Induction and Rejoining of DNA Double-Strand Breaks in Human Cells after Exposure to Ionising Radiation: an Experimental and Modelling Approach

a Thesis submitted to the University of London for the degree of

Doctor of Philosophy in Physics

2002

Cell and Molecular Biophysics Group, Gray Cancer Institute

Department of Oncology, University College London

Supervisors:
Dr. Kevin M. Prise
Prof. John A. Hartley

presented by:
Massimo Pinto
BSc in Physics
University of Naples 'Federico II'

Abstract

The induction of DNA double-strand breaks (DSBs) by ionising radiation and subsequent rejoining were studied in normal human fibroblasts *in vitro*, using radiation of different qualities. Radiation of increasing linear energy transfer (LET) can induce local hot spots of energy deposition that may result in DNA damage that is difficult to repair, and can potentially be mis-repaired. Due to the spatial association of the energy deposition events after the passage of ionising radiation, double-strand breaks (DSBs) and other types of DNA damage may be induced at genomic distances that reflect chromatin structure and radiation quality, introducing higher orders of damage complexity. The pulsed field gel-electrophoresis (PFGE) technique was used to resolve the fragmentation patterns after induction and rejoining of DSBs, separating double–stranded DNA fragments between 30 kbp and 5·7 Mbp. Several analytical and numerical methods of quantification of DNA damage were used and critically analysed. A novel method of DSB quantification based on random breakage was developed, which was applied to an extensive data–set along with several other methods. Results of this comparative analysis suggest that conventional methods of DSB quantification may be misleading, due to the way they handle the unwanted background damage that is produced during manipulation of the samples. Significant deviations from the random breakage predictions were observed for ^{238}Pu α-particle irradiation, using a numerical method based on DSB clustering to analyse experimental data. In order to have an indication of the relative biological relevance of DSBs induced by radiation of different LETs, DSB rejoining kinetics were measured in living cells, and a detailed fragmentation analysis was carried out. A simple rejoining kinetics numerical model was designed and developed, based on a semi-empirical approach. The kinetic model was applied to the analysis of many experiments from this study. The results of the computer simulations are in good agreement with the experimental data. Even if the initial fragmentation patterns were significantly different for X-rays vs α-particles, DSBs induced by both radiations seem to rejoin according to a first order kinetics with two decay components, that do not depend on the size of the fragments being rejoined. For the molecular–weight size distribution that was observed in this project, the results indicate that the complexity of individual DSBs, rather than proximity effects between distinct DSBs, determine the rejoining kinetics.

Preface

This doctoral study aims at giving a contribution to the field of radiation research, with an emphasis on radiation protection and radiotherapy research. Radiation protection aims at evaluating the risks of exposure of humans to radiation, establishing the acceptable limits for occupational, medical and certain environmental exposures. In radiotherapy, the property of ionising radiation of killing living cells is explicitly used for curing malignant cells in tumours. At first sight, radiation protection and radiotherapy research may seem rather different, but they are in fact very deeply connected, since advance in both sciences relies heavily on understanding the basic mechanisms of radiation-induced cell injury.

That radiation can kill living cells has been known since the beginning of the 20^{th} century, when radiologists began to employ ionising radiation to kill tumours (1903). Little was known about the mechanisms through which radiations cause cell damage, and further investigations were required in physics, chemistry and biology, before it became clear that the main cellular target had to be in the nucleus (Lea, 1946; Munro, 1970; Schrödinger, 1944), then identified in the DNA double helix (NCRP, 1979; Painter, 1979; Ragni and Szybalski, 1962; Sparrow, 1965). Radiation research can help to improve both radiotherapy and radiation protection by answering the following questions:

- which type of damage is most severe,
- what is the mechanism of its production,
- how it is processed by the cells when trying to repair it,
- what are its biological consequences

In principle, progress in this field will provide methods that could help modify the cellular radiation response in radiotherapy, in healthy and malignant cells selectively, in order to improve radiotherapy protocols.

At present, it is widely accepted that DNA is the most sensitive target to radiation for cells of high-eukaryotes systems, and that only some relatively infrequent types of DNA damage are most relevant. This project aims to contribute in the characterisation of the

most lethal forms of radiation-induced DNA damage, currently thought to be a form of DNA double-strand break (DSB).

The work in this project has been based on experimental, mathematical and computer-modelling approaches. The results obtained in this thesis have only been possible due to the close interplay between the model development and experimental data sets obtained.

To facilitate reading and finding specific arguments that may be of interest to the reader, the electronic portable document format (PDF) version of this Thesis, which can be found in the CD-rom attached to the third page of the hard-cover, contains a hyperlinked Index. The table of contents, the list of figures and tables, and every reference to tables, figures or equations in the text body is hyperlinked, with the sole exception of hyperlinks inside rotated tables. There are also hyperlinked 'back-references' to bibliography citations throughout the text. For example, if you find that your work relates to an article that is listed in the bibliography, you can quickly go to the pages where this article was cited using the hyperlinks provided. For example:

> AGER, D. D. and DEWEY, W. C., 1990, Calibration of pulsed field gel electrophoresis for measurement of DNA double-strand breaks. *International Journal of Radiation Biology*, **58**, 249–259. 52.

If you are reading the electronic version of this Thesis, you can go to page 52 by clicking on the hyperlink above, otherwise just turn the pages manually.

Contents

List of Tables

List of Figures

List of Program Codes

Dedicato a Lorenzo e Renata

Chapter 1

General Introduction

1.1 The interaction of ionising radiation with matter

Ionising radiation interacts with matter via excitation and ionization of the atoms and/or molecules of the surrounding environment. Whenever electromagnetic radiation, charged particles or neutrons hit matter, electrons are ejected due to Coulomb interaction (with charged particles) as a consequence of the primary hit, or due to electromagnetic interaction (with photons) or nuclear reactions.

Both excitations and ionisations of the target material upon interaction with a charged particle may cause a given target molecule to enter a very reactive state, which lasts for a short time, in the order of 10^{-9}–10^{-6} seconds. Radiation may hit the target molecule *directly*, causing either an excitation to an unstable state, which upon de-excitation may lead to a lesion of the target molecule, or causing a direct ionization to the target molecule. Since the chemical bond in a molecule depends on the spatial distribution of its electrons, the loss of even one electron, due to a radiation-induced ionization, may trigger a re-arrangement of the molecule's electronic distribution. The major consequence is that this re-arrangement may lead to the formation of a break in a chemical bond (Tainer, 2000). A radiation-induced indirect damage to a biomolecule is mediated by another molecule which, if able to diffuse, reaches the biomolecule and transfers the damage to it. Indirect damage to a biomolecule may be limited by means of scavengers, as described in § 1.2. The distinction between direct and indirect effects made here may be over-simplified, as it is believed that there is a type of indirect damage that is non-scavengeable, which takes place in close vicinity to the target molecule (called the hydration layer if in water; Becker and Sevilla 1993; Ward 1994) referred to as quasi-direct damage. Ionising radiation is capable of inducing direct, indirect and quasi-direct damage to a target molecule, in relative proportions that depend on the properties of the environment, such as the presence of scavengers and their concentration, as well

as on properties of radiation itself. It is common to distinguish radiation depending on its quality, as described in § 1.1.1. In an aqueous environment, most of the indirect damage to a target molecule originates from the radiolysis of water, resulting in the production of $^{\bullet}$H and $^{\bullet}$OH radicals and the hydrated electron $e^{-}_{\mathrm{aq}}{}^{\bullet}$, the $^{\bullet}$OH radical being the most reactive species with DNA.

1.1.1 Dose, radiation quality and RBE

As radiation traverses matter it loses energy which is absorbed via excitations and ionisations (see § 1.1). A macroscopic quantity called dose is defined as the *energy absorbed per unit mass of irradiated material*. In the International System, its unit is the Gray (Gy), defined as an energy of 1 Joule absorbed in 1 kg of target material.

$$1\ \mathrm{Gy} = \frac{1\ \mathrm{Joule}}{1\ \mathrm{Kg}} \tag{1.1}$$

1 Gy delivered to a cell causes damage that may be lethal depending on the radiosensitivity of the cell line examined. For an estimate of the damage that is made to a cell after a dose of 1 Gy, see table 1.1.

The number of molecules that are hit in a Kg of target material is proportionally small, even after a very copious exposure to ionising radiation. In fact if 13·5 eV is the binding energy of the electron occupying the outer molecular orbital of water, then 1 Joule, equivalent to $1/1.69\times10^{-19}$ eV would be expected to produce roughly 4×10^{17} ionised water molecules, while a kg of water contains $\approx 55.5 \times 6 \times 10^{23} = 3.3 \times 10^{25}$ water molecules. Only one in 10^{8} water molecules is then ionised. Dose, however, is an average quantity that does not provide information about the energy that is absorbed everywhere in the target material, that is, in any given volume of observation. The difficulties of the concept of dose illustrated above are considered by the use of Microdosimetry, which

> *"studies the physical properties of ionising radiations, their interactions, and their patterns of energy deposition, with particular emphasis on the heterogeneities and stochastic nature of the interactions" – D. T. Goodhead*

Microdosimetry allows extrapolations to be made to the macroscopic environment. Dose is a quantity that measures the energy absorbed by the medium after the passage of radiation through the medium itself. However, it does not give information on the spatial distribution of the energy deposition events in the microscopic environment of the medium. One parameter commonly used to define different radiations is the 'unrestricted' linear

energy transfer which is defined as the *quotient of the differential energy dE imparted to the medium per unit length dx of medium traversed* (see also ICRP, 1980, for the 'unrestricted' property).

$$\mathrm{LET} = \frac{\mathrm{dE}}{\mathrm{dx}} \tag{1.2}$$

The LET of a given radiation is normally expressed in keV of energy imparted per μm of medium traversed. The unrestricted LET depends on parameters of both radiation and target, as reported in eq. 1.3, simplified from the original Bethe-Bloch formula:

$$-\frac{\mathrm{dE}}{\mathrm{dx}} \propto \frac{Z_t Z_p^{*2}}{m_p v_p^2 A_t} \tag{1.3}$$

where Z_t and A_t are the atomic and mass number of the target material, Z_p^*, m_p and v_p are the effective charge (smaller than the chemical charge because of shield-like effects of the electron cloud of the target material, given by the Barkas' formula), the rest mass and the speed of the primary charged particle.

In the definition of unrestricted LET it is assumed that radiation transfers energy to the medium linearly in space along its direction of travel. When a certain amount of energy is absorbed locally in a medium after the passage of a charged particle, for example, it is very likely that one or several electrons are freed. These electrons, often referred to as secondary electrons or 'δ-rays', leave the site of primary ionization with a kinetic energy that is proportional to the energy initially imparted, so that they may potentially transfer energy to the medium themselves, may be far away from the site of primary ionization, leading to diffusion in space of the energy deposited, and potentially damaging biomolecules or even cells nearby. The three-dimensional energy deposition pattern can thus be very complex. This can only be described accurately by means of sophisticated charged-particle transport computer codes, which are written to simulate numerically the ionisation events that follow the passage of a given radiation. It was found in a series of experiments that radiation of different types, specifically light ions like protons or α-particles of the same LET had significantly different values for the radiation biological effectiveness (defined ahead in eq. 1.5) for DSB induction (see § 1.3), mutation or cell killing (Belli *et al.*, 1993, 1991, 1989, 1986, 1987, 1992; Folkard *et al.*, 1989, 1996; Jenner *et al.*, 1992; Prise *et al.*, 1990) This was an indication that the unrestricted LET concept may be an incomplete descriptor of the energy deposition pattern of radiation in a medium, and that microscopic features in track structure play an important role in determining the biological effect of ionising radiation.

For a given LET, depending on the mass of the primary particle, the speed of the

particle varies as written in eq. 1.3. Since the speed of the primary particle has a direct effect on the energy of the secondary electrons (Chatterjee *et al.*, 1973) , the δ-rays freed have different energy deposition patterns for charged particles of same LET but different mass. As protons travel slower than α-particles at the same LET, their δ electrons have less energy, hence they have a shorter range and have a higher LET themselves than δ-rays from α-particles. As such, unrestricted LET may not be the ideal parameter for estimating the biological impact of radiation (see the RBE-LET relationship in figure 1.1), a datum that is required in the estimation of radiation risk. To allow for part of the energy transported away by the δ-rays, other quantities have been proposed to replace unrestricted LET. One quantity is the restricted LET (Harder, 1987) where dE in eq.1.2 refers to energy that is transferred locally around the primary charged-particle track. Restricted LET is quantified by considering in the calculation only the energy that is transferred to the medium by the primary and secondary tracks up to 100 eV. An example may clarify the subtle difference between restricted and unrestricted LETs. If a secondary electron is freed with 500 eV of kinetic energy, only the first 100 eV deposited nearby are included in the calculation of the restricted LET. The 100 eV limit is the most used in the restricted LET but by no means a standard, so the limiting value is always reported in eV. For example:

$$\mathrm{LET}_{100} \equiv \left.\frac{\mathrm{dE}}{\mathrm{dx}}\right|_{100} \tag{1.4}$$

Despite the limitations illustrated above, unrestricted LET remains often more practical than restricted LET, and for this reason the former has been widely used as the physical parameter related to the radiation effectiveness (see Goodhead, 1987, for a review). In this Thesis, every reference to LET will be referred to the unrestricted LET. Since the two types of radiation used in this study are very different from each other (one sparsely and one medium-densely-ionizing) the unrestricted LET is reasonably adequate to characterise them.

In radiobiology studies, to quantify the efficacy of a given radiation quality in relation to that of a reference radiation, a dimensionless quantity named radiation biological effectiveness (RBE) is defined. This is expressed as the *quotient between the dose of the reference radiation and that of the test radiation that is required to attain the same level of biological effect*:

$$\mathrm{RBE} = \left.\frac{\mathrm{D_{reference}}}{\mathrm{D_{test}}}\right|_{\text{iso-effect}} \tag{1.5}$$

If the dose of test radiation needed to cause a specific effect is smaller than that required with the reference radiation, the radiation biological effectiveness (RBE) of the test radiation is larger than one, the test radiation is more effective.

As high-LET radiations are characteristic for their high ionisation density, which can potentially cause severe damage to DNA, it could be thought that the effectiveness of radiation monotonically increases with LET. Nevertheless, for virtually all the biological end-points in repair-proficient eukaryotic systems, there is a characteristic non-monotonic RBE–LET relationship, which was first described in detail by Barendsden (1968) and shown in figure 1.1. For a given end-point, the RBE first increases with LET up to a maximum which is located in the order of a few hundreds of keV/μm, then falls rapidly with LET. A commonly accepted explanation for this behaviour is based on the assumption that radiation is most effective in causing DNA damage when a certain critical level of ionisation is deposited in or near the DNA, sufficient to cause a potentially irreparable damage (see § 1.3 for a characterisation of biological relevance of classes of DNA damage). Ionising energy deposition events below this value are generally causing easily repairable damage, whereas ionisation densities above the critical value will cause additional but ineffective damage. Any extra hit is considered an 'overkill' event. For virtually any end-point, the RBE–LET curve is not unique but shows dependence on the particle charge, as described earlier. Although RBE is a useful descriptor, great care has to be taken in its use for quantification of effects. This is because it is a function of the particular system, its repair capacity, the level of effect and the chemical (*e.g.* oxygen, repair inhibitors) and physical (*e.g.* dose rate, temperature) conditions of exposure.

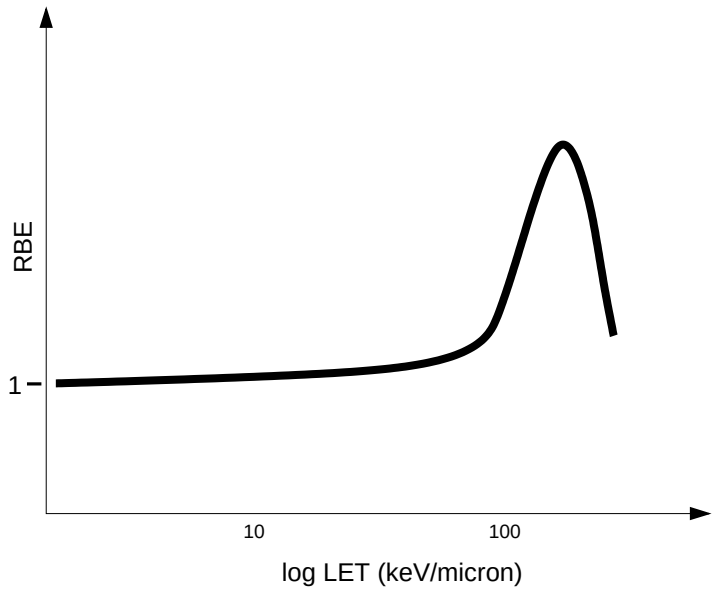

Figure 1.1: The RBE-LET relationship

1.2 DNA, Chromatin structure and function

According to the classical paradigm of radiation biology, radiation causes cell injury via DNA damage that is produced either via direct or indirect effect in the cell nucleus. In order to understand the nature of radiation-induced cell injury, it is important to know which are the targets of radiation inside the nucleus, as well as their structure and their function. Scavenging (Johansen, 1965) effects are specific to the gaseous and liquid phase, where molecules can diffuse easily and the result of a ionization may be seen at a relatively long distance away from the site of its creation. Scavengers are molecules that 'neutralise' water radicals, or radicals of other chemical species present in water, by interacting with them, before these reach the biomolecules. Alternatively, one can have restitution of a damaged biomolecule, for example by means of a H-atom donor. Glutathione (GSH) is endogenous to cells and operates by restoring damaged biomolecules (Roots and Okada, 1972) so as to minimise the damage induced by radiation. GSH is the most abundant thiol in cells, although not the only one. The higher the concentration of scavenging molecules, the less likely is the production of radiation-induced indirect damage (Lea, 1946).

Human cells, like all the eukaryotic cells, have a structurally separate nucleus, defined by the nuclear membrane in which the genomic DNA is contained and organised with the aid of the histone proteins, closely associated to the double helix, and those that form the nuclear matrix (reviewed by Berezney, 1991). About 1% of the total DNA within a cell is mitochondrial DNA present outside the cell nucleus, in a circularised form 16,500 bp long. During cell division at metaphase, chromatin is highly condensed such that is visible in the form of chromosomes by microscopy. For non-cycling cells or cells not in metaphase (inter-phase) the DNA is still highly organised in repeated structures, visible by electron microscopy. These repeated structures are held in a stable configuration by attachment to a non-chromatin structure present in the nucleus, called the nuclear matrix, a complex three-dimensional 'scaffold' in the nuclear interior. Apart from being a structure that can be isolated from the nuclei of cells, the nuclear matrix seems to have a vast number of functions: its DNA attachment sites, called scaffold-attached regions (SARs) by Mirkovitch *et al.* (1987), may be three-dimensionally organised in the nuclear volume to keep the chromosomes in separate territories, as well as being involved in DNA replication, gene transcription and RNA splicing.

DNA is highly compacted in the nucleus by means of several orders of chromatin folding, so that approximately 2 metres of DNA double helix may be accommodated in a nucleus of about 10μm diameter (see figure 1.2). Beginning from the naked DNA double helix itself, one can distinguish the following organised structures (see Filipski *et al.*,

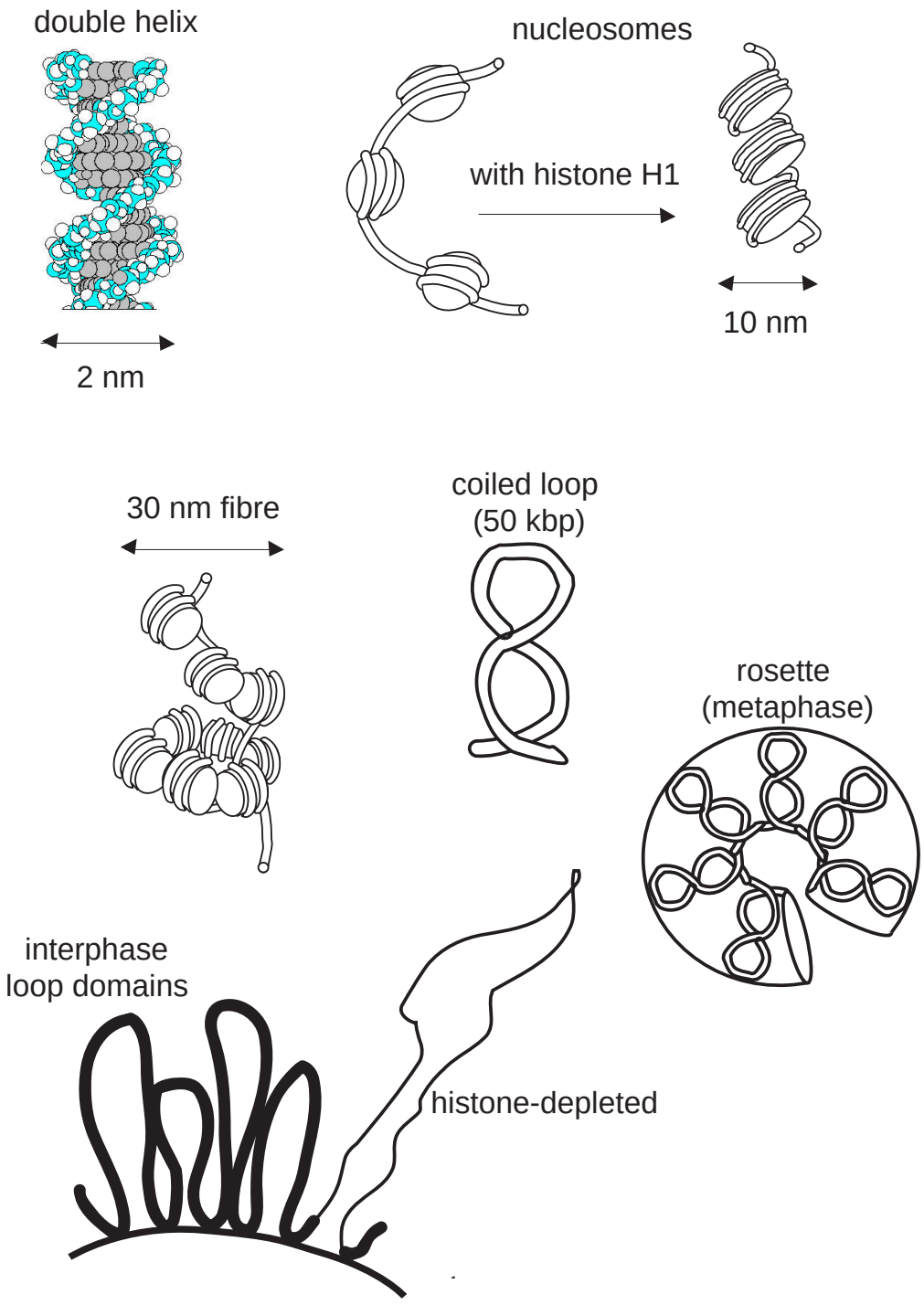

Figure 1.2: DNA high-order organisation in the mammalian cell nucleus. The double helix is known to wrap around nucleosomes, which in turn coil into the 30 nm chromatin fibre. In interphase, the fibre is believed to form looped structures attached to the nuclear envelope. For chromosome condensation, it has been proposed that coiled loops are formed, which in groups of six form rosettes, the elementary part of a condensed chromosome (Filipski *et al.*, 1990).

1990; Widom, 1998, for a review):

- **The nucleosome octamer core plus the linker DNA.**
  The DNA double helix is wrapped around an octamer protein complex made of 4 distinct histone proteins: H2A, H2B, H3 and H4. Together they form the nucleosome core, around which a DNA double helix of well defined length of about 146 base pairs (bp) is wrapped (Widom, 1992). Nucleosome cores are linked together by a short sequence of 'linker DNA', bound to the H1 linker histone. The nucleosome core and the DNA linker together form the nucleosome, a structure that may be inscribed in a cubic volume of size 10 nm.

- **The 30 nm chromatin fibre.**
  Nucleosomes are further folded into a 30 nm fibre that has been long thought of resembling a solenoid structure (Finch and Klug, 1976), each turn consisting of six nucleosomes and approximately 1 kilo-base pairs (kbp) of DNA double helix. The linker histone H1 is responsible for keeping the 30 nm chromatin fibre in a condensed form. In this conformation, the nucleosomes are not only defining a precise structure, but appear to be functionally involved in sensing DNA DSBs for enzymatic repair, as demonstrated by Rogakou *et al.* (1998) and by Paull *et al.* (2000). Due to the compacted shape of the 30 nm chromatin fibre, part of the DNA may be more accessible from the exterior, whereas other parts may be less accessible. This is by no means a permanent organisation: during gene transcription and DNA synthesis, part or the entire DNA sequence needs to be accessed and this requires transient relaxation of the compacted form. Some sequences may be even permanently unbound to nucleosomes, to facilitate access to the DNA transcription machinery, such as the promoters of housekeeping genes (Wallrath *et al.*, 1994).

  Recent computer-modelling studies, supported by experimental evidence, have thrown doubt on the solenoid model for the 30 nm chromatin fibre and have proposed an alternative three-dimensional zig-zag arrangement of the nucleosomes (Rydberg *et al.*, 1998).

- **The chromatin fibre loop domains.**
  The 30 nm chromatin fibre *in vivo* is further folded into higher-order structures. The first distinct structure are super-coiled DNA loops whose size is estimated at 50-100 kbp and seem to vary with cell type. These chromatin loops are held in place by means of the scaffold-attached regions. Each of these 50-100 kbp loops may be a separate DNA replication unit (Berezney, 1991).

- **The next level** of chromatin organisation is still controversial and at least two models have been proposed, mostly based on *in situ* experimental observations and computer-modelling. These two models may also have overlaps in the structure, as the chromatin changes organisation from interphase to cell division and vice-versa:

  - **Rosettes.** The super-coiled 50 kbp loops of chromatin fibres may be organised in groups of 6 to form a circular rosette (containing 300 kbp, as in figure 1.2). These rosettes may be linked to each other on a random walk three-dimensional path during interphase, but they may form a coil, or a wave or again a double helix that would become visible as the unit length of metaphase chromatid during cell division (Filipski *et al.*, 1990).

  - **'Giant' loops.** Scaffold-attached regions that maintain loop domains may be transient, occurring during replication and possibly during transcription, but it has been proposed that more permanent SARs are located near sites where DNA replication is initiated. In some experiments where the weaker SARs bonds are digested, 'giant' loops of size 2.9 Mega-base pairs (Mbp) are identified (Johnston *et al.*, 1998a,b). These may not be present as individual loops *in vivo*, since smaller loops are identified as illustrated above. Support for Mbp-sized, well-defined chromatin structures of size above 50 kbp has also come recently from co-ordinated experimental and modelling approaches (Manuelidis, 1990; Sachs *et al.*, 1995; Yokota *et al.*, 1995).

- **Chromosome territories.** Experimental *in situ* evidence has lead to the emerging view that each inter-phase chromosome is organised in a discrete chromosome territory (CT) inside the cell nucleus. Surrounding CTs, an inter-chromatin compartment (IC) would contain macromolecular complexes that are required for transcription, replication, splicing and also DNA repair (Cremer and Cremer, 2001). Chromosome territories and the inter-chromatin compartment could occupy non-mutually exclusive volumes inside the nucleus, with IC protruding into the CT space and vice-versa. The CT-IC model proposed by Cremer and Cremer also predicts a specific topology of transcriptionally active genes. In fact, since the transcription machinery would reside only in the inter-chromatin compartment, a gene must be in close proximity to the surface that defines the border between a chromosome territory and the inter-chromatin compartment in order to be accessible to transcription. According to this model, gene silencing would be accomplished by moving DNA farther away from the inter-chromatin compartment, whereas up-regulation would be achieved by bringing it closer. The highly dy-

namic DNA compartmentalisation predicted by the CT-IC model is compatible with a three dimensional nuclear matrix, although the existence of the latter may not be necessary.

The chromatin structures mentioned above and schematically drawn in figure 1.2 have a significant influence in determining both the type and extent of DNA damage induced by a given radiation quality and its subsequent repair. These two aspects will be dealt with in the following sections of this and subsequent chapters.

1.3 DNA damage

In 1944, Schrödinger elegantly described the mutations that X-rays can induce in humans, remarking that these mutations appear to be the same as those that arise spontaneously. Nothing was known at that time about the molecular nature of the damage that leads to mutations, and it was speculated that these lesions were caused by ionisation events in genes, caused by radiation, called 'explosions' by Schrödinger. Timofèeff-Ressovsky *et al.*, studying X-ray-induced mutations, suggested that the dimensions of the target that was hosting genes, which was thought to be made of proteins rather than DNA at that time, had to be roughly those of a cube with sides between one and 10 μm (Timofèeff-Ressovsky *et al.*, 1935). Today it is known that biological effects of ionising radiation, including gene mutations, are consequences of DNA damage (see for example Cole *et al.*, 1980; Elkind, 1985).

It was written in § 1.1 that exposure of a material to ionising radiation can induce breaks in chemical bonds. For biological systems, the main interest over the last 50 years has been the DNA double helix, long considered the main target of radiation. The spectrum of lesions that may be induced by radiation via chemical modification involving breakage of bonds is very large, but only a subset of these lesions has the ability to participate in causing significant biological effects, like reproductive cell death, mutation or transformation, division delay (see Ward, 1998, for a review). Although a range of lesions of differing yields are produced, enzymatic repair processes allow many of these to be removed, therefore the response of a cell to a radiation exposure is a consequence of both damage induction and repair. It should be noted that some of these radiation-induced lesions are structurally identical to endogenous lesions, which despite being very frequently induced in cells (see table 1.1) are repaired very efficiently. The simplest classes of radiation-induced DNA damage include simple, 'clear cut' isolated single-strand breaks (SSBs) and excised bases, which are produced in abundance in healthy cells, but repaired efficiently. What makes ionising radiation so lethal to cells is

its ability to produce DNA damage in clusters: even if the total number of lesions to DNA induced by a dose of 1 Gy is significantly lower than the number of lesions caused by endogenous processes per day, they are considerably more effective in causing severe biological consequences, as reviewed by Burkart *et al.* (1999).

DNA damage induced by radiation includes base damage, strand breaks, DNA-DNA cross-links and DNA-protein cross-links (Cole *et al.*, 1980). These should be regarded as classes of lesions, since there are, for example, several types of damaged bases and many different types of strand breaks (Eastman and Barry, 1992; Von Sonntag *et al.*, 1981). Some of these lesions have little biological relevance, like isolated SSBs and some damaged bases, as they can be easily repaired. An indication of the relative abundance of some of the lesions caused by 1 Gy of low-LET radiation is given in table 1.1. The value indicated for the DSB yield in 1.1 is given with approximation, since one of the

Event	Yield (Gy^{-1})
Ionisations and excitations (nucleus)	100 000
Ionisations and excitations (DNA)	4 000
Damaged bases	1 000
DNA single-strand breaks	1 000
DNA-protein cross links	150
DNA double-strand breaks	$\approx$ 40
Mean number of lethal events	0·5
Total *endogenous* lesions (per day)	10 000

Table 1.1: Extent of DNA damage caused by ionising radiation in the cell nucleus after 1 Gy of low-LET radiation. For comparison, the total number of lesions caused by endogenous processes is also shown in the last row of the table (produced with data from Burkart *et al.*, 1999; Goodhead, 1994).

main aims of this work was to critically review the methods of quantification of DSBs and to develop more reliable methods. As will be discussed in chapters 3 and 4, quantification of DSB yields depends to a significant extent on the data analysis methods used (see also Prise *et al.*, 2001).

If the DNA double helix were just a long polymer, stretching along one dimension in space, when hit by radiation it would experience a relatively limited class of damage: base damage or strand breakage, or a combination of these two, often referred to as locally multiple damaged site (LMDS). These are locally damaged sites, at the level of a few base pairs from each other (Ward, 1981). The complexity of LMDSs is function of radiation quality (Prise, 1994) and the higher the level of complexity, the more biologically relevant is the lesion. LMDSs are not the only type of clustered damage that ionising radiation induces in DNA. For simplicity, it may be assumed that every time a charged-particle track intersects DNA it causes damage, although this may not happen

for sparsely ionising radiation. Since the DNA is three-dimensionally organised in nucleosomes, 30 nm chromatin fibre, and supercoiled loops/rosettes/coils and chromosome territories (§ 1.2), the damaged spots that are correlated in Euclidean space along the direction of the charged particle (an electron, or a more massive particle) will also be correlated along the genomic distance of the double helix. These can range from a few tens to several 10^6 bp. For each order of chromatin structure that is being hit, there is a corresponding level of regionally multiply damaged site (RMDS), as originally defined by Rydberg (1996) to refer to the damage clustered at the nucleosomes and 30 nm fibre level. Due to the folding of DNA at the nucleosome level, a relative abundance of radiation-induced DNA damage, correlated to genomic distances that reflect these structures, is expected (Holley and Chatterjee, 1996; Rydberg, 1996). For each of the super-structures mentioned before, there is a corresponding order of RMDS.

In principle, it should be possible to detect experimentally this 'fine structure' of DNA damage. The experimental technique that was employed in the work for this Thesis, described in § 2.6, allows detection of DNA damage than can be associated within the 30 kbp-5.7 Mbp size region. Due to the genomic DNA content of a nucleosome ($<$200 bp) and 30 nm chromatin fibre (1kbp), correlated DNA damage at the level of these structures may be at 'resonant' genomic distances up to approximately 2 kbp, which falls below the sensitivity limit of the techniques employed in this study. Conversely, radiation-induced clustered DNA damage at chromatin structures of higher order may be at genomic distances that could be probed. The detection of this damage and its interpretation by the cellular repair machinery will be extensively discussed in the following chapters.

1.3.1 DNA double-strand breaks

The discovery that ionising radiation causes some type of breakage in the chromatin dates back to 1948 with the work by Taylor *et al.*, where a change in the viscosity of DNA was detected after exposure to radiation. A few years later, with the double helix model for the DNA, it was understood that the changes in the sedimentation of DNA molecules were due to radiation-induced double-strand breakage of long stretches of the double helix. It became possible to measure the breakage yields with the aid of some mathematical modelling of fragmentation of long polymers (Charlesby, 1953; Montroll and Simha, 1940).

There is a large body of experimental evidence in support of a major biological role of DSBs over the other types of lesions induced by ionising radiation (Burkart *et al.*, 1999; Goodhead, 1994; Iliakis, 1991; Olive, 1998; Ward, 1994, 1995; Whitaker *et al.*, 1995).

This evidence is based on the following arguments.

A DSB causes a physical interruption in the DNA sequence. Attempts of the cell repair machinery to eliminate a DSB may not necessarily be effective, with potential loss of (coding) sequences that could result in mutations or chromosomal damage leading to loss of genetic information. DSB repair-deficient mutants have been shown to be significantly more radio-sensitive than normal cells, while the same cell lines showed normal SSB repair (Jeggo and Kemp, 1983; Kemp *et al.*, 1984), also recently reviewed by Fox and Prise (1993) and Jeggo (1998b). These findings are in support of a biological role of DSBs relative to SSBs. Also, in mutant cell lines that show reduced DSB repair activity, the number of un-repaired DSBs correlates well with yields of chromosome aberrations data (Darroudi and Natarajan, 1991), which in turn correlate with biological end-points such as reproductive death (Cornforth and Bedford, 1987; Durante *et al.*, 1994).This evidence is in support of a biological role for DSBs that were not enzymatically repaired, although the picture is known to be more complex (see § 1.4).

Initially it was believed that DSBs were a biologically relevant lesion because their yield was found to increase with LET, like the RBE for several cell responses (Christensen *et al.*, 1972). Shortly after it was found that it is not the initial, total number of DSBs that correlates with radiation sensitivity, since there is not a causal relationship between the formation of a DSB and biological consequences (Foray *et al.*, 1997a). In fact, a considerable proportion of the initially induced DSBs is efficiently repaired by the cells (see § 1.4). That the initial DSB yield does not correlate with biological response has also been confirmed more recently with the aid of more accurate experimental techniques and methods to analyse data (Belli *et al.*, 1994; Iliakis *et al.*, 1988; Prise *et al.*, 1987, 1990), reviewed by Prise *et al.* (1998). It is appropriate then to ask the following question:

> If DSBs are a critical lesion, why does the total DSB yield not correlate with changing biological effectiveness due to different LETs?

A possible explanation is that what is measured experimentally with the current techniques as DSB does not reflect the way the cells interpret that lesion, and that DSBs of different orders of local complexity are all detected as mere DSBs (Olive, 1998). An additional and related problem may be that the number of DSBs is not correctly estimated (Prise *et al.*, 1998), and/or that only some DSBs are quantified and these may be those that are less relevant (Prise *et al.*, 2001). Even in the ideal case of perfectly unbiased experimental techniques, it could be argued that not every DSB is equally lethal to a cell. The problem underlying the lack of correlation between DSB induction and biological effects, as found in several experiments, may be in what is defined as a double-strand break.

The term DSB clearly gives a general picture of this class of lesion in that the DNA sequence is interrupted by a break in the double helix. Nevertheless, such a name gives a very poor description of the several sub-classes of DNA double-strand break where the two opposite strands are broken in close vicinity, namely within a few base pairs. The nucleotides at the two 'ends' formed may be intact, with an hydroxyl group $^{\bullet}$OH on one end and a phosphate group on the other end of each of the two interrupted strands (see for example Eastman and Barry, 1992, for a description of the quality of strand break ends). This simplest case only requires an annealing process to restitute the original sequence. The phosphate/sugar backbone at the breakage site itself may be also damaged, requiring the action of excision enzymes before the sequence can be re-established by re-annealing of the strands. At a higher level of DSB complexity, the damaged ends may be accompanied by other damaged sites nearby: abasic sites (a base has been lost), bases showing a wide range of damages or additional SSBs with or without damaged sugar backbone at their ends (locally multiple damaged site). The DSB spectrum is hence very large, and it would be tempting to postulate that not all of these forms of DSB may be repaired with the same efficiency by the cells, with the repair enzymes failing to recognise and/or to process the damaged sites.

Using radiation of different LET to modulate LMDS complexity (Prise, 1994; Prise *et al.*, 1994; Ward, 1994), it is shown that the lethality of a single DSB correlates with LET (Fox and Prise, 1993). Specifically, it was suggested that while a DSB from a 100 keV/μm α-particle has approximately 5% chance of killing a cell, a DSB induced by 250 KeV X-rays has about a 1% probability.

If local DSB complexity greatly influences the severity of a single, isolated DSB, RMDSs (see § 1.3) add another level of complexity to the problem of characterising the relevant type of DNA double-strand break. In fact, two regionally associated simple DSBs may be even more difficult to repair than a sparse, single locally complex DSB (see § 1.4). Since DSBs that are correlated at the level of RMDS are significantly more frequent after high-LET radiation, as described in chapter 3 and confirmed by analysis of experimental data in chapter 4, the regional association and the local complexity of DSBs may need to be considered in order to characterise relevant lesions. To answer all of these questions, DSBs repair studies may provide very useful information.

1.4 DNA double-strand break repair

Elkind and Sutton first showed in a bacterial system that ionising radiation-induced DNA damage can be repaired (Elkind and Sutton, 1959), setting the scene for the vast field of DNA repair. The work for this Thesis has focused on double-strand breaks (DSBs)

and consideration of DNA repair will be limited to that of this type of damage. In order to find the relevant DNA lesion, experimental observations have moved from quantification of initial DSBs (§ 1.3.1) to evaluating the fraction of DSBs that remain un-repaired after several hours of cell incubation, or the rejoining DSB kinetics, or, more recently, to repair fidelity, in order to distinguish between correct vs incorrect DSB repair (Löbrich *et al.*, 1995). As there are DSBs that are not repaired by cells correctly, it is important both to characterise the lesions, as described ealrier, and the mechanisms of enzymatic repair of DSBs. Mammalian cells have more than one pathway for repair of DSBs available (Haber, 2000; Jeggo, 1998a,b; Pastink *et al.*, 2001). These pathways involve several proteins which have been partly identified using mutants that were defective in DSB repair. Three major pathways are distinguished:

- homologous recombination (HR)
  is the principal DSB repair mechanism in Yeast, requiring extensive regions of DNA sequence homology to operate. Every time that a DSB is to be repaired, the intact sequence on the homologous chromosome to the one that has experienced the DSB has to become available for the HR enzymes to operate. Conversely, HR is very seldom used in higher eukaryotes, namely in cells undergoing meiosis and in the cells of the immune system (Kuzminov, 1996). During interphase, chromosomes of higher eukaryotes are thought of occupying well defined domains in the cell nucleus, as detailed in recent high-resolution cytometry studies (see Boyle *et al.*, 2001, and the CT-IC model in § 1.2). Chromosomes belonging to neighbouring domains are the only ones likely to interact, so that for the major part of the cell cycle, when sister chromatids are absent and the homologous sequences may be too far away to interact with each other in HR, other DSB repair processes may be used. The majority of DSBs in high eukaryotes are in fact repaired by the NHEJ repair pathway, although HR may play an important role in the S and G2-phase when sister chromatids are present.

- non-homologous end-joining (NHEJ)
  Extensive regions of sequence homology are not necessary for the non-homologous end-joining DSB repair process, which seems to be the main repair process in mammalian cells, including human cells. The NHEJ repair pathway shares several enzymes with a process called Variable (Diversity) Joining (V(D)J) recombination. The V(D)J process is used during the development of the immune system (Jeggo, 1998b) and is used to generate sequence diversity, by introducing multiple DSBs in vicinity and re-arranging the DNA sequence of some genes. This is a key feature for the development of the immune system, but it is certainly not desirable for the

re-constitution of the correct sequence at the site of any DSB, such as those introduced by ionising radiation. Chromatin organisation in higher eukaryotes (§ 1.2) may help this DSB repair pathway to operate correctly. Specifically, when a DSB is introduced in a DNA helix, this is interrupted and its two ends may separate away from each other by diffusion. In yeast, which lacks high-order chromatin structures, the two ends are virtually free to diffuse, so that if many DSBs are present in the genome at the same time, it is very likely that the NHEJ process would join the incorrect ends of different DSBs. In this case, one has a *mis-repaired* DSB. In mammalian cells, high order chromatin structures secure the two ends of a DSB so that they do not diffuse freely, since there would be a stretch of DNA nearby that is attached to the nuclear matrix via means of a covalent bond to a SAR (§ 1.2). For this reason, when using NHEJ, it is believed that mammalian cells are not exposed to the same risk to which yeast is exposed when using the same pathway. Nevertheless, if chromatin loops maintain the ends of one DSB in vicinity before the recruitment of the competent repair enzymes, *multiple* DSBs within a chromatin loop domain would inevitably free double-stranded stretches of DNA, considerably enhancing the risk of sequence deletion and/or mis-rejoining (Johnston *et al.*, 1998a,b).

NHEJ may have become the prevailing DSB repair pathway in high eukaryotes also because the fraction of their genome that is coding for proteins is at most 30%, so even if NHEJ fails to re-constitute the correct DNA sequence, this may not necessarily cause biological consequences. The mis-rejoining event would then be tolerated, since it may not lead to a non-functional protein. In yeast, as well as in *E. Coli*, where the fraction of coding genome is 95% or more, a simple but error-prone repair mechanism like NHEJ is not an affordable choice, and HR is probably a better solution to the DSB threat.

- single-strand annealing (SSA)
  This process is known to occur in areas of the genome where repeated sequences are present (Kuzminov, 1996). It proceeds via annealing of two complementary strands, after the other two opposite strands have been digested. The mechanism is explicitly causing sequence deletions in those regions of the genome where repeated sequences are found, like at the telomere sites. The involvement of the single-strand annealing process in repair of radiation-induced DSBs in mammalian cells has been proposed recently, since cells that were defective in the NHEJ repair pathway were found to show an enhanced rate of chromosome re-arrangements after exposure to ionising radiation (P. Jeggo, personal communication).

Disagreement has often been found in the results of experiments where residual DSBs were measured after the cells had been allowed long times to carry out DSB rejoining. Some data report good correlation between residual, un-repaired DSBs and cellular radiosensitivity (Blocher, 1988), other show lack of correlation (Badie *et al.*, 1995; Foray *et al.*, 1997b; Olive *et al.*, 1994), see also Jeggo (1998b), Olive (1998) and Foray *et al.* (1997a) for reviews.

The extent of DSBs that appear to have been repaired may not be representative of the toxicity of the DSBs. Despite the fact that an un-rejoined DSB is a potential threat to a cell, attempts to remove it may not necessarily imply restitution of the intact sequence, hence correct repair, since mis-rejoining of DSB ends may cause DNA sequence re-arrangements and deletions. There are in fact several cell lines that show normal DSB rejoining activity but are nevertheless highly radiosensitive (Fox, 1990), which may suggest that a considerable proportion of the initial DSBs are repaired incorrectly. It is in such kind of cell lines that extent of DSB rejoining does not correlate with radiosensitivity.

If DSBs are biologically relevant lesions, but neither total initial DSB yields nor fraction of un-rejoined DSBs correlate with high-order biological effects, it is likely that the subclass of DSB that is biologically relevant is the one that carries a higher potential of being involved in a mis-rejoining event. Another feature that has been explored in DSB repair is the rejoining kinetics, an argument that will be discussed more extensively later in the Thesis (chapter 5). With DSB rejoining kinetics one observes the rate of DSB rejoining during cell incubation after exposure to ionising radiation (or incubation of an *in vitro* system with cellular or bacterial extracts of repair enzymes). An overall slow rejoining rate may suggest more complexity of the substrate for the repair machinery, for example because more breaks have to be introduced during repair of some lesions (the involvement of the base-excision repair (BER) mechanism in the repair of a LMDS may introduce *de novo* DSBs) which is a competing process to DSB repair, appearing as an overall slow-down of the entire rejoining process. Early experimental work showed that DSBs induced by radiation of increasing LET repair more slowly (Coquerelle *et al.*, 1987; Fox and McNally, 1988). Along with the considerations made before about the local complexity of individual DSBs and radiation quality (§ 1.3.1), it would be reasonable to believe that since high-LET-induced DSBs are more complex, the operations that the enzymes need to carry out to repair them may take several steps, which may potentially be not synchronous and could take longer, as opposed to a simple DSB with 'blunt' ends that may be processed in a more straightforward manner. Nevertheless, not even total DSB rejoining kinetics have provided a good correlation with the RBE for high biological effects, as discussed by Olive (1998).

Recent experiments have begun to provide answers to another question, specifically if the vicinity of a DSB to another damaged site nearby, which may not necessarily contain a DSB itself, affects the repairability, or possibly the repair fidelity, of the first DSB. In other words, it may not only be the local complexity of a DSB that influences its correct repairability, but also proximity to other damaged sites, referred to as RMDS earlier (Prise *et al.*, 2001). Some experiments have pointed out that RMDSs at the chromatin fibre loop domain sites (§ 1.2) involving DSBs were responsible for the fraction of DSBs that repair with slower kinetics with the NHEJ mechanism, whereas single, sparse DSBs (Johnston *et al.*, 1998a,b) appear to be removed more easily. Other recent evidence supports the hypothesis that the NHEJ process is faithful when sparse DSBs are distributed in the cells, but if these are to be found 'close in space (Euclidean space) and at the same time', for example after the passage of a densely-ionising particle or in conditions of high dose-rate exposure to sparsely ionising radiation like X-rays, NHEJ processes are likely to fail to reconstitute the original sequence (Rothkamm *et al.*, 2001).

Since high-LET radiation is more effective than sparsely-ionising radiation in causing clustered damage, hence LMDS but also RMDS at the DNA level, it is tempting to hypothesise that proximity of DSB has an important role in determining high-order biological responses. The effect of local complexity vs regional association of DNA DSBs has been critically investigated in the present Thesis, as discussed experimentally in chapter 5 and theoretically in chapter 3.

1.5 DNA fragmentation studies

For several years, studies aiming at the quantification of DNA DSBs only employed techniques that measure total yields of DSBs. It was generally found that the total DSB yields show little variation with radiation quality (Belli *et al.*, 1994). When they showed variations, these could not explain the significant differences in the RBE values measured for other biological end-points (Löbrich *et al.*, 1993; Prise *et al.*, 1998). With the recent introduction of PFGE techniques, which allow measurements of total DSB yields *and* their spatial distribution, it was found that DSBs are often induced non-uniformly along the genome, and in excess of the predictions based on a purely uniform, random DNA breakage mechanism (Löbrich *et al.*, 1996; Newman *et al.*, 1997). These findings paved the way for a number of other studies where the hypothesis that regionally correlated DNA damage (RMDS) could explain the high RBEs for high-LET radiation could be tested, independently of local damage complexity (LMDS, see § 1.3). 'Fragmentation analysis' has provided a powerful method to test random breakage models of DSB induction (Belli *et al.*, 2001, 2002; Höglund *et al.*, 2000; Höglund and Stenerlöw, 2001;

Newman *et al.*, 1997; Pinto *et al.*, 2002) and to investigate DSB repair in greater detail than allowed with previous techniques and methods (Höglund and Stenerlöw, 2001; Pinto *et al.*, in prep.; Stenerlöw *et al.*, 1996; Stenerlow and Hoglund, 2002; Stenerlöw *et al.*, 1999, 2000). The achievements of this project were mostly based on the choice of fragmentation analysis as a tool to assess DNA DSBs induction and rejoining kinetics.

1.6 Modelling induction and rejoining of DSBs

Mathematical models provide ways to make hypotheses and quantitative predictions that can be tested against experimental data. In DNA damage studies, early analytical models described the fragmentation of long-chain polymers after induction of breaks (Charlesby, 1953; Contopoulou *et al.*, 1987; Cook and Mortimer, 1991; Litwin, 1969; Montroll and Simha, 1940). All these models were based on the simple assumption that breaks are introduced randomly and according to a uniform distribution, that is, they can occur anywhere in the polymer with equal probability. These 'random breakage' models have provided analytical functions that can be employed for regression analysis of experimental data of DNA fragmentation, in order to estimate the breakage frequencies. The recent experimental findings, which tend to conflict with the random, uniform breakage paradigm (see §1.5), have set the scene for a new class of DNA damage models, which aim at a more reliable characterisation of the mechanism of radiation-induced DNA breakage. The complexity introduced by abstracting DNA structures and radiation quality-dependent energy deposition patterns have forced the models to change from an analytical approach and move to computational techniques. The stochastic nature of radiation-induced DNA breakage can be well described by means of a Monte Carlo approach, where breakage is simulated in one cell at a time, for example, and several quantities may be evaluated, which can also be measured experimentally, for comparison. In these models, different hypotheses for chromatin structure and high-order structures are made (§ 1.2), which can be tested by experimental measurements based on fragmentation analysis (Friedland *et al.*, 1999, 1998; Holley and Chatterjee, 1996; Ponomarev *et al.*, 2000; Rydberg *et al.*, 1998; Sachs *et al.*, 1998, 1999a).

In this project, some of the most common analytical approaches that are freely available for the quantification of initial DNA breakage have been tested by applying them to the data obtained during the project itself. Deficiencies that were observed in some of these approaches (described in § 3.2.1 and § 3.2.4) lead to the design of new methods, whose simplicity lies in their semi-empirical nature. Quantitative methods were designed and implemented in order to describe experimental data that are obtained from PFGE experiments. Using the most up-to-date programming techniques available, the computer

programs developed allowed both qualitative and quantitative description of experimental DSB induction and rejoining data, together with low-dose predictions that can be tested with other experimental techniques (§ 4.5 and 5.4).

1.7 Scientific objectives of this project

The main aims of this project were:

1. To measure DSBs induced by X-rays and ^{238}Pu α-particles, with emphasis on the fragmentation patterns that result from the interaction between charged particle track-structure and chromatin geometry.

2. To measure rejoining kinetics of DSBs induced by radiation of different qualities, employing fragmentation analysis to assess the relative importance of LMDS *vs* RMDS to the repairability of the DSB.

3. To develop novel analytical and/or numerical methods of quantification of radiation-induced DSB yield and distribution that are not biased by the influence of background damage.

4. To develop novel analytical and/or numerical methods of quantification of DSB rejoining kinetics, which could also account for background damage, in order to investigate the relative relevance of radiation-induced RMDSs and LMDSs.

A noticeable aspect of this doctoral work is the feedback between mathematical modelling and experiment. Experimental and modelling work have been carried out in synchrony, with experimental results setting the grounds for the hypotheses of the mathematical/computer models, which were developed following both semi-empirical and mechanistic approaches.

Chapter 2

Experimental Methods

2.1 Introduction

The experimental methods used in this project are summarised in the following chapter. Briefly, normal human fibroblasts are exposed to varying doses of radiation of different linear energy transfers (LETs) to induce double-strand breaks (DSBs), under conditions where initial damage yields and distributions are measured, or repair is allowed to occur for pre-determined periods of time. DNA is purified from intact cells and separated according to size by pulsed field gel-electrophoresis (PFGE), currently the best method for analysing DNA fragmentation. Quantification of DNA damage is made possible by pre-labelling DNA with a radiolabelled precursor, and the results are analysed with a variety of analytical and numerical methods. This chapter describes the general experimental material and methods which were routinely used during the course of this project. These include cell culture conditions, irradiation sources and conditions, double-strand break rejoining, protocols for isolation of DNA, PFGE run and 'early' analysis of PFGE data. Analytical and numerical methods of analysis of DNA fragmentation are described separately in chapter 3.

2.2 Cell culture

All studies have been performed with primary human foreskin fibroblast, AG01522B, obtained from the National Institute of Ageing, Bethesda, Maryland, (USA). Normal human fibroblasts are very useful and commonly employed for studies similar to the present one, since fibroblasts are well renowned for their excellent resistance to high radiation doses if held in G_0 phase at confluence, as reviewed by Foray *et al.* (1997a) and also demonstrated recently by Rief and Löbrich (2002). One can then be assured that the

experimental observations that are carried out at high doses, due to the sensitivity constraints that the experimental techniques are setting, are not biased by disfunction of the cellular metabolism due to cell death, at least up to a few hours after the initial injury. AG01522B cells were stored in liquid nitrogen at passage 9 in 70% (w/v),[1] 20% (w/v) fœtal calf serum (FCS) and 10% (w/v) dimethyl sulphoxide (DMSO) in sterile filtered α-minimum essential medium (MEM) (all supplied by Sigma-Aldrich), before the beginning of the project.

For recovery of cell stocks from liquid nitrogen, cryogenic vials containing 1 ml of cell suspension are rapidly pre-warmed to 37°C in water-bath. The cell suspension is diluted to 1:4 in the cryogenic vial, then transferred to a sterile vial and further diluted to 1:2. Finally the suspension is seeded into four 25 cm^2 tissue culture flasks (T25) and incubated in humidified atmosphere (95% air and 5% CO_2) at 37°C. After four hours of incubation to allow for attachment of cells to the flasks, which is assessed using a phase-contrast microscope, the media is replaced by fresh α-MEM to minimise exposure to DMSO which is toxic at 37°C.

Fibroblasts are routinely grown in 25 cm^2 or 75 cm^2 tissue culture flasks (TCS or Corning) between passage 10 and 15 in α-MEM in humidified atmosphere of 95% air and 5% CO_2 at 37°C. The medium is supplemented with 20% (w/v) FCS, 100 μg ml^{-1} benzyl-penicillin and 100 μg ml^{-1} streptomycin (Gibco, Hemel Hempstead, UK), 200 mM L-glutamine (Gibco), 1$\times$non-essential aminoacids (Sigma) and a mixture of deoxynucleotides (2-deoxyadenosine, 2-deoxycitidine, thymidine, adenosine, cytidine, guanosine, uridine, all from Sigma). After passage 15, an extensive proportion of cells enters a senescence status and is not used further.

For cell detachment, a 0.25% (w/v) trypsin solution prepared in ethylene diamine tetra acid (EDTA) buffer is used. Cells are incubated with 2 ml (T25 flasks) or 6 ml (T75 flasks) of trypsin at room temperature for a maximum of 2 minutes to limit trypsin-induced damage to cell membranes, before the flasks are gently shaken to encourage cell detachment. A volume of fresh α-MEM equal to twice the volume that is used for trypsin is finally added to the flask for neutralisation. The cell suspension is then pelleted by centrifugation at 700g, 4°C for five minutes and then re-suspended at the desired concentration for re-seeding.

For experiments, cells are seeded in 60 mm diameter disposable sterile tissue culture plastic Petri dishes (Corning, TCS) for X-irradiation, or in custom-made 27 mm diameter glass-walled dishes consisting of a base of 3μm thick mylar film. The latter are sterilised for several days before each experiment by γ-irradiation using a ^{60}Co-γ source.

[1] Abbreviations used when expressing percentages in chemical recipes are v/v: volume/volume, w/v: weight/volume

2.2.1 DNA radioisotope labelling

Radiolabel is incorporated into DNA of growing cells by supplementing the culture medium with 0.05 μCi mmol^{-1} [2-^{14}C] thymidine (specific activity 52 mCi mmol^{-1}, Amersham International, Amersham, UK). Quantification of DNA DSBs and subsequent repair is based on counting β-decays of ^{14}C as described in § 2.7, using scintillation counting. To avoid competition between radiolabelled and non-radiolabelled thymidine that is normally supplemented in the culture medium (it is estimated for the labelling conditions specified above that for every 2 [2-^{14}C]thymidine molecules there are 5 'cold', non-labelled thymidines) a culture medium is prepared specifically for cells that are grown for experiments, which is identical to the medium employed for routine AG01522B culture (see § 2.2), with the exception that 'cold' thymidine is not added to the nucleotide mixture. It has been proved in this study that this correction in the protocol sensibly improves the relabelling efficiency, measured, on average, as 0.02 dpm per cell. Cells are grown in ^{14}C -labelled medium for seven to ten days to reach confluence, with 90-95% of the population synchronised in G_0-phase (flow-cytometry measurements kindly performed by Dr. Andrea Malcolmson), then the medium is replaced with fresh α-MEM for one day incubation before irradiation.

2.3 Irradiation

Before irradiation, α-MEM is replaced with fresh 20 mM HEPES-buffered α-MEM. Following irradiation, for experiments measuring initial DSBs induction, monolayers attached in Petri dishes are washed repeatedly with fresh phosphate-buffered saline solution (PBS) that has been kept on ice. The dishes are then kept on ice before further treatment on the same day, normally within a few hours (see § 2.5). For DSB rejoining experiments (see § 2.4) dishes are maintained on ice for a few minutes, before being prepared for post-irradiation incubation. Two radiation qualities have been employed in this project: 240 kVp X-rays as a low LET source and ^{238}Pu-α particles as high LET source.

2.3.1 240 kVp X-rays

240 kVp X-rays have been produced on using a commercial Pantak IV system that is fitted with a 0·25 mm Cu and a 0·5 mm Al filters. The system is equipped with several interchangeable jigs where tissue culture flasks or Petri dishes can be accommodated. The jig that has been employed regularly can accommodate up to three 60 mm diameter plastic Petri dishes. Photons reach the cells from above the dishes, after they have

traversed a volume of air and a volume of culture medium in which the cells are maintained during irradiation. Traversing water before reaching the cells is in fact required to allow electrons to build-up in number at the cell surface, or the dose distribution could be inhomogeneous.

X-rays are produced by the slowing down (*Bremsstrahlung*) of electrons that are first accelerated in an electric field. X-rays dosimetry had been performed before the beginning of this project using a Baldwin-Farmer instrument coupled to an ionisation chamber. Dose to be delivered to the samples is set on the Pantak IV control unit in form of 'irradiation divisions'. The correspondence between irradiation divisions and dose in Gy is given by the dosimetry in the form shown in eq. 2.1.

$$\frac{\text{divisions}}{\text{1 Gy}} = \sigma \times \frac{\text{P}}{\text{T}} \tag{2.1}$$

P and T in eq. 2.1 are the atmospheric pressure in mmHg and the temperature of the room in degrees Kelvin. σ is a dosimetric constant, having dimensions [K][mmHg]$^{-1}$[Gy]$^{-1}$. The value of σ that was provided at the beginning of the project was 228.7. For example, if the atmospheric pressure is measured as 758 mmHg and the room temperature is 298 K, then 581.7 irradiation divisions are required to deliver a dose of 1 Gy. These dosimetry settings have been employed for the entire project. Nevertheless, toward the end of the project, dosimetry measurements and calculations have been repeated by the laboratory staff and it has been estimated that the correct value for the dosimetric constant σ is 199. The ratio of the early to the newer, correct estimate for the dosimetric constant σ is 1.15, which means that every time a dose of 10 Gy was set, for example, 11.5 Gy were effectively delivered, for every experiment using X-irradiation in this project. This systematic dose-shift does not introduce any practical problem, except for the fact that comparisons between α-particles and X-ray data should be made on measurements normalised to the dose, wherever possible. The dose rate for X-rays is 0.027 Gy s^{-1} equivalent to 1.62 Gy min^{-1}, so that 10 Gy are delivered in little more than 6 minutes, while 100 Gy are delivered in approximately one hour, during which cells are held on Petri dishes, covered by 4 ml of pre-cold HEPES-buffered MEM, cooled by laying the irradiator's jig on ice.

2.3.2 ^{238}Pu α-particles

$^{238}_{94}$Pu is an unstable nucleus that decays to $^{234}_{92}$U by ejecting an α-particle of predominant energy 5.59 MeV, accompanied by minor emission of γ photons. The half life of ^{238}Pu is 87 years. The α particle irradiator, built in the Gray Cancer Institute on a design

based on that of an irradiator described by Thacker *et al.* (1982), consists of a 1090 MBq ^{238}Pu source which is housed in an aluminium cylinder (figure 2.1). The irradiator itself is filled with helium gas and is equipped with a mylar exit window, from which α-particles can leave the irradiator to reach the samples to be exposed, which are normally held in an aluminium jig that sits externally, on top of the irradiator. In this configuration, the dishes containing attached cells, covered by 5 ml of HEPES-buffered MEM, are held horizontally and the α-particles reach the cells from underneath the dishes, after they have traversed a volume of helium gas, mylar, air, mylar.

^{238}Pu is brushed on a thin metal disk and the energy of the α-particles reaching the cells can be varied by changing the distance between the Pu source and the irradiator's mylar window, by means of a graduated thumb-wheel. α-particles in fact deposit part of their initial energy to the molecules of the gas that fills the cylinder, which become ionised (see § 1.1). The larger the distance of the source from the mylar window, the higher the energy lost by the α-particles. The range of α-particles in air is very limited, due to the relatively high stopping power of air (see eq. 1.3). Helium is preferred because of its small atomic number which minimises the α-particles energy loss, circulated through the irradiator at a rate of a few cc min^{-1} to avoid accumulation of ionised He atoms in the cylinder, which could change the energy deposition characteristics of α-particles. Before reaching the cells, α-particles must also pass through the thin irradiator's mylar window, a few millimetres of air, and the mylar film that constitutes the base of the custom-made glass-walled dishes. The source in the irradiator is always set to the same position for all the α-particle irradiations in this project, so that the energy of the α-particles when reaching the cells is 3·5 MeV and the volume-averaged LET is calculated at 110 keV μm^{-1} (Folkard *et al.*, 1989). The dose rate is 0.88 Gy s^{-1}, equivalent to 52.8 Gy min^{-1}, so that 10 Gy are delivered in approximately 11 seconds, while 100 Gy are delivered in slightly less than 2 minutes. Unlike the X-ray irradiation conditions, the glass-walled dishes are not cooled on ice during exposure to radiation. In order to prevent DSB re-joining activity due to temperature increases during irradiation, the dishes are pre-cooled on ice for 30 minutes before irradiation, and the volume of HEPES-buffered MEM in the dishes is increased from 1.5 ml, which is normally used for culturing cells in these glass-walled dishes, to about 5 ml. Once irradiation is completed, the dishes are immediately transferred to ice. For measurements of initial DSBs induction by radiation, cells that have been irradiated are treated as described in § 2.5. For rejoining experiments, cells are transferred to an incubator for different times as described in the following section.

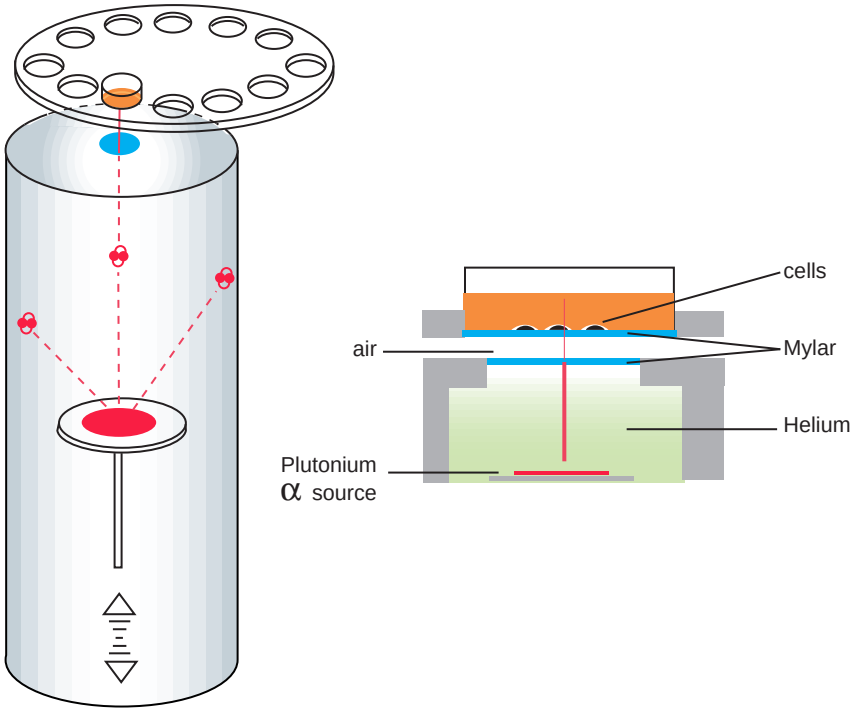

Figure 2.1: The ^{238}Pu α-particle irradiator.

2.4 DSB rejoining

Cells monolayers are allowed to repair radiation-induced DSBs in Petri dishes, by incubating them at 37°C in humidified atmosphere of 95% air and 5% CO_2. For post-irradiation incubation, HEPES-buffered medium that has been used during irradiation is replaced by fresh α-MEM that has been pre-warmed to 37°C in a water-bath.

Early experiments in this project have been carried out with cells attempting to repair DSBs while embedded in agarose (see § 2.5) immediately after irradiation. It has been found from measurements on unirradiated control cells that incubation of cells embedded in agarose promotes extensive DNA fragmentation which can be appreciated after approximately 24 hours of incubation, which is believed to be due to the stress condition to which the cells are exposed. The same result was also found by another group (Stenerlöw, personal communication) and was the subject of several studies by Kysela (1994), together with a targeted experiment by Whitaker and McMillan (1992b). Using a relatively low-sensitive method based on quantification of the fraction of activity released (FAR) below a certain DNA fragment length, described in § 2.7, Kysela observed that the uncontrolled DNA fragmentation measured in unirradiated cells incubated when embedded in agarose was cell line-dependent (see also Cedervall and McMillan, 2002), and limited to a maximum of 10% FAR, which was only observed after overnight incubation. During this project, other quantities have been adopted along with the FAR to measure DSB-induced DNA fragmentation. Using relatively more sensitive methods, it has been estimated that the damage induced in cells incubated embedded in agarose can be surprisingly extensive, as can be observed from the fragmentation patterns in figure 4.5.

All the results reported in this Thesis refer to experiments in which cells have been allowed to repair as monolayers attached in Petri dishes. Cells have been embedded in agarose only after both irradiation and rejoining are completed. For each experiment, DSB rejoining is allowed for several times in incubator, ranging from 10 minutes to 24 or 48 hours. After the longest period in incubation of 48 hours to repair the damage initially induced by radiation, measurements indicate that DNA fragmentation takes place in competition with DSB rejoining, which is believed to be related to a form of cell death, probably not apoptosis since fibroblasts seldom trigger this form of organised cell death. The experimental measurements performed on the cells that have been incubated for 48 hours post-irradiation have normally not been included in regression analysis, unless specified.

At the end of the required time of incubation for each sample, the dishes are taken out of the incubator at fixed times and α-MEM is replaced by fresh PBS that has been

kept on ice, to minimise the activity of repair enzymes. After several washes in fresh PBS, the samples are incubated on ice before further treatment within the same day, as mentioned before.

2.5 DNA extraction and preparation of PFGE samples

In order to perform any measurement of DSB yields and distribution in the nuclear DNA, this first needs to be isolated from the rest of the cell content. The general protocol for DNA isolation has been adapted from Schwartz and Cantor (1984) and Newman *et al.* (1997) with some minor modifications. Firstly, cells are detached by treatment for 10 minutes with 0.25% (w/v) trypsin/EDTA on ice to minimise unwanted repair enzymes activity. Dishes are then gently shaken to allow cell detachment, then fresh α-MEM that has been kept on ice is added to neutralise trypsin. Cell suspensions are pelleted by centrifugation at 4°C , 700 g-force for five minutes and re-suspended in ice-cold PBS, at concentrations in the order of 10^6-10^7 cells ml^{-1}. The cells suspensions are then kept on ice.

For practical purposes and to preserve the integrity of DNA, which could be damaged by shear forces during the manipulation of the samples, cells are embedded in agarose plugs before DNA is purified and loaded in agarose gels for electrophoresis. The concentrated cell suspensions, obtained as described above, are mixed with low melting point agarose (Sigma, gelling point approximately 18°C), in either tris acetic acid (TAE) or tris borate acid (TBE) buffers (see specification for each PFGE protocol in tables 2.1, 2.2) kept at 37°C in a water-bath. Eppendorf tubes containing the concentrated cell suspensions are removed from ice and heated to 37°C in the water-bath for approximately 10 seconds, then a volume in the order of a few μl is sampled and transferred to an equal volume of the low melting point agarose solution prepared earlier and maintained at 37°C , using a Gilson type pipette. The suspension is mixed using the pipette for a maximum of 20 seconds at 37°C in water-bath. The suspension is then immediately pipetted into purpose-made plastic casting moulds (BioRad), pre-cooled in a refridgerator at 4°C , which allow the agarose to set in a box-shape, commonly referred to as plug, having the same size of the agarose gel wells in which the plugs will be loaded for electrophoresis. Each casting mold has 10 separate compartments which are clearly marked to distinguish the samples, to be immediately stored at 4°C in a refrigerator to let the agarose set. About 90 seconds elapse from the time when the Eppendorf tubes are removed from ice and exposed to 37°C , to the moment when the casting moulds containing the cell/agarose suspesion are refridgerated. During this time, repair enzymes are potentially activated and unwanted DNA repair could occur. This sets a theoreti-

cal lower limit of 90 seconds for the minimum repair time that can be controlled during an experiment, although in practise the minimum repair time allowed was 10 minutes. For experiments aiming at quantification of initial DSB yields and distribution, initial fragmentation is intended inclusive of a maximum of 90 seconds DSB repair throughout this Thesis. The plastic tips used with the Gilson pipettes are always pre-cut to avoid shear forces that could introduce unwanted additional DSBs.

The number of cells to be embedded in each plug is chosen on the basis of fragment size detection limits requirements. In order to characterise the mechanisms of DSB induction and rejoining, as well as to test different models for DNA organisation in the nucleus, it is desirable to carry out measurements of DNA fragmentation over the widest possible molecular weight range, ideally covering the size of the entire Genome. PFGE has significantly improved the sensitivity of conventional constant field gel-electrophoresis (CFGE) approaches, by broadening the molecular weight region where DNA fragments can be detected. Nevertheless, the sensitivity of PFGE assays is limited by several factors:

1. specific DNA labelling efficiency,
2. radiation dose,
3. methods of analysis of PFGE data.

The first two factors deal with the design of the experiment, whereas the third factor is more related to the way data are analysed after the laboratory procedures. As for the labelling efficiency, in this project a ^{14}C -based approach has been adopted (§ 2.2.1).

[2-^{14}C]-thymidine, which is incorporated uniformly in the strands of DNA of dividing cells, undergoes β decay with a half life of 5700 years. The ejected electron is detected by means of scintillation counting. Larger DNA fragments contain more thymidine and hence more disintegrating ^{14}C atoms, per unit time, hence their signal is larger. Detection of smaller and smaller fragments is most difficult and it would require, in principle:

- the largest possible DNA labelling efficiency that can be achieved, without affecting cell viability. More radioactive nuclei could be employed, which may even be incorporated in more than one nucleotide. In practise, one cannot increase the DNA uptake of radioactive material indefinitely, since at some point the endogenous radioactivity would be too high and the radiation dose would be toxic to the cells. A different approach consists of labelling DNA after the electrophoresis run. Labelling could be achieved by 'tagging' the ends of DNA fragments using a very radioactive nucleus, like ^{32}P. This procedure has proved unsuccessful since the ends of DSBs that are produced by radiation are chemically highly variable and

often not recognised by the enzymes that are employed in the experiment to tag the fragments with ^{32}P (Newman et al, unpublished observations, and Tobi and McMillan 1997). Also, DNA can be labelled after the electrophoresis run using a fluorophore such as Ethidium Bromide, Propidium Iodide or SYBR Green, which binds specifically to DNA and that can fluoresce by excitation with UV or even visible light. These techniques are gradually becoming more popular than ^{14}C DNA labelling, supported by recent advances in computer imaging techniques (Sutherland *et al.*, 1996).

- a larger number of cells, so that the total number of fragments available in the gel of any size is increased, thus bringing the signal from smaller and smaller fragments into the detectable range. An example may help to clarify this concept and provide an idea of the sensitivity of the technique used in this project. The measured average activity incorporated into each cell is approximately 0.02 disintegrations per minute (dpm). With a total diploid genome content of 6.4 Gbp, this means that every bp in a single cell provides as little as $\approx 3 \times 10^{-12}$ dpm. In theory, it would then take at least 3×10^{12} cells to be able to detect the only one dpm that small DNA stretches 1 bp long would produce. Nevertheless, for an amount of DNA mass to be detected by scintillation counting, this must be above the noise level, so that one needs to count at least 20-30 dpm, not just one. Single cell studies are not possible using this technique since, in order to reach a level of 30 dpm one needs the total DNA content of at least 1500 cells. In practise, if one needs to spread this signal over a wide molecular weight region resolved by PFGE, if one wants to carry out fragmentation analysis, it takes many more than 1500 cells. As described in § 2.7, scintillation counting is carried out in several gel segments, in order to quantify the mass of DNA in many molecular weight size ranges. Therefore enough signal must be present in each molecular weight range of interest. But fragmentation of DNA cannot be controlled in a way to compress all the DNA of a cell in a molecular weight window: fragments of virtually every size are generated by the DSBs. Many more cells are hence needed, and several breaks have to be introduced in each cell in order to produce an extensive fragmentation, so that small DNA fragments become also detectable. A combination of high dose and large number of cells is needed. That a high dose is required to extend the experimental observations to smaller and smaller DNA fragments appears clear from the results in chapters 4 and 5, which are obtained only when doses as high as 50–100 Gy are employed.

Methods used for data analysis may also have an impact on the overall sensitivity

of the assay. It has been demonstrated in a number of studies that the use of some quantities that are related to the number of DSBs may lead to inaccurate estimates of DSB yields, distribution, rejoining kinetics parameters, and ultimately RBE values (see for example Prise *et al.*, 2001; Stenerlow and Hoglund, 2002; Stenerlöw *et al.*, 2000).

For all the experiments in this project, $10^5 - 10^6$ cells were embedded in each plug, which corresponded to $10^3 - 5 \times 10^4$ dpm per plug. As reported in chapters 4 and 5, this approximately translates to a sensitive molecular weight region in the fragment size range [30 kbp-10 Mbp], although this is only achieved at the cost of exposing the samples to a dose that is often much higher than what normally used in other radiobiological investigations. After agarose plugs containing intact cells have solidified in the casting moulds, plugs are processed for DNA purification, using a lysis solution that contains proteinases and detergents. These eliminate virtually everything but nuclear DNA, which is left free of all histones (DNA organisation is described in § 1.2) in the form of a 'naked' double helix. The lysis solution is prepared using 1% N-laurylsarcosyne (Sigma), 0.5 mg ml^{-1} proteinase K (Invitrogen) in 0.5 M EDTA. For DNA extraction, the agarose plugs are held in 1.5 ml plastic Eppendorf centrifugation tubes with a lysis solution volume of 1 ml. These are first stored on ice for one hour, during which the lysis solution permeates through the outer cell membrane and the nuclear membrane, called equilibration, but during which it is almost completely enzymatically ineffective, due to the low temperature. Then the Eppendorf tubes are transferred to a water-bath that has been pre-heated to 50°C, where they remain for 24 hours. Only when the temperature is raised, the lysis solution is activated and enzymes begin DNA purification. If cells were immediately immersed in the lysis solution at 50°C, this would begin degrading the outer cell membrane, and cell sensors located inside the cell's membrane would trigger a suicide-like response, which includes endogenous DNAase activity, so that the DNA would become extensively fragmented, increasing the background damage already present. After 24 hours of incubation at 50°C, plugs containing purified DNA are transferred to 24 wells plates (Corning), where they are washed repeatedly with 1×tris-EDTA (TE), to remove traces of lysis solution. To help the lysis solution diffuse out of the plugs, the 24 wells plate is kept on a shaker and the TE buffer is replaced at least four or five times. The complete washing procedure takes about three hours and ends when there are no visible traces of contaminating lysis buffer in the wells.

Although de-proteinated DNA in plugs has been previously shown to be stable (Kysela, 1994; Schwartz and Cantor, 1984), in this project DNA has always been pre-labelled before lysis of the membranes and DNA purification with [2-^{14}C]thymidine, at a high cell density per plug, equivalent to a maximum of 30,000-50,000 dpm per plug. At the level of radionuclide incorporation used here, it is important to minimise the total

experimental time so that the β decays produced do not lead to significant strand breakage. Therefore, plugs are stored in a refrigerator at 4°C for the minimum time necessary before the gel electrophoresis run, which either starts immediately after the plugs are washed or within 24 hours from the completion of the washing procedure.

2.6 Pulsed-field gel electrophoresis

Electrophoresis technique allows separation of electrically-charged molecules of varying size in a semi-solid viscous support by application of an electric field. For DNA, the support is normally polyacrylamide, for detection of oligonucleotides, or agarose, for larger fragments, as in this project. DNA is normally negatively charged due to the presence of phosphate groups (PO_4^-) in the helix backbone. The total charge of a DNA molecule is linearly proportional to the size of the molecule itself, often expressed in base pairs (bp), kbp or Mbp, where size and molecular weight are used as synonyms. From the dynamics of a body subject to a constant force (for this case that exerted by the electric field $\vec{E}$ on the charged DNA fragment) and the constant breaking force of a viscous medium, it can be determined that the speed v of the DNA fragments in the gels is proportional to the charge Q (in case of the DNA proportional to the size) of the fragments but inversely proportional to a factor β which is function of the fragments three-dimensional geometry and the medium viscosity.

$$\mathrm{v} = \frac{\mathrm{QE}}{\beta} \tag{2.2}$$

For a given electrophoresis time, the smaller fragments which have a smaller Q/β ratio migrate further in the gels since, despite their minor electric charge, they are subject to minor resistance in the viscous agarose matrix, compared to larger DNA fragments. Nevertheless, DNA filaments undergo reptation under the action of the electric field. In practise, the Q/β ratio remains approximately constant for DNA fragments larger than 50 kbp, so that the fragments cannot be separated according to size.

PFGE allows separation of fragments larger than 50 kbp (currently the limit is about 10 Mbp) by explicitly avoiding reptation of long DNA molecules. By pulsing the electric field in two directions, the fragments maintain a coiled form except for short times when the fragments undergo partial reptation and penetrate through the pores of the agarose matrix (Chu *et al.*, 1986; Deutsch, 1988; Schwartz and Koval, 1989) to maintain a forward vector. This is schematically shown in figure 2.2. Several factors influence the mobility of DNA fragments and the overall PFGE performance:

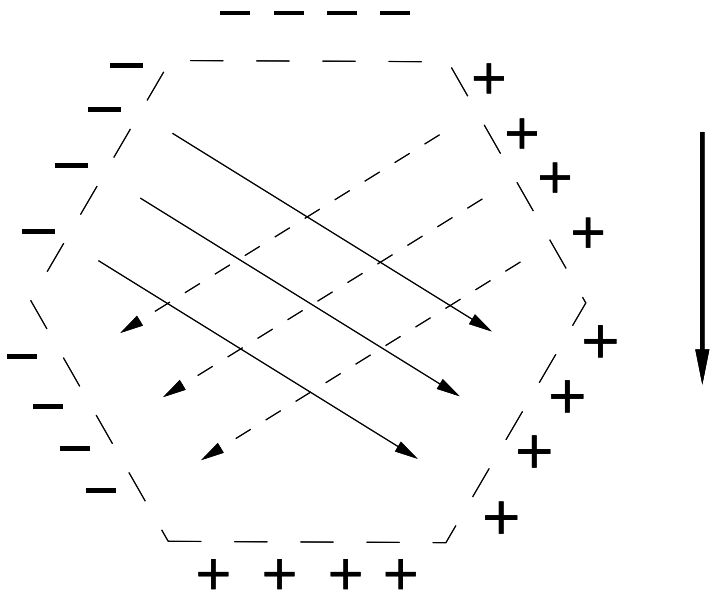

Figure 2.2: The principle underlying PFGE: by pulsing an electric field in two directions, reptation of DNA fragments is avoided. First, the electric field is stretching the DNA fragments in one direction. After one pulse switch period, τ, the direction is changed. The effective direction of migration is shown to the right of the diagram.

1. electric field strength $\left|\vec{E}\right|$,
2. electric field pulsing angle φ,
3. electric field pulsing frequency ν, or pulse switch period τ=1/ν
4. ionic strength of the buffer,
5. electrophoresis buffer temperature,
6. gel agarose concentration,
7. total electrophoresis time

DNA molecules are stretched along the instantaneous field direction, until the direction of the electric field is changed according to the pulse angle, after one pulse period. The re-orientation time of fragments is related to their size, with larger fragments taking a longer time to re-orientate than smaller ones. Fragments whose size is such that the time they take to orientate to the new electric field direction is close to or larger than the pulse switch period τ will spend most of the time re-orientating to the continuously changing electric field direction, rather than proceeding further in the gel (Schwartz and Cantor, 1984). Therefore, only fragments whose size is such that their re-orientation time is smaller than τ shall proceed in the gel. In practise, the value of τ is ramped between

a minimum and a maximum value that can be set on the PFGE run controller, so that ultimately a very wide size range of DNA fragments is separated in the gel according to their size. The ionic strength of the running buffer and the buffer temperature, which is maintained stable via circulation through a chiller unit, influence the effective charge of the DNA molecules. The agarose gel concentration also affects the mobility of the DNA fragments, as the higher the agarose concentration the larger the viscosity (high β in eq. 2.2).

Three PFGE protocols have been employed in this project. For electrophoresis, gels are prepared using 250 ml solutions of 0.8% (w/v) or 1.0% (w/v) concentration of rapid agarose (Sigma) and TAE or TBE buffer (see tables 2.1, and 2.2 for PFGE protocols specifications). Gels are cast in purpose-built moulds, equipped with combs for the formation of 30 wells for agarose plugs insertion. Agarose plugs are gently pushed into the gel wells and sealed with low melting point agarose, prepared as previously described. Along with the samples that have been irradiated, and in some cases incubated for repair, samples of control unirradiated cells are also loaded onto the gels. Control samples are processed exactly the same as irradiated samples to evaluate and quantitate the background damage that is present in the cells or as part of the technique. Treatment of unirradiated controls in PFGE played a major role in this project as discussed in detail in the following chapters. Molecular weight markers are also run alongside the unirradiated controls and the irradiated samples for calibration of the gels (see for example figure 4.1). The molecular weight markers are purified DNA fragments of known molecular weight, either embedded in agarose plugs that are cut to the size of the gel wells, or in suspension, in which case they are embedded in agarose plugs before being loaded.

PFGE PROTOCOL I	
block 1, 44 hours	
electric field strength $\lvert\vec{E}\rvert$	2 V cm^{-1}
electric field pulsing angle φ	106°
pulse switch period τ	20–40 min
block 2, 4 hours	
$\lvert\vec{E}\rvert$	6 V cm^{-1}
φ	120°
τ	7–114 s
ionic strength of the buffer	1×TAE
running buffer temperature	13.5°C
gel rapid agarose	0.8% (w/v) in 1×TAE
total electrophoresis time	48 hours
Markers separation region	5.7 Mbp–12 kbp

Table 2.1: PFGE protocol I. Adapted from the protocol of Elia and Nichols (1993).

	PFGE PROTOCOL II	PFGE PROTOCOL III
electric field strength $\left\|\vec{E}\right\|$	6 V cm^{-1}	
electric field pulsing angle φ	120°	
pulse switch period τ	0.1–17.3 s	50–60 s
ionic strength of the buffer	1×TBE	1×TAE
running buffer temperature	13.5°C	
gel rapid agarose	1.0% (w/v) in 1×TBE	1.0% (w/v) in 1×TAE
total electrophoresis time	7.5 hours	18 hours
Markers separation region	285–12 kbp	825–12 kbp

Table 2.2: PFGE protocol II (Newman *et al.*, 1997) and III (Löbrich *et al.*, 1996).

It is assumed that the mobility of each molecular weight marker in the gel is identical to the mobility of DNA fragments in the samples having the same size of the markers. It should be noted, however, that the technique cannot fully differentiate between DNA fragments having different conformations which may influence migration, for example linear fragments which have been circularised. In general, several markers are adopted, in combinations that vary according to the molecular weight region that is being explored with one of the three PFGE protocols used in this Thesis (see table 2.3).

DNA Molecular weight markers	
S. Pombe	3·5, 4·6, 5·7 Mbp
S. Cerevisiae	225, 285, . . . 450 . . . 825 kbp . . . 1·02, 1·6, 2·2 Mbp
λ ladder	48·5, 97, 147·5, 198·kbp, ...
8–48 kbp standard	8, 9, 10, 11, 12. . . 48 kbp
1 kbp standard	512, 1024, 2048 bp,. . . 8, 9, 10, 11, 12 kbp

Table 2.3: Size of the linear DNA double stranded fragments that are employed as molecular-weight markers in PFGE gels.

2.7 Analysis of PFGE gels

After electrophoresis, gels are stained with 0.5 μg ml^{-1} ethidium bromide prepared in a fresh buffer for approximately one hour, and then de-stained in fresh buffer on a shaking platform. A photograph is taken (see figure 4.1) for record keeping with a digital camera (Cohu) on a UV trans-illuminator, and the image acquired is stored as a 16 bit TIFF file.

Gels are then cut into sections according to sample type (unirradiated controls, 10 Gy, 50 Gy, repair for one hour, etc) vertically, along the direction of migration, and across the lanes, according to the position of the molecular weight markers, thus defining molecular weight regions in which measurements of DNA content are to be carried out. Each

individual gel section is put in a plastic vial for scintillation counting (Beckman). Before scintillation fluid is added to each vial, the gel sections are melted so to decrease the degree of sample quenching, 200 μl of 1 M HCl are added to each vial, and the agarose sections are melted for two hours in an oven at 95°C . Once cooled, the agarose remains in liquid form since the presence of HCl inhibits re-polymerisation. 10 ml of scintillation fluid (Beckman Ready Safe) are added to the vials and scintillation counting is performed using a Beckman LS 6500 instrument. Some agarose gel sections from lanes that have not been loaded with ^{14}C -labelled DNA are counted to monitor background activities. These sections have similar sizes to the other sections and are treated as mentioned above. The activities expressed in counts per minute (cpm) averaged over several non-radioactive samples, per experiment, are then used as the cpm background, to be automatically subtracted by the scintillation counter from the cpm of the radioactive samples.

For quantification of DSBs with all the methods of analysis employed in this project (chapter 3), the dpm signal measured in each gel segment is first transformed into fraction of total activity detected, F_i. This is obtained by dividing the number of dpm counted in a given section by the total number of dpm in the gel lane to which the section belongs, as in eq. 2.3

$$\mathrm{F_i} = \frac{\mathrm{dpm(section_i)}}{\sum_j \mathrm{dpm(section_j)}} \tag{2.3}$$

Assuming that [2-^{14}C]-thymidine is uniformly incorporated throughout the DNA, F_i also measures of the fraction of DNA mass present in section i, characterised by an average molecular weight $\overline{\mathrm{M}}_i = M$ and a molecular weight range $\Delta\mathrm{M}_i$. It can be easily demonstrated that F_i has the following approximate relationship with M and $\Delta\mathrm{M}_i$:

$$\mathrm{F_i} \simeq \frac{n\left(\overline{M}_i\right) \times \overline{M}_i \times \Delta M_i}{H} \tag{2.4}$$

where H in eq. 2.4 is the size of the diploid human genome (in this project this is known to be 6.4 Gbp, International Human Genome Sequencing Consortium, 2001) and $\mathrm{n}(\overline{\mathrm{M}_i})$ is the frequency of DNA fragments, normalised to the width of the interval $\Delta\mathrm{M}_i$. The goodness of the approximation in eq. 2.4 depends on the validity of the inequality $\Delta M_i/\overline{M}_i \ll 1$ (calculations not shown) which translates to the need to cut as many thin gel sections as possible. On the other hand, thin gel sections contain less amounts of DNA, which limits detection as described above, so a compromise is required.

The experimental frequency n of fragments is a very useful quantity that can be used to make comparisons with continuous frequency distributions. This can be related to F_i using eq. 2.4, as shown in eq. 2.5a.

The number of DNA fragments $\mathcal{N}$ that are contained in the section i is a more in-

tuitive quantity which can also be estimated using eq. 2.4, as shown in eq. 2.5b, where $\mathcal{N}\left(\overline{M}_i\right) = n\left(\overline{M}_i\right) \times \Delta M_i$.

$$n_i \equiv n\left(\overline{M}_i\right) \simeq \frac{H\, F_i}{\overline{M}_i\, \Delta M_i} \tag{2.5a}$$

$$\mathcal{N}_i \equiv \mathcal{N}\left(\overline{M}_i\right) \simeq \frac{H\, F_i}{\overline{M}_i} \tag{2.5b}$$

The advantage of $\mathcal{N}_i$ over n_i is that by summing all the $\mathcal{N}_i$ values available one has a *direct quantification* of DSBs in the experimental region available (see for example Höglund *et al.*, 2000; Höglund and Stenerlöw, 2001; Pinto *et al.*, 2002). This very simple method of DSB quantification is described in § 3.2.2.1. The disadvantage of $\mathcal{N}_i$ is that its value strongly depends on the width of the gel section, since the larger the section the greater the number of fragments. To make data more consistent one should try to combine gel sections together, so to have comparable numbers of DSBs in different sections (as shown in Stenerlow and Hoglund, 2002).

Other useful quantities may be defined for analysis of PFGE data. Q values are obtained from integration of the fragment size mass distribution over varying windows, delimited by an upper and a lower limit. (Cedervall and Kallman, 1994). Similarly, the FAR is defined as the fraction of total DNA mass below a certain threshold size k, which may either be the exclusion size of the gel, defined as the molecular weight size above which fragments remained trapped in the wells, or the size of one of the markers that are run with the other samples. If $\mathrm{M}_{\max}(j)$ is the largest fragment in section j, the FAR_k may be written as the sum of all the F_j that contain fragments not larger than k, as specified in eq. 2.6.

$$\mathrm{FAR}_k = \sum_{j:\mathrm{M}_{\max}(j)<k} F_j \tag{2.6}$$

Chapter 3

DNA Fragmentation and DSB rejoining kinetics models

3.1 Introduction

Mathematical models have provided invaluable tools in this project for qualitative and quantitative analysis of the experimental data that have been obtained as part of the project. In this chapter, some of the existing models of DNA fragmentation and DSB rejoining kinetics are briefly presented. It is shown how new models have been developed in this project from a knowledge of the limitations of previously utilised models available in the literature. The design of the new models will be described in detail along with their development with the aid of diagrams, while their application to experimental data can be found in chapters 4 and 5.

3.2 Analytical models

Analytical models are very useful since they provide ready-to-use mathematical functions that are analytical at least in the experimental data range where regression needs to be carried out. These functions may be used for regression analysis by virtually anyone who has access to a statistics computer package supporting least squares fitting routines. In this project, several analytical functions have been employed for non-linear regression analysis using χ^2 minimisation with the Levemberg-Marquardt algorithm, part of the Origin data analysis software package (Microcal, Northampton, MA, USA). In non-linear regressions, the functions employed are non-linear in the parameters to be estimated. For example, if a is the parameter to be estimated and x is the independent variable, in both $y = x^a$ and $y = a^2x$, y is non-linearly related to a. Conversely,

$y = ax + bx^2$ is linear in both a and b. Models of induction of DSBs are described separately from DSB rejoining kinetics models in this chapter.

3.2.1 Induction of DSBs

When breaks are introduced in a long segment of DNA, fragments of the segment each of smaller size result, leading to a fragmentation pattern. Such a pattern reflects the way the breaks were introduced in the original long segment, and how many were introduced. The greater the number of the breaks, the smaller the average size of the fragments that are generated. If the breaks are spatially associated, by being preferentially localised close to each other, then one would expect to find many short fragments, accompanied by fewer larger ones, as shown in figure 3.1. If breaks are introduced randomly and independently of each other, then one would expect to find a different fragmentation pattern. In summary, the number of fragments can directly tell us the number of breaks introduced, while the size distribution of the fragments can give an indication of how the same number of breaks were distributed. If one could detect all the fragments generated by the induced breaks, without any limitation on the size of these fragments, then understanding the breakage mechanism and counting the number of breaks would be simple. However, human chromosomes are very large (50-250 Mbp) and the experimental techniques that are currently available do not allow detection of intact chromosomes or some of the smaller fragments that are generated when breaks are introduced. One may either measure intact chromosomes and some large fragments, down to several Mbp, as in cytogenetics, or focus on smaller fragments but neglecting the intact chromosomes. We shall now focus on the second case, since the region of detection of PFGE is from a few kbp up to a maximum of 10 Mbp (§ 2.6), which is only a small fraction of the size of the intact human chromosomes. Therefore experimental observations are made in a restricted size region and used to extrapolate to other size regions, in order to make an estimate of the complete fragmentation pattern.

Early experiments employing PFGE to measure DNA fragmentation also faced problems with quantifying the number of DSBs that caused the fragmentation of chromosomal DNA. DSB yields were initially expressed indirectly as fraction of DNA released from the gel wells, versus dose (Ager and Dewey, 1990; Iliakis, 1991; Stamato and Denko, 1990). Since this quantity is not linearly related to the number of DSB (Blöcher, 1990) a mathematical model is needed to estimate breakage yields from experimental measurements of DNA fragmentation.

Models of DNA breakage that assume random location of breaks are the most common by far. Random may be generally considered as a synonym of stochastic. Never-

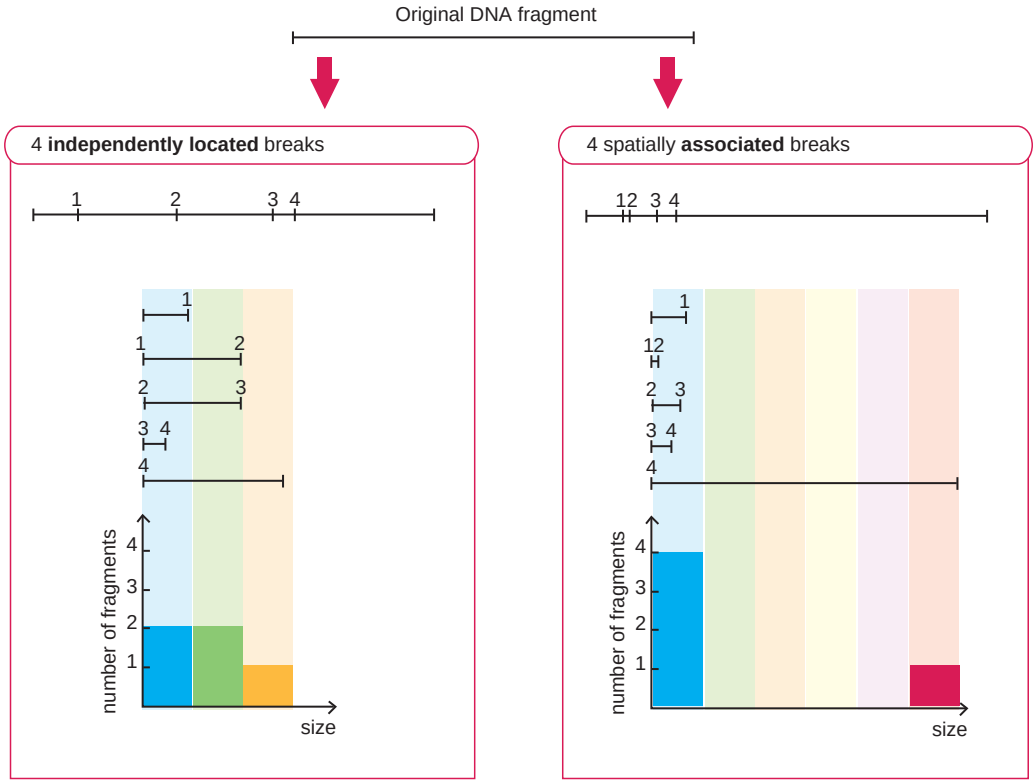

Figure 3.1: Random vs spatially clustered breakage mechanisms. In both panels, four breaks were introduced in the original intact segment shown above, leading to the formation of five smaller fragments. In the **left panel**, the breaks are distributed randomly on the intact segment, independently of each other, producing fragments of various sizes which are grouped in a frequency histogram. **Right panel**: if the same four breaks are located in spatial association, not independently of each other, smaller fragments are produced compared to the picture shown on the left, and no intermediate sizes are detected before a much larger fragment is found.

theless, in DNA fragmentation, randomness has commonly, although improperly, been referred to a phenomenon that is more than just stochastic. In fact, random breakage of DNA is often thought of a breakage mechanism such that individual breaks are located in a chromosome, or in the entire genome, according to a uniform probability distribution, randomly. This is equivalent to saying that breaks have the same probability of being located anywhere in the DNA, independently of each other. A random but different process may be one that locates breaks according to a normal distribution centred around a breakage hot-spot, which may be regarded as an example of a process where breaks are clustered. This is discussed separately in § 3.3.1.1. From the random breakage model, a number of analytical functions have been independently derived that can describe very general experimental data of DNA sedimentation, a leading technique before filter elution and electrophoresis were introduced (Charlesby, 1953; Litwin, 1969; Montroll and Simha, 1940). When electrophoresis techniques became available, the random breakage model was invoked again to derive analytical functions that could be used to describe typical electrophoresis data. These recent applications of the random breakage model are briefly presented in the following sections. It is worth stressing that the methods of analysis that follow may differ in the way they are applied to analysis of data, but the breakage mechanism that is assumed is always the same, namely breaks are induced randomly and independently.

3.2.1.1 Integral approaches: the *Q* function and FAR analysis

In electrophoresis experiments, the irradiated DNA is distributed along several gel lanes along the direction in which the electric field was applied (or the effective direction in pulsed field gel-electrophoresis, § 2.6). With the aid of molecular-weight markers, one can define regions of the gels in which the mass of DNA within each section can be quantified. Both the *Q* function method and the FAR method provide an estimate of the number of DSBs that should have been randomly and uniformly distributed in the genome to cause a DNA fragmentation that resembles that observed experimentally. From the observation of the DNA fragmentation pattern in a limited molecular weight region, these methods attempt to extrapolate to the total DSB yield, assuming random breakage occurred.

The *Q*-function method was proposed by Cedervall and Kallman (1994) and subsequently revised (Cedervall and Lange, 1998; Cedervall and Radivoyevitch, 1996; Cedervall *et al.*, 1995). Quoting from Cedervall and Kallman (1994), the *Q*-function method is mathematically equivalent to an integration of the DNA fragment size distribution as described by Contopoulou *et al.* (1987), which is presented in § 3.2.2.2 and provides the same results, although via an independent derivation, of the FAR method by Blöcher

(1990).

PFGE techniques are intrinsically more sensitive to the presence of large fragments rather than to small ones. This is simply because the signal measured with PFGE is proportional to the mass of DNA, and one very large DNA fragment weighs more than many much smaller fragments. The *Q*-function and the FAR method are examples of integral methods, because they require that the experimental DNA mass distribution is integrated over a relatively wide molecular weight range, compared to other methods that are described in the following sections. Since the signal from fragments of different sizes is accumulated in the *Q*-value or in the FAR-value, the major disadvantage of this fragment size-dependent approach is that one cannot easily detect any fine structure in the fragmentation patterns. For example, fragmentation patterns caused by radiation of different LETs due to single charged-particle tracks traversal of chromatin structures, would not be easily detected when integral approaches are employed (Prise *et al.*, 2001).

In its most recent version, the *Q*-function method is employed to analyse DNA fragmentation data in a large molecular weight window which is selected at the tail of the DNA mass distribution, consisting of smaller fragments, rather than focusing on the fragments of larger molecular weight (Cedervall and Lange, 1998) which make the analysis insensitive. An interesting feature of the *Q*-function method is that is does not require a correction of experimental data for the DNA damage that is estimated from measurements on the unirradiated control samples. In his PhD thesis, Cedervall mentions the presence of unwanted background damage in PFGE and describes potential ways to correct data for it. Due to the experimental procedures, additional DSBs are introduced independently of radiation (see chapter 2). These additional DSBs cause a variation in the fragment size distribution that is produced by radiation, thus biasing the experimental datasets. Corrections made directly on the experimental data for the effect of the background damage are error prone and do not seem to eliminate the problem (§ 3.2.2.3). Rather than correcting the data for the background damage, the *Q*-function method assumes that the effect of the background damage to DNA is like a dose-shift, which is based on the hypothesis that radiation and background damage distribute DSBs according to the same mechanism. The *Q*-value is related to the radiation-induced yield of breaks per Mbp r, the size of the marker below which the mass is accumulated k, the average chromosome size S and the number of breaks per Mbp due to background damage, r_b as detailed in eq. 3.1.

$$Q = \frac{1}{A}\left\{1 - \exp[-k(r - r_b)]\left[1 + k(r - r_b)\left(1 - \frac{k}{S}\right)\right]\right\} \tag{3.1}$$

The influence of the experimental background damage on all the measurements car-

ried out on the irradiated samples has had a central role in the present project. As discussed in § 3.2.2.3 and in § 6.1, treatment of the PFGE experimental background damage is a complex problem which is not satisfactorily solved neither by subtraction, or by considering the mechanism of its induction equivalent to that of radiation. For this reason, the *Q*-function method has not been adopted during this project. For integral DSB quantification methods, the more widely diffused FAR-method has been preferred to the *Q*-function method.

The FAR analysis method was proposed by Blöcher (1990) and has been widely adopted for the analysis of PFGE data, particularly in DSB rejoining measurements (as in Kysela, 1994; Kysela *et al.*, 1993b) and as a popular predictive assay for radiotherapy outcome (see for example Kiltie *et al.*, 1997, 1999). The popularity of the FAR assay lies in its simplicity and in the assumption that it can be used as a marker for DSB yields and provide biologically relevant answers from analysis of data that are relevant for both radiotherapy and several end-points in radiation biology. The FAR is the amount of DNA mass smaller than a fixed threshold size as a fraction of the total DNA content per cell, defined in eq. 2.6. The threshold is normally the gel exclusion size, *i.e.* that of the largest fragment leaving the loading wells, determined by the electrophoresis protocol used, but it may also be the size of any molecular weight marker loaded in the gel wells. The analytical function that describes the relationship between FAR, number of breaks and molecular weight is, as defined in Blöcher (1990):

$$F_{<k} = 1 - \exp\left(-\frac{rk}{n}\right) \cdot \left[1 + \frac{rk}{n}\left(1 - \frac{k}{n}\right)\right] \tag{3.2}$$

Based on random breakage, eq. 3.2 predicts the fraction of DNA mass $F_{<k}$ of DNA below a threshold size k (the FAR with k threshold) due to fragmentation of a polymer, in this case a chromosome, of initial size n after the induction of r uniformly distributed breaks. Eq. 3.2 describes the dependency of FAR on the number of radiation-induced breaks only. Since experimental background damage is also present, the data need to be corrected for the background damage before FAR analysis with eq. 3.2, in order to eliminate the influence of the DSBs that are not introduced by radiation. The type of correction that has been carried out on FAR data during this project, and similarly in many other published works, is simple subtraction of FAR values measured in unirradiated controls from the corresponding FAR values measured in the irradiated (and rejoined if prescribed) samples. Other groups have employed a correction for the background damage with the FAR method similar to that of the *Q*-function method described earlier (Belli *et al.*, 2001, 2002). A correction based on a subtraction of FAR values assumes additivity, but the FAR is non-linearly related to the number of breaks (Blöcher, 1990), so

that subtraction of FAR values does not imply subtraction of number of breaks (see also Pinto *et al.*, 2000). As for the *Q*-function method, the FAR value at a given dose, hence a given r value in eq. 3.2, is weighted by the presence of the largest DNA fragments, which can be excluded by lowering the exclusion size k, to consider only the production of smaller fragments.

In early PFGE experiments, FAR was the method of choice for quantification of initially induced DSBs and subsequent repair. Experiments showed that one could measure radiation-induced fragmentation of DNA of mammalian cells due to DSBs with as little as 2.5 Gy (Stamato and Denko, 1990). When expressed as FAR, the experimental background damage caused extraction of a few % of the total DNA mass at maximum (Kysela, 1994). More recently, the apparent low levels of background damage, measured by FAR methods, have been found to conceal a very high level of DSBs (Belli *et al.*, 2002; Höglund *et al.*, 2000; Pinto *et al.*, 2000, 2002) when fragmentation analysis is performed (see § 3.2.2 and following). There has been increasing experimental evidence questioning the validity of FAR approaches. Above all, there was a lack of correlation between RBE values measured for the initial yields of DSBs and biological effects such as reproductive cell death or mutation for different radiation qualities (Heilmann *et al.*, 1995; Prise *et al.*, 1998, 2001). To overcome this problem, studies employing PFGE techniques have moved toward a new type of analysis: detailed observation of the fragmentation distributions after induction and repair of DNA DSBs (Höglund *et al.*, 2000; Höglund and Stenerlöw, 2001; Löbrich *et al.*, 1996; Newman *et al.*, 1997, 2000; Pinto *et al.*, 2002; Stenerlow and Hoglund, 2002; Stenerlöw *et al.*, 1999) to include DSBs that FAR with Mbp-sized thresholds fails to detect. The following paragraphs deal with the analysis of DNA fragmentation, using the fragmentation analysis procedure.

3.2.2 Fragmentation analysis

Due to the sensitivity restrictions of current PFGE techniques, one cannot measure the number of fragments of any size with an infinite resolution. Whether videofluorometry or radioactive labelling techniques are employed for detection of DNA fragments, the best that can be done is to accumulate the mass signal of fragments in a molecular weight range; the higher the sensitivity, the narrower the molecular weight window that can be observed. For integral approaches, this window represents the major part of the molecular weight range that is resolved in the gels after electrophoresis. For FAR, the total mass below a specified threshold is integrated. Alternatively, one can measure the fraction of DNA in several, narrow windows, which added together cover the same range as for the FAR method, but providing multiple determinations of DNA

mass fractions in several contiguous molecular weight regions.

With the aid of the set of equations 2.5, one can relate the fraction F_i of DNA mass, measured in each of the gel section i, identified by the positions of the calibration markers (see § 2.7), to the frequency n_i or number $\mathcal{N}_i$ of DNA fragments. While the number of DNA fragments strongly depends on the width of gel sections, the frequency is normalised to the width of the molecular weight range, showing less dependency on how the gel was cut. In fact, both quantities depend on several properties of the gel regions, namely how much DNA mass is present, the average size and the molecular weight range (eq. 2.5). If the same gel was analysed with many different sectioning arrangements, as can be done by virtual sectioning using quantitative imaging techniques (as in Sutherland *et al.*, 1996), the frequency and number of breaks values would vary, although the ultimate result of the fragmentation analysis should remain approximately the same. Nevertheless, if the assay allowed detection of DNA fragments reflecting breakage of fine chromatin structure, this would be best observed for specific gel sectioning schemes that isolate fragments whose size is close to the expected size (figure 3.10). The measured frequency distribution $n(M)$ can be analysed with theoretical frequency distributions derived from random breakage assumptions, as described in § 3.2.2.2 and § 3.2.2.3, or with numerical models, which can extend from random breakage to DSB clustering concepts (§ 3.2.2.3). Alternatively, the number of fragments in each section may be used for a more straightforward type of analysis, called direct quantification.

3.2.2.1 Direct quantification

Eq. 2.5b allows conversion of the measured fraction of DNA mass F_i to the numbers of fragments in a given gel section, $\mathcal{N}_i$. It should be remembered that, starting from one long fragment, the total number of smaller fragments created after breakage is equal to the number of breaks plus one (compare to figure 3.1). This simple relationship nevertheless does not apply to total number of breaks induced per cell and number of fragments whose size is contained in a specified molecular weight interval. The correspondence in this case can be understood if the DNA fragmentation pattern is observed globally, rather than locally (see also § 3.2.2.3. Cumulative addition of the $\mathcal{N}_i$ values for all the sections available in the gel allows the total number of fragments present in the region covered by the markers in the PFGE run to be quantified. Since fragmentation of the human chromosomes may lead to DNA fragments of size larger than the largest molecular weight markers resolved in the gel, the fragmentation pattern that is observed experimentally is incomplete, hence, direct conversion *per se* under-estimates the total number of DSBs per cell.

To extrapolate to the total DSB yields, some assumptions are needed. For example,

it is convenient to assume that the number of breaks present above the largest DNA marker, for example the PFGE protocol-specific exclusion size ε, is negligible compared to that measured in the gel lanes. In experiments measuring the initial induction of DSBs, this is referred to as 'high-dose approximation' (Höglund *et al.*, 2000; Stenerlöw *et al.*, 2000) because at high doses very few large fragments, large enough to remain trapped in the wells, are left. For DSB repair experiments, after long incubation times, double stranded fragments will have been joined to each other to the extent that a significant proportion of them may be above the largest marker, and the high-dose approximation could be inappropriate.

For extrapolation from the (under-)estimates of the direct quantification to the total number of breaks per cell, an alternative approach is proposed in this project. This approach makes the assumption that random (and uniform) breakage holds, using the broken stick method, eq. 3.4. A functional relationship is provided between the number of fragments measured in any molecular weight region [M_1, M_2] and the total number of breaks μ that should be present in the entire genome if random breakage holds. This is obtained from integration of eq. 3.4 in [M_1, M_2], which results in the approximate relationship shown in eq. 3.3 (see also Pinto *et al.*, 2002).

$$\mathcal{N}_{\mathrm{DSB}}\left(\mu, H, M_1, M_2\right) = \sum_{[M_1, M_2]} \mathcal{N}_i \simeq (\mu+1)\cdot\left[\exp\left(-\frac{\mu M_1}{H}\right) - \exp\left(-\frac{\mu M_2}{H}\right)\right] \quad (3.3)$$

In eq. 3.3, H is the size of the human diploid genome. Given the measurement for $\mathcal{N}_{\mathrm{DSB}}$ in the interval [M_1, M_2], the solution for μ may be obtained via numerical inversion of eq. 3.3. It is also convenient to plot the correspondence DSB(μ), as in figure 3.2 to solve graphically for μ.

3.2.2.2 Broken stick, Distribution shape

An important step toward a more correct quantification of radiation-induced DSBs was taken by Contopoulou *et al.* (1987), later adapted for data analysis from assays employing gene-probes (Cook and Mortimer, 1991). The broken stick method describes the frequency n of fragments of size x when μ breaks are introduced randomly and uniformly in a polymer of initial size H, which in this context may represent the average size of a human chromosome (139 Mbp), or the size of the complete diploid human genome, (6.4 Gbp International Human Genome Sequencing Consortium, 2001).

$$n\left(x, \mu, H\right) = \frac{\mu}{H}\left[2 + \mu\left(1 - \frac{x}{H}\right)\right]\exp\left(-\frac{\mu x}{H}\right) \quad (3.4)$$

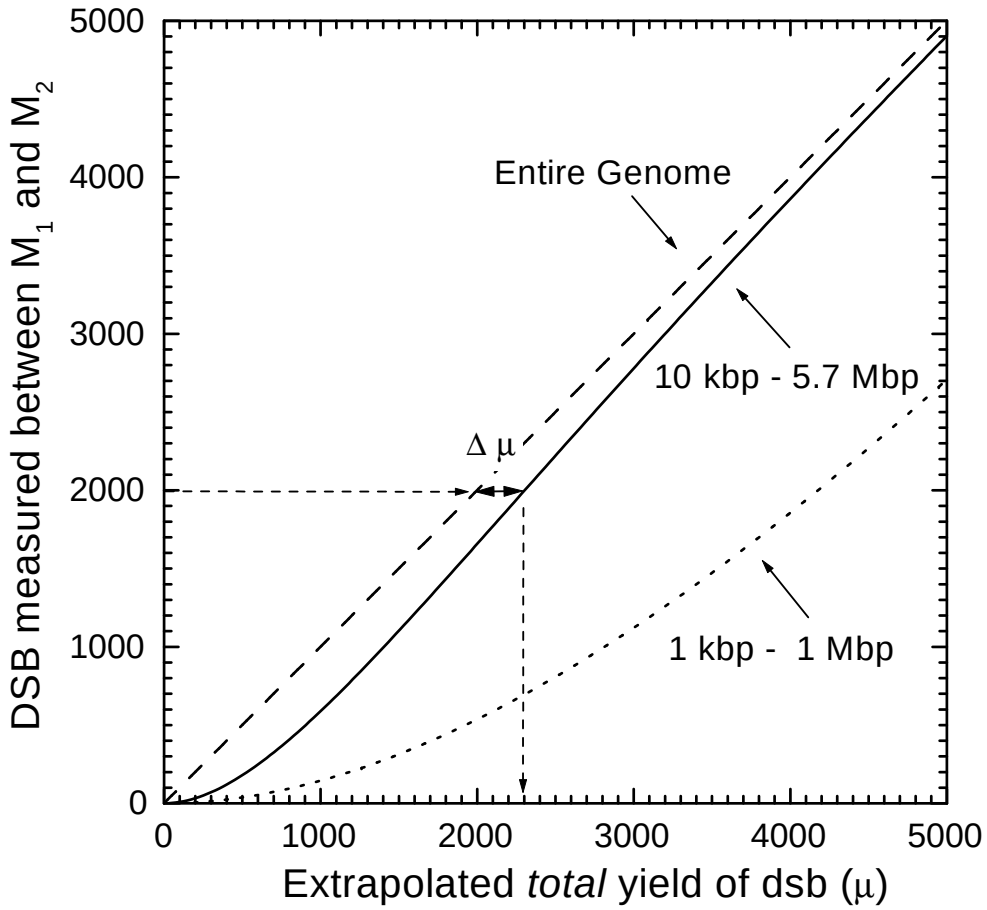

Figure 3.2: When DSBs are measured using the 'direct quantification' method, in a limited molecular-weight region, the broken stick method can be used to extrapolate to total DSB yield per cell. Using the solid curve relative to [10 kbp-5.7 Mbp], if 2000 DSBs are measured, 2300 are predicted to be distributed in the entire genome. The underestimation $\Delta\mu$ is then approximately 15%. When 2000 DSBs are measured in a more restricted window [1 kbp-1 Mbp] (dotted curve), the error made because of underestimation becomes over 100%.

For data analysis with the broken stick method in this project, experimental values of frequency of DNA fragments have been plotted vs molecular weight at a fixed dose, and eq. 3.4 has been used for non-linear regression analysis for estimation of μ. Alternatively, experimental data can be plotted vs dose, for a fixed molecular weight region. In this second case, eq. 3.4 may be used again for non-linear regression analysis, but μ is replaced by $r \times D$, where D is the dose and r is the estimated breakage yield per unit dose. This second type of analysis with the broken stick method is illustrated in the work by Newman *et al.* (1997). Correction of experimental data for the effect of the additional unwanted DSBs introduced during the experimental procedures has been carried out by simply subtracting the frequency values measured in the unirradiated control samples from the corresponding values measured in the irradiated samples, for each molecular weight region available in the gels. As for FAR approaches, this correction is an oversimplification (Pinto *et al.*, 2000, 2002). A high-dose approximation of the broken stick method was derived several years earlier by Lehmann and Ormerod (1970). This non-integral approach was found to be particularly sensitive to the shape of the DNA fragmentation pattern by Cedervall *et al.* (1995), who called it the 'distribution shape' method. Lehmann and Ormerod applied random breakage concepts to describe the same relationship $n(x)$, reported in eq. 3.5.

$$n(x) \simeq \frac{\mu^2}{H} \exp\left(-\frac{\mu x}{H}\right) \tag{3.5}$$

It can be easily seen that eq. 3.5 is a good approximation of eq. 3.4 when μ becomes large and $x \ll H$. The first condition is satisfied when large numbers of breaks are present, for example at high doses for initial DNA fragmentation, which at approximately 30 DSB per Gy per cell means a few Gy, but not after long times of DSB rejoining, when most the initial breaks have been removed. The condition $x \ll H$ is normally met in PFGE experiments when human DNA is separated, since the experimental region analysed contains fragments that are much smaller than the size of the intact chromosomes/genome. This would not be met in smaller genomes such as Yeast systems, where the intact chromosomes are completely separated in the gels.

The analogy between the broken stick and the distribution shape methods may be also extended to other methods described earlier. Since the broken stick, the distribution shape, the *Q*-function and the FAR methods are all based on the random breakage model, the functions that they provide should be easily convertible into each other, as schematically shown in figure 3.3.

For analysis of experimental data with the distribution shape method, data are plotted as frequency of DNA fragments, obtained from mass fraction determinations as shown

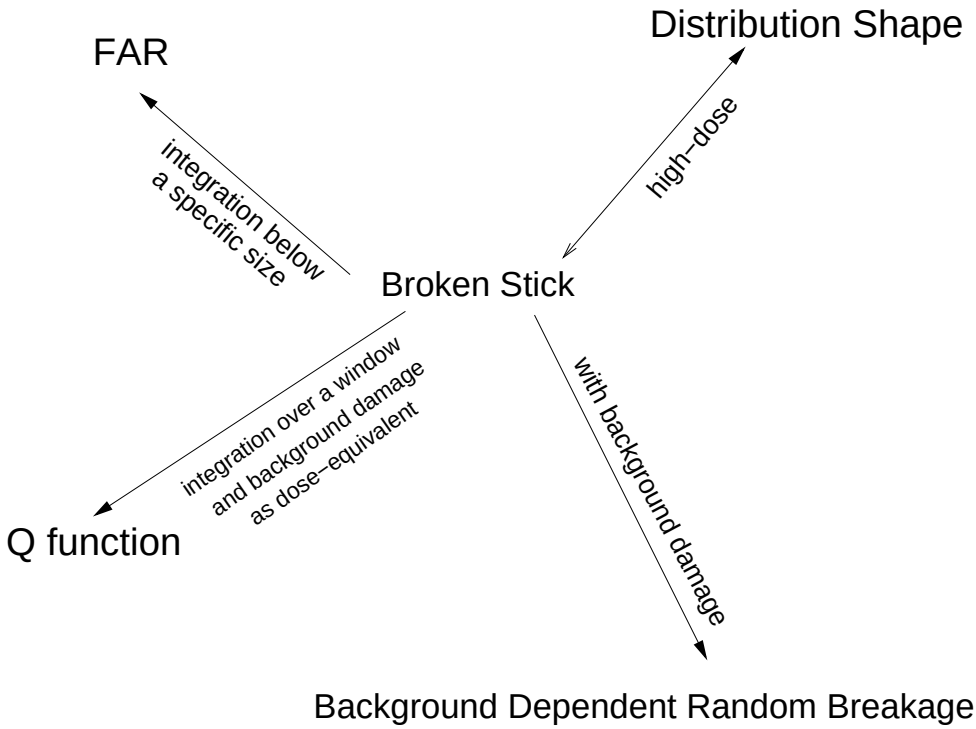

Figure 3.3: The relation between the many implementations of the random breakage model. The broken stick method was put in the centre of the diagram for illustration, since any other method could have been used instead.

in eq. 2.5a, on a logarithmic scale versus the corresponding molecular weight on a linear scale. A linear regression using formula 3.5 allows estimation of the DSB yield per cell from the slope of the best linear fit. For this reason the distribution shape method has often been called the distribution shape–slope analysis. The method was applied by Newman *et al.* (1997) and by Cedervall *et al.* (1995), who made a critique to the slope analysis method and its sensitivity).

3.2.2.3 Background-dependent random breakage method and analysis of control DSBs in PFGE experiments

With the exception of the *Q*-function method, all the random breakage implementations described so far refer to radiation-induced DSBs only, and require some sort of correction of the experimental data for the unwanted DSBs that are induced during the experimental procedures. For the *Q*-function method this statement does not apply, since this method treats the background breaks as if they were caused by an additional radiation dose, see also § 3.2.1.1 and Pinto *et al.* (2000). The background correction normally consists of subtraction, either of FAR values or of mass fraction values, for each gel section. The latter, corrected mass fractions are then transformed into number

of fragments $\mathcal{N}_i$ in a given gel segment with eq. 2.5b or frequencies of DNA fragments n_i normalised to the width of the gel section, with eq. 2.5a. Subtracting experimental determinations of mass fractions, to correct for the additional DSBs that are induced during the experimental procedures, assumes a linear dependence of the DNA mass fraction in a molecular weight window on the total number of breaks. This is clearly not the case for FAR (Blöcher, 1990), nor is the case for any method of fragmentation analysis (as also illustrated in Pinto *et al.*, 2000, and discussed ahead). The problem underlying corrective procedures based on subtractions of mass values is that the de-polymerisation of a molecule, like the DNA of a chromosome, cannot be described in full by observing the fragmentation patterns locally, that is, in a restricted molecular weight region delimited by any two markers in the gel. As more breaks are introduced in a chromosome, larger DNA fragments are reduced in size, so that the measured mass shifts the length distribution of the fragments toward smaller molecular weight values. Figure 3.4 shows the fragmentation pattern that results from the super-imposition of the two sets of breaks that generated the fragmentation patterns shown in figure 3.1. The two distributions of breaks from figure 3.1 have been re-drawn in figure 3.4 for clarity and the symbols changed. The one on the top left is caused by random breakage, the other one is caused by a clustered breakage process, although for what follows the two mechanisms could be the same. Let us assume that the 4 clustered breaks are introduced first: these produce the fragmentation pattern that was drawn in figure 3.1 (bottom right) where a fragment much larger than all the others was found. Following, 4 breaks are randomly distributed by radiation, on top of the breaks already distributed, altogether producing the fragmentation pattern sketched in the bottom cartoon of figure 3.4. It can be seen that while the total number of breaks is additive, and likewise the total number of fragments, subtracting the fragmentation pattern obtained after 4 clustered breaks from the pattern obtained from all breaks superimposed does not lead to the pattern due to the 4 randomly distributed breaks. In fact, after such subtraction, one even has a negative value for the frequency histograms at large fragment sizes, since one count in the very large fragments region is subtracted from zero counts. The mass of the longest fragment that was shown in the frequency histogram in figure 3.1, right panel, has been distributed among smaller fragments when 4 extra breaks were induced. There is now way one can get that mass back by means of a section-by-section subtraction of frequency histograms, which results in under-estimation of large fragments. This can also be seen using the broken stick method. Figure 3.5 is an additional example that allows to visualise the distortion that is caused to the fragmentation patterns when size-dependent subtractions are carried out. The corrected profile obtained from subtraction of the control from the irradiated profiles is distorted in a way that small fragments are overestimated and larger fragments are un-

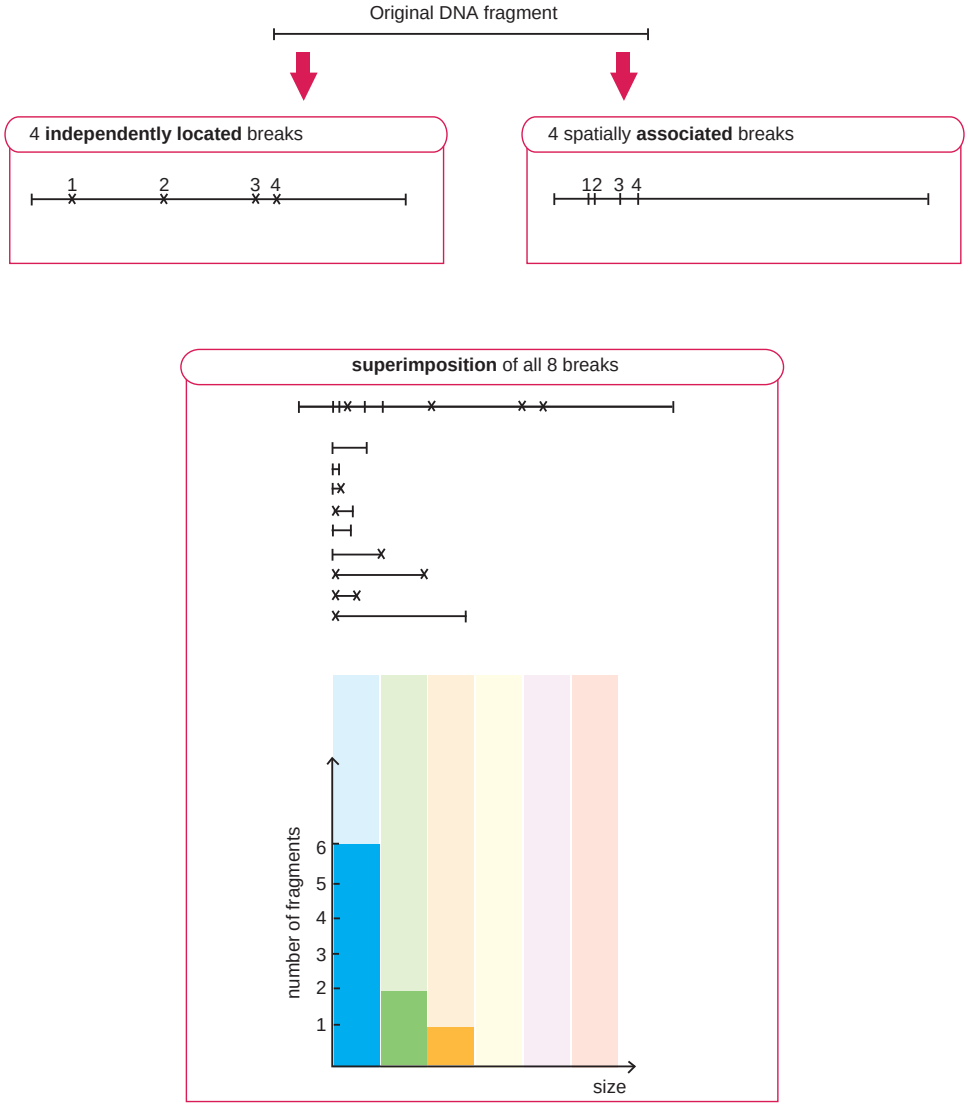

Figure 3.4: The fragmentation pattern that is produced from the super-imposition of all the breaks shown in figure 3.1.

derestimated, compared to a correct fragmentation profile (see right panel in figure 3.5). This fragment size-dependent distortion leads to a chain reaction of erroneous observations. It shall be seen in § 5.3.1 how the experimental inference can be biased by the subtractive procedures. In the *Q*-function method (§ 3.2.1.1), experimental data are not corrected for the presence of the background breaks before non-linear regression analysis. Nevertheless, the *Q*-function method is an integral approach which suffers from low sensitivity for smaller DNA fragments, and more importantly makes the assumption that radiation and background DSBs are introduced according to the same mechanism. One aim of this project has been the development of a new analytical approach, based on fragmentation analysis and not requiring any correction to be applied to the experimental determinations for the background damage observed. This background-dependent random breakage (BDRB) approach has also paved the way for the development of numerical approaches in this project and that are described in § 3.3 and following. This following section deals with the derivation of the background-dependent random breakage (BDRB) analytical approach.

The rationale behind the BDRB approach is the evidence that unwanted DSBs introduced during the PFGE experimental procedures are non-uniformly distributed in the genome, and should be treated separately from radiation-induced DSBs. In fact, the shape of the fragmentation profiles observed in the unirradiated control samples in PFGE experiments suggests that these breaks are spatially associated (like in figure 3.1, right panel) rather than being distributed independently (Belli *et al.*, 2001, 2002; Erixon and Cedervall, 1995; Höglund *et al.*, 2000; Pinto *et al.*, 2000, 2002).[1] The DNA fragmentation patterns observed in the unirradiated control samples in PFGE experiments show a lack of Mbp-sized fragments with correlated excess of smaller fragments of a few hundreds of kbp and below, compared to the fragmentation profiles that are theoretically predicted from pure random breakage. The mechanism that leads to the production of these fragments is unknown. The fragmentation patterns in the controls may be empirically described with a power-law where the exponent is a real number (Pinto *et al.*, 2000, 2002). Power-laws normally indicate phenomena with strong correlations. A power-law does not normally add much information as to the fundamental underlying mechanisms, and has appeared in radiation biology several times, for example in the context of late effects of radiation on normal tissues (reviewed in Alper, 1990). In the specific case of background DSBs observed in the unirradiated controls, it seems that these are prefer-

[1] Deviations from random breakage in the unirradiated control patterns were in fact not described by Erixon and Cedervall on the basis of their experimental determinations of DNA mass fractions. Data from Erixon and Cedervall (1995) were converted to frequency n_i of DSB using eq.2.5a and information on the molecular weight markers found in the original paper, in order to estimate deviations from uniform random breakage in the unirradiated controls (not shown here).

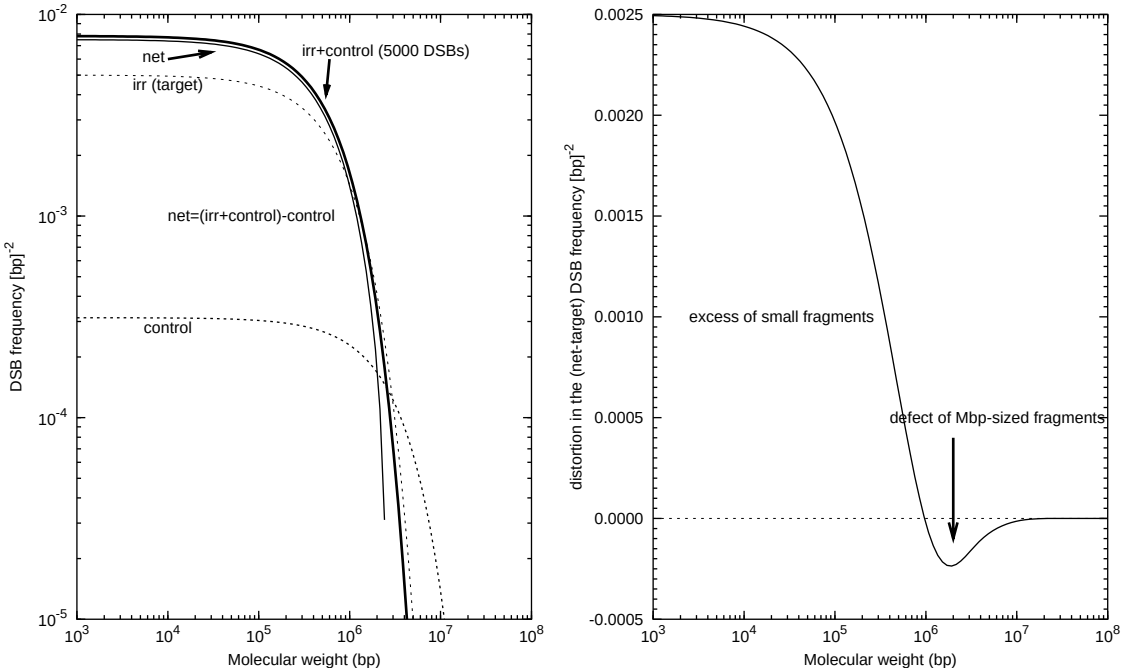

Figure 3.5: The distortion produced in a DNA fragment-size distribution that is obtained from subtraction of two other distributions. **Left panel**: DSB frequency distributions from eq. 3.4 are plotted for several numbers of total DSBs per cell. In the example shown, a first fragment size distribution relates to 5000 DSBs induced randomly 'irr+control', but it is assumed that only 4000 are due to radiation (random breakage) the remaining 1000 being induced during the manipulation of the samples, also based on a random distribution . When only these 1000 DSB are allocated one has the pattern referred to as 'control'. Subtraction of the background signal from the total signal produces a corrected profile (net) which is significantly different from the true fragmentation pattern caused by 4000 DSBs only (target). **Right panel**: The difference between the corrected and the target profiles (net-target) are displayed in the same molecular weight region, but on a linear y axis to show the positive *and* negative distortions that arise from the subtraction procedure. Absence of distortion would give the straight line for $y = 0$ shown on the plot. It is clearly shown how the subtraction leads to a fragmentation pattern with excess (> 0) of fragments smaller than approximately 1 Mbp, accompanied by a defect (<0) of larger Mbp-sized fragments. What is shown here is a simplification, since one cannot describe the background profile as due to DSBs induced randomly (see text). The background breaks are in fact preferentially induced in close spatial association, leading to fragmentation patterns that are very different from those produced via random breakage (figure 3.7).

entially accompanied, rather than uniformly along chromosomes. It is unlikely that the number of DSBs measured in the unirradiated controls is representative of a DNA fragmentation *in vivo*. Nevertheless, studies employing γ-H2AX hybridization (Paull *et al.*, 2000) which is believed to occur at the sites of DSB specifically, show a background level of endogenous DSBs in unirradiated cells (Kai Rothkamm, personal communication).

Before developing a relatively complex mathematical approach for the description of radiation-induced DSBs on top of background DSBs, it is worth considering whether the fragmentation patterns observed in the unirradiated controls are a consequence of a pre-existing background damage, or systematic errors are biasing the experimental observations. Stenerlöw *et al.* (2000) suggested that background breaks may represent the effect of amplification of a signal in a molecular weight region where the measurements are dominated by noise. This possibility is considered in the discussion chapter (§ 6.1).

Mathematical details of the derivation of the BDRB model are reported in Pinto *et al.* (2000) and in Pinto *et al.* (2002) with some improvements. The principles behind the BDRB analytical approach are mentioned here. The fragmentation of a long chain polymer described by the broken stick method by means of eq. 3.4 is the starting point for the derivation of the BDRB method. In the broken stick approach, it is assumed that the only DSBs present are those induced by radiation, and that without radiation one has a mono-dispersed fragment size distribution that is centred, for example, on the average size of an intact chromosome.

Rather then having a mono-dispersed fragment-size distribution before irradiation, in the BDRB approach it is assumed that radiation adds DSBs on top of a poly-dispersed distribution, which is the one that is measured in the unirradiated controls of each experiment. Being based on the broken stick method, the BDRB method is implicitly based on the assumption that radiation induced DSBs are distributed randomly and uniformly. It is also assumed that DSBs are introduced during the sample manipulation procedures independently of radiation-induced DSBs, hence it is not relevant which mechanism acts first. It is likely that the background breaks are introduced after radiation in the experiments, since samples are further manipulated for electrophoresis (see the experimental procedures for DNA extraction in § 2.5). It is nevertheless mathematically convenient to model a situation where the radiation-induced breaks are induced on top of a distribution of DNA fragments that has already been fragmented due to the sample manipulation procedures. The background-dependent random breakage approach may then be viewed as a broken stick approach applied to a continuous distribution of intact fragments of varying size. In this context, intact is meant only from the perspective of radiation action, since the fragments have otherwise already been broken down from intact chromosomes during the induction of background damage. The size of a DNA fragment can only take

discrete values, although for very large fragments as in this study it is convenient to treat the size as a continuous variable. Nevertheless, the number of monomers contained in the DNA fragments detected in PFGE is so large that discreteness can conveniently be replaced by continuity.

The continuous distribution which is going to be fragmented further by radiation is that measured in the unirradiated controls. Firstly, one needs a good analytical description of the fragment-size distribution caused by the background-induced DSBs. Since the mechanism by which the DSBs are introduced is not known, a semi-empirical approach is used. As mentioned before, experimental data suggest a power-law behaviour, at least in the region where measurements are available. On double logarithmic scales, the power-law is shown as a straight line, whose slope is the exponent. A linear regression on the background frequency of DNA fragments data provides an estimate of the parameters A and B of the linear model $y = A + Bx$. In the first derivation of the BDRB model (Pinto *et al.*, 2000) it has been assumed that a power law can also describe the fragmentation of DNA in regions of molecular weight above the resolution limit, for fragments that remain in the wells of the agarose gels. Nevertheless, after application of the model to several experimental data-sets it has often been found that the extrapolation of the power-law implies an anomalous genomic DNA content, either above or below the currently estimated size (6.4 Gbp International Human Genome Sequencing Consortium, 2001). The approach has then been updated (Pinto *et al.*, 2002) to preserve the diploid genome content, which is set fixed by a constraint. For fragments larger than the exclusion size of the gel ε, or larger than the size of a specific marker, it is assumed that 46 (for human cells) 'virtual' chromosomes are present, having for mathematical convenience all the same size C', smaller than the original intact average size (H/46), as seen in eq. 3.6 and 3.7. According to Charlesby (1953), exact details on the size distribution of intact molecules before radiation introduces breaks does not influence the distribution that is observed after radiation, provided that each of the original intact molecules is hit at least four or five times. For this reason, when large numbers of breaks are involved, it is convenient to assume that the chromosome have all the same size, the average human chromosome size. For low doses and/or long repair times, the size of the individual chromosomes should be considered, as for example in the low dose-oriented rejoining-misrejoining numerical approach by Hill and Johnston (unpublished). The size-reducing factor $\mathrm{FAR}_{\mathrm{exp}}$ in eq. 3.7 is chosen to depend on the extent of the manipulation-induced fragmentation, as measured from the unirradiated control samples using the values of A and B estimated in the former linear regression. This discontinuity in the background frequency distribution function $y(S)$ in ε does not affect the analytical behaviour of the

BDRB fitting function in the experimental data region, which always lies below ε.

$$y(S) = \begin{cases} AS^B \text{ for S} \in [1, \varepsilon] \\ 46\,\delta(S - C') \text{ for S} > \varepsilon \end{cases} \tag{3.6}$$

where

$$C' = \frac{H}{46} \cdot (1 - \mathrm{FAR}_{\mathrm{exp}}) \tag{3.7}$$

and

$$\mathrm{FAR}_{\mathrm{exp}} = \frac{A}{H} \cdot \frac{\varepsilon^{B+2} - 1}{B + 2} \tag{3.8}$$

The function that describes the radiation-induced DNA fragmentation, derived with the BDRB approach is written in eq. 3.9, in which μ is the number of radiation-induced DSBs, to be estimated in the non linear regression, A and B are the parameters of the background frequency distribution $y(S)$, H is the diploid genome content, ε is the point of singularity of $y(S)$, and C' is as in eq. 3.7.

$$\begin{aligned} n(x, \mu, H, A, B, \varepsilon) &= A \cdot \frac{\mu}{H} \left[\frac{\mu}{H} \frac{\varepsilon^{2+B} - x^{2+B}}{2 + B} + \frac{\varepsilon^{1+B} - x^{1+B}}{1 + B} \left(2 - \frac{\mu x}{H} \right) \right] \exp\left(-\frac{\mu x}{H} \right) \\ &+ 46 \cdot \frac{\mu}{H} \left[2 + \left(\frac{\mu}{H} \right) \cdot (C' - x) \right] \exp\left(-\frac{\mu x}{H} \right) \\ &+ A x^B \exp\left(-\frac{\mu x}{H} \right) \end{aligned} \tag{3.9}$$

In eq. (3.9), A replaces base^A, with 'base' being that of the logarithm used for the linearisation of the power law for estimation of the parameters in eq. 3.6. Formula (3.9) has been employed for regression analysis of several data-sets, presented in § 4.3.4 and also in Pinto *et al.* (2002).

3.2.2.4 Analytical models supporting clustering of radiation-induced DSBs

For medium and high LET radiation, there is experimental evidence for significant deviations from uniform mechanisms or DSB induction, as evident from results of α-particle irradiation in § 4 and from several other studies (Belli *et al.*, 2001, 2002; Höglund *et al.*, 2000; Löbrich *et al.*, 1996; Newman *et al.*, 1997, 2000). In fact, attempts to fit DNA fragmentation data from experiments employing densely-ionising radiations to random breakage models have failed (Kraxenberg *et al.*, 1998). Cluster breakage analysis, an extension of the random breakage model, has been developed (Sachs *et al.*, 1998), successfully used to analyse DNA fragmentation data (corrected for the background damage) after exposure to radiation of about 100 keV μm^{-1}. Other models have been developed that incorporate mathematical equations in Monte Carlo routines. The ran-

domly located cluster (RLC) formalism was also successfully applied to subtracted experimental data from high LET irradiation (Ponomarev *et al.*, 2000; Sachs *et al.*, 1999b). More flexible models of DSB induction that support clustered breakage are discussed in § 3.3.1 in the context of numerical methods.

3.2.3 Conclusions on analytical models of DSB induction

As summarised in figure 3.3, all the analytical models introduced so far are interrelated, since they are essentially based on the same assumption: the induction of DSBs by radiation is random, with breaks distributed in the genome uniformly, independently of each other. Starting from the function derived with the broken stick method, which describes the DNA fragment size distribution after breaks have been distributed randomly and uniformly in an originally intact molecule (formula 3.4), one can obtain almost all the functions that can be derived with the other approaches. The direct quantification method is slightly different. Although this method is not derived from random breakage concepts, it may also be supported by random breakage when extrapolating to total DSB yields per cell. Most of the methods described above may be used to analyse fragmentation patterns that reflect radiation-induced breakage, and the effect of other breaks, such as those that may be present in the background, is taken into account by simple subtraction. The subtractions that are normally carried out to correct FAR or mass fraction values, for each segment, for the effect of the additional DSBs introduced during the sample manipulation procedures have been shown to distort the distributions. Ultimately, this has consequences on the results of the DSB induction and rejoining analysis, as shown in chapters 4 and 5. A step forward has been made in DNA fragmentation analysis, which takes into account the effect of the background damage on the fragmentation profiles that are measured in the irradiated samples. Rather than being subtracted, information regarding the background damage is incorporated in a modified random breakage model, which is used for regression analysis on experimental data measured in the irradiated samples. An approach that is conceptually very similar to BDRB has been derived independently by Belli *et al.* (2001), and also applied to the analysis of DNA fragmentation after low LET radiation.

The principle underlying the BDRB analytical approach is used to underpin a numerical version of the method, which extends random breakage concepts to incorporate DSB clustering, in order to describe fragmentation data also from high LET radiation (§ 3.3.1.1).

3.2.4 DSB rejoining kinetics models

In repair experiments of DNA damage, the overall rejoining kinetics and the extent of repair after long hours of post-irradiation incubation are taken as markers of the severity of the damage inflicted to DNA. More recently, experimental assays that measure repair fidelity have become available, provided yields of mis-rejoined fragments located in different parts of the genome (see Kühne *et al.*, 2000; Löbrich *et al.*, 2000, 1995; Rothkamm *et al.*, 2001). Repair kinetics plots show the disappearance in time of the damaged species, in the present case DNA double-strand breaks. Typically these are represented with bi- or multi-exponential decay in many experiments assessing repair of several radiation-induced DNA damage species (for clinical and experimental data of DNA repair kinetics see Fowler (1999) and references therein, for DSBs see Höglund and Stenerlöw (2001); Kysela *et al.* (1993a,c); Stenerlow and Hoglund (2002); Stenerlöw *et al.* (1999, 2000)). In fact, data on repair of DNA damage can seldom be described with a single exponential decay. Underlying single or multi-exponential decays is the assumption that repair is a 'first order process', in which the repairable unit is the DSB. First order kinetics means that the repair rate is related to the number of repairable species, as in equation (3.10). Second order may also occur, with the DSB ends being the repairable entities (reviewed by Sachs *et al.*, 1997b). In second order kinetics, the repair rate is proportional to the square of the number of repairable species. Zero order kinetics is such that the repair rate does not depend on the number of repairable species present. In this section, the existing models of DNA DSB rejoining kinetics are briefly described to introduce the kinetic approach that has been adopted in this project and the new numerical approach that has been developed.

1. **First-order kinetics: single or multiple exponential components.**
   A typical repair formula assuming that DSBs are the repairable entities is

$$\frac{dN}{dt} = -\lambda N \tag{3.10}$$

   which mathematically states that repair occurs in proportion to the yield of the damaged species. The solution to eq. 3.10 is the simple exponential decay $N = A\exp(-\lambda t)$, where λ (or $\tau = 1/\lambda$) is a repair constant which measures the velocity of the process. A more general solution of equation (3.10) is provided to allow for the occurrence of distinct repair kinetics phases:

$$N(t) = A\exp\left(-\frac{t}{\tau_1}\right) + B\exp\left(-\frac{t}{\tau_2}\right) + \ldots + K \tag{3.11}$$

   The common interpretation of experimental data that are well described by eq. 3.11

is that a proportion of DSBs repairs with fast kinetics, while other breaks may repair slowly. In turn, this is interpreted as due to the fact that the slowly rejoining DSBs are more difficult to repair and/or they are involved in illegitimate recombination processes.

2. **Second order kinetics.**
   If the repairable entities are the ends of a double-strand break, then each repair event involves two ends and the process is said to be of second order. Mathematically this can be written as:
   $$\frac{dN}{dt} = -\lambda N^2 \tag{3.12}$$
   The case of a purely second order process has been recently described by Fowler (1999). A physical picture of the role of first and second order kinetics was given by Tobias (1985): second order may be related to mis-rejoining events, since each illegitimate reunion process requires two ends, belonging to different DSBs, whereas first-order may be related to correct repair, since one can see a break disappearing. From this perspective, the repairable entities are the DSB ends, but when the two correct ends are joined to each other, this may also be seen as one DSB being correctly removed, hence the appearance of first order kinetics.

3. **variable repair half time (VRHT).**
   The multiple-component first-order kinetic model has many adjustable parameters, therefore Foray *et al.* proposed a simplified model in which a continuous spectrum of repair probability, reflecting a continuous spectrum of lesion complexity, rather than two or more types of DSBs (as in eq. 3.11) is postulated and mathematically represented by a variable repair half time (Foray *et al.*, 1996). According to the VRHT model, as the process of DSB rejoining continues, only the more complex breaks are left unrepaired, so that the repair rate is decreased.

4. **Kinetics based on DSB-repair enzyme complexes.**
   From the interaction of repair enzymes with DNA, Cucinotta *et al.* showed the natural appearance of slow and fast kinetics components, due to the time delay that was caused by the action time of the enzymes. If enzymes are not provided in sufficient proportion to the number of lesions, the pool of available enzymes becomes depleted and repair cannot proceed according to pure first order kinetics. Cucinotta *et al.*'s numerical-analytical model could also describe the kinetics of the formation of simple chromosome exchanges on the basis of competitive DSB repair pathways.

5. **Mis-rejoining kinetics and size distribution of mis-rejoined fragments.**

Radivoyevitch *et al.* demonstrated that PFGE and premature chromosome condensation (PCC) data support the hypothesis that two types of DSBs exist. One type of DSBs would be refractive to mis-rejoining, though available for correct restitution of intact sequences. It was suggested that these breaks may be either easily repairable DSBs, or SSBs on opposite strands, a few base pairs from each other, which would not be interpreted as DSBs by the cells but could be converted into DSBs during the experimental procedures, such as during lysis at 50°C or during the PFGE run itself (Radivoyevitch *et al.*, 1998c). The other type of DSBs may be active for mis-rejoining, although they would not be prevented from rejoining correctly (Radivoyevitch *et al.*, 1998a,b,c).

6. **TLK model**.
   The two-lesion kinetic (TLK) model by Stewart (2001) attempts to link biochemical processing of the DSB to cell killing. According to the TLK model, there are two types of DSBs: those that are complex and those that are simple, with different repair characteristics. The repairable entities are the break ends from both types of DSBs, for a first and second order rejoining kinetics process, as explained above. The break ends may form irreversible lethal damages, that is a mis-repair event is not reversible, or non lethal damages. The model is designed having in mind the ability to predict cell survival, as well as DSB induction and rejoining rates. Fit to FAR data from PFGE can also be carried out.

7. **Zero order kinetics**.
   The repair machinery does not answer proportionally to the injury. The rejoining kinetics rate is constant. An example of zero order repair kinetic model was described by Přidal and Lokajiček (1984).

3.2.5 Conclusions on analytical DSB rejoining kinetics models

The picture given above in support of the existence of at least two types of DSBs may have to be re-considered from the perspective that multiple DSBs repair pathways exist, and that requirement for a radiation-induced DSB to be repaired with a specific repair pathway or another are not fully understood (see section 1.4). At least two orders of complexity may influence DSB repairability:

1. the local complexity of each individual DSB

2. the spatial association of multiple DSBs in specific chromatin domains. The relative importance of these two orders of complexity is faced in § 5.3 when data from this project are analysed, and discussed in § 6.3.

A recent study demonstrated that complex DSB, which should be more frequent after exposure to high-LET radiation, are often not recognised by the non-homologous end-joining repair-pathway enzymes, hence are left unrepaired, at least by this pathway (Winters *et al.*, 2001). DSB repair requiring specific repair-pathways may not proceed stochastically. In fact, homologous recombination, the predominant pathway in yeast, requires homologous sequences to become spatially associated, so that DSBs are repaired one at a time via a step-by-step process (zero order) rather then proceeding at a rate that is proportional to the number of lesions present.

In this project, DSB rejoining kinetics data have been preferentially analysed using the first-order kinetics model, with two decay phases, reported in eq. 3.11. Advances in the analysis of DSB rejoining kinetics data have been made in understanding the influence that the additional DSBs induced during the experimental procedures have on the estimation of kinetics parameters, when any kinetic model is applied.

3.3 Numerical Models

Numerical approaches provide the flexibility that is often needed to solve problems which are not satisfactorily described with an analytical model, or are too complex for analytical treatment. For the implementation of numerical models, the C++ programming language has been adopted in this project, since it supports the popular object-oriented (OO) programming approach also found in Monte Carlo codes. The advantage of the object-oriented approach is that the programmer can think in terms of objects that interact with each other according to rules that he/she specifies (see for example the introduction of the books by Cohoon and Davidson, 1997; Flowers, 2000). Once designed, the objects can be easily re-used throughout the code and extra features may be added later, if needed, without affecting the meaning of code written earlier and the way it was used. For the design of the DNA breakage and rejoining models in this project, the objects `DNAfragment` and `DSB`[2] have been most useful. Their descriptions are reported in listings A.1 and A.2 in the Appendix. In the computer-program code, a DSB object is characterised by the quality of its ends and by its position in one of the 46 human chromosomes. The quality of the break determines the way it is handled during the actual computer simulation, particularly for repair. Background breaks are of type '0' and are not processed by the repair machinery, since it is assumed that these are not present in viable cells, but are the result of the experimental handling procedures. Repairable radiation induced DSBs are of type '1', whereas chromosome ends are given a different flag since these may be considered natural, endogenous virtual

[2] names written in `typewriter` font refer to C++ program objects or program entities

break ends (type '2'). By selectively tagging several types of double-strand breaks in the computer-simulations, one can also follow the length distribution of DNA fragments that are delimited by a given type of break. For example, one may ignore the presence of the control DSBs. This can be very useful if one wants to have a clearer picture of the physical process of radiation-induced breakage alone (see also figure 3.12). Also, ignoring the 'control' DSBs is useful if the results obtained from analysis of PFGE data are to be generalised to other techniques like the premature chromosome condensation (PCC), where the background damage is negligible compared to the background damage in PFGE. Other types of DSB quality are conceivable for the purposes of development of computer simulations. For example, a DSB that is not repairable may be of type '3', and a mis-rejoining event may also be recorded specifically. Mis-rejoining could not be detected with the PFGE technique employed in this study, hence mis-rejoining events have not been computer-simulated to fit experimental data from this project.

An object of type `DNAfragment` is characterised by the size of the DNA fragment that it represents, the quality of its two ends and its location in one of the 46 chromosomes. For correct repair, removal of a DSB is equivalent to saying that two contiguous fragments have joined to each other to form one larger fragment. Nevertheless, for some aspects it is more convenient to think in terms of DNA fragments, for example when looking at length distributions. In case mis-rejoining is to be simulated, than one should allow illegitimate ends to combine, and thinking in terms of fragments and their ends could be more convenient than using `DSBs`. The objects `DNAfragment` and `DSB` have been designed in a way that the pool of double-strand breaks can be transformed into the corresponding pool of DNA fragments and vice-versa whenever needed, so that one can think of the set of `DNAfragments` and that of `DSBs` on the chromosomes similarly to dual coordinates that describe DNA fragmentation. Some examples of functions that operate to make these conversions possible are given in Appendix A.

The standard template library (STL) tools and algorithms have been used extensively in the program codes. `Vectors` provided by the library have been used to store all the `DNAfragment` and `DSB` objects. Sorting and finding routines have been used for the development of several algorithms incorporated in the computer simulations. A selected number of examples is also reported in Appendix A.

The numerical models that have been designed and developed in this project are presented in this section, along with models that have been developed by other investigators, for comparison. Models of initial DNA fragmentation are described in § 3.3.1, whereas DSB rejoining models are discussed in § 3.3.3.

3.3.1 Initial DNA fragmentation

In this project, numerical approaches have allowed us to extend random breakage mechanisms to DSB clustering, in order to provide a better description of fragmentation induced by medium-high LET radiation. Sophisticated computer models exist which give a mechanistic description of the action of ionising radiation on DNA, based on Monte Carlo charged-particle transport codes, like the PARTRAC approach (see Ballarini *et al.*, 2000, and references therein) which has been also applied to fragmentation analysis studies (Friedland *et al.*, 1999, 1998, 1997). Independently developed approaches have focused on the formation of very small DNA fragments originating from multiple breaks to the 30 nm chromatin fibre (Holley and Chatterjee, 1996; Rydberg, 1996; Rydberg *et al.*, 1998). Other recent studies have focused on DNA fragmentation at low doses, including DSB clustering at the Mbp scale (Ponomarev *et al.*, 2000, 2001a,b).

No attempts have been made in this project to reproduce in any part the models of induction of DSB by radiation developed by other investigators. Rather, the problem of the influence of background DSBs (introduced in § 3.2.2.3) on the analysis of every DSB induction and rejoining PFGE experiment has been addressed. DSB induction and rejoining models have been designed specifically for the interpretation of the experimental data that were measured in this project, but the programming approach is generic. Although the existing models of DNA fragmentation mentioned earlier are often very sophisticated, they do not take into account the presence of background DSBs and their effect, probably because the experimental data that the models have tried to reproduce were already corrected for the background damage. Recently, a Russian group has attempted to give a mechanistic interpretation to the background damage in PFGE (Khvostunov and Andreev, 2001).

3.3.1.1 Clustering extensions to the BDRB method

In the analytical version of the background-dependent random breakage method (§ 3.2.2.3), the size distribution of DNA fragments measured in the unirradiated control samples of PFGE experiments is described by means of a power-function, as written in eq. 3.6. This appears as a straight line on a double logarithmic scale, at least in the molecular weight region that is resolved in the agarose gels. Departures from straight lines are occasionally observed in the region analysed in experiments, especially for fragments of size 4-6 Mbp (see figure 4.5) and nothing can be assumed about the relevance of the power-law for larger fragments, outside the experimental region. Nevertheless, it may be assumed that the power-law still holds, with the constraints given by the conservation of the total genome content (an approach also adopted by Belli *et al.*, 2001),

or that the power-law does not hold, but some large intact fragments are present. More flexibility may be given to the description of the control fragmentation patterns if a numerical approach is used. Figure 3.6 shows schematically each step of the numerical simulations of both DSB induction and rejoining developed here. The steps involved in

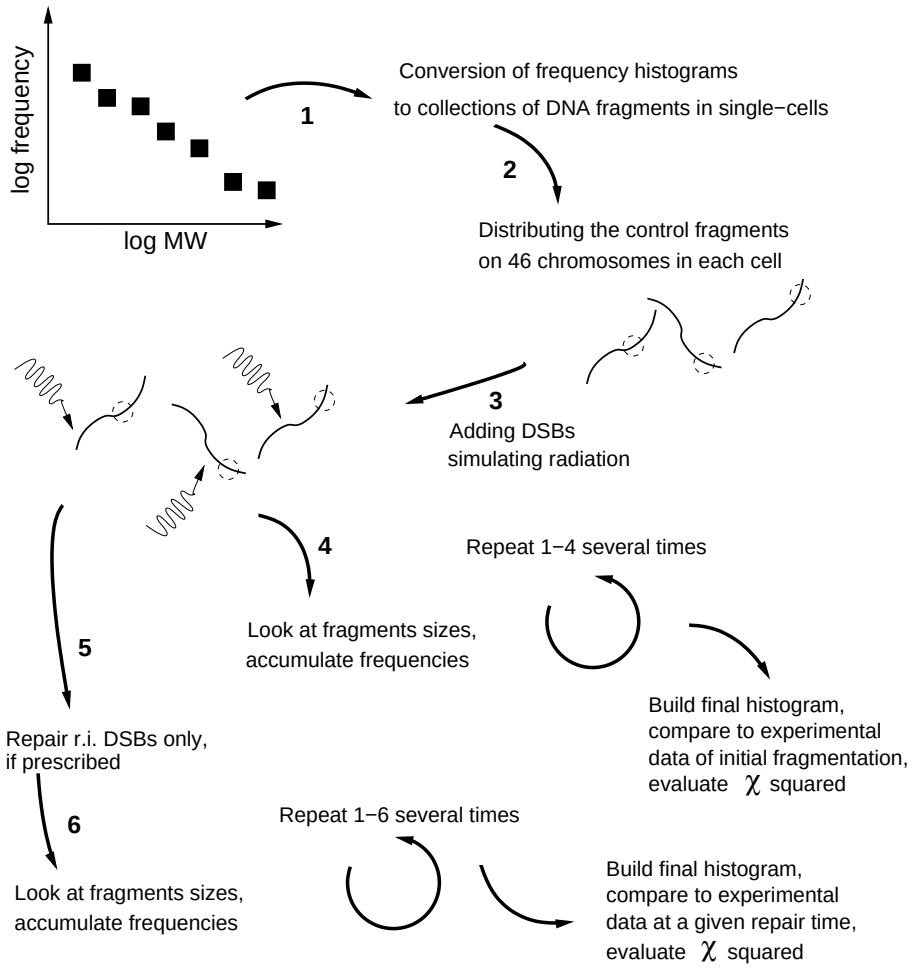

Figure 3.6: Step-by-step procedures followed in the numerical simulations of both DSB induction and rejoining.

the simulation of initial DSB induction are described below, whereas the additional rejoining module is described in § 3.3.3.1. Briefly, unirradiated control patterns are used as input data to the simulation to build, stochastically, a collection of background fragments which meets the conditions set by the inputted histogram (1). Then these fragments are localised on the 46 chromosomes of each cell, at a random position on each chromosome (2). Radiation-induced breakage is simulated by adding new breaks either in spatial association, according to a clustered breakage mechanism, or according to random breakage (3). This operation is repeated for several cells, and finally an averaged fragmentation pattern is outputted in the form of a frequency histogram, which is com-

pared to the experimental determinations of initial DNA fragmentation via χ^2 evaluation. Alternatively, after step 3, if repair is prescribed, a specified fraction of radiation-induced DSBs is rejoined, and frequencies of sizes of the fragments remaining after repair are accumulated as above for a fit to the experimental data relative to a certain repair time. Each of these steps is described in more detail below.

Conversion of frequency histograms to collections of DNA fragments in single-cells.

In the first step of the computer simulations of DSB induction, and also for DSB rejoining, the frequency values n_i measured in the control samples in one experiment are read from an input data file and stored in standard template library's `vectors`. Each experimental data set is employed separately in the computer simulations. A collection of DNA fragments is then generated, stochastically, that conforms to the starting frequency histogram, as described in figure 3.7. Generating such a collection of DNA fragments is conceptually the inverse operation of building a frequency histogram from a population sample. When a frequency histogram is built, data from a population are grouped in separate bins and the frequencies are counted, so that for a specific arrangement of bins one has a unique frequency histogram. If the bin arrangement changes, for example if one has less but wider bins, then the frequency histogram also changes, but for each bin arrangement there is still one and only one frequency histogram. The frequency histogram is used here as an input, and one has to extract from it each time, that is for each simulated cell, one of many data-sets that conform to the input histogram. For example, let us assume that in the bin 4.6–5.7 Mbp one measures a total DNA mass equivalent to 90 Mbp (figure 3.7 can be used as a guide). A number of DNA fragments having size included in the range specified is generated stochastically, until the total mass of 90 Mbp is allocated, within a specified level of tolerance. To generate fragments in each bin stochastically, a probability distribution is required, whose shape and amplitude should reflect the expected relative abundance of fragments as a function of their size in that bin. Such a probability distribution may be sampled from interpolation of the frequency distribution observed experimentally, which was described by means of a power-law in eq. 3.6 in the analytical version of the BDRB approach. For simplicity, a uniform probability distribution is used here in each bin, *i.e.* gel segment. The thinner the gel sections the more accurate is this approximation. The Mersenne-Twister random number generator has been employed (Matsumoto and Nishimura, 1998) for the computer-generation of random numbers according to all the probability distributions used in the simulations in this project, in its C++ implementation by Richard Wagner. Since generating the collection of DNA fragments that conforms to the input frequency histogram is a stochastic operation, it is repeated several times, in order to improve statistics, a fundamental re-

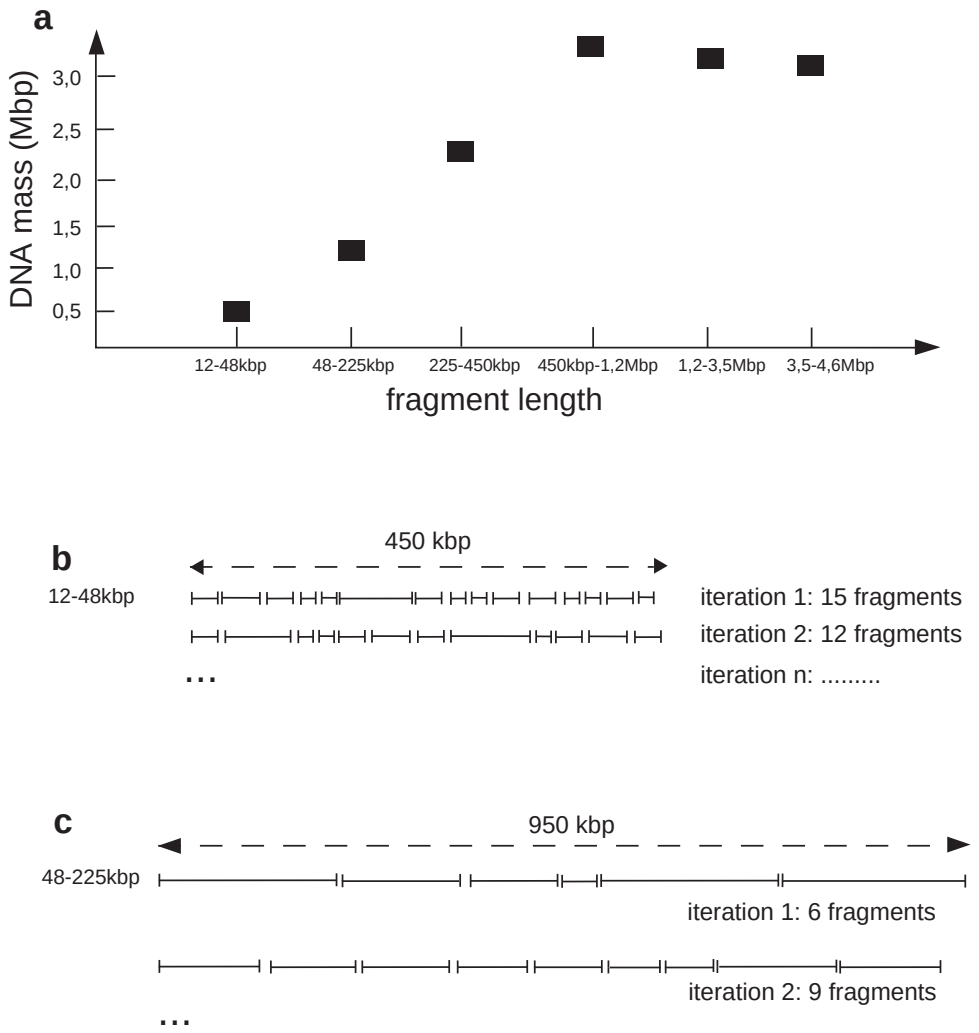

Figure 3.7: A collection of background fragments is stochastically generated using the information provided by the input frequency histogram. Fragments are first generated in each bin, stochastically, satisfying mass constraints, then they are shuffled and distributed on the chromosomes as shown in figure 3.8.

quirement of any Monte Carlo simulation.

The more variable is the phenomenon simulated, the larger should be the number of Monte Carlo cycle repeats, to make sure that the variability of the phenomenon itself is also reproduced in the simulation. The precision of the simulations in this project has been set to be slightly better than the experimental uncertainties. Interestingly, it takes less 'cells' in the computer simulations, *i.e.* Monte Carlo cycle repeats, than the number of cells that are effectively loaded in the gels, to obtain similar uncertainties. The computer-simulations focus on single cells and on single DNA fragments, with a sensitivity that cannot be currently achieved with PFGE. In practice, the statistical variations in the results of the simulations on 100 cells have been found to be already significantly smaller than the experimental uncertainties, which by contrast are achieved on tens of thousands cells.

A collection of control fragments, *i.e.* originating from the DSBs induced during the experimental procedures, as estimated from the unirradiated controls, is again generated for each cell, so that, in the computer simulation, each cell has a variable background damage pattern, but always conform to the frequency histogram that is measured in the experiment. This approach assumes that the background damage that is measured in the lanes of the unirradiated controls of a PFGE gel is representative of the damage that is caused to every single cell in the population, rather than to a sub-population. The hypothesis that the background damage observed is the result of DNA fragmentation in a cell-subpopulation could be made, as addressed in the discussion, § 6.1.

Distributing the control fragments on 46 chromosomes in each cell

Once the collection of control DNA fragments for a single cell has been generated, the fragments are randomly distributed on each of the 46 chromosomes. No information is currently available on the background damage regarding its distribution in the different chromosomes, and where on a chromosome they are preferentially located. One observation available from measurements on the unirradiated controls is the mass of DNA extracted below a given size, expressed in eq. 2.6, the fraction of activity released for example below the exclusion size of the gel ε. It is then assumed in the computer simulations that the FAR value measured in the controls is representative of the proportion of length of each chromosome that is occupied by control fragments (see also figure 3.8). As for the BDRB analytical approach, 46 chromosomes of equal size, the average human chromosome size, 139 Mbp, are considered per cell. Typically, control FAR values are between 5% and 10%. Hence, each chromosome has a region accounting for approximately 5% to 10% of its total length that is occupied by background breaks resulting in fragments having size $\leq$10 Mbp. For each chromosome, the location of the region populated by background breaks is chosen randomly according to a

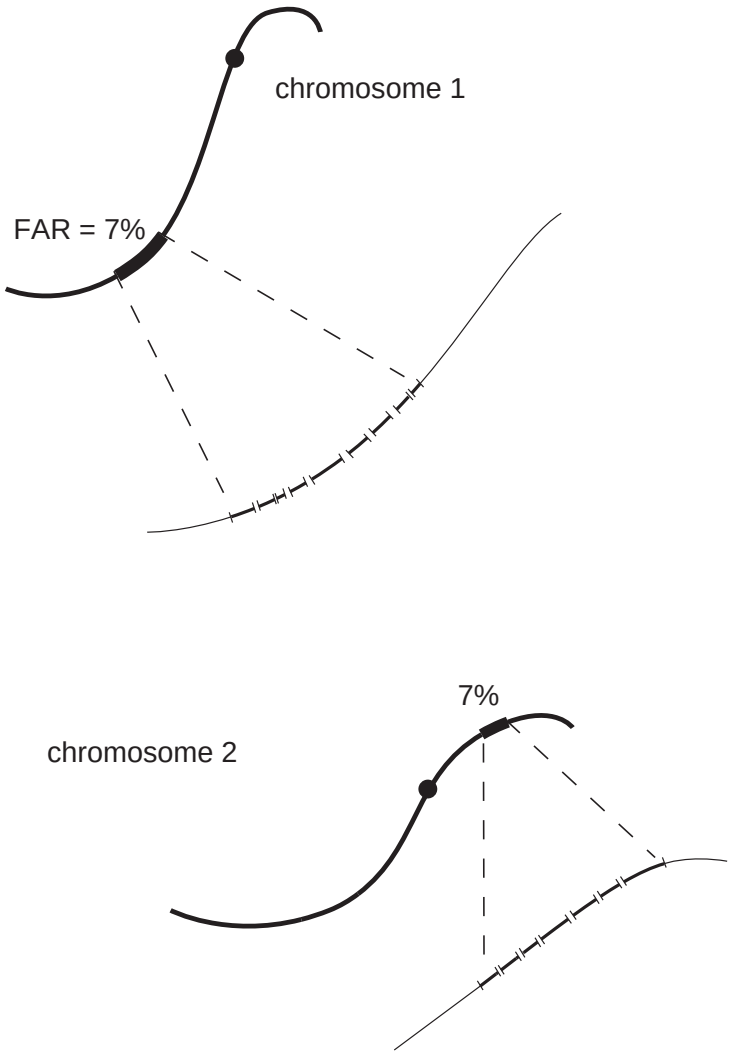

Figure 3.8: The collection of control DNA fragments is equally distributed on each of the 46 chromosomes, on a cell-by-cell basis. Background breaks are assumed to be concentrated in one region, which is also accessible to radiation-induced DSBs. In the example shown, each of these regions covers 7% of the chromosome size.

uniform probability distribution (see figure 3.8). The fact that approximately 5% or 10% of each chromosome is occupied by background DSBs does not imply that this region is not accessible to radiation-induced DSBs. Background and radiation-induced DSBs are in fact assumed to be independently allocated. After background breaks have been distributed on the chromosomes of one cell, background DSBs are labelled to be distinguished from the chromosome ends and from the radiation-induced DSBs that are about to be allocated with the next program module.

Modelling radiation-induced DSBs

With the analytical version of the BDRB approach, analysis of the initial DNA fragmentation is carried out to estimate the total number of DSBs induced in a cell, at a given radiation dose, for each experiment. Regression analysis is carried out using eq. 3.9, based on χ^2 minimisation with the Levenberg-Marquardt algorithm, implemented in many commercial packages for statistical analysis. Numerical approaches do not normally provide analytical functions that may be used in the way just described. In some cases it is possible to follow the way the result of the computer-simulation varies with different values of the input model parameters, and try to find an analytical function $\mathcal{F}$ that describes these results. The function $\mathcal{F}$ would depend on some parameters which are in one-to-one correspondence with the model parameters, as in equation 3.13. Supposing the model has three formal parameters, p_1, p_2, p_3, the outcome of the computer simulation may be described by means of an analytical function of three parameters, t_1, t_2, t_3:

$$\mathrm{model}(p_1, p_2, p_3) \Leftrightarrow \mathcal{F}(t_1, t_2, t_3) \tag{3.13}$$

The function $\mathcal{F}$ may be used for regression analysis of the experimental data with the Levenberg-Marquardt algorithm, and the best values for its parameters t_1, t_2, t_3 would be estimated. Finally, the best values for the original model parameters p_1, p_2, p_3 would then be estimated from t_1, t_2, t_3 by means of the relationship in eq. 3.13. When such strategy is adopted, the main goal is to find such relationship. This approach has nevertheless been found to be too complex for the computer simulations in this project. Without an analytical function, the model parameters that best reproduce the experimental observations may still be estimated, but χ^2 minimisation should be carried out differently, without using the Levenberg-Marquardt algorithm. In the present project this has been done on the basis of a discrete sampling of χ^2 values in the space of the computer model parameters. The numerical extension of the BDRB approach that includes DSB clustering concepts has several input parameters:

- the number of independent clusters of DSB, $\mathcal{N}_{\mathrm{cl}}$
- the average multiplicity of each cluster, ν

- the maximum cluster radius, ϱ
- the number of cells in which DNA fragmentation is going to be simulated, N.

N has been normally kept constant to about 100, since this provides results that are accurate enough, as mentioned earlier. All the other parameters are variable and best-fit values are to be estimated. A complete computer simulation is run for a certain set of initialisation values for the model parameters, and a χ^2 value is estimated from the comparison between the experimental data and the outcome of the simulation. For the particular point in the parameter space, specified by the four coordinates $(\mathcal{N}_{\rm cl}, \nu, \varrho, N)$, one has a χ^2 value. The computer-simulation is then repeated each time with different initialisation values for the model parameters, in practice, several hundreds of different combinations are tested, and a sorted table of $\chi^2(\mathcal{N}_{\rm cl}, \nu, \varrho, N)$ values is written as the program runs. Once all the simulations for each of the hundreds of different combinations of initialisation values for the model parameters are completed, the values that lead to the simulation with the minimum χ^2 are considered the best values of the model parameters, namely the best fit of the clustered breakage simulation of one particular data-set. On an Intel Pentium 166 MMX laptop computer a best fit to one data-set was achieved after an overnight simulation run. When uniform, random breakage, is simulated, DSBs are located independently of each other, that is the cluster multiplicity is null, and any property of the cluster becomes meaningless, like the radius of the cluster. Each chromosome to be hit is selected randomly, and every chromosome has the same chance of being hit, given also that in this implementation one has 46 chromosomes of equal size (see also Sachs *et al.*, 1997a, for the random process of targeting different chromosomes). Within each chromosome, every stretch of DNA is assumed to be equally exposed to radiation, hence a single DSB is located randomly, according to a uniform probability distribution. The difference between the computer simulation of random breakage and the analytical version of the BDRB method is that the numerical approach provides a more realistic picture with 46 chromosomes, each carrying background DSBs, on which additional DSBs are induced by radiation. In contrast, with the analytical version , each of the fragments defined by the distribution of background DSBs, in practise many more than 46 chromosomes, is a potential target to radiation; either the fragment 'survives' with no hits, remaining of the same size, or it is hit by one or more DSB and fragmented further, with its fragmentation described by the broken stick approach (§ 3.2.2.2).

As extension of random breakage, n this project, the DSB clustering process has been designed to simulate clustering of DSBs that is expected to originate from the intersection of a single charged-particle track with chromatin structures, using the simplest approach possible. Such a process has not been designed mechanistically, *i.e.* simulat-

ing the physical passage of a charged-particle, with the accompanied energy deposition events, in a three-dimensional space filled with folded chromatin, described atom by atom and attached to nuclear matrix and membrane structures (see for example the PARTRAC charged-particle transport codes, applied to DNA fragmentation by Friedland *et al.*, 1999). DSBs have been *located* on a simplistic abstraction of inter-phase chromosomes, clustered according to rules that aim at summarising the entire physical and physical-chemical events caused by the passage of a charged particle through the nucleus of a mammalian cell, solely from the perspective of DSB formation. Other types of DNA damage are in fact not accounted for. Although far less accurate and predictive than mechanistic-atomistic approaches, the computer models have been designed to a level of sophistication that allows a good quantitative description of PFGE data with the experimental precision available. An atomistic model of DNA structure would probably be superfluous, since the PFGE technique adapted in this project allows quantification of DNA fragments of at least 10 kbp. Computer-simulation of DSBs of different orders of complexity, mentioned in § 1.3.1, is also not strictly necessary since all DSBs are detected in the same way with the PFGE assay used. Complexity of DSBs may be inferred from results of computer-modelled rejoining kinetics, as described following.

For simulation of clustered DNA breakage, the origin of each cluster is one DSB that is located randomly on one chromosome, as described earlier for pure random breakage. The radius that defines the interval within which additional, clustered DSBs are to be located around the origin, on the same chromosome, since inter-chromosome clustering is not considered, is then drawn randomly, its value being limited by a *maximum cluster radius* ϱ that is specified as one of the input parameters to the simulation. Each independent cluster spans over a region of variable size, with such size limited from above by an inputted value (figure 3.11). It is assumed for simplicity that the radius of each cluster varies according to a uniform distribution, that is all values between 0 and ϱ are equally likely. This is surely an approximation that could not account for fine structures in the expected length distributions, as schematically shown in figure 3.10. Nevertheless, as result of this choice, production of small fragments due to clustering of DSBs is favoured, as suggested from the experimental evidence. For a uniform distribution U(0,ϱ), the average value is ϱ/2, so one has an immediate relationship between the value inputted and the average cluster radius in the simulation. The maximum cluster radius is a property of both radiation quality and chromatin structure (figure 3.9). For a very short-ranged charged-particle, one would expect that correlated DNA damage would not extend beyond a certain number of base pairs away from the primary damaged site. For low-energy photons, for example, which lead to the production of photo-electrons that can travel a few nm or tens of nm away from the site of their production, one expects

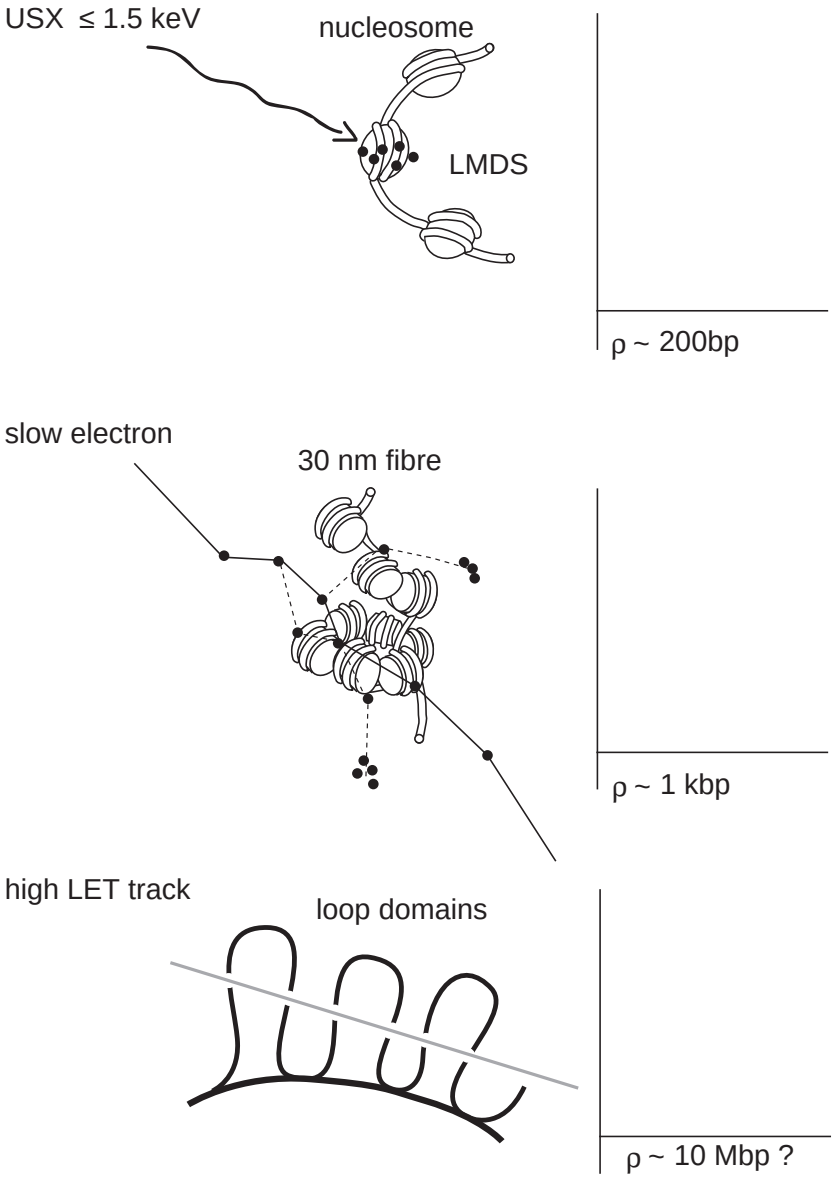

Figure 3.9: The maximum cluster radius ϱ used in the computer simulation relates to radiation quality and chromatin structure. For Ultra Soft X-rays, for example, clustering of DNA damage due to a single photon may extend only up to a few hundreds of base pairs, due to the limited photo-electron range in water. For a slow electron, whose range is sufficient to travel across the 30 nm chromatin fibre, clustering of DNA damage is expected to extend further. For a high-LET particle, clustered damage may extent up to several Mbp, and a single particle may cross a whole cell nucleus intersecting one or more chromosome territories, depending on cell shape.

correlated breakage at the level of the repeated units that define the 30 nm chromatin structure, so the maximum cluster radius may be in the range of a few kbp. Ultra Soft X-rays (USX) are in fact known for their ability to produce highly locally clustered DNA damage, typical of high-LET radiation, but not regionally-clustered damage at level of 100 kbp or above. For charged-particles of longer range, the maximum cluster radius may be in the order of a few tens or hundreds of kilo-base pairs, if a single track may intersect more than one chromatin stretch within a single looped domain. For a particle that is expected to traverse the whole nucleus, the maximum cluster radius may become more a property of chromatin structure rather than radiation quality. For very heavy ions, particle velocity and radial dose distribution may have to be modeled, but this level of accuracy was not needed in this work (see also Kraxenberg *et al.*, 1998).

Track structure is emulated also by means of another parameter. This additional parameter for the simulation of DSB clustering is classified as the *expected multiplicity* of the cluster, ν. This is regarded as the number of expected additional breaks clustered around the primary DSB, the origin of the cluster. The multiplicity of a single cluster is considered a Poisson-distributed variable, so that the multiplicity of each cluster is drawn randomly during the simulation for each cluster, according to the Poisson distribution with the expected multiplicity ν that is given as input parameter. In summary, the combination of a variable cluster radius and a variable cluster multiplicity per cluster aim at simulating the effect of the intersection of a charged-particle track of varying LET with the many orders of chromatin structures that can be probed for with the PFGE technique adopted in this project (see also figures 3.11 and 3.10). These two parameters are not fixed *a priori*, but are estimated by means of χ^2 minimisation after a large number of fragmentation simulations are run for different values of these two parameters, along with the total number of independent clusters $\mathcal{N}_{\mathrm{cl}}$, which is related to the number of independent hits. The additional DSBs, whose number is set by the multiplicity for the current cluster, are allocated in each cluster, within the temporary cluster radius from the DSBs that sets the origin of the cluster, according to a uniform probability distribution, which acts as proximity function. This may be regarded as another simplification, since it could be expected that depending on the chromatin structure that is hit, fragments should be produced of size resonant to the size typical of the specific chromatin structure, as shown in Rydberg *et al.* (1998). Nevertheless, despite the choice of a uniform distribution as a simplified proximity function, the agreement with the experimental data is remarkable, suggesting that a finely structured probability distribution for the localisation of the clustered breaks is not necessary to fit data in this particular study. This may be due to the limited sensitivity of the PFGE technique, which makes detection of fine structures in the fragment-size distribution difficult. In fact, for each order of chromatin organisation (§ 1.2) there should

be a certain probability of generating DNA fragments of a particular size, as shown in figure 3.10. Once the prescribed number of DSBs set by the current cluster multiplicity has been located in the cluster within the temporary radius, a new cluster is started on another randomly selected chromosome. In fact, with a probability of 1/46 this may be the same chromosome where the last cluster was located.

Accumulation of DNA fragment size frequencies.

Each time the computer-simulation has finished processing a single cell, frequencies of fragments of varying sizes are accumulated using the same bin arrangement as in the experimental frequency histograms, for evaluation of χ^2 for the goodness of the fit. At the end of the simulation, a final frequency histogram is built, reflecting the fragmentation pattern averaged from all the cells simulated. Frequencies of DNA fragments are accumulated from cell to cell during the simulation, since the simulation is attempting to reproduce data of a PFGE experiment, where one measures a fragmentation pattern that is averaged over several cells, rather than a single-cell. The design of the computer-codes written for the simulations allows radiation-induced breaks and background DSBs to be distinguished from each other. It is thus possible to measure the size-distribution of fragments that are delimited by DSBs of any type, but in particular by radiation-induced DSB only. The latter feature is unique to the numerical method, since PFGE measurements refer to the fragmentation pattern due to the background and radiation damage without distinction (see figure 3.12). Observation of the fragmentation pattern produced by radiation only may be helpful for an idealised PFGE damage-independent fragmentation analysis, or for comparison to results from other simulations which normally do not include the background damage. It may also be useful to focus on radiation action solely, without the profile shape bias that is caused by radiation-induced breaks.

When DNA fragmentation has been simulated in the prescribed number of cells, that is a number of Monte Carlo cycles (typpically 100), the final frequency histograms are built, one to include the effect of the background damage on DNA fragmentation, the other one excluding the background breaks, to account for the effect of radiation only, as explained above. The first of the two fragment-size frequency histograms is compared to the experimental fragmentation pattern, and the χ^2 value for the goodness of the fit is estimated and recorded in the previously mentioned sorted table of χ^2 values, in the appropriate row. Computer simulation of radiation-induced DNA-fragmentation is started again for different values of number of independent clusters, maximum cluster radius and expected cluster multiplicity, seeking minima in $\chi^2(\mathcal{N}_{\rm cl}, \nu, \varrho, N)$.

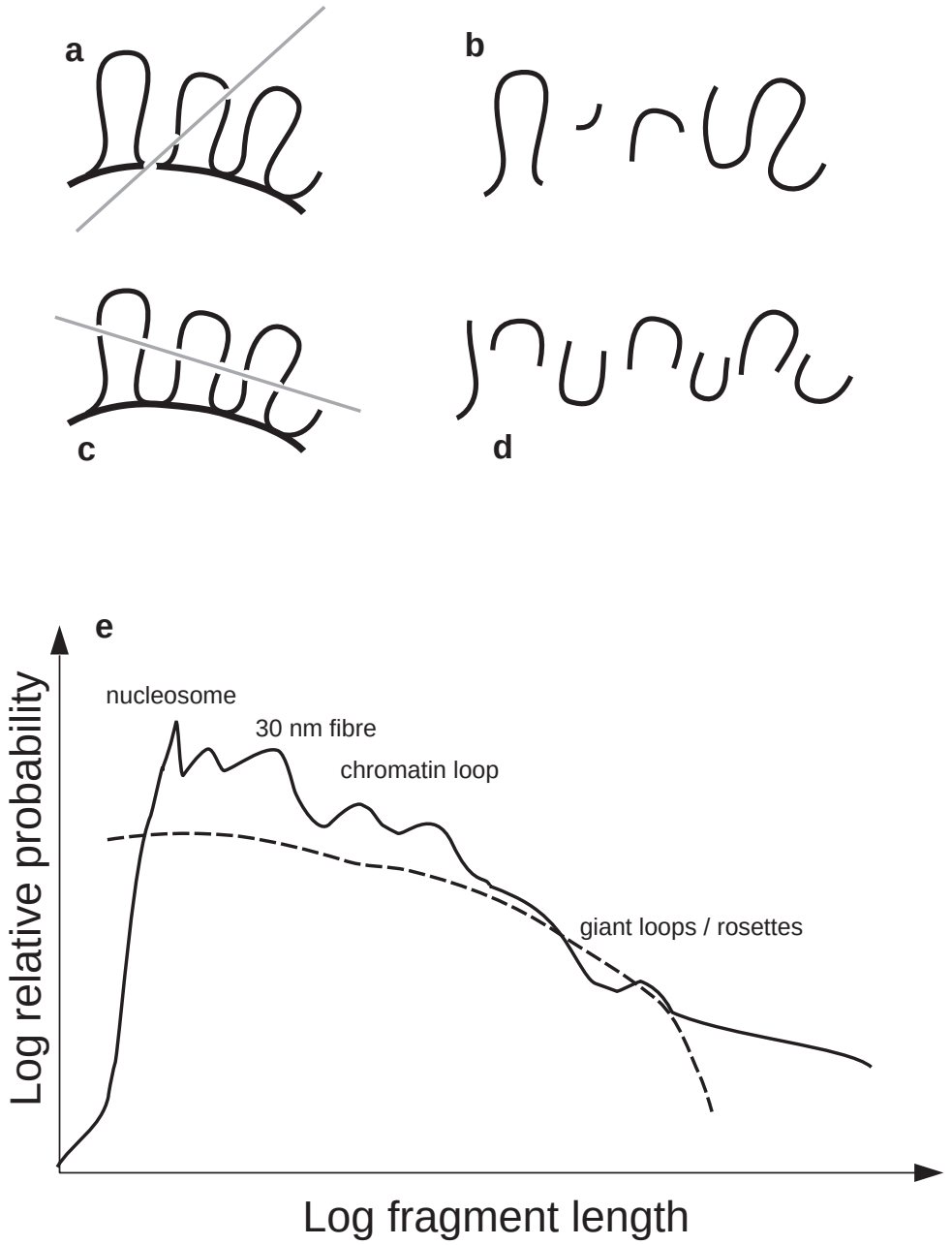

Figure 3.10: (a) As result of the intersection of a charged particle track with several chromatin loops, the fragmentation pattern reported in (b) is produced. In (c) the particle intersects the loops with a different angle producing the fragmentation pattern shown in (d). If one considers every order of chromatin organisation, for a given radiation quality there should be a theoretical expected fragmentation pattern, schematically shown in panel (e) with a solid line, where the pattern that is expected from random breakage is also shown for comparison with a dashed line. The peaks in the theoretical distribution are put in correspondence to the many orders of chromatin organisation known (see also § 1.2).

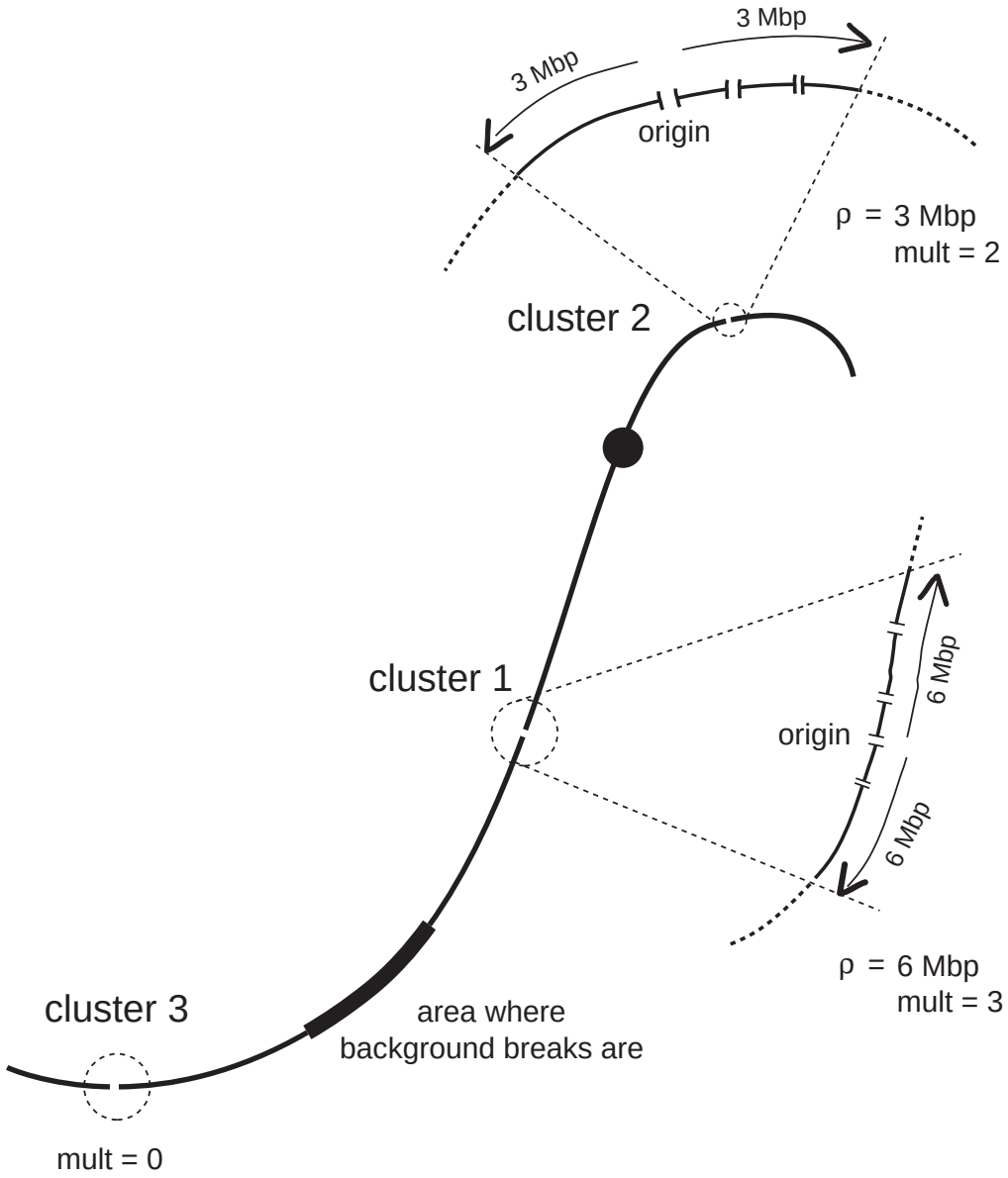

Figure 3.11: How DSBs are clustered along chromosomes to simulate the effect of a traversal of a single charged-particle. In the example shown, the chromosome contains three cluster of DSBs, one counting 4 breaks altogether, one three breaks, and one being simply an isolated break.

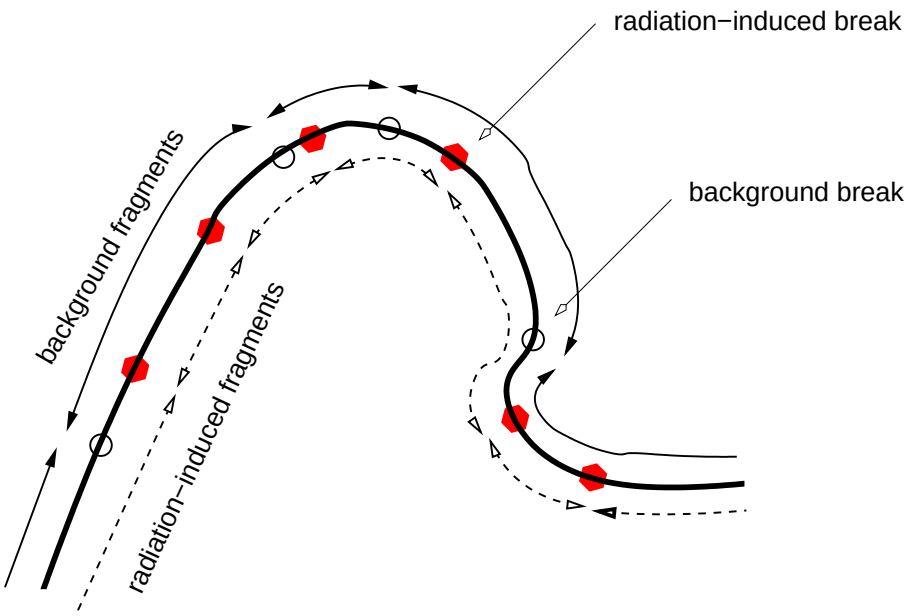

Figure 3.12: DNA length-distributions may be measured for fragments that originate from background breaks, as well as from fragments whose ends are radiation induced breaks, in each case ignoring the presence of other types of breaks. Besides, frequencies of fragments whose ends are of any type can be counted (not shown in figure).

3.3.2 Conclusions on numerical models of DSB induction

The numerical extension of the BDRB method illustrated in § 3.3.1.1 provides a relatively simple method that allows the quantification of the yields and distributions of DSBs that are induced by radiation of different LETs. The quantitative analysis does not suffer from the distortions caused to experimental data by conventional methods to correct for the background DNA damage in PFGE experiments.

Several features of the computer-simulations of clustered breakage developed in this project have been designed with simplicity in mind, with the intent of providing an unbiased method of quantification of DNA fragmentation that can be observed in PFGE experiments, not a comprehensive description of radiation-induced DNA damage. From this point of view, the method developed in this project is far less sophisticated than several other computer-models of DNA fragmentation that have been mentioned in § 3.3.1. For example, the only type of DNA damage modelled is the double-strand break, and there is no reference to different types of DSBs and their relative yields. Nevertheless, the method developed provides an adequate quantitative description of PFGE experimental data, without the need to use highly sophisticated program codes, as shall be seen in the following two chapters.

The method described has also provided useful data that have been used as input to another computer-simulation, namely that of DSB rejoining (§ 3.3.3), which has been em-

ployed for the analysis of repair data in this same project. It is suggested that treatment of background damage to DNA used here may be incorporated in more sophisticated computer-models of DNA fragmentation, for a more accurate prediction of yields and distributions of DSB and possibly even other types of DNA damage.

3.3.3 DSBs rejoining kinetics

Analytical-numerical models of DSB repair exist that focus on chromosome aberrations formation (see for example Sachs *et al.*, 1999a) and mis-rejoining of DNA fragments (Radivoyevitch *et al.*, 1998b). A novel approach that assumes initial random breakage and supports illegitimate end-joining, based on proximity of repairable DSB ends is being developed by Hill and Johnston (unpublished). In their model, Hill and Johnston simulate low doses of sparsely-ionising radiation and the formation of several types of simple and complex aberrations, making quantitative predictions that can be tested experimentally with fluorescence *in situ* hybridization (FISH) techniques. Unfortunately, these sophisticated computer models of DSB rejoining are either too accurate for PFGE, which also does not represent the best tool for low-dose investigations of chromosome aberration formation caused by mis-repair, or are not correctly applicable to the conventional PFGE data of total DSB rejoining, because of the distortions caused to fragmentation analysis by the PFGE background damage.

As for the interpretation of experimental data of initial DNA fragmentation, in this project there has been a need to describe in simple terms, both qualitatively and quantitatively, the results that have been collected during the experimental part of this same project. Background damage in PFGE and how to treat it has played a central role, also in fragmentation analysis of repairing DNA, hence a correct method of analysis of experimental data that have not been corrected for the background damage, rather than a sophisticated rejoining kinetics model, was needed.

3.3.3.1 Modelling radiation induced DSB rejoining kinetics

Background DSBs are presumably not present as frank DSBs in viable cells, so rejoining of radiation-induced DSBs only has been considered in the computer-simulations. Part of the discussion focuses on this particular issue, § 6.1. PFGE experimental data of initial DNA fragmentation do not allow us to distinguish between control and radiation-induced DSBs. If experimental data of initial fragmentation of DNA are to be used as input data to the rejoining-simulations, a method must be found to distinguish radiation-induced breaks from background breaks. To distinguish background DSBs among the totality of the breaks present, a ‘recognise and tag’ approach was developed and employed

first. A computer-program has been written that first reads the control fragmentation pattern and generates a collection of control fragments in single cells that conforms to the experimental frequency histogram, using the routines described earlier in § 3.3.1.1. The procedure then generates a second collection of DNA fragments that conforms to the measured distribution of the totality of fragments, that is the fragments that are delimited by DSBs of any type, reading from the experimental data measured on the irradiated samples. This second collection is generated as described before, only the data relative to fragmentation induced by both background and radiation damage are used as input. After these two collections of `DNAfragments` are converted to the corresponding collections of DSBs (the programming objects described in § 3.3.1.1 and in listing A.1), another program procedure attempts to recognise, among the totality of the breaks present in the second collection, those that are distributed approximately like the DSBs of type '0' in the first collection. These breaks are then tagged as background breaks. This type of approach has faced several practical difficulties. To make an association between background breaks in the first collection and (where only type '0' breaks are present) and breaks in similar positions in the second collection was quite difficult. The number of breaks 'tagged' was very low, so that most of the breaks present remained attributed by exclusion to radiation, particularly those that were closely associated, and the approach has been abandoned.

The solution to the problem of distinguishing background breaks from radiation-induced breaks for the DSB rejoining kinetics simulations has been provided by the successful computer-simulations of initial DNA fragmentation based on DSB clustering (described in § 3.3.1.1 and applied to fit data in chapter 4). These simulations have in fact provided a method to generate a complete initial DNA fragmentation pattern in single cells, where DSBs of type 'background' and type 'radiation' are already well distinguished. In these simulations there is no need to 'recognise and tag' background breaks, since the radiation-induced breaks have been located, in a controlled manner, and separately, on top of background DSBs that have been distributed earlier. It has been thought that the initial fragmentation pattern generated in single cells as described above could be used as the substrate for the rejoining simulation, which effectively becomes an additional program module that plugs into the existing program code for the simulation of initial DSB induction, as shown in the diagram 3.6. In fact, the DSB rejoining simulation is very similar to the DSB induction simulation, but for a few extra functionalities that allow rejoining kinetics to be computer simulated for fragments of *any* size, so that one can compare the simulated data to measurements of rejoining kinetics evaluated in separate molecular weight regions, testing specific rejoining kinetics mechanisms. This is shown in chapter 5 for many experiments.

Every DSB rejoining kinetics experiment carried out in this project includes samples that have been irradiated and not incubated for repair of the damage induced. These irradiated but unrepaired samples are first analysed with the numerical extended BDRB approach described earlier (§ 3.3.1.1) in order to estimate the relevant parameters that describe the initial DNA fragmentation. The same parameter values (number of independent clusters, maximum cluster radius and expected cluster multiplicity) are then used in an independent DSB rejoining simulation to generate the initial DNA fragmentation pattern in single cells, which becomes the substrate of the rejoining program module.

The DSB rejoining kinetics module.

The concept of repair time is not explicitly incorporated in the DSB rejoining kinetics simulation. The model does not postulate that either first or second order rejoining kinetics apply, nor single or multi-component exponential repair kinetics (§ 3.2.4). DSBs are repaired one after another, according to a zero-order step-by-step process that is similar to the one suggested by Přidal and Lokajiček (1984), at least from a practical point of view. The analogy to the model by Přidal and Lokajiček is in fact not extended to the actual DSB repair mechanism, which they proposed to be based on the formation of pairs of homologous chromosomes as in the homologous recombination process, a situation that may seldom apply to repair of DSBs in human cells (see § 1.4).

For a specified *fraction* of radiation-induced DSBs to be repaired, breaks on different chromosomes are individually selected, by randomly choosing the chromosome in which a break is about to be repaired (if there are any left to be repaired on the selected chromosome) and randomly selecting the individual break to be repaired on such chromosome. Every DSB is equally likely to be repaired in unit time, and breaks produced in the same cluster are not repaired in concert. The rejoining procedure may then not be viewed as the inverse operation of the DSB clustering procedure. Repair is here intended as restitution, or correct removal of double-strand break. Similarly, the process may be pictured with two adjacent DNA fragments, separated by one radiation-induced DSB, that join to each other to form a fragment whose length is the sum of the lengths of the former two. The fact that the breaks are selected at random for removal, during the simulation, is equivalent to saying that the probability of rejoining two fragments does not depend on size, and this rejoining mechanism has been given the name of 'fragment size-independent rejoining kinetics'.

The rejoining simulation is repeated several times for the specified number of cells, each time removing a different fraction of the initial DSBs, ranging from 1% to 100%, for simulation of several different repair stages, up to complete repair, when all but the irreparable background breaks have been removed. For each simulated fraction of breaks repaired, the resulting fragmentation patterns are described quantitatively by construct-

ing a frequency histogram as described earlier. Each frequency histogram is stored in a separate data file and compared to the fragmentation patterns measured experimentally at all the available times of post-irradiation incubation, for the particular experiment analysed, in order to evaluate the χ^2 for the goodness of the fit. For example, the experimental DNA fragmentation pattern measured after one hour of incubation is compared to each of the patterns obtained after simulated removal of several fractions breaks, and for each theoretical distribution obtained a χ^2 value for the goodness of the fit is calculated. The simulated pattern which gives the minimum χ^2 value gives the best estimate for the only rejoining parameter to be estimated: the fraction of DSBs repaired at that repair time, $\mathcal{F}_t$. This procedure is repeated for the experimental data measured at all the repair times available for the particular experiment under analysis, so that one eventually has an estimate, for each repair time, of how many radiation-induced DSBs have been repaired, assuming that DSBs are simply removed. Nevertheless, there is no general functional relationship between any $\mathcal{F}$ value and repair time, since $\mathcal{F}$ values are only known for the repair times available. An additional step is required to have a more complete rejoining kinetics time picture.

The computer-simulation provides a method to quantify the number of DSBs repaired as if correct repair took place. The estimates obtained for different experimental repair times may be plotted vs incubation time, in order to evaluate the more traditional total DSB rejoining kinetics curve. These data can be fitted to a rejoining kinetic model, assuming for example first order repair, using single or multiple exponential decay components (§ 3.3.3). Regressions provide a functional relationship $\mathcal{F}(t)$, which can be inverted to $t(\mathcal{F})$. It is only at this stage that computer-simulated fragmentation patterns for different fractions of DSBs rejoined may then be associated to time. The greatest advantage by far is that this allows us now to follow the kinetics, vs time, of fragments of *any* size, testing visually the hypothesis of fragment size-independent kinetics. This type of analysis in shown in figures 5.6, 5.7, 5.10 and 5.11 in chapter 5.

3.3.3.2 Modelling DSB rejoining kinetics on experimental data corrected for the background damage

Although the lack of accuracy of the subtraction procedure that corrects for the background damage has been pointed out several times in this chapter, some early rejoining simulations have been run in this project to describe the rejoining kinetics of experimental data that were corrected for background damage by subtraction. This analysis is reported in this Thesis for two experiments for illustration purposes, one for each radiation quality (see figure 5.12) merely to show how significantly different can be the results if compared to those obtained when data are not subtracted and radiation induced breaks

only are selectively rejoined, leaving the background breaks untouched.

For rejoining simulations that aim to reproduce the experimental 'net' (*i.e.* corrected for the background breaks by subtraction) frequency distributions, there is no need to distinguish between radiation-induced breaks and control breaks, since it is assumed that the experimental fragment size distributions are consequence of radiation-induced breaks only. The rest of the simulation is essentially identical to what has been described above, with breaks to be selected at random on chromosomes also selected randomly, equivalent to a fragment size-independent rejoining kinetics mechanism.

3.3.4 Conclusions on DSB numerical rejoining models

The numerical method of analysis of DSB rejoining kinetics developed in this project and described in § 3.3.3.1 is not as sophisticated as other existing repair models, in terms of hypothesis made on kinetics. In fact, it assumes that breaks are removed one after another, at a constant rate in an arbitrary time, independent of actual time measured during DSB repair experiments. A reference to real time is made explicit only at the end of the simulations, when results are analysed with a first order kinetics model, although any other kinetics model may be in principle applied. In summary, the rejoining kinetics model combines analytical and numerical methods. Nevertheless, a major advantage of the rejoining kinetics model developed is that this allows us to estimate the number of repaired DSBs without making manipulations to the experimental data that would distort them and bias the results. This is particularly evident from the application of the same type of simulation to the experimental data that are either corrected for the background damage or not corrected, as shown in figure 5.12.

An interesting feature of the numerical method developed for the analysis of DSB rejoining kinetics data is that it describes the fragmentation of the entire genome in single cells, not only in the experimental region where PFGE data may be measured. The disappearance and reappearance of very large fragments may be followed as rejoining proceeds toward the restitution of intact chromosomes, well above the limits of resolution of PFGE assays, but in the sensitive region of other techniques, like in premature chromosome condensation (PCC)-assay. Predictions of fragmentation patterns in regions unresolved with PFGE requires extrapolations, both to the low-dose region and to large fragments size region (§ 4.5). For extensions of the DSB rejoining kinetics model to the analysis of chromosome aberrations, mis-rejoining of incorrect ends should be modelled, and more detailed simulations of inter-phase chromatin structure and inter-chromosome clustering of single charged-particles track-correlated DSBs would be needed. This was beyond the scope of this project.

Chapter 4

Initial DNA fragmentation: Experimental results

4.1 Introduction

Results of analysis of radiation-induced initial DNA fragmentation are presented in the following chapter for both X-ray and α-particle radiation. Analysis using analytical methods for the quantification of DSB yields and distributions is presented first. Then the application of numerical methods of analysis of DNA fragmentation is considered, providing a more detailed characterisation of the DSB clustering properties of the types of radiation employed in this study. Finally, a computer-simulation of a PCC experiment measuring initial yields of chromosome breaks is presented, based on extrapolations from results obtained from PFGE data analysis.

4.2 Raw PFGE output data

Before showing the analysis of radiation-induced DNA fragmentation using PFGE with a variety of analytical and computer-based methods, it is useful to illustrate the raw PFGE data, as they are collected from early analysis of electrophoresed gels, in order to appreciate how these are treated and modified for subsequent analysis. After the gels are sectioned as described in § 2.7, and after scintillation counting, results are in the form of a table of dpm per gel section. For a given a gel lane, dpms are then accumulated for all the sections available, and the measured signal in each section is normalised to the total number of counts per lane. One thus obtains the fraction of DNA mass present in each gel section (see also § 2.7). An example of DNA mass-size distribution is shown in panel A of figure 3.7, where the molecular weight regions to which the measurements

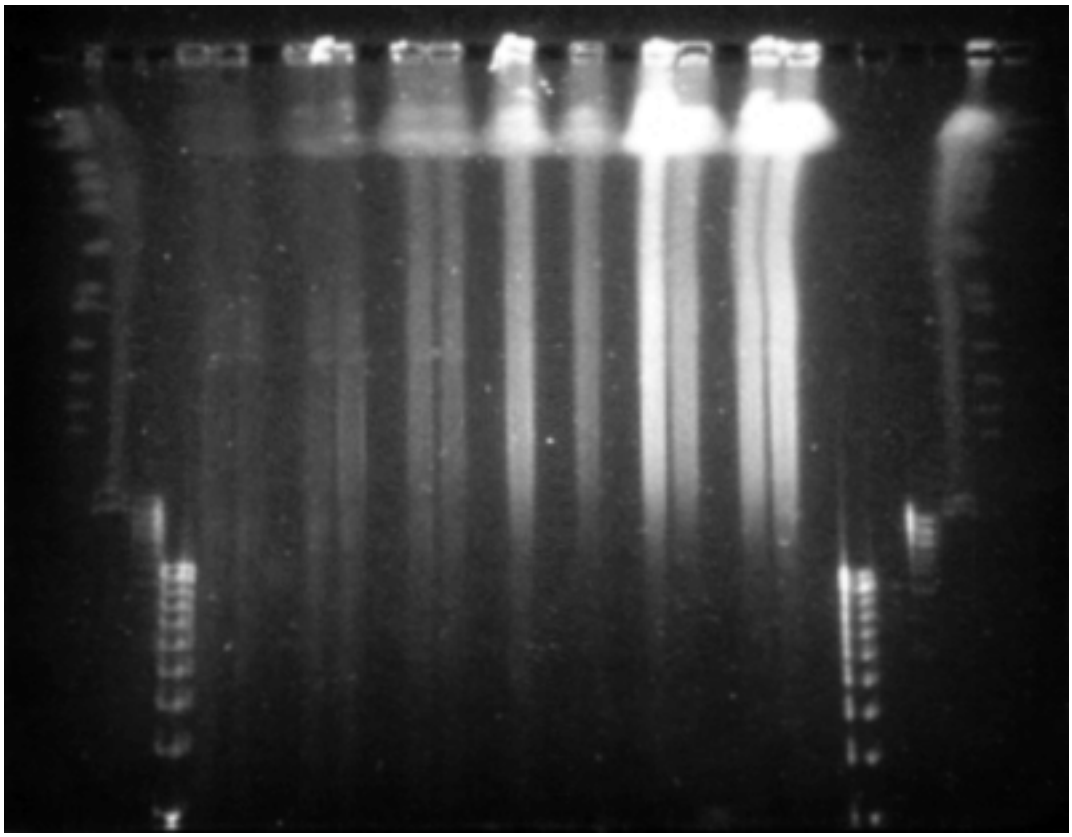

Figure 4.1: A photography of a typical PFGE gel stained in EtBr and observed over a UV trans-illuminator. The photography shown refers to the 18 hours electrophoretic protocol (table 2.2). Molecular weight markers are loaded on each side of the gel. Unirradiated control samples are located next to the markers on the left, followed on the right by samples that have been irradiated at increasing radiation doses, ranging from 10 to 200 Gy.

refer are specified (not to scale).

Mass fraction values are then converted to other quantities as described in eqns. 2.5 for further analysis. The most useful quantities are the number of breaks in a gel section and the frequency of fragments normalised to the width of the molecular weight interval defined by a gel section.

4.3 Analysis of initial radiation-induced DNA fragmentation with analytical methods

Several different analytical methods of analysis of radiation-induced DNA fragmentation have been employed in this project for the quantification of yields and distributions of DSBs. All the methods of analysis used are based on or supported by random breakage concepts, according to which breaks in a polymer are introduced randomly, with equal probability of being located anywhere in the molecule that is being hit, and independently of each other (see figure 3.1 for a graphical description of the random breakage mechanism). The following sections present the result of the analysis of initial DNA fragmentation carried out with the 'FAR' method (which was described in § 3.2.1.1), the 'direct quantification' method (§ 3.2.2.1) and the 'BDRB' method (§ 3.2.2.3)

4.3.1 Application of the FAR method

The fraction of activity released (FAR) method has been used as representative of analysis of DNA fragmentation with integral methods, *i.e.* that require integration of the DNA mass signal over a relatively wide molecular weight interval (see § 3.2.1.1). Experimental determinations of the fraction of DNA smaller than a specified molecular-weight threshold k have been first corrected for the background damage caused to DNA by the experimental procedures. The correction is carried out by subtracting the FAR value measured in the unirradiated controls from the FAR value measured in the samples that have been irradiated, for the same integration threshold k value. The FAR value obtained in this way is considered 'corrected' for the effect of the background damage, hence unbiased and representative of DNA fragmentation produced by radiation-induced breaks only after a pre-determined dose. Alternatively, background damage may not be subtracted from the FAR measured in the irradiated samples, but it could be treated like a radiation dose scaling factor (see for example Belli *et al.*, 2001). FAR values corrected for the background damage by subtraction are then averaged from several independent experiments, at the same dose. Mean FAR values, together with their standard devia-

tions, are plotted vs dose, and least-squares regression analysis is carried out in order to estimate breakage yields per unit dose, using the analytical relationship between FAR, number of breaks introduced in a cell per Gy r, and integration threshold k, reported in eq. 3.2. In the analysis of DNA fragmentation with the FAR method, the fraction of DNA mass measured in a restricted molecular weight region is used to estimate what the total DSB yield per cell would be to reproduce the experimental findings in that molecular weight region observed. A question is whether the result of the analysis with the FAR method, namely the total DSB yield per cell and per Gy of radiation, depends on the choice of the experimental region where the regression analysis is carried out. For a breakage mechanism that is purely random (§ 3.2.1) one would expect that estimates of total DSB yields are not influenced by the choice of the experimental region analysed. In fact, for random breakage and a given total number of breaks introduced per cell (to be estimated) the number of DSBs measured in a limited part of the genome should be linearly proportional to the size of the experimental region under observation. When expressing DSB yields extrapolated per cell or per unit base pairs, these would be constant. The picture would be rather different for a breakage mechanism that favours spatial association of DSBs (see figure 3.1 for comparison to random breakage) leading to the formation of an excess of small fragments and a defect of larger fragments, compared to random breakage, as also shown by Höglund and Stenerlöw (2001). By focusing the experimental observation on smaller DNA fragments only, one would conclude that a large number of breaks must have been randomly and uniformly introduced in each cell in order to observe such an extensive DNA fragmentation. Conversely, when trying to estimate total DSB yields from quantification of larger DNA fragments, it would be concluded that a relatively small number of breaks must have been randomly and uniformly introduced in the chromosomes of each cell to observe such a limited DNA fragmentation at the level of the fragments of large size. By varying k values in the FAR analysis one would then expect to find different estimates for r, indicating deviations from the random breakage mechanism (see Höglund and Stenerlöw, 2001).

For data analysis with the FAR approach, FAR values have been calculated below 12 different molecular weight thresholds k, 8 of which are shown in figure 4.2 in separate panels (a-h). The DSB yields r estimated can be then compared as function of k, as shown in figure 4.3, which shows that when large fragments are included in the FAR integration, the total DSBs yields are higher for X-rays than for α-particles (panels 4.2a-c). However, as the threshold size is reduced to below approximately 1 Mbp (panel e) the extraplated yields of DSB induced by α-particles increase above those of X-rays and the FAR-dose curve for α-particles shifts above that for X-rays. At the largest threshold size studied, the FAR signal is weighted to the larger DNA fragments, and therefore for more

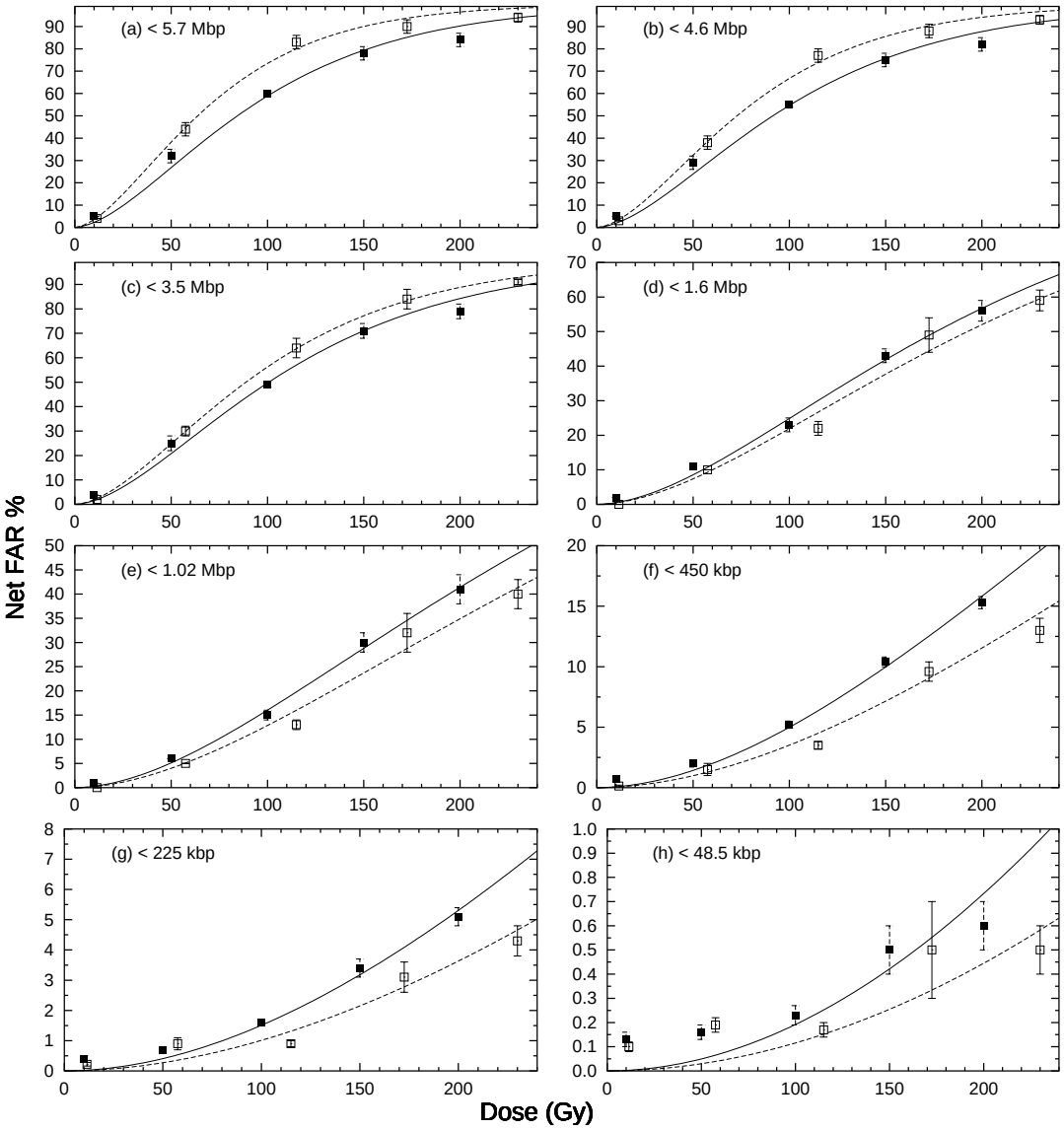

Figure 4.2: Panels (a-h) depict FAR values (with controls subtracted, thus ”net”) for α-particles (■) and X-rays (□) with each panel representing a different exclusion size (k in eq. 3.2).

sparsely-located breaks. Widely separated breaks are expected to be produced more effectively after sparsely ionising radiation. By lowering the threshold size, sparse breaks are no longer contributing to the integrated signal, and the FAR becomes more sensitive to the closely associated breaks, which are expected to be produced more effectively by densely ionising radiation.

Figure 4.3 summarises the estimates for the extrapolated total DSB yield and the RBE, based on regression analysis, as was shown in figure 4.2, with varying threshold size. By varying k from 5.7 Mbp to lower molecular weight values, down to 200 kbp,

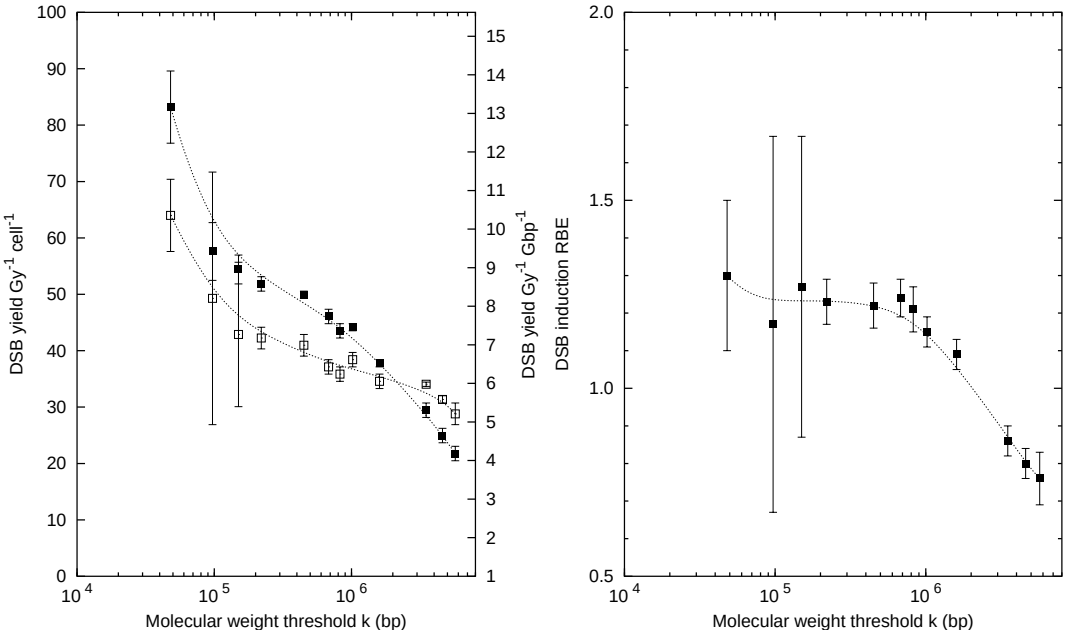

Figure 4.3: Results of quantification of DSB yields with the FAR method. Left: total DSB yields evaluated as DSB per Gy per cell or per Gbp as function of the molecular weight threshold k: (■) α-particles, (□) X rays. Right: RBE value for DSB induction shown as function of molecular weight threshold k.

the data points are non-horizontal, indicating a deviation from random breakage as discussed earlier. With the exclusion of the data shown for k values 48·5 kbp, 97 kbp and 147·5 kbp, where the experimental uncertainties appear to be dominant, linear regressions in the range 225 kbp–5·7 Mbp on apparent scales, *i.e.* on the semi-logarithmic scales as shown in the left panel of figure 4.3 result in slopes different from zero at 95% confidence level (slope B=-9$\pm$2 for X-rays and -22$\pm$4 for α-particles, with standard error). It should be stressed that this was observed not only for FAR analysis conducted on α-particles data, but even for X-rays, suggesting that X-rays could induce DSBs that are non-randomly distributed. This conclusion will be further analysed in chapter 6 when results obtained from the application of a variety of methods of DSB quantification will all be compared. Results obtained with the FAR analysis method, shown in figure 4.3, are

also summarised in table 4.1.

4.3.2 Fragmentation analysis with the Broken Stick method or the Distribution Shape method

The 'broken stick' method (§ 3.2.2.2) may be used to quantify radiation-induced DSBs from analysis of DNA fragmentation patterns in which the only breaks present are those introduced by radiation. The method cannot be used to quantify radiation-induced breaks when the fragmentation patterns result from more than one breakage mechanism, for example radiation and PFGE background damage together. In order to adapt PFGE data for analysis with the broken stick method, experimental measurement of DNA mass distributions are normally corrected for the background damage by simple subtractive methods (see § 3.2.2.2). Nevertheless, this type of background damage correction is flawed, since it is biased by distortions of the fragmentation patterns that are non-uniform throughout the size-distribution of DNA fragments, as shown in figure 3.5. The biasing effect of background correction procedures on the experimental inference is also evident in the estimation of DSB rejoining kinetics in § 5.3.1. For this reason, analysis of both initial DNA fragmentation and fragment-size distributions during DSB rejoining has not been carried out with the broken stick method as extensively as with other methods of quantification of DSBs yields and distributions and will not be shown here. Similarly, analysis of DNA fragmentation patterns with the distribution shape method (slope analysis, § 4.3.2) is also biased by the subtraction procedures that are required to correct the experimental determinations for the background damage. The distortions caused to the fragmentation profiles by the data correcting procedures in particular lead to the finding that low-LET radiation induces a singificant level of charged-particle track-correlated DSBs.

4.3.3 Fragmentation analysis with the Direct Quantification method

Individual PFGE experiments have been carried out using one of the three PFGE running conditions, in which different DNA molecular weight markers are employed, so that three molecular weight intervals are identified from the smallest and the largest molecular-weight markers available in each gel, [M_1,M_2]. Measurements of DNA mass-intensity have been converted by means of eq. 2.5b to number of DNA fragments for each gel section, and then added together for every gel section in the same gel lane. From the number of breaks measured between M_1 and M_2, *i.e.* added together from all the sections available and corrected by subtraction of the corresponding number of

FAR method - Results - Yields of DSBs·Gy^{-1}·Gbp^{-1}

Radiation	<5·7 Mbp	<4·6 Mbp	<3·5 Mbp	<1·6 Mbp	<1·02 Mbp	<825 kbp
α-particles	3·4±0·2	3·9±0·2	4·6±0·2	5·9±0·1	6·9±0·1	6·8±0·2
X-rays	4·5±0·3	4·9±0·1	5·32 ± 0·06	5·4±0·2	6·0±0·2	5·6±0·2
RBE	0·76±0·07	0·80±0·04	0·86±0·04	1·09±0·04	1·15±0·04	1·21±0·06

	<685 kbp	<450 kbp	<225 kbp	<147·5 kbp	<97 kbp	<48·5 kbp
α-particles	7·2±0·2	7·8±0·1	8·1±0·2	8·5±0·4	9·0±0·8	13±1
X-rays	5·8±0·2 (△)	6·4±0·3 (△)	6·6±0·3	6·7±2 (△)	8±3 (△)	10±1
RBE	1·24±0·05	1·22±0·06	1·23±0·06	1·27±0·04	1·1±0·4	1·3±0·2

Table 4.1: Results obtained using the FAR method for the quantification of initial DSB yields per Gy per Gbp. Data are shown as means ± s.e.m for X-rays and α-particles calculated using the FAR method for 12 different molecular weight thresholds with eq. 3.2. In some cases (△), corresponding to particular molecular weight thresholds, data have been obtained by only considering the FAR values at 115 Gy (n=6). Data are plotted in figure 4.3a for convenience. Also shown are the calculated RBE values with standard error, plotted in figure 4.3b.

background breaks, the total DSB yield per cell has been extrapolated using the relationship reported in eq. 3.3 and plotted in figure 3.2, although a numerical solution is also possible. Experimental data have been analysed exclusively at 115 Gy for X-rays irradiation and 100 Gy for α-particle irradiation. Results of fragmentation analysis with the 'direct quantification' method, extrapolated to total DSB yields per cell, are shown in figure 4.4 for several independent experiments.

DSB yields extrapolated to whole cells have then been averaged for PFGE experiments that are analysed in the same molecular weight interval. Averaged estimates are reported in table 4.2 together with α-particles RBE values for DSB induction as assessed by 'direct quantification' of DSBs.

Direct Quantification method - Yields of DSBs·Gy^{-1}·Gbp^{-1}			
Radiation Quality	48 kbp-5.7 Mbp	12 kbp-825 kbp	12 kbp-225 kbp
α-particles	5.6 $\pm$ 0.2 (●)	8.2 $\pm$ 0.4 (▲)	10 $\pm$ 2 (■)
X-rays	4.7 $\pm$ 0.2 (○)	5.5 $\pm$ 0.5 (△)	6 $\pm$ 2 (□)
α-particles RBE	1·19$\pm$0·07	1·5$\pm$0·1	1·6$\pm$0·5

Table 4.2: Results of the application of the 'direct quantification' method with the supplementary use of a method based on random breakage to extrapolate to total DSB yield per cell (the method is illustrated in figure 3.2). The analysis is restricted to the 115 Gy data-set for X-ray experiments and the 100 Gy data-set for α-particle irradiation experiments. The values reported are mean $\pm$ s.e.m from the results of the application of the 'direct quantification' method on each separate experiment, shown in figure 4.4. The mean values were calculated separately per three molecular weight regions. The symbols shown in parentheses in this table indicate that the average values were obtained from experiments that are marked with the same symbols in figure 4.4.

4.3.4 Application of the BDRB analytical method

The background-dependent random breakage (BDRB) method is described in § 3.2.2.3. The first step that is required for the application of the BDRB method for fragmentation analysis is the estimation of the unwanted damage caused to DNA by the experimental handling procedures. The extent of such damage is quantified by means of a linear regression of frequencies of DNA fragments measured in the unirradiated control samples, plotted on double logarithmic scales (linear fit on apparent scales, see § 3.2.2.3). Figure 4.5 shows the DNA fragmentation patterns measured in the unirradiated controls of several independent PFGE experiments. A reproducible inverse relationship between DNA fragments frequency and size of the fragments is evident, approximating to a linear relationship. Stenerlöw *et al.* have questioned the reliability of the apparent linear relationship between the frequencies of DNA fragments measured in the unirradiated

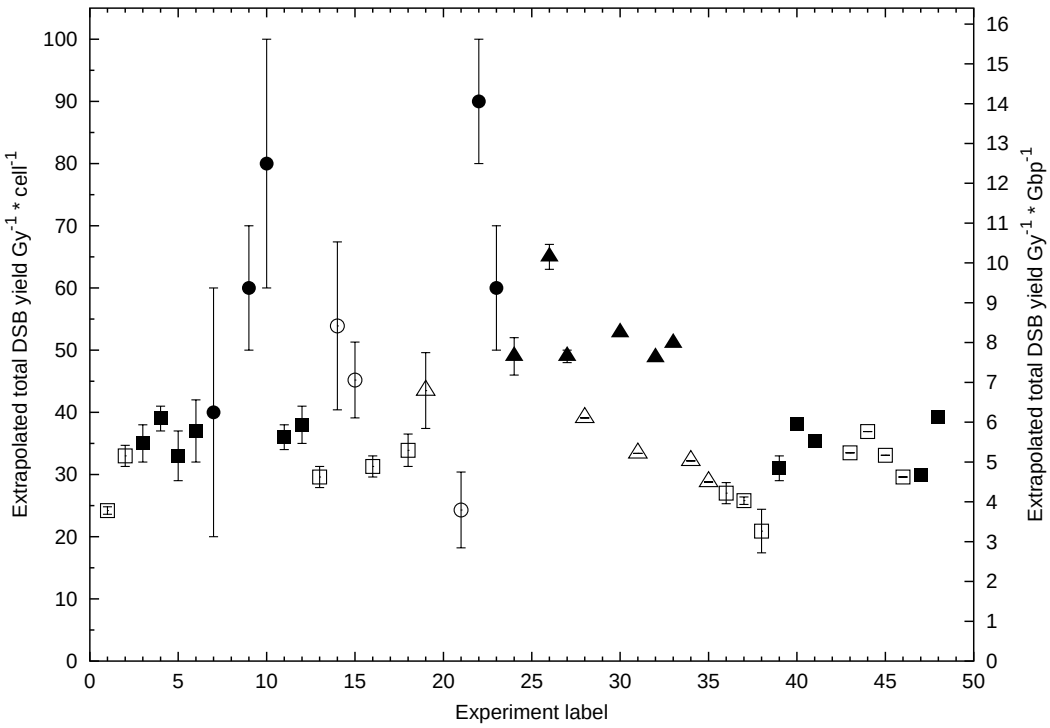

Figure 4.4: Results obtained with the 'direct quantification' method applied to each separate experiment. Open symbols: X-ray single dose 115 Gy, bold symbols: α-particles single dose 100 Gy. Error bars shown represent s.e. from a single experiment. Interval **48 kbp-5.7 Mbp**: X-rays (□), α-particles (■), experimental interval **12 kbp-825kbp**: X-rays (△), α-particles (▲). Interval **12 kbp-225 kbp**: X-rays (○), α-particles (●). The values shown are reported, averaged for each group, in table 4.3 and they are also compared to those obtained with other methods in table 4.4.

controls and their sizes. In particular, Stenerlöw *et al.* showed that the linear relationship observed could be the result of a biased operation that allows the conversion from measured fractions of DNA mass to frequencies of DNA fragments, reported in eq. 2.5a, and that a fixed line slope would result from a given gel sectioning scheme. The origin of the such bias would lie in the amplification of measurements that are carried out in a region that is affected by noise, due to the sensitivity limits of the PFGE technique, as discussed in § 6.1. Several gel sectioning arrangements have been used in the experiments of this project, as indicated in § 4.3.3, although for experiments with identical gel sectioning arrangements, *i.e.* with symbols having the same abscissas in figure 4.5, data suggest that the slope of the regression lines vary significantly from experiment to experiment, which in turn suggests that the conversion to frequencies of DNA fragments using eq. 2.5a is unbiased, though this may hold only in the experimental region studied. An

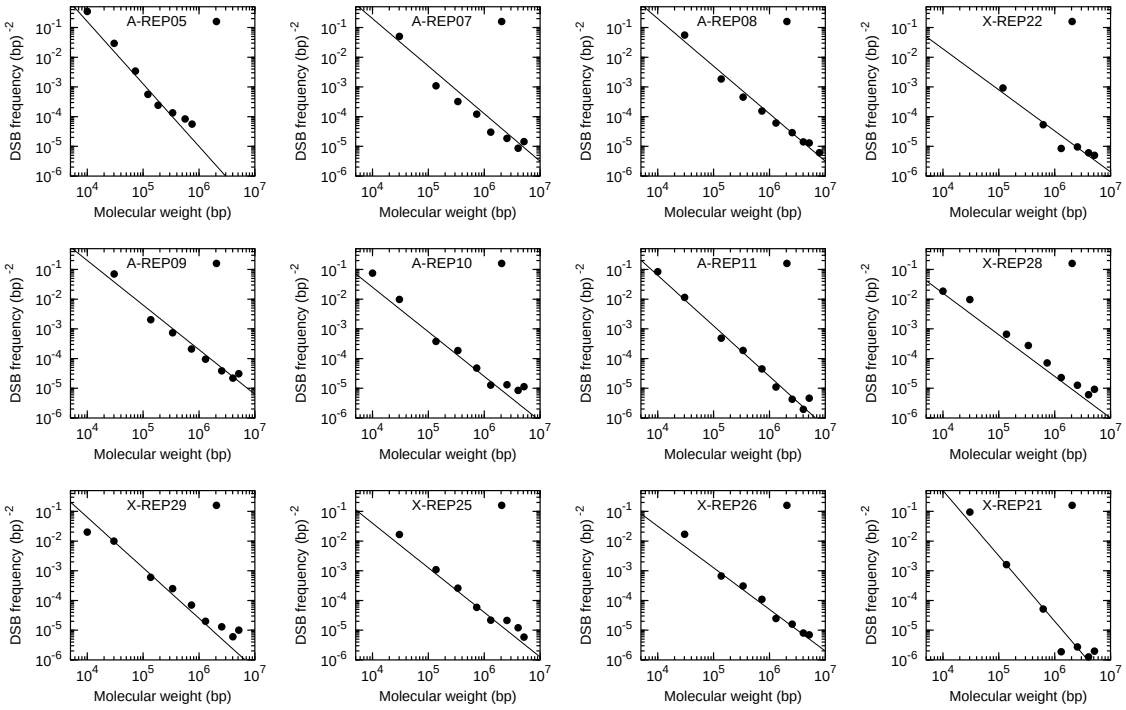

Figure 4.5: DNA fragment size-distributions measured in the unirradiated control samples of several PFGE experiments. Each panel shows the experimental frequency of DNA fragments in an independent experiment, normalised to the width of each gel section (see eq. 2.5a). The axes scales are the same on all the panels displayed for better comparison by eye of the slopes of the best-fit lines. The labels shown beginning with 'A' or 'X' refer to DNA fragmentation data in unirradiated control samples from experiments employing α-particle or X-ray irradiation.

excess of larger fragments in the 4·6-5·7 Mbp region is frequently observed, as shown in figure 4.5, compared to the linear prediction, which may indicate that extrapolations

of the linear relationship to regions of large molecular weight fragments may be error-prone and should be avoided. The fragmentation pattern above the size of the largest DNA marker resolved in the gel has been described in the BDRB method framework as consisting of 46 'virtual' chromosomes whose mass is set by cell total DNA content constraints (see § 3.2.2.3). The estimates for the slope and intercept of the best regression lines are then incorporated in the BDRB function (eq. 3.9) for non-linear regression of frequencies of DNA fragments produced after irradiation. The limit of validity for the power-law that describes the fragmentation in the unirradiated control samples is set as constant parameter, while the extrapolated total number of DSBs at a given dose is the parameter to be estimated by least-squares fitting. Figure 4.6 shows the best-fits to a number of data-sets from several independent experiments. Some experiments have

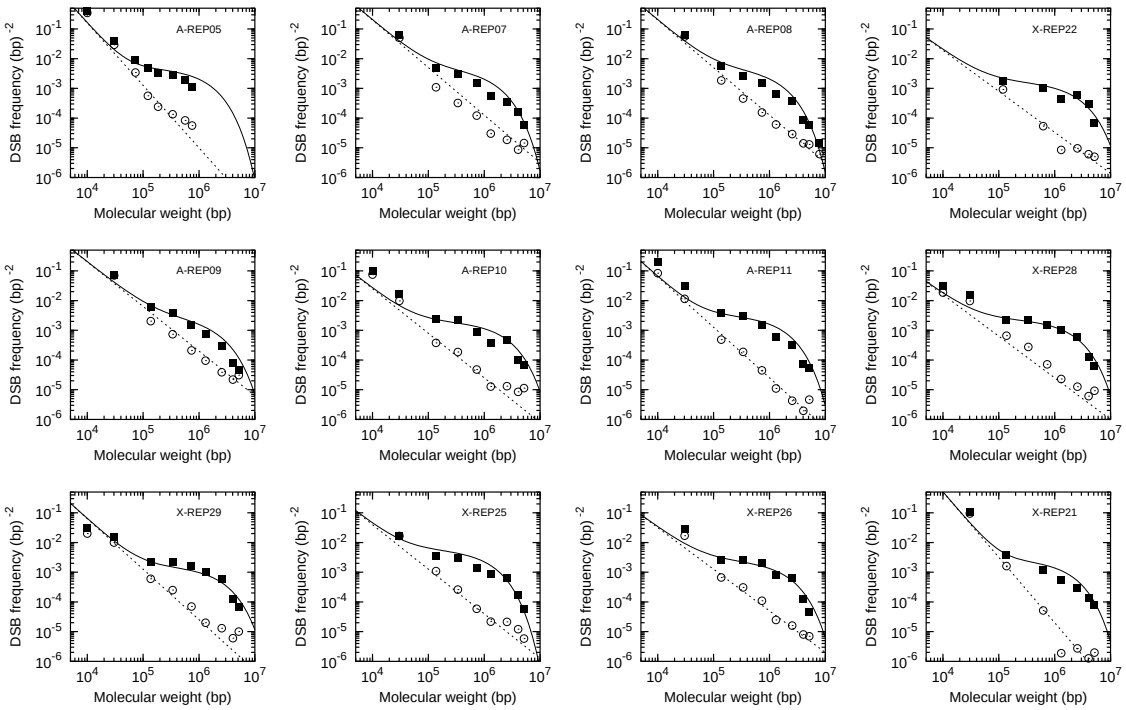

Figure 4.6: Application of the BDRB method to data from several independent experiments where a 115 Gy dose of X-rays or 100 Gy dose of α-particles was used to induce DSBs. For all panels, (■) represent single determinations for the frequency of DNA fragments, per unit base pair per cell, measured in the irradiated samples and *not* corrected for the background damage. (○) are the corresponding values measured in the unirradiated controls. Dotted lines correspond to linear regressions on the unirradiated control profiles to estimate the parameters 'A' and 'B' of eq. 3.6, needed for the non-linear regression with eq. 3.9. Solid lines are curves from the best BDRB fit restricted to data-points above 100 kbp. The labels shown beginning with 'A' or 'X' refer to DNA fragmentation data from α-particle or X-irradiation experiments, respectively.

provided measurements of DNA fragmentation profiles at multiple dose values, in which case the BDRB method has been applied to the analysis of data for each individual dose. The results of the BDRB regressions in these experiments where measurements are available at multiple doses, for the same experiment, have been plotted *vs* dose, and a linear regression has been carried out (assuming linearity of DSBs induction with dose, forcing the lines to pass through the origin of the axes on the plots, *i.e.* A=0) to calculate the total DSB yield per cell and per Gy. This is shown in figure 4.7 for one typical experiment in which samples have been irradiated with an X-ray dose ranging from 11·5 to 230 Gy. Five different dose values have been used for this multi-dose BDRB analy-

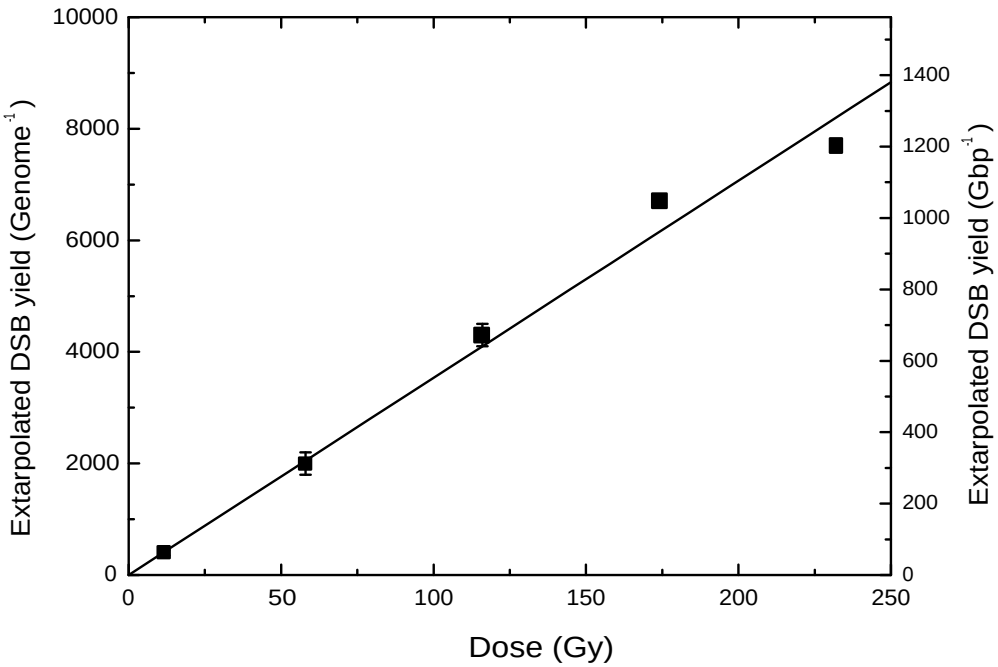

Figure 4.7: An example of linear regression on BDRB results, evaluated on data at a fixed dose, *vs* dose, for the *same* experiment. Each of the (■) symbols with error bars shown (visible where larger than the symbols) is the estimate, with its standard error, obtained applying the BDRB method on a data-set at a fixed dose, as shown in figure 4.6. After data from the same experiment have been analysed at the various dose points available, the BDRB estimates are plotted *vs* the corresponding dose value, and a linear regression is carried out to estimate the breakage yield per unit dose. For the experiment shown, where X-rays have been used to induce DSBs, the breakage yield was estimated as (35·3 $\pm$ 1·2) DSB Gy^{-1} cell^{-1}. This value, together with the results from other experiments that have been analysed in the same way, is plotted in figure 4.8.

sis, per separate experiment (10, 50, 100, 150, 200 Gy for α-particles and 11·5, 57·5,

115, 173, 230 Gy for X-rays). Figure 4.8 shows the results of the BDRB regressions on each of the experiments carried out in this study, expressed as total extrapolated DSB yields per Gy and per cell (or per Gbp on the right y-axis). A different symbol is used in figure 4.8 for each radiation quality and each of the three molecular weight regions in which the method has been applied. Further, a different symbol is used to distinguish between experiments that are analysed with the BDRB method at a single-dose *vs* those analysed at multiple dose values, as shown for one experiment in figure 4.7, given the same radiation quality and the same molecular weight region analysed.

Results of DSB yields obtained with the BDRB method, plotted in figure 4.8 have then been averaged, grouping experimental data for X-rays and α-particles, in each molecular weight region. For the averaging procedure, results from experiments analysed at a single dose value have been grouped together with experiments that have been analysed at multiple dose points (for the same radiation quality and same molecular weight region analysed) since no evidence has been found for significant difference between the DSB yields estimates from one group of experiments over the other. These averaged estimates for the total extrapolated DSB yields obtained with the BDRB method are summarised in table 4.3, expressed as mean $\pm$ s.e.m. together with the calculated RBE values for initial DSB induction.

BDRB analytical method - Yields of DSB·Gy^{-1}·Gbp^{-1}

Radiation Quality	225 kbp-5.7 Mbp	225 kbp-825 kbp	225 kbp-285 kbp
α-particles	7·0 $\pm$ 0·3 (■,♦)	7·6 $\pm$ 0·9 (▲,▼)	9$\pm$2 (●)
X-rays	5·5$\pm$0·4 (□,◊)	4·9$\pm$ 0·2 (△)	6·2 $\pm$ 1·4 (○)
α-particles RBE	1·3$\pm$0·1	1·6$\pm$0·2	1·5$\pm$0·5

Table 4.3: Results obtained with the BDRB method applied to several data from independent experiments. Each experiment has provided data that have been analysed in one of the three molecular weight regions shown in the table. Results of the BDRB analysis on homologous experiments have been then averaged, and the mean $\pm$ s.e.m. are shown in separate columns in the table. Results from individual experiments, in the same experimental regions reported in this table, are plotted in figure 4.8. Symbols shown in parentheses here indicate that the average values are obtained from homologous experiments that are marked with the same symbols in figure 4.8.

Table 4.4 summarises the DSB yields estimated with all the three analytical methods of DSB quantification described.

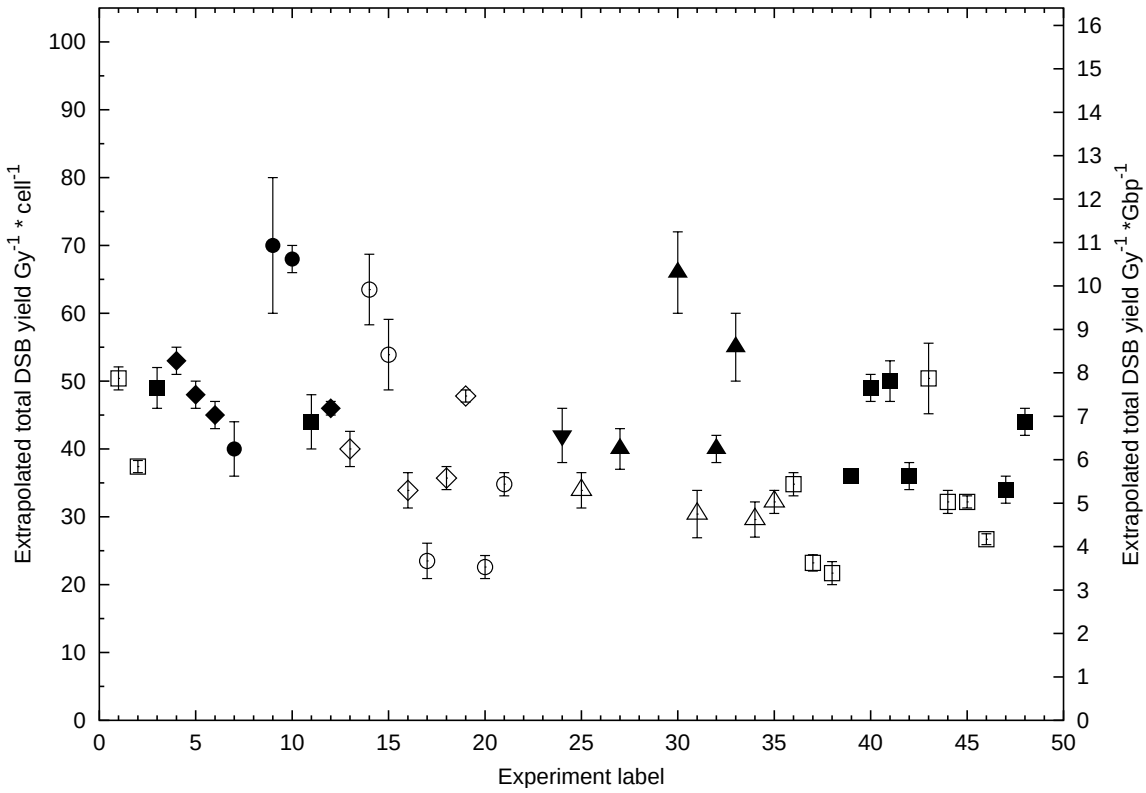

Figure 4.8: Results of the BDRB regression analysis performed on several independent experiments. Symbols shown, with error bars, are best value $\pm$ s.e. from regression analysis with eq. 3.9 carried out on 42 independent experiments. Full symbols show extrapolated total yields of DSBs from 100 Gy α-particle irradiation data, open symbols relate to 115 Gy, X-rays data. Experimental interval **225 kbp-5.7 Mbp**: single BDRB regression of X-ray data (□), or BDRB X-ray dose-response (◇) as shown for one example in figure 4.7, single regression of α-particles data (■) or α-particles BDRB dose-response (⧫). Experimental interval **225 kbp-825 kbp**: single BDRB regression of X-ray data (△), α-particles BDRB single regression (▲), α-particles BDRB dose-response (▼). Experimental interval **225 kbp-285kbp**: X-ray BDRB dose-response (○), α-particles BDRB dose-response (●). Results obtained from the BDRB analysis shown in this plot are averaged in separate groups and summarised in table 4.3.

Summary of total extrapolated DSB yields estimated using analytical methods

	DSBs·Gy^{-1}·Gbp^{-1}					
	FAR		BDRB		Direct quantification	
Radiation	$<$5·7 Mbp	$<$48 kbp	0·225–5·7 Mbp	225–285 kbp	0·048–5·7 Mbp	12–225 kbp
α-particles	(3·4$\pm$0·2)	(13$\pm$1)	(7·0$\pm$0·3)	(9$\pm$2)	(5·6$\pm$0·2)	(10$\pm$ 2)
X-rays	(4·5$\pm$0·3)	(10$\pm$1)	(5·5$\pm$0·4)	(6·2$\pm$1·4)	(4·7$\pm$0·2)	(6$\pm$2)
RBE	(0·76$\pm$0·07)	(1·3$\pm$0·2)	(1·3$\pm$0·1)	(1·5$\pm$0·5)	(1·19$\pm$0·07)	(1·6$\pm$0·5)

Table 4.4: Total yield of DSBs per cell, for X-rays and α-particles, calculated from data analysis with the FAR approach, the BDRB method and the direct quantification of DSBs, adapted from the previous tables. For each method, two estimates for the DSB yields are shown, with their standard error for the FAR method and with s.e.m for the 'direct quantification' and the BDRB method. The smaller DNA fragments were contributing less than the larger fragments to the first DSB yield estimate, shown on the left, for each method. For the second estimate, the analysis was more focused on the contribution of the smaller DNA fragments.

4.4 DNA fragmentation analysed with numerical methods

Experimental measurements of initial DNA fragmentation after exposure to α-particles and X-rays analysed in § 4.3 have also been compared to the computer simulations described in § 3.3.1.1. Before the Monte Carlo simulations were run to fit experimental data, some other simulations were run to test the quality of the random number generator, the 'core' of all the computer simulations in this study. The Mersenne Twister random number generator that has been employed for all the numerical simulations presented in this chapter and in chapter 5 has passed a long series of very stringent quality tests of randomness which are not repeated in this study. Nevertheless, a few tests have been carried out on the Mersenne Twister random number generator to show its fidelity in producing Poisson deviates, which have been largely employed in the computer simulation module dedicated to clustering of DSBs on DNA (see § 3.3.1.1). In fact, a random number generator chosen earlier in this project had to be rejected, since its low accuracy resulted in errors in the number of DSBs that were set to be distributed in the DNA. Figure 4.9 shows the frequencies f_i that have been accumulated after 100,000 Poisson deviates are generated with mean value μ ranging from 0.0 to 3.0, displayed in four different panels, compared to the theoretical Poisson probability distribution $P_\mu(x)$ for the same mean value. Also shown in each panel is the average value $\bar{x} = \sum_i f_i \cdot x_i$ calculated from the simulated f_i values, compared to the theoretical mean value μ enclosed in square brackets. For all the panels in figure 4.9 it is evident that Poisson deviates are generated with accuracy such that deviations are in the order of 0.1%.

For the computer simulations of DNa fragmentation to be compared to PFGE data from independent experiments, measurements of DNA mass distributions in single lanes of PFGE gels are used for the computer-generation of a background collection of DNA fragments in single cells. Such a collection of DNA fragments is generated stochastically, according to the method illustrated in figure 3.7, conforming to the experimental frequency histogram measured in the unirradiated control samples and used as input data to the computer-simulation. The fragment size frequency histogram reflecting the DNA computer-simulated fragmentation in unirradiated controls is in excellent agreement with the experimental data (compare for example the experimental control fragmentation pattern and the computer-simulated pattern in figure 4.10). After a collection of background double-stranded fragments is stochastically generated for one cell, the computer simulates radiation injury by allocating DSBs according to the clustering mechanism that is described in figure 3.11. The construction of the background fragmentation pattern and the introduction of radiation-induced DSB is repeated for 100 cells (see § 3.3.1.1 for a

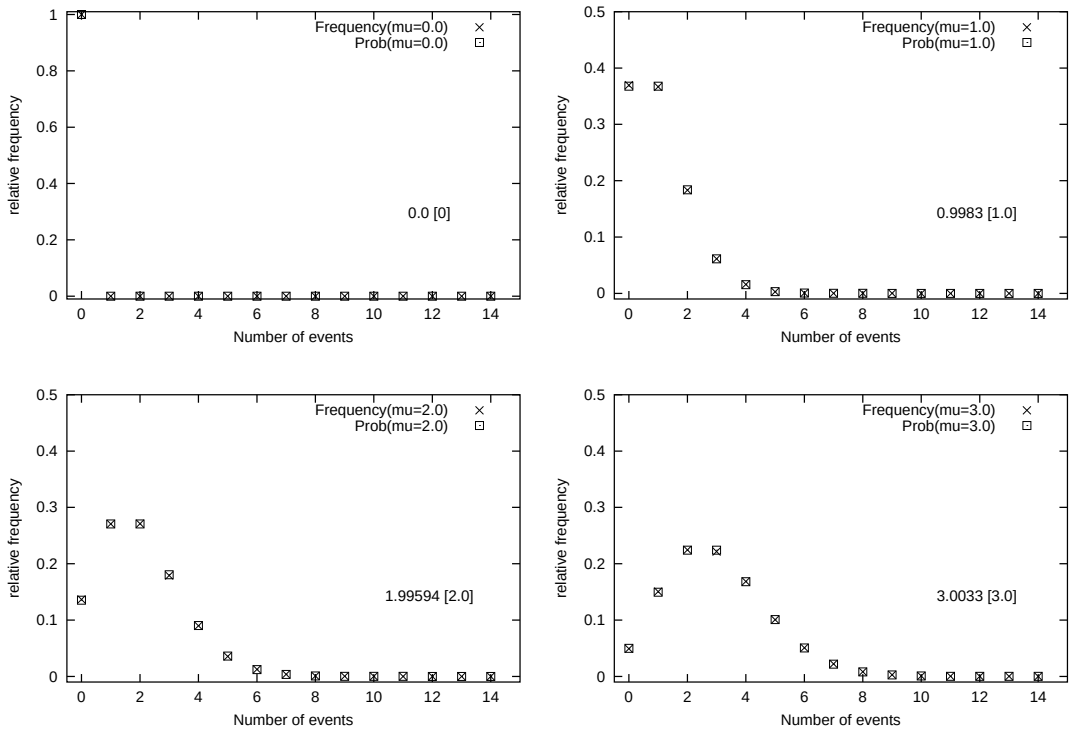

Figure 4.9: Quality test of the Mersenne Twister random number generator for the production of Poisson deviates. Each panel shows the frequency histogram collected after simulation of Poisson deviates for different average values μ (X), compared to the corresponding expected theoretical Poisson distributions (□). The numbers reported in each panel are the mean values evaluated from the frequencies, $\sum_{i=1,100000} f_i \cdot i$, compared to the expected mean value shown in square brackets.

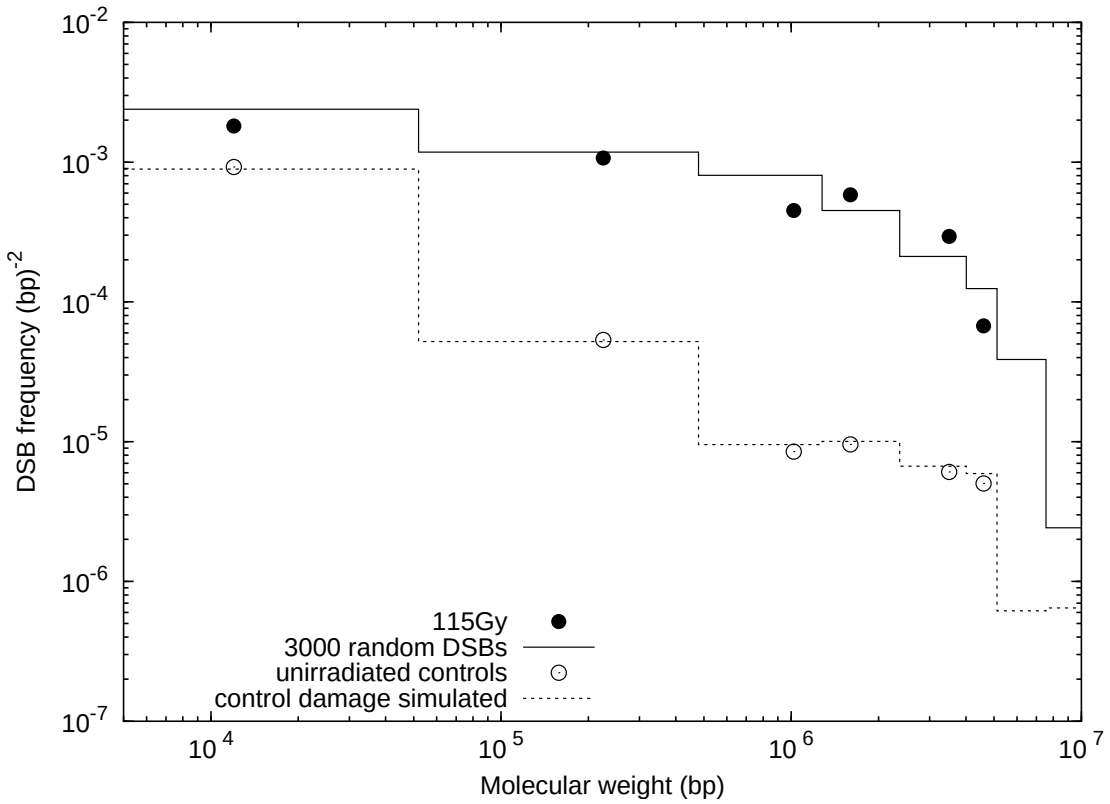

Figure 4.10: Application of the numerical extension of the BDRB method for the quantification of the DSB yield in one particular experiment, where samples have been X-irradiated with 115 Gy. (○) experimental fragment-size frequency histogram in unirradiated controls. (●) fragmentation profile observed after 115 Gy. The dashed line represents the fragment size distribution built from the computer-simulation of background damage in single cells. The solid line is the best fit of the DSB induction simulation to the particular experimental data-set shown.

discussion on the number of cells that have to be simulated in order to limit the uncertainties to below or equal the experimental error) and a fragment-size frequency histogram is finally built and compared to the experimental fragmentation pattern. This comparison is made quantitative by evaluation of the χ^2 for the goodness of the fit for several different settings of the computer-model parameters. According to the least squares method, the result of the computer-simulation of DNA fragmentation is the set of model parameter values ($\mathcal{N}_{\mathrm{cl}}, \nu, \varrho, N$, see § 3.3.1.1) that minimises the χ^2 for the goodness of the fit to the experimental frequency histogram. Since both the experimental and computer-simulated frequencies of DSBs span over several orders of magnitudes (see for example the y-axis scales in figures 4.10 and 4.11) and departures of the model from the experimental data at larger frequencies of DSB values would weigh more in the computation of the χ^2, this is evaluated on the logarithms of the frequencies, for a χ^2 minimisation on 'apparent' scales:

$$\chi^2 = \sum_i \frac{\left[\log\left(f^i_{\mathrm{exp}}\right) - \log\left(f^i_{\mathrm{th}}\right)\right]^2}{\left|\log\left(f^i_{\mathrm{exp}}\right)\right|} \tag{4.1}$$

where f^i_{th} and f^i_{exp} are the computer-simulated and the experimental frequency of DNA fragments values for each gel section i. It should be noticed that the χ^2 is evaluated on the fragmentation patterns that are consequence of *both* radiation and background breaks, as also shown for data analysis with the analytical version of the BDRB method (§ 4.3.4). It is then ideal to have the best possible agreement between the experimental and the computer-simulated background fragmentation patterns before proceeding with simulation of radiation-induced breakage, or the χ^2 evaluation for the goodness of the fit would be biased by the inaccurate description of the background DNA fragmentation. It is evident from the fidelity of the reconstruction of the background fragmentation patterns in figure 4.10 and figure 4.11 that the numerical extension to the BDRB approach provides greater fidelity than its analytical version which did not have the same flexibility in the reproduction of the background pattern (see figure 4.5 for comparison).

The best fit of the computer-simulation of initial radiation-induced DNA fragmentation to a particular experimental X-ray data-set is shown as a fragment size frequency histogram in figure 4.10. For the particular data set shown, the result of computer-simulated radiation-induced DNA breakage suggests no clustering of double-strand breaks. The best fit of the computer-simulation yields 3000 randomly and independently located DSBs. Error bars are not displayed since the points shown in figure 4.10 are single determinations in one particular experiment. Nevertheless, it is estimated that a relative error in the order of 10% is associated with each data point (calculation not shown). Although confidence intervals for the estimates of DSB yields (and all the other computer-model parameters of DSB induction by radiation) are not provided by the simulation from the

analysis of single experiments, these can be obtained by averaging the results for the model parameters values estimated in several independent experiments.

An example of the application of the computer-simulation of clustered breakage on an α-particle data-set is shown in figure 4.11. In this case, the best fit of the computer-

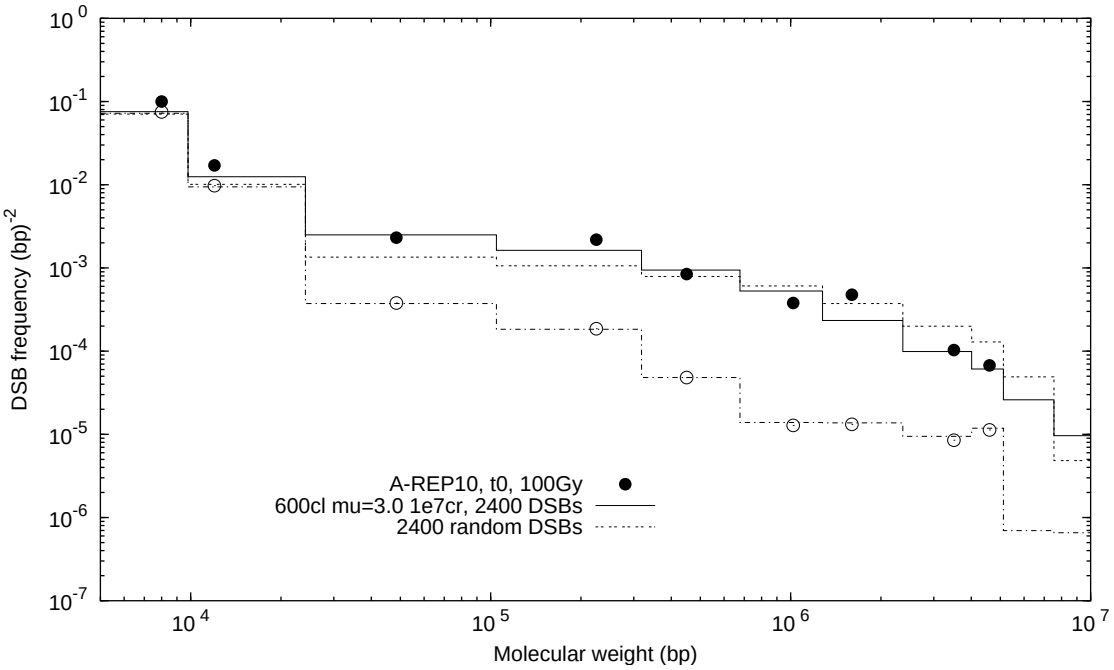

Figure 4.11: Simulation of radiation-induced DNA breakage after α-particle irradiation in one particular experiment. (○) experimental fragment-size frequency histogram in unirradiated controls. (●) fragmentation profile observed after 100 Gy. The dashed-dotted line represents the fragment size distribution built from the computer-simulation of background damage in single cells. The solid line is the best fit of the DSB induction simulation to the particular experimental data-set shown (2400 DSBs, distributed in 600 clusters having average multiplicity 3). The dotted line shows the fragmentation pattern due to 2400 randomly-distributed breaks.

simulation of clustered breakage predicts that 600 clusters ($\mathcal{N}_{\rm cl}$) have been randomly and independently distributed in the genome, each having on average 3 additional DSBs (ν) randomly and independently located within a radius that varies for each cluster, but that is always below a maximum value (ϱ) estimated at 10 Mbp. A fragmentation pattern produced by random breakage for the same total number of DSBs predicted in the DSB clustering simulation, in this case 2400 in total, is also shown for comparison in figure 4.11. It is evident that the same number of clustered DSBs results in less Mbp-sized DNA fragments and relative excess of smaller DNA fragments compared to randomly-located DSBs, overall resulting in better agreement with the experimental fragmentation pattern. Computer-simulations of clustered DNA breakage after exposure to radiation of varying LET have been run for several independent experiments. Figures 4.12 and 4.13

show the best computer-simulation fits to a collection of X-rays experimental data-sets of DNA fragmentation after 115 Gy and α-particle data-sets after 100 Gy, respectively. The computer-simulations of DSB clustering have also been run to fit data of experi-

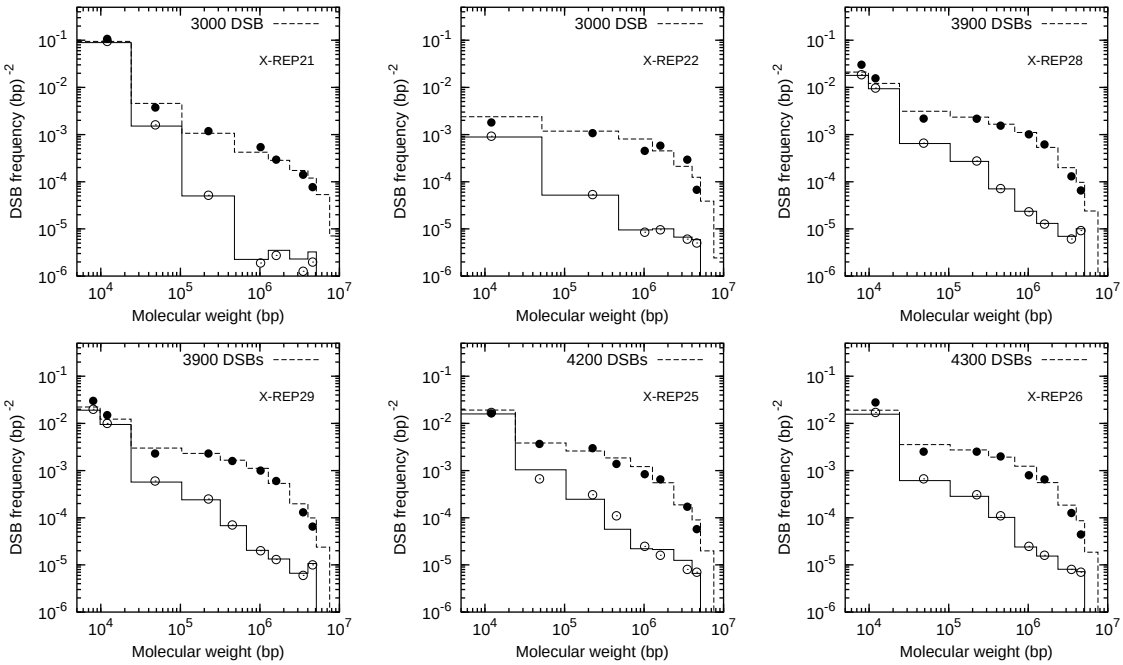

Figure 4.12: Results of computer-simulations of clustered breakage applied to several independent X-ray experimental data-sets of fragmentation after a dose of 115 Gy. In all the panels shown, symbols are experimental determinations and the lines are computer-simulations

ments where initial DSB induction has been assayed at several different dose values, as was shown for the BDRB analytical method in figure 4.7. An example of this type of analysis is shown for X-ray-induced DNA fragmentation in figure 4.14. With the exception of the fit to the 57·5 Gy data-set, where 1500 independent clusters are predicted with an average multiplicity of 0·5 and a maximum cluster radius of 900 kbp, the fit to all the data-sets shown in figure 4.14 suggests random breakage for the particular experiment analysed.

Application of the DSB clustering Monte Carlo procedure to data-sets relative to different doses also serves as a test of the clustering model employed. When applying the computer-simulations of DSB clustering to the analysis of initial radiation-induced DNA fragmentation, it is interesting to investigate the dependence on dose of the computer model parameters that result from the best fit to the experimental data. Although it would be expected that the total number of DSBs induced is linearly related to radiation dose, it remains to be seen whether the other model parameters specific to the DSB clustering are also a function of dose. For example, it should be expected that the number of inde-

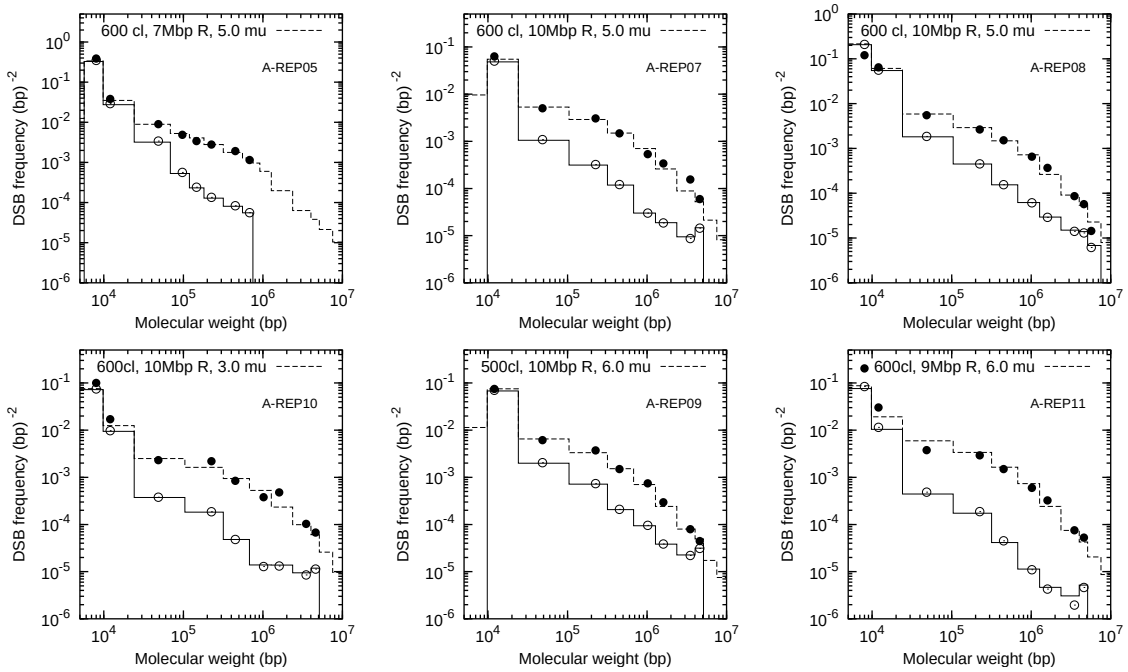

Figure 4.13: Results of computer-simulations of DSB clustered breakage applied to several independent α-particle data of DNA fragmentation after a dose of 100 Gy. For each panel, the best-fit model parameter values $\mathcal{N}_{\rm cl}, \varrho, \nu$ are also shown.

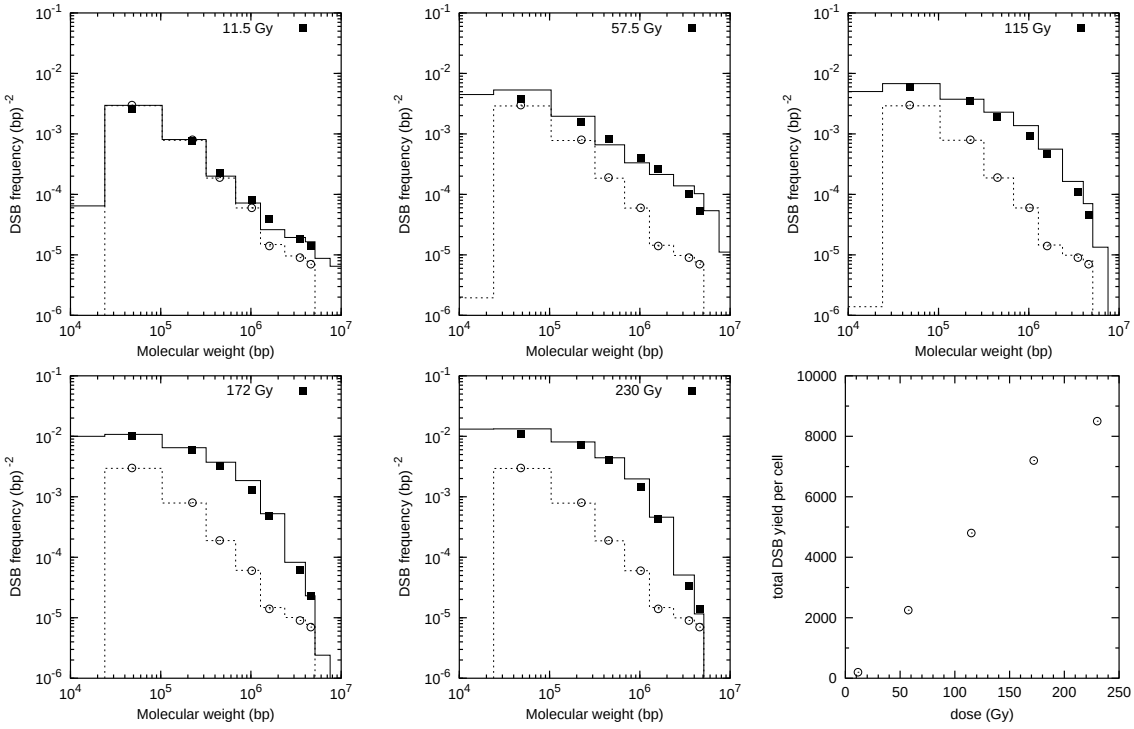

Figure 4.14: Computer simulations of DNA fragmentation in one experiment at several different radiation dose values. Samples have been irradiated at 11·5, 57·5, 115, 172 and 230 Gy with X-rays. The bottom-right panel displays the result for the total DSB yield estimated from the data-sets at different dose values plotted in the other five panels.

pendent clusters is dose-dependent, while the average cluster multiplicity should remain constant, if all the breaks in one cluster are consequence of the damage induced by the same charged-particle track. These conditions should hold as long as independent clusters remain distant from each other, a condition that may not be satisfied at very high doses, when clusters induced by different charged-particle tracks may overlap and not be distinguished any more. In this case it could be expected that the cluster multiplicity ν should rise, as well as the cluster radius, although the number of independent clusters should fall since some would have merged together and be counted as a single cluster. This is not observed for the X-ray data where the DSB induction mechanism appears to be random. Results of the application of the DSB clustering analysis at several dose values on a particular α-particle experiment are shown in figure 4.15 as fragment size frequency histograms that best fit the experimental data. The dose-dependence of the

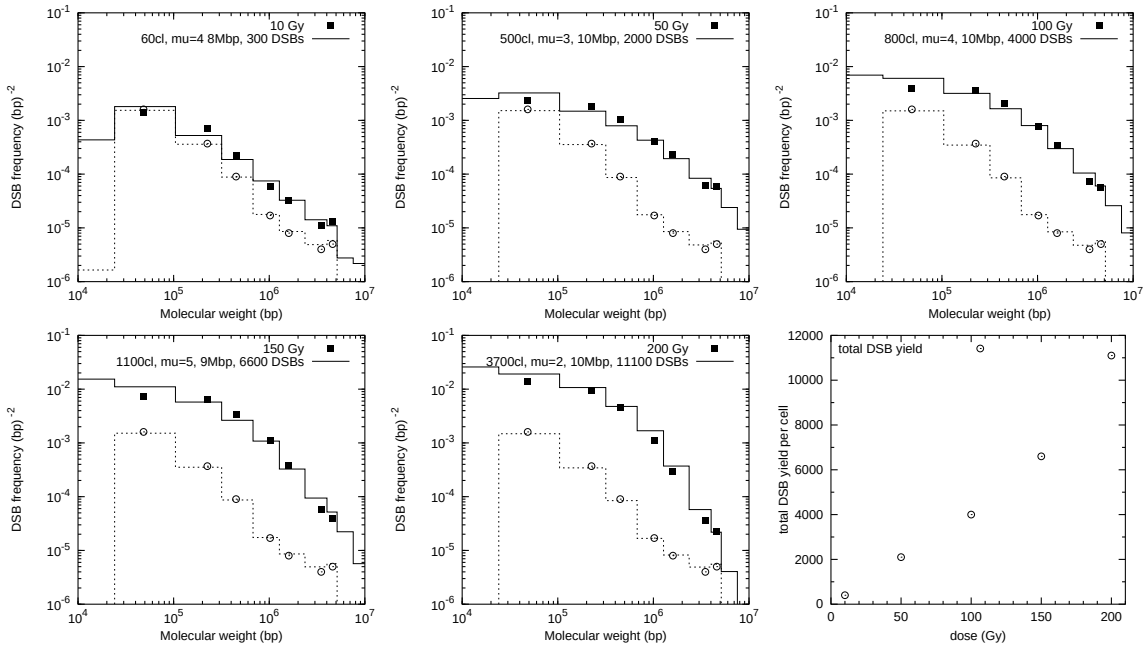

Figure 4.15: Computer simulations of DSB clustering for one experiment at several different radiation dose values. Samples have been irradiated at 10, 50, 100, 150 and 200 Gy with α-particles. The bottom-right panel displays the result for the total DSB yield estimated from the data-sets at different dose values plotted in the other five panels. The dose-dependence of the best fit computer model value-parameters is displayed in figure 4.16. Focusing on the 10 Gy data set, top left panel, '60cl, mu=4, 8Mbp, 300 DSBs' means $\mathcal{N}_{\rm cl}$, ν=4, ϱ=8 Mbp, for a total of $60 \times (4+1) = 3000$ DSBs.

computer-model parameters relative to the best fits in figure 4.15 is shown for each parameter in a separate panel in figure 4.16. With the exception of the 200 Gy data-set, where the result of the best fit appears to be anomalous, perhaps going in the opposite direction of what predicted above for high doses, the total DSB yield and the number of

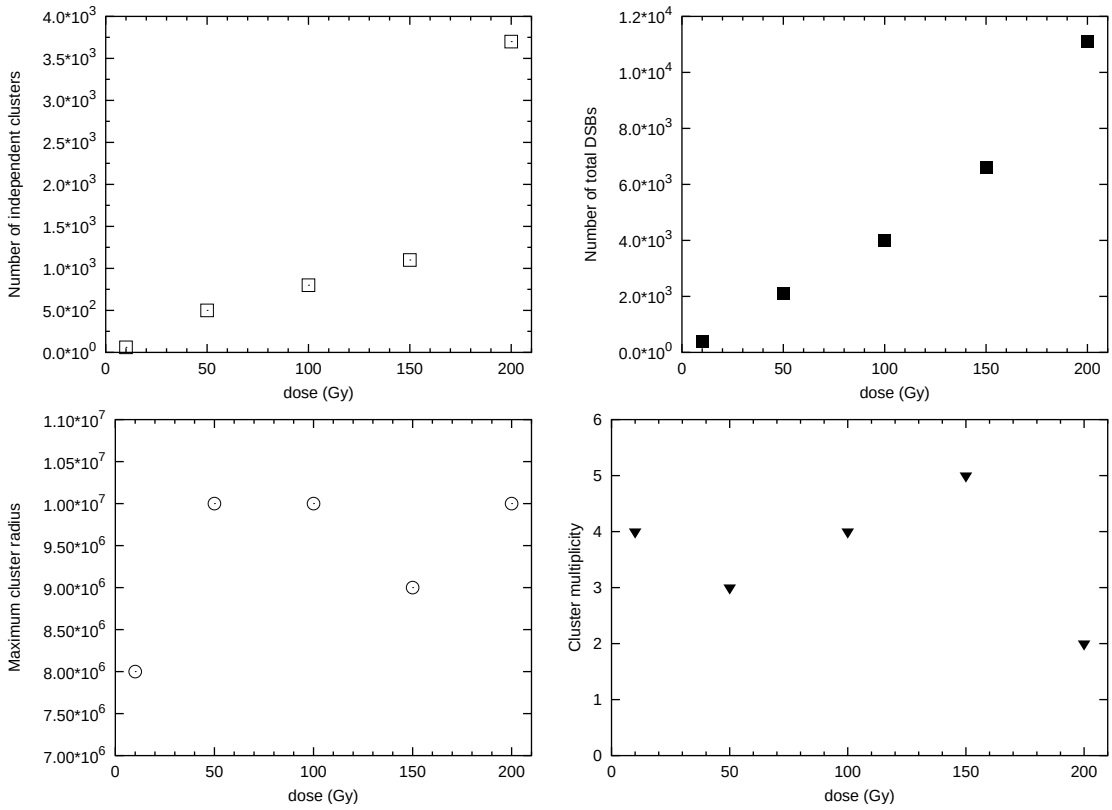

Figure 4.16: Dose-dependence of the computer-model parameters evaluated from the best fit shown in figure 4.15 for one particular α-particle experiment.

independently located clusters increases linearly with dose. Conversely, neither the average cluster multiplicity nor the maximum cluster radius appear to be function of dose, at least up to the maximum dose employed. Results of the computer-simulation of initial DSB induction by α particles and X-rays are summarised in table 4.5, averaged from those shown in figure 4.12 and 4.13. Since the computer-simulations suggest that X-rays induced double-strand breaks are not clustered, values for the computer model parameters that characterise DSB clustering have been omitted in table 4.5 for X-rays. RBE values for α particles are consequently only shown for the total DSB yield per unit dose.

Summary of DSB clustering properties

Radiation	DSBs·Gy^{-1} per cell	$\mathcal{N}_{\mathrm{cl}}$·Gy^{-1} per cell	ν	ϱ (Mbp)
α-particles	35±6	5·7±0·5	5±1	9·3±1·2
X-rays	32±5	–	0	–
RBE	1·1±0·2	–	–	–

Table 4.5: DSBs yields and clustering properties evaluated after the application of the computer simulation of radiation-induced initial fragmentation to six independent experiments per radiation quality as shown in figures 4.12 and 4.13. $\mathcal{N}_{\mathrm{cl}}$ is the number of independent clusters induced per unit Gy, ν is the expected number of extra correlated breaks in one cluster (multiplicity) and ϱ is the maximum radius of each cluster, varied stochastically during the simulation (see also § 3.3.1.1 for a detailed description of the model parameters). Values shown are means and standard errors (n=6).

4.5 Computer-simulation of a low-dose PCC experiment

In PCC experiments with cells in G1 phase of the cell cycle, chromatin condensation is achieved after irradiation by fusing the cells that have been irradiated with a mitotic cell population (Pantelias and Maillie, 1983). After cell fusion and chromosome condensation are complete, which normally takes about one hour, one can count the number of excess fragments to the number of intact chromosomes of the two cell types combined together. During this time, repair of DNA damage cannot be completely prevented, although there are methods available that seem to limit the extent of repair and reveal the presence of a fast kinetics phase (see for example Durante *et al.*, 1998b).

The number of excess PCC fragments, as measured with PCC, has often been used as a measure of initial yield of DNA DSBs. This number is typically reported as 6 excess fragments per cell per Gy of low-LET radiation, with RBE values around 2 for α-particles (Bedford and Goodhead, 1989), although a recent study employing ions up to 140 keV μm^{-1} show substantially constant yields of initial excess fragments (Durante

et al., 1998a). Estimates for yields of initial PCC fragments are hence significantly lower than those obtained with PFGE, which for this study only are summarised in table 4.5 (see table 6.1 for comparison to results from published works). The discrepancy is normally attributed to two factors:

1. PCC can only detect fragments above a threshold size, as smaller fragments are invisible under a microscope. On the other hand, PFGE allows measurements of DNA fragmentation down to fragments sizes that are much smaller than those visible with PCC. A higher DSB yield should be observed from measurements in a wide molecular weight range.

2. Unwanted repair during chromosome condensation in PCC eliminates a fraction of the initial DSBs, whereas with PFGE the uncontrolled repair time is generally less than a few minutes.

Results of the analysis of initial DNA fragmentation, obtained from the best fit of the computer simulations of PFGE data in this study, provide estimates of DSB yields and distribution properties for both X-rays and α-particles (table 4.5). These estimates have been obtained at high doses, but if one assumes linear proportionality with dose, they could be used to simulate the initial DNA fragmentation in cells exposed to low doses of ionising radiation, extrapolating PFGE estimates to the PCC dose region. Since the computer simulations have been tested in the molecular weight region that can be studied with PFGE, making predictions in the PCC fragment size region is an additional extrapolation. For both radiation qualities, that is for different DNA fragmentation mechanisms, one could provide an estimate of how many fragments are *missed* in an ideal PCC experiment, *i.e.* in the hypothesis that no unwanted repair takes place at all, so that PCC fragments detected reflect the initial DNA fragmentation. However, the following extrapolated results are only qualitative, since for low doses some of the approximations made in the design of the computer-simulations may not hold. Firstly, chromosomes are assumed here to have all the same average size. According to Charlesby (1953), the initial distribution of intact fragments does not determine the final distribution *i.e.* after radiation, provided that *each* of the original fragments is hit at least four or five times. For low doses, and especially for clustered breakage, some chromosomes may remain intact and would be found again in the final fragment-size distribution. Secondly, it cannot be guaranteed that the proportionality between dose and number of independent clusters can be extrapolated to low doses. Statistical fluctuations in the number of charged-particle tracks/independent clusters may in fact dominate in the low-dose region.

In the attempt of linking PFGE to PCC results, a low dose PCC experiment in which formation of excess fragments can be measured has been computer simulated, assum-

ing 20 Mbp or 5 Mbp as the threshold size for a fragment to become visible under PCC conditions. These choices represent two likely extremes based on personal communications by several investigators. According to Kodama *et al.* (1997), this threshold size may be in fact $\geq$10 Mbp. Additional frequency histograms are outputted by the computer simulations of initial DNA fragmentation, the same that were run in § 4.4, that counts the number of fragments larger or smaller than 20 Mbp (5 Mbp). For a given simulated radiation dose, the number of fragments larger than 20 Mbp (5 Mbp) is compared to the total number of fragments, which relates directly to the total number of DSBs induced per cell. Results of this simulation are shown in figure 4.17 for the dose range 1-7 Gy. In these simulations it has been assumed that there is no background damage to DNA, as opposed to simulations of PFGE. At 0 Gy, one has 46 chromosomes of average size 139 Mbp. It is shown in figure 4.17 that for both radiation qualities the number of breaks

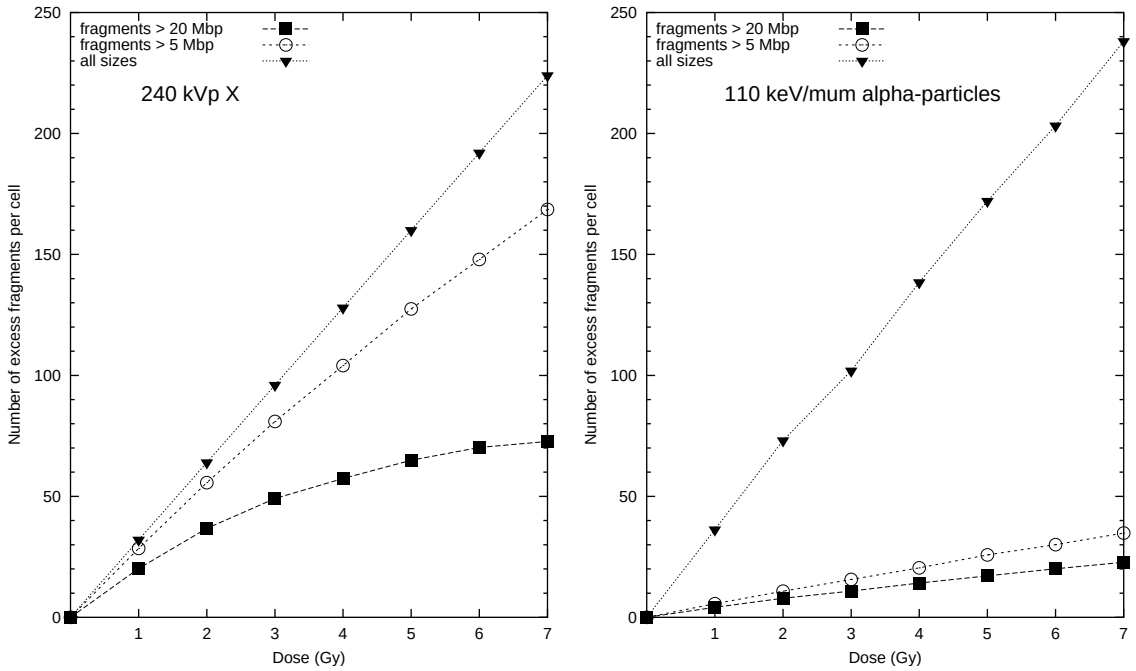

Figure 4.17: Simulation of a dose-response PCC experiment

detected via observation of PCC fragments is only a fraction of the number of breaks introduced in the entire genome. For X-rays, left panel, the yields of PCC visible fragments $\geq$20 Mbp is first increasing linearly, then it reaches a plateau. At this point, the average number of breaks induced per chromosome is about five, so fragments whose size falls below 20 Mbp may be present in significant proportion to the total fragments, so that many fragments are mimssed. The yield of all the fragments is otherwise linear, since it has been assumed that a linear relationship between number of breaks and dose holds. For 110 keV/μm α-particles (right panel in figure 4.17) the total fragments yield

also increases linearly, and is also steeper, since the RBE for total DSBs was estimated to be greater than one in these simulations which employed PFGE-based estimates (see table 4.5). The line shown for the yield of fragments of any size is slightly irregular since, for each simulated dose, the number of independent clusters to be located has been rounded to the nearest integer. For example, at 2 Gy one should have 5.7$\times$2=11.4 independent clusters, but since this value in the simulation has got to be an integer it was rounded to 11. Fewer α-particles induced PCC visible fragments are predicted than for X-rays, for both the size thresholds used. Due to the DSB clustering properties of α particles, at low doses there will be several chromosomes that have not been hit at all, whereas other chromosomes may have one cluster with an average of six breaks spanning a region of size 2$\times$9 Mbp at maximum. The average size of a fragment inside a DSB cluster decreases to below 5 Mbp, so that most of the α-particle induced fragments are not visible in PCC, according to this simulation.

The non-linear behaviour for the yield of PCC 'visible' fragments under X-irradiation implies that the RBE value for DSB production is dose-dependent, but more importantly it is predicted to be always smaller than one, in disagreement with other published results (Badie *et al.*, 1995; Nasonova *et al.*, 2001). Perhaps the very fast rejoining phase, normally not detected in PCC as mentioned earlier, accounts for a major fraction of the low-LET induced breaks than for high-LET, so that after the fast phase is complete a major fraction of low-LET induced breaks has been removed, compared to the high-LET induced breaks. The presence of a very fast rejoining phase would be also in support of the hypothesis that DSB yields estimated from PFGE are significantly higher than PCC yields, due different uncontrolled repair times in the two techniques. Fast rejoining kinetics phase may also incorporate heat-labile sites (HLSs), which may be detected in PFGE as DSBs, but undetected in PCC, since with the latter technique there is more time for repairing them.

Perhaps also the conditions for extrapolating PFGE data to predict the outcome of a PCC experiments are not satisfied. The computer simulations cannot be tested to the experimental data available here for clustering of damage involving distances that are larger than 10 Mbp, the maximum size of fragments that are succesfully extracted in the gels. If a single particle track intersected a single chromosome territory twice, with the sites of clustered damage separated by, for example, 50 Mbp, then this would fit PFGE data at high doses just as well as if two clusters were in separate chromosome territories. Nevertheless, this would make a substantial difference in a PCC experiment, since the formation of a 50 Mbp fragment would be detected, in principle, and the yield of α-particle induced fragments would increase along with the RBE value for DSB induction. If this was the case, the computer-modelled DSB clustering procedure

may need refinement to account for single-track multiple clustering events on the same chromosome, before carrying out an extrapolation to the PCC dose and fragment size region. Figure 4.18 shows the computer-simulated yield of fragments that are smaller

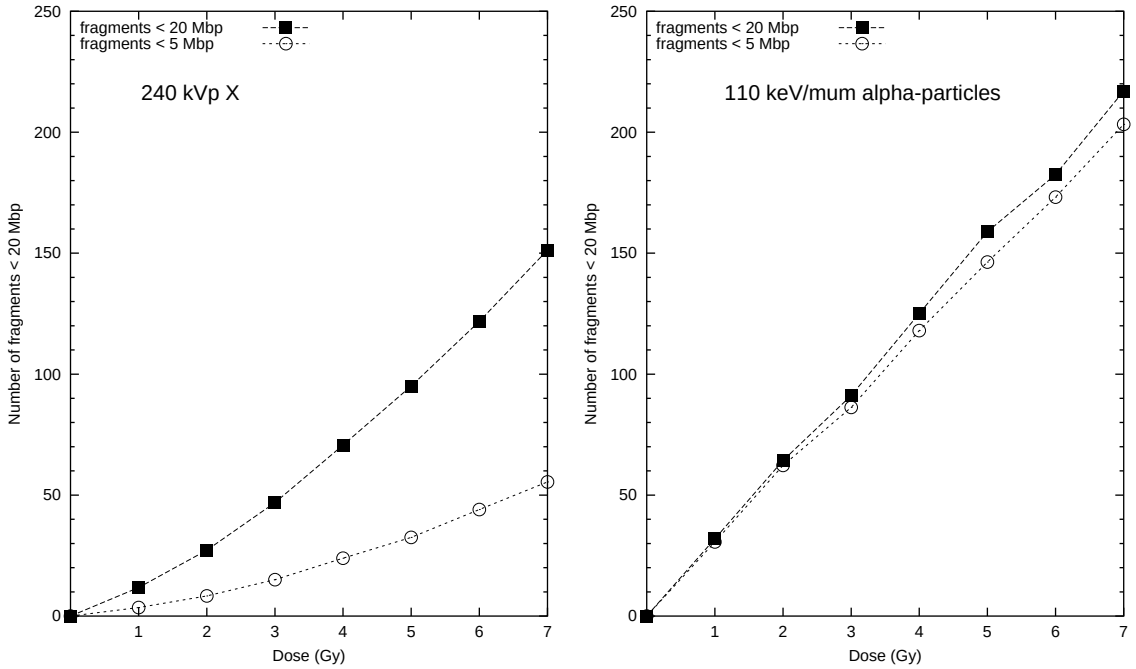

Figure 4.18: Simulation of a dose-response yield of fragments that are not detectable with PCC, when the critical size is either 20 Mbp or 5 Mbp.

than 20 Mbp or 5 Mbp, *i.e.* those that are assumed to be invisible in PCC. It is shown in the right panel that α-particles produce many more small fragments than X-rays, whose 'excess' visible fragments are shown in the left panel, and also that there is a linear dose-component for α-particles, whereas for X-rays this seems to be more quadratic. Since the cluster radius is about 9 Mbp for α-particles in these simulations, each cluster shall contribute to the formation of an average of 5 fragments that are all smaller than 20 Mbp, although some may be occasionally larger than 5 Mbp. Since it is assumed that the yield of independent clusters is proportional to the dose, small fragments also are expected to be formed linearly with dose. Conversely, X-rays produce randomly-distributed DSBs and it takes two independently located breaks ($\propto D^2$) to form fragments smaller than 20 Mbp or 5 Mbp. A linear component for the formation of a small fragment is also expected from location of a DSB near a chromosome end. For α-particles, the difference between the yield of fragments $\leq$20 or $\leq$5 Mbp is very small, following the arguments made above. This is because the clustering of DSB with α-particles at low doses, either a very small, undetectable fragment is formed, or none at all.

Chapter 5

Rejoining of double-strand breaks: Experimental results

5.1 Introduction

Experimental measurements of double-strand break (DSB) rejoining kinetics are presented in the following chapter, together with predictions based on numerical methods of analysis of DSB rejoining data, which are described separately in chapter 3. When cells are incubated at 37°C , DSBs induced by radiation are processed by the cellular repair machinery, which attempts to restitute the intact DNA sequences. By sampling cells that have been repairing DNA damage for different times after the initial acute exposure to radiation, pulsed field gel-electrophoresis is employed to monitor the variations that occur in the shapes of the DNA fragmentation profiles, as consequence of the on-going repair process. By using a method that allows us to estimate the number of DSBs from the fragmentation profiles, one can also give a quantitative description of the DSB rejoining process. Methods of quantification of DNA DSBs based on random breakage are commonly employed for analysis of DNA fragmentation during DSB repair, despite the fact that this operation is only approximate. In fact, when using a model of DNA fragmentation, based on random breakage, to describe the molecular weight distributions that result from DSB rejoining, it is implicitly assumed that the fragmentation profiles after repair reflect randomly distributed breaks. This assumption is valid only if the following conditions apply:

1. The initial fragmentation pattern should originate from randomly distributed breaks,
2. breaks distributed initially should be 'removed' by the cellular repair machinery randomly, *i.e.* each break independently of any other break and independently of its location in the genome.

In summary, breaks are induced randomly and removed randomly, for a totally reversible process, so that those breaks that at a given time are left unrepaired are still distributed randomly. The validity of the first assumption of the two made above is challenged by the results reported in chapter 4, as well by results of other works (see for example Gauter *et al.*, 2002). In this Thesis it is in fact shown that α-particle induced DSBs are spatially associated. For the validity of the second assumption, particular attention is required, since for the breaks to be removed randomly, the cellular repair machinery must process every DSB:

1. independently of its vicinity to other DSBs, which may in principle hamper the repairability of the first break (see § 1.4 for a description of DSB repair mechanisms and the types of DSBs that they can repair successfully).

2. complete repair of all DSBs is allowed to occur, *i.e.* every break is ultimately removed from the initial pool. This would apply even in case mis-rejoining events take place, which theoretically should be leaving spurious, un-coupled ends that cannot participate in the repair process any more since they are too far from another DSB end to recombine with.

Experimental evidence for DSB mis-rejoining events and formation of chromosome aberrations, including micronuclei formation, after exposure to ionising radiation, indicates that this second set of assumptions may not hold. For this reason, quantification of DSBs during post-irradiation incubation has been accomplished via the application of only one of the already existing analytical methods of analysis of DNA fragmentation that have been used in chapter 4, namely 'direct quantification', since this appears to be dependent to a lesser extent on the random breakage model (see § 3.2.2.1 for a description of the method). Other recent studies have shown that the shape of the fragmentation patterns after post-irradiation incubation deviates from that predicted on the basis of random breakage (Gauter *et al.*, 2002).

A more extensive analysis of DNA fragmentation during DSB repair has been carried out using numerical methods. The computer-simulations of DSB rejoining kinetics which have been developed as part of this Thesis project (described in detail in § 3.3.3.1) help to test the validity of the assumptions that are made when analytical methods of analysis of DNA fragmentation based on random breakage are employed for the quantification of DSBs during the rejoining process. In particular, the numerical approach developed here provides a method to simulate, on a cell-by-cell basis, the fragmentation patterns that are measured after exposure to both low and high LET radiation, without necessarily requiring that the DSB are introduced in the chromosomes randomly. Indeed, the influence of charged-particle track-structure on the shapes of the fragmentation profiles

is described here by means of a simplified clustered breakage procedure (§ 3.3.1.1) so that the initial fragmentation profiles accurately fit the experimental determinations (see § 4.4). The computer-simulated initially injured cells are thus used as an input for the repair machinery during the computer-simulation of DSB rejoining kinetics.

Results obtained from the application of the 'direct quantification' method are presented first, while the application of the numerical method for the analysis of DSB rejoining kinetics data is shown in § 5.3. Finally, a computer-simulation of a premature chromosome condensation (PCC) experiment, in which DSB rejoining kinetics is measured after low doses of ionising radiation, is presented in § 5.4.

5.2 Application of the Direct Quantification method

The 'direct-quantification' method has been applied to quantify DSB yields during post-irradiation incubation in the same fashion as described in § 4.3.3, when initial DSB yields, *i.e.* without any repair incubation, were measured in several X-ray and α-particle irradiation experiments. Briefly, using eq. 2.5b one can convert the fraction of DNA mass measured in any molecular weight region, i, into number of double-stranded fragments $\mathcal{N}_i$. By summing the $\mathcal{N}_i$ values over all the molecular weight regions available, one has an estimate of the number of double stranded fragments $\mathcal{N}(\mathrm{M}_1, \mathrm{M}_2)$ in a region between two molecular weight markers M_1 and M_2, which normally spans the 6.4 Gbp human diploid genome size for a few orders of magnitude (approximately 30 kbp–5.7 Mbp). The value obtained for $\mathcal{N}$ is then corrected by subtraction for the corresponding determination on the unirradiated control samples of the same experiment. The total DSB yield per cell is then extrapolated using the relationship reported in eq. 3.3 for calculation of yields or can also be plotted using the same function as shown in figure 3.2. Six independent X-ray-induced DSB rejoining kinetics experiments have been analysed with this method. For each time point available in each experiment, the number of DSB per cell (extrapolated) is calculated and the kinetics are described by means of an exponential decay with one or two components, predicting a first-order repair mechanism (see § 3.3.3). The fitting functions are repeated here in the set of equations 5.1 for clarity:

$$1 - \mathcal{F} = F_{\text{fast}} \exp\left(-t/\tau_{\text{fast}}\right) + \left(1 - F_{\text{fast}}\right) \exp\left(-t/\tau_{\text{slow}}\right) \tag{5.1a}$$

$$1 - \mathcal{F} = (1 - a) \exp(-t/\tau) + a \tag{5.1b}$$

where $\mathcal{F}$ is the fraction of DSBs rejoined at time t, F_{fast} is the fraction of DSB that rejoin with fast kinetics, τ_{fast} and τ_{slow} are the fast and slow repair time-constants (or τ the only

constant in eq. (5.1b), and a is the fraction of DSBs that remain un-repaired. When using two decaying exponential components (eq. 5.1a) it has been assumed that all breaks are eventually re-joined, whereas for a single exponential decay it has been assumed that an un-rejoined sub-population may exist, merely to provide better fits. The hypothesis that eventually all the breaks are rejoined is supported by recent evidence from M. Löbrich *et. al.*, where it has been shown that virtually all the slowly repairing breaks are ultimately *mis*-rejoined, although after many days from the initial injury (unpublished results). Results of the kinetics analysis carried out on 'direct quantification' data obtained from its application to X-irradiation experiments are shown in figure 5.1. Grouped data from 6 experiments are shown in the lower, wider panel, as means $\pm$ s.e.m., and the individual experiments plotted in the other panels above. For rejoining of X-ray-induced DSBs, it is often observed that the measured signal falls below the background level measured in the unirradiated control samples, just after a few hours of post-irradiation incubation (discussed in § 6.3). When performing the correction for the background by subtraction, this gives negative values which are excluded from the kinetics plots. The first-order DSB rejoining kinetics model has been applied to both averaged measured values and individual experimental determinations in figure 5.1. This is mainly for comparison of best-fit values obtained on 'direct quantification' data of DSB yields to the values obtained with the numerical approach (see table 5.3 in § 5.3) as well as to show inter-experimental variability in the rejoining kinetics. Best-fit values of curves shown in figure 5.1 are summarised in table 5.1. It is evident that in virtually every experiment the number of DSB remaining unrepaired falls to zero after a few hours of post-irradiation incubation, partly due to the correction for the background damage that has been applied by subtraction of the number of breaks per cell. When the first-order repair kinetics model is applied to fit individual experimental data, the best fit is obtained using a single exponential decay, except for experiment X-REP22 where a double component is used. Conversely, when data are averaged together from the six experimental data-sets, a double exponential component provides a better fit to the averaged results. This may be due to the fact that only when data are averaged together from many experiments one has several determinations spanning a wider time interval, where a single exponential may not have enough degrees of freedom to fit the data. The same type of analysis has been carried out on six independent α-particle irradiation experiments, with results shown in figure 5.2. Compared to X-ray data, analysis of rejoining kinetics of DSBs induced by ^{238}Pu α-particles indicates two exponential decay components. Experiment A-REP09 showed an increased number of double-stranded fragments in the first 30 minutes relative to the initial value: this particular data-set was not analysed individually as the other five shown in figure 5.2. The best fit to the averaged values from five experiments also suggests two

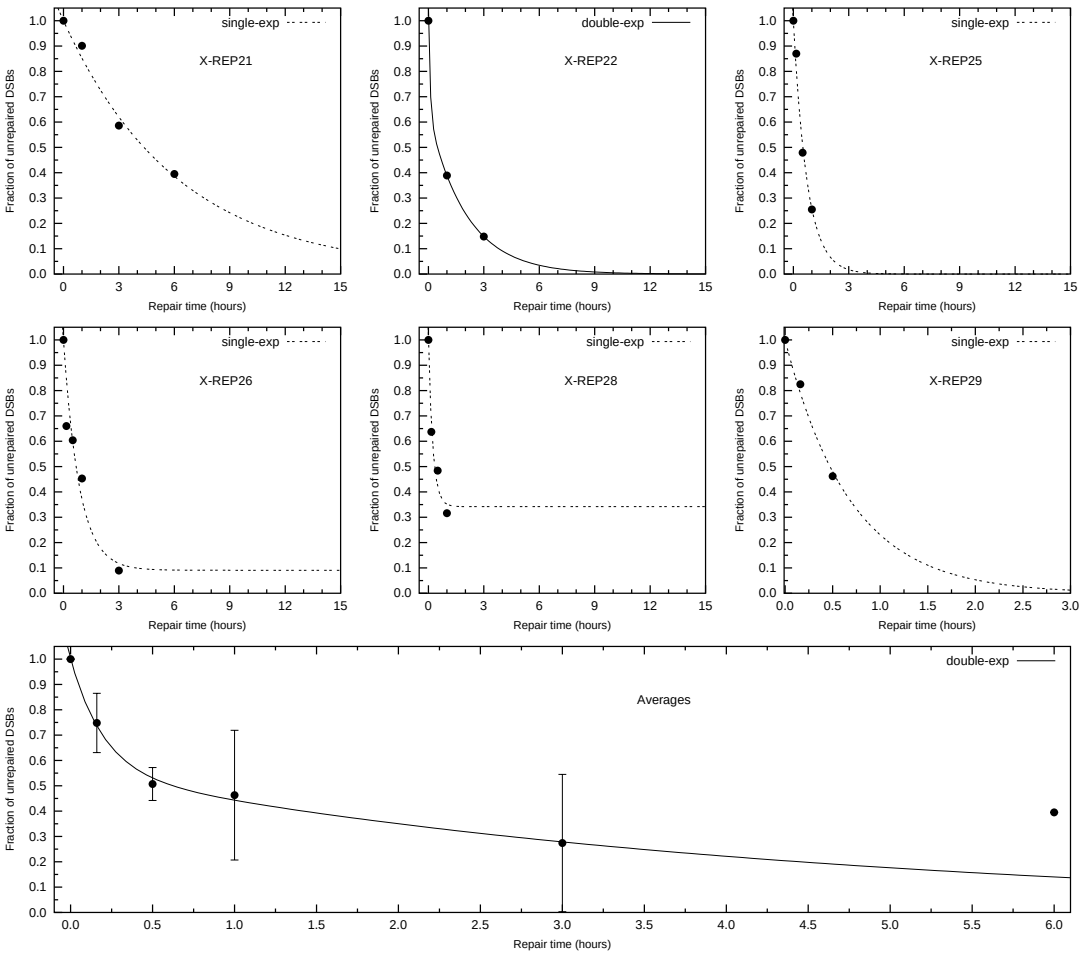

Figure 5.1: DSB rejoining kinetics analysis of the results of the application of the 'direct-quantification' method for the quantification of DSBs that were induced after a 115 Gy X-ray dose in 6 independent experiments. Data in the lower, wide panel are averages $\pm$ standard errors from data values that are plotted in the other six panels. Lines shown are best fit with the first-order repair kinetics model, employing one (dashed line, eq. 5.1b) or two exponential decay components (eq. 5.1a, solid lines). Best fit value parameters of either function used are summarised in table 5.1.

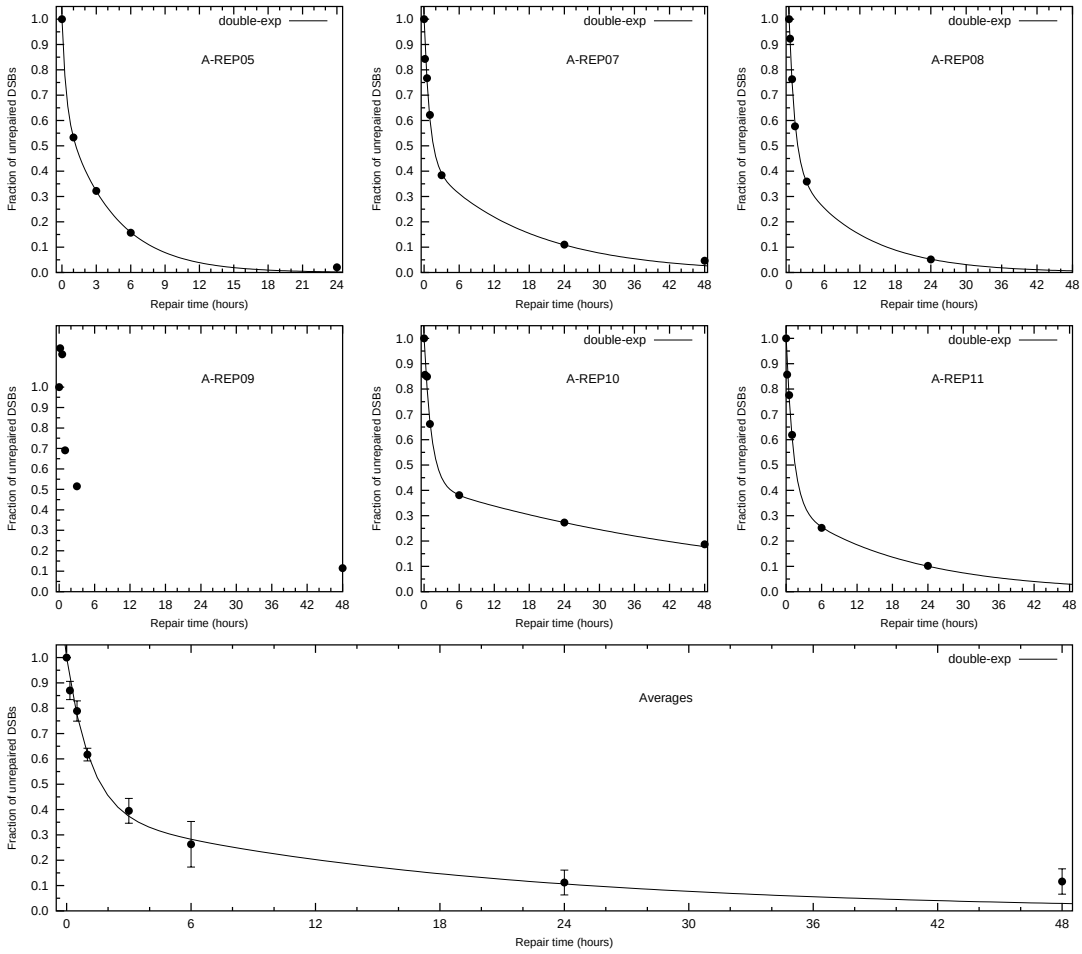

Figure 5.2: DSB rejoining kinetics analysis of the results of the application of the 'direct-quantification' method for the quantification of DSBs that were induced after a 100 Gy α-particles dose in 6 independent experiments. Data in the top panel are averages from data values that are plotted in the other six panels. Solid lines shown are best fit with the first-order repair kinetics model, employing two exponential decay components (eq. 5.1a). Best fit value parameters of either function used are summarised in table 5.2.

Total DSB rejoining kinetics - X-rays - 'Direct Quantification' method

Experiment	F_{fast}	τ_{fast} (h^{-1})	τ_{slow} (h^{-1})
X-REP21	a=0		τ=6±4
X-REP22†	0.37	0.1	2.07
X-REP25	a=0		τ=0.74±0.06
X-REP26	a=0.09±0.15		τ=0.9±0.3
X-REP28	a=0.34±0.06		τ=0.24±0.07
X-REP29	a=0		τ=0.68±0.05
mean±s.e. (n=6)	F_{fast}	τ_{fast} (h^{-1})	τ_{slow} (h^{-1})
	0.45±0.05	0.20±0.04	4±1

Table 5.1: Total DSB rejoining kinetics of X-ray-induced breaks: best fit values with s.e. using the first-order kinetics model (see eqns. 5.1) to the results of the application of the 'direct quantification' method, as shown in figure 5.1. Experiments marked with a † symbol have no degrees of freedom during the regression analysis and best fit values are provided without error. In other cases, parameters whose values are reported without error were kept constant during the regression.

repair kinetics components, both the repair time constants being slower than for X-ray induced DSBs (see tables 5.1 and 5.2 for comparison). Interestingly, the fraction of DSBs rejoining with fast kinetics is larger for α-particles, although the repair time constant for the fast component is much slower. Finally, it should be also observed that rejoining kinetics analysis of data relative to α-particles induced DSBs in individual experiments (figure 5.2) was probably more accurate than for X-rays, due to the availability of more data points per experiment. This may be due to the slower repair kinetics for high-LET induced DSBs, so that it takes more time before the measured signal falls to the level of the background level, thus avoiding rejection of data points in one experiment.

Total DSB rejoining kinetics - α-particles - 'Direct Quantification' method

Experiment	F_{fast}	τ_{fast} (h^{-1})	τ_{slow} (h^{-1})
A-REP05	0.35±0.07	0.3±0.3	4.3±0.6
A-REP07	0.56±0.08	0.9±0.2	17±6
A-REP08	0.57±0.04	1.0±0.1	11±2
A-REP09	no rejoining kinetics analysis available		
A-REP10	0.58±0.08	1.2±0.3	60±40
A-REP11	0.66±0.08	1.2±0.2	20±8
mean±s.e. (n=5)	F_{fast}	τ_{fast} (h^{-1})	τ_{slow} (h^{-1})
	0.61±0.05	1.2±0.2	19±5

Table 5.2: Total DSB rejoining kinetics of α-particles induced DSB: best fit values with s.e. using the first-order kinetics model (see eq. 5.1a) to the results of the application of the 'direct quantification' method, as shown infigure 5.2.

5.3 Application of a Monte Carlo method for the description and quantification of DSBs rejoining kinetics

A detailed description of the computer-simulations of DSB rejoining kinetics in single cells is given in detail in § 3.3.3. In this section, these DSB rejoining kinetics simulations are employed to give a quantitative description of DSB rejoining kinetics as assayed via PFGE in this project. The computer-simulations of DSB rejoining kinetics are contained in an additional module in the initial DNA fragmentation program that was applied in § 4.4. The first step of the analysis of DSB rejoining data is hence the quantification of initial DSB yield and distribution, by means of a DSB clustering approach. The initial fragmentation pattern is simulated in single cells and then used by the computer-simulated repair machinery, which simply removes breaks from the pool of those initially available and assumed to be repairable, by joining ends of contiguous double-stranded fragments. Repairable breaks are assumed here to be all the radiation-induced breaks, but not the background breaks, which are thought to be absent in cells at the time of post-irradiation incubation.

Here, contiguous is to be intended to reflect fragments that originate from a larger fragment after introduction of a DSB. After a given fraction of DSB $\mathcal{F}$ has been repaired in the computer simulation, given as input value to the simulation, and for several cells, the resulting DNA fragmentation profile is described by means of a fragment-size frequency histogram that is compared to an experimental data-set at a certain post-irradiation incubation time, for χ^2 evaluation of the goodness of the fit. A χ^2 minimisation approach is adopted to estimate the best $\mathcal{F}$ value for a given time of post-irradiation incubation. Result of the application of this method are shown in figure 5.3 for an experiment where an X-ray dose of 115 Gy was delivered (experiment X-REP26). The same value-parameters estimated from the simulation of initial fragmentation have been used here, before applying the rejoining kinetics simulation module, namely, 4300 randomly distributed breaks for this experiment (see figure 4.12). Every panel in figure 5.3 shows the experimental fragmentation profiles observed in the unirradiated control samples, together with the computer-simulated background fragmentation profile, shown with a dashed line. Also shown is the fragmentation profile in cells that are irradiated and not yet incubated (the 'time zero' t_0 profile) with the corresponding computer-simulated fragmentation profile that produces the best fit, reproduced from figure 4.12. Each different panel shows experimental determinations of DNA fragmentation at a given repair time (10 minutes, 30 minutes, 1 hour, 3, 24 and 48 hours), along with the computer-simulated DNA fragmentation pattern that best fits the particular data-set. For example, in figure 5.3, upper left panel, after 10 minutes of post-irradiation incubation at 37°C , the best fit of the computer

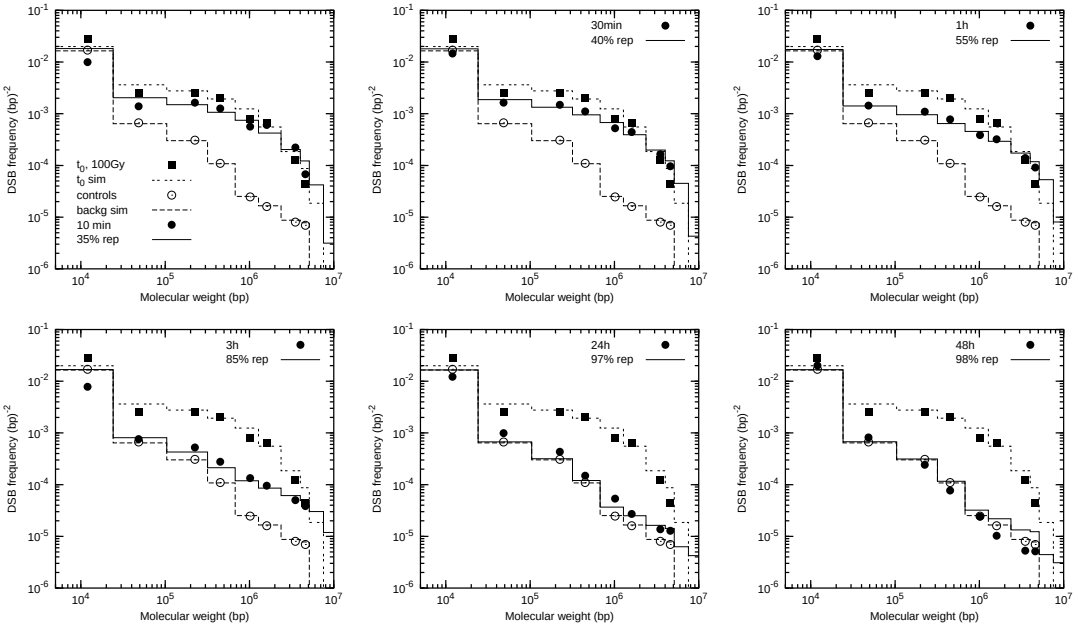

Figure 5.3: Application of the Monte Carlo simulation of DSB rejoining kinetics to the 'X-REP26' experimental data-set. Symbols are experimental determinations: (○) unirradiated controls, with best-fit (dashed line), (■) initial DNA fragmentation with best fit (short dashed line), (●) fragmentation pattern after repair incubation for the specified time, and best fit (solid line) with best $\mathcal{F}$ value specified.

simulation to the data-set shown indicates that 35% of the breaks have been removed from the initial pool (for experiment X-REP26 only). Similarly, in the other panels, a best fit to experimental data-sets reflecting the fragmentation profiles at the other repair times available in this experiment is produced using the least squares method. The best fit curves in every panel of figure 5.3 indicate good agreement, with the exception of the longest repair times. After 48 hours of post-irradiation incubation (bottom right panel) there is an indication of a *de novo* extensive fragmentation process that may be the result of a form of cell death, considering the lethal radiation dose employed. Compared to the fragmentation profiles observed in the unirradiated controls, after incubation for 48 hours there seems to be in fact a depletion of large, Mbp-sized double stranded fragments, accompanied by an excess of smaller fragments. This fragmentation process, probably endogenous, is competing against the DSB rejoining process and is not taken into account in the computer-simulation, which assumes a stable background. As consequence, while the fragmentation pattern relative to simulated repair approaches the experimental background pattern, the experimental pattern after long incubation times may not. Another example of Monte Carlo simulation of DSB rejoining kinetics is shown in figure 5.4 for experiment X-REP25. Very similar considerations apply here, where an extensive fragmentation after long incubation times is also observed. The type of

analysis performed on experiment X-REP26 and X-REP25 has been carried out on 6 independent DSB rejoining kinetics experiments after X-irradiation. The initial fragmentation patterns for these six experiments were all shown in figure 4.12. For each DSB

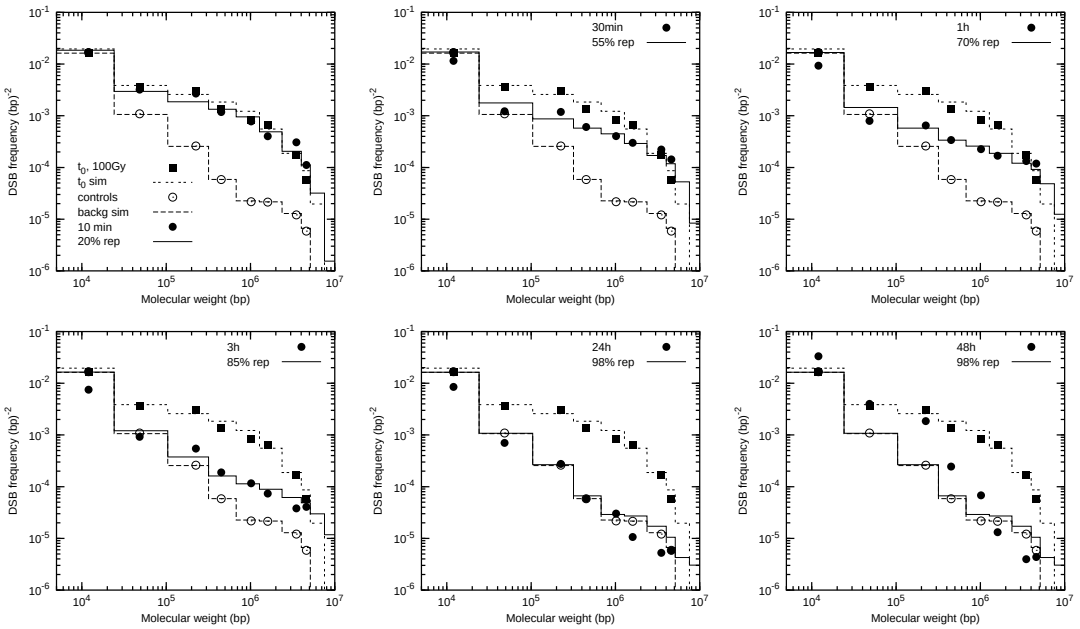

Figure 5.4: Application of the Monte Carlo simulation of DSB rejoining kinetics to the 'X-REP25' experimental data-set. Symbols are experimental determinations: (○) unirradiated controls, with best-fit (dashed line), (■) initial DNA fragmentation with best fit (short dashed line), (●) fragmentation pattern after repair incubation for the specified time, and best fit (solid line) with best $\mathcal{F}$ value specified.

rejoining kinetics experiment, at the end of the type of analysis shown in figures 5.3 and 5.4, one has a set of best-fit $\mathcal{F}$ values (fraction of DSBs repaired) corresponding to different experimental repair times. These values may be used to study the total DSB rejoining kinetics, as reported in § 5.2, when total DSB kinetics data obtained with the direct quantification method were fitted against a first-order rejoining kinetics model, with either one or a double exponential function. Figure 5.5 summarises total DSB rejoining kinetics for experiment X-REP25, X-REP26 and other four experiments, shown in the same order as they appeared in figure 4.12. In figure 5.5, data-points shown in each of the six upper panels are complement to one of best-values obtained from χ^2 minimisation, like the values explicitly reported in the separate panels of figures 5.3 and 5.4 for experiments X-REP26 and X-REP25, respectively. Error bars represent a maximum error which is due to the finite step used when changing the value of the fraction of DSB rejoined in the computer-simulation. This step was normally 0.05 (i.e. 5% of the total breaks rejoined, although near the time rejoining began, 'time zero', and toward rejoining completion, a more fine-tuned step of 1% was used). The error bar shown is to be

intended as the maximum error, hence without any information regarding the level of statistical significance. Total DSB rejoining kinetics analysis was carried out on individual

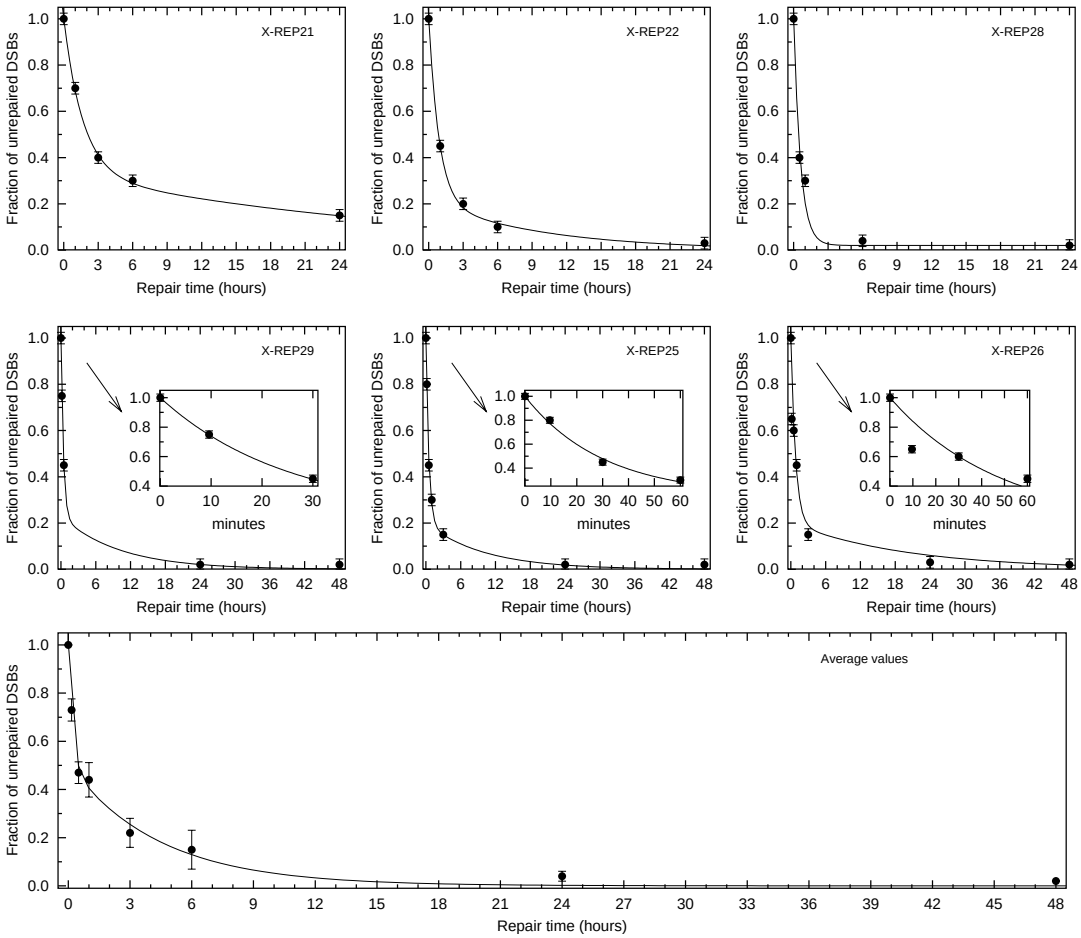

Figure 5.5: Upper 6 panels: DSB rejoining kinetics analysis on the best-fit results of the Monte Carlo simulations of 6 independent X-ray data-sets (including X-REP25 and X-REP26 of figures 5.3 and 5.4). Error bars provide an estimate of standard deviation of the best value, given as half the step used when varying the computer simulation model's $\mathcal{F}$ value in the simulations (see text). The lower, wider panel shows the best fit to the means$\pm$s.e. (n=6) of the data sets shown in the other six panels. Solid lines are best-fits using the first-order rejoining kinetics model; best-fit values are reported in table 5.3. In-sets: expansions of the kinetics curves in the first hour of post-irradiation incubation.

experiments, as in § 5.2 for the direct quantification method, to show inter-experimental variability. Nevertheless, the best-fits shown for individual experiments (with best values and errors reported in table 5.3) were carried out also for another reason that is described below.

A central hypothesis of the computer simulations of DSB rejoining is that kinetics are independent of fragment size. Alternatively, from the perspective of the DSBs, it is hy-

Total DSB rejoining kinetics - X-rays - Monte Carlo analysis

Experiment	F_{fast}	τ_{fast} (h^{-1})	τ_{slow} (h^{-1})
X-REP21	0.67±0.03	1.68±0.05	30±6
X-REP22	0.79±0.06	0.9±0.1	10±4
X-REP25	0.80±0.05	0.49±0.05	10±2
X-REP26	0.85	0.8±0.2	20±30
X-REP28	a=0.02±0.03	τ = 0.6±1	
X-REP29†	0.77	0.41	10
mean±s.e. (n=6)	F_{fast}	τ_{fast} (h^{-1})	τ_{slow} (h^{-1})
	0.50±0.06	0.21±0.06	4±1

Table 5.3: Rejoining kinetics of X-ray-induced DSBs: best fits using the first-order kinetics model of eqns. 5.1 to the data estimated with the Monte Carlo approach and displayed in figure 5.5. Experiments marked with a † symbol have no degrees of freedom, hence regression analysis does not provide statistical errors. For experiment X-REP26, F_{fast} was kept constant during regression. Also shown are the best-value parameters and s.e. of the best fit to the values averaged from the six independent experiments analysed.

pothesised that vicinity to another DSB does not influence individual repairability of each break. To test this hypothesis, it is interesting to observe rejoining kinetics of double-stranded fragments in separate molecular weight regions, probing for fragments of any critical size that rejoin at a different rate. The numerical approach adopted for the design and the development of the rejoining kinetics simulation provides enough flexibility to predict what the kinetic curves should look like for fragments of any size, even outside the experimental region resolved, in the hypothesis of fragment size-independent rejoining kinetics. In fact, this feature is used to extrapolate PFGE data to simulate PCC low-dose experiments of initial fragmentation (§ 4.5) and rejoining kinetics (§ 5.4). In figures 5.3 and 5.4, if one could follow the value of the normalised frequency of DSB per unit base pair, in a given molecular weight range, as it varies across the six time points shown, one could draw a plot in which rejoining kinetics are studied in separate molecular weight regions. Concentrating on individual molecular weight regions also allows us to display more conveniently the number of fragments (breaks) vs time, other than the normalised frequency (see also eq. 2.5b for the link between these two quantities). In fact, the normalised frequency is less intuitive and becomes useful only when the complete fragmentation pattern is shown. This fragment size-independent rejoining kinetics study has been done in figure 5.6 for experiment X-REP25, which shows experimental data of rejoining kinetics and computer-simulated curves in 6 different molecular weight regions. To explain how the step-lines were produced, it is worth remembering that the rejoining kinetics computer-simulation module's only free parameter is the fraction of DSB rejoined, $\mathcal{F}$. One could then plot computer-simulated rejoining kinetics curves for fragments belonging to a given size interval as a function of $\mathcal{F}$. Nevertheless, a rejoining

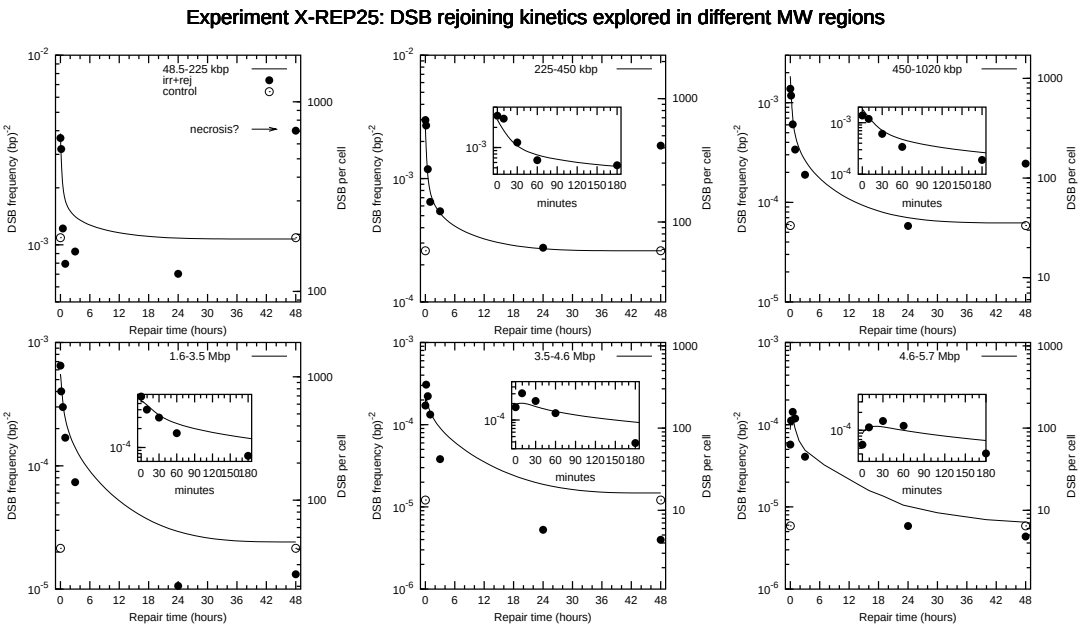

Figure 5.6: DSB rejoining kinetics observed in separate molecular weight regions in experiment X-REP25. (●): normalised frequency of DNA fragments per unit base pair or number of DNA fragments, irradiated samples; (○): same for unirradiated controls. Data are shown without errors since they refer to single determinations in one experiment. Lines are computer-simulations and the x-axis scale of the inset plots is in minutes, expanded in the first three hours of post-irradiation incubation.

kinetics curve is better understood if time is shown explicitly, as in figures 5.1 and 5.2, so it would be better to transform the computer-simulation parameter $\mathcal{F}$ into real time. The best-fit curves shown in figure 5.5 provide a functional relationship between time of post-irradiation incubation and the fraction of DSBs rejoined $\mathcal{F}$, free parameter of the computer-simulations. This correspondence allows us to associate a time value to each $\mathcal{F}$ value for which the computer-simulations are run, which varies from 0.01 to 1.0, with an interval of 0.01 or 0.05, as mentioned earlier. Since the function written in eq. 5.1a cannot be solved for time analytically, a table of ($\mathcal{F}$, time) values is built, serving as a 'look-up' table for a purpose-written interpolation computer-program, such that every computer-simulated $\mathcal{F}$ value available is put in correspondence to a repair time by interpolation in the 'look-up' table of ($\mathcal{F}$, time) values. In this way, the computer-simulated rejoining kinetics curves can be plotted vs time for each experiment, as shown in figure 5.6 for experiment X-REP25. The power of these plots is their ability to show what the kinetics of fragments of many different sizes should be like in the hypothesis of fragment size-independent rejoining kinetics. It is worth stressing that the rejoining kinetics curves in any selected distinct molecular weight region (each panel in figure 5.6) cannot be described by means of one or two exponential decay components, as usually done for total DSB rejoining kinetics. The case shown here is made more complex because, focusing on one molecular weight region at a time, there are both fragments moving out of the region and fragments migrating from regions populated by smaller double-stranded fragments (see § 3.2.2.3). A mathematical solution in closed form to this problem does not exist. For larger fragments, at short incubation times, it is evident that the measured signal increases, which is not what one would expect when repair takes place, where depletion of fragments should be observed. The number of fragments smaller than the ones being observed at the Mbp-scale, which participate to the rejoining process, tend to populate the Mbp region at a rate that is faster than that of those Mbp-sized fragments which, due to rejoining, tend to leave the region. Curves departing from experimental data in particular molecular weight regions would suggest that kinetics are fragment size-dependent. It can be observed that for experiment X-REP25 there is an indication of an excess of small DNA fragments (48–225 kbp) at incubation times exceeding 24 hours. Coupled to this, the larger fragments' signal falls below the level of the unirradiated controls. This may be interpreted as due to breaks that are introduced *de novo* and that counteract the rejoining process, as proposed earlier in this chapter. In experiment X-REP26 (figure 5.7) the *de novo* DNA fragmentation at long incubation times seems less pronounced than for X-REP25. In the Mbp region, the simulated rejoining curves appear to lie above the experimental data, bound to the constraint that only radiation-induced breaks can be rejoined and there is no additional fragmentation process during

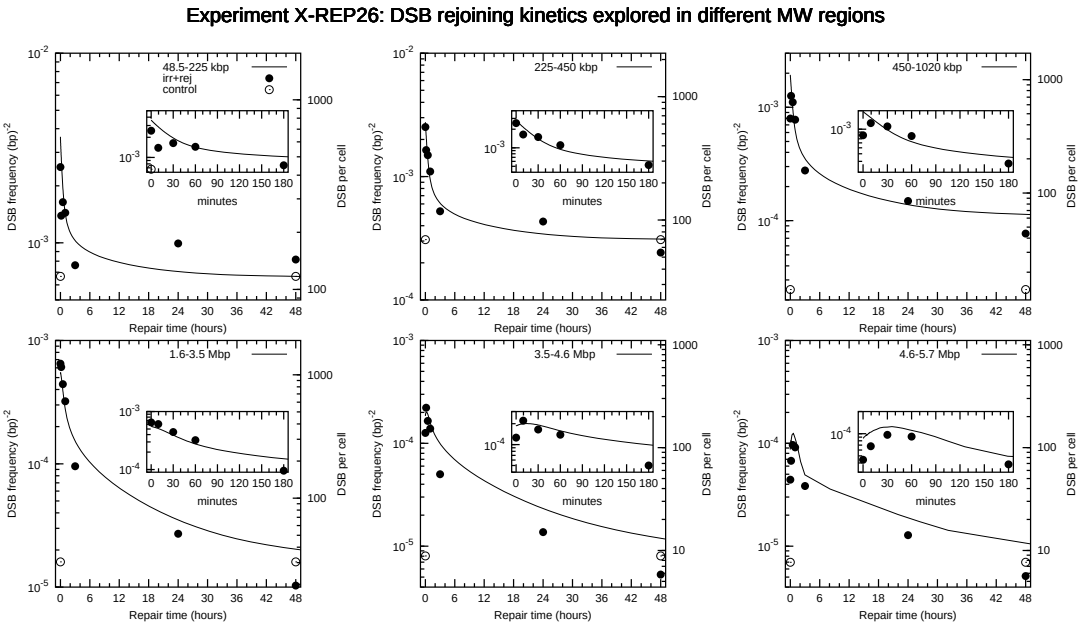

Figure 5.7: DSB rejoining kinetics observed in separate molecular weight regions in experiment X-REP26. (●): normalised frequency of DNA fragments per unit base pair or number of DNA fragments, irradiated samples; (○): same for unirradiated controls. Data are shown without errors since they refer to single determinations in one experiment. Lines are computer-simulations and the x-axis scale of the inset plots is in minutes, expanded in the first three hours of post-irradiation incubation.

incubation. There is generally a good agreement.

The same type of analysis has been carried out on the same six independent experiments that employed α-particles to produce the initial fragmentation and that were analysed with the 'direct quantification method' in § 5.2. Figure 5.8 shows an example of the application of the Monte Carlo DSB rejoining kinetics simulation to experiment A-REP08, where 100 Gy were delivered to the fibroblasts. As shown for experiments X-REP26 and X-REP25 in figures 5.3 and 5.4, respectively, every panel in figure 5.8 shows the experimental fragmentation profiles observed in the unirradiated control samples, together with the computer-simulated background fragmentation profile, shown with a dashed line. Also shown is the profile for cells that are irradiated and not incubated (the 'time zero' t_0 profile) with the corresponding computer-simulated fragmentation profile that produces the best fit, reproduced from figure 4.13 using the same value parameters estimated with the DSB clustering simulation. The computer-simulated step-lines give a

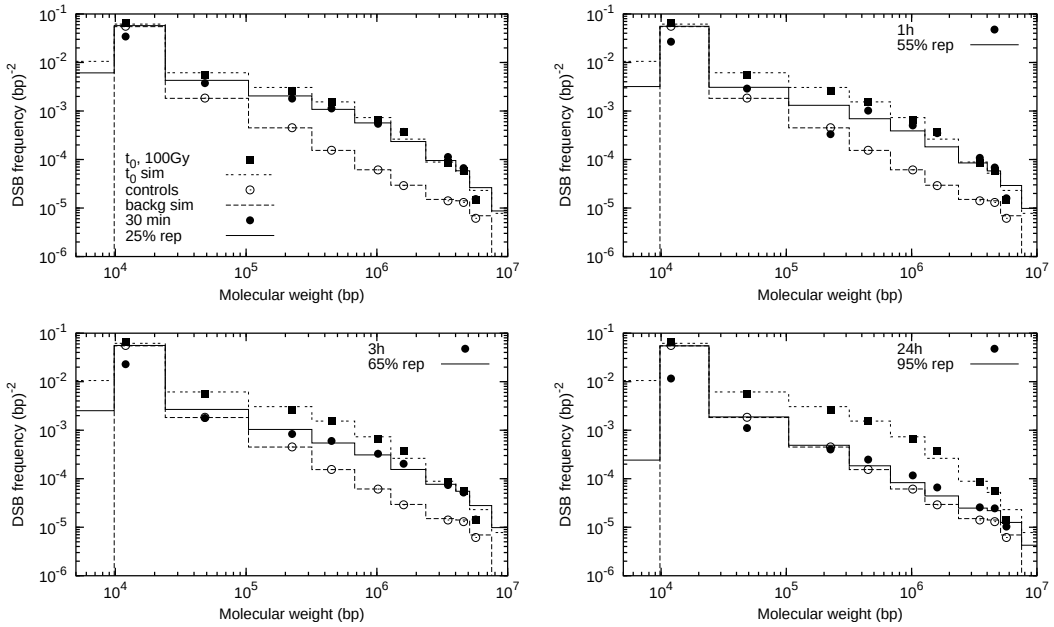

Figure 5.8: Application of the Monte Carlo simulation of DSB rejoining kinetics to the 'A-REP08' experimental data-set. Symbols are experimental determinations: (○) unirradiated controls, with best-fit (dashed line), (■) initial DNA fragmentation with best fit (short dashed line), (●) fragmentation pattern after repair incubation for the specified time, and best fit (solid line) with best $\mathcal{F}$ value specified.

good fit to the data, with exception of the region of smallest molecular weight fragments, where the signal measured is weaker and noise could be influencing the result. The main difference from the regression analysis of X-rays data shown earlier is that the kinetics appear to be slower, as suggested by the $\mathcal{F}$ values shown in the panels. The type of analysis performed on experiment A-REP08 has been carried out on other 5 α-particle

independent experiments, as for the direct quantification method. As before, the best-values for $\mathcal{F}$ in separate experiments have been averaged together and fitted against a first-order kinetic model with two exponential decay components (eq. 5.1a). $\mathcal{F}$ values from single experiments have been plotted vs time and fitted with one or two exponential decay components function (as in 5.1b) as shown in figure 5.9.

DSB rejoining kinetics analysis has also been performed on $\mathcal{F}$ values from individual experiments, in order to relate the $\mathcal{F}$ values to repair time and plot DSB rejoining kinetics curves in separate molecular weight regions *vs time*.

The best-fit value parameters relative to curves shown in figure 5.9 are summarised in table 5.4. Rejoining kinetics in separate molecular-weight regions are shown in fig-

Total DSB rejoining kinetics - α-particles - Monte Carlo analysis

Experiment	F_{fast}	τ_{fast} (h^{-1})	τ_{slow} (h^{-1})
A-REP05	0.70±0.03	1.0±0.1	60±30
A-REP07	0.65±0.09	0.8±0.2	20±10
A-REP08	0.58±0.09	0.6±0.2	12±6
A-REP09	α=0.0		τ = 3.4±0.8
A-REP10	0.6±0.1	1.2±0.4	30±20
A-REP11	0.41±0.09	0.16±0.11	10±4
mean±s.e. (n=6)	F_{fast}	τ_{fast} (h^{-1})	τ_{slow} (h^{-1})
	0.6±0.1	0.8±0.3	20±10

Table 5.4: Total DSB rejoining kinetics of α-particles-induced DSB:best fits using the first-order kinetics model of eqns. 5.1 to the data estimated with the Monte Carlo approach and displayed in figure 5.9. Also shown are the best-value parameters and s.e. of the best fit to the values *averaged* from the six independent experiments analysed.

ure 5.10 for experiment A-REP10 (100 Gy, repair times 10′, 30′, 60′, 6, 24 and 48 hours). The computer-simulations are generally in good agreement, although in this case there is also a hint of a *de novo* DNA fragmentation starting after 24 hours. This is clear from the 48.5-225 kbp region, although *de novo* fragmentation in the Mbp region is not as evident as in the X-ray experiments shown earlier. It is evident in the panel referring to fragments in the 1.6–3.5 Mbp region in figure 5.10 that if the agreement at time zero is poor, the chances of having a good agreement during DSB repair are reduced. Moreover, since DSB rejoining kinetics involves fragments of varying sizes in a complex fashion, the chances of having good fits to the experimental data in any molecular weight region during repair time depend on the quality of the best-fit to data of initial DNA fragmentation in every ‘next neighbour’ region. For experiment A-REP10, a possible explanation for the poor fit at short times in the 3.5–4.6 Mbp fragment size region may be related to the behaviour of smaller fragments. Since fewer fragments between 1.6 and 3.5 Mbp are predicted than experimentally measured, fewer are moving to larger

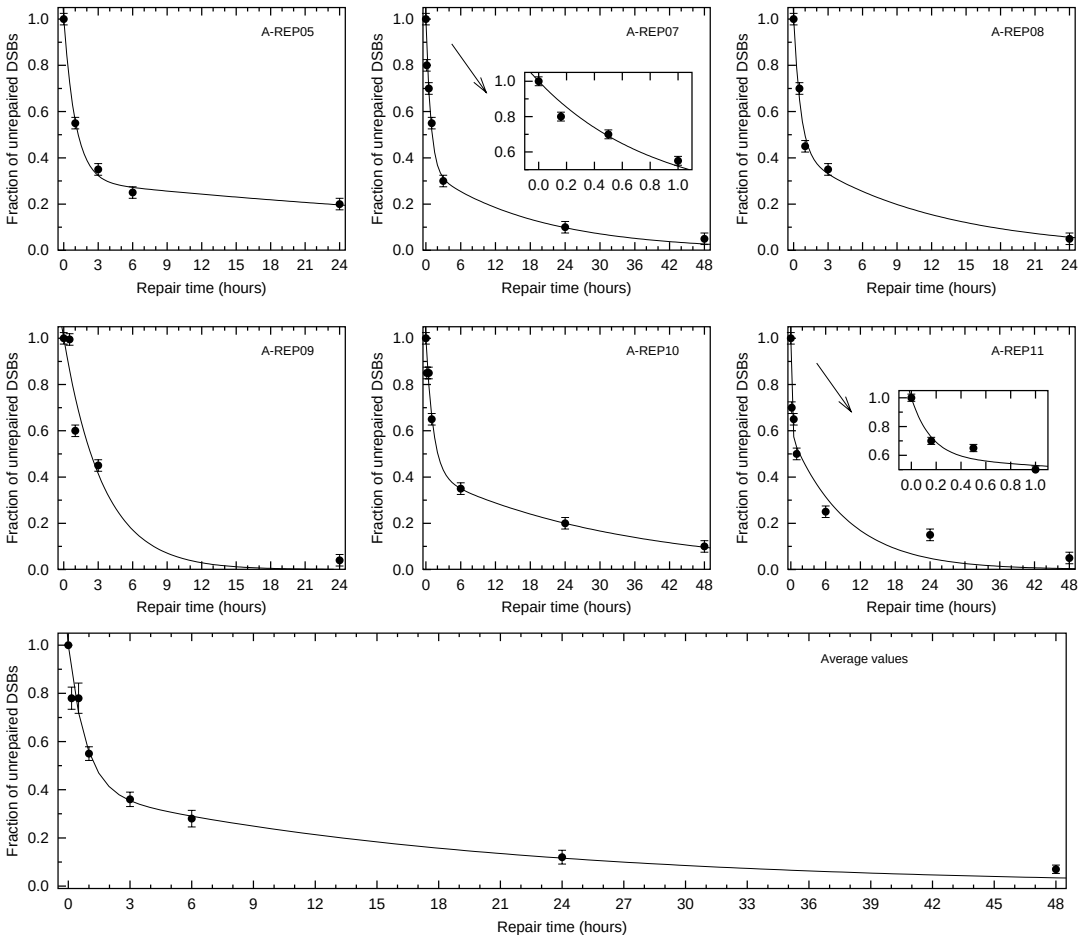

Figure 5.9: Total DSB rejoining kinetics evaluated in 6 independent experiments where α-particles were employed to produce an initial DNA fragmentation. The lower, wider panel shows the best fit to the means$\pm$s.e. (n=6) of the data sets shown in the other six panels. The six panels shown refer to experimental data (•) that were analysed for initial DNA fragmentation and shown in the same order in figure 4.13, error bars providing an estimate of the standard deviation of the best value, given as half the step that was used when varying the computer-simulation model's $\mathcal{F}$ value. Solid lines are best-fits using the first-order rejoining kinetics model; best-fit values are reported in table 5.4. In-sets: expansions of the kinetics curves in the first hour of post-irradiation incubation.

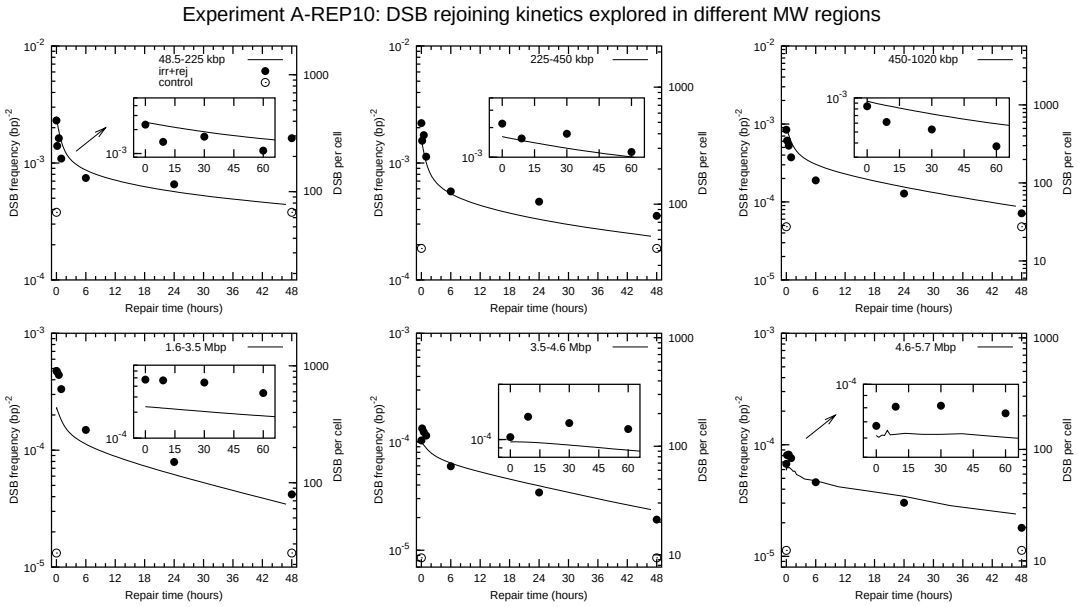

Figure 5.10: DSB rejoining kinetics observed in separate molecular weight regions in experiment A-REP10. (●): normalised frequency of DNA fragments per unit base pair or number of DNA fragments, irradiated samples; (○): same for unirradiated controls. Data are shown without errors since they refer to single determinations in one experiment. Lines are computer-simulations and the x-axis scale of the inset plots is in minutes, expanded in the first hour of post-irradiation incubation.

fragments as repair takes place, so that the simulated curve in 3.5–4.6 Mbp fails to rise. Similar considerations would apply relatively to the 3.5–4.6 Mbp and the 4.6–5.7 Mbp regions. Another example of DSB rejoining kinetics monitored in separate molecular weight regions is shown in figure 5.11 for experiment A-REP07. The top left panel representing kinetics data in the region 48.5–225 kbp shows that after a few hours incubation the signal detected in the irradiated samples fall below the level of the unirradiated controls. This feature has been observed several times for independent experiments and it may be an artifact. It should not be confused with the *de novo* fragmentation observed earlier, appearing as depletion of large fragments. The measured signal falls below the controls with a defined trend, so it is unlikely that noise may be responsible for this observation. On the other hand, the computer-simulated rejoining kinetics curves cannot fall below the level of the controls, since it is postulated that only radiation-induced DSBs are repairable, and that no new breakage process takes place during DSB repair (see also § 6.1). In fact, the computer-simulated curves always approach the background level from above. Table 5.5 summarises the results of the DSB rejoining kinetics analysis car-

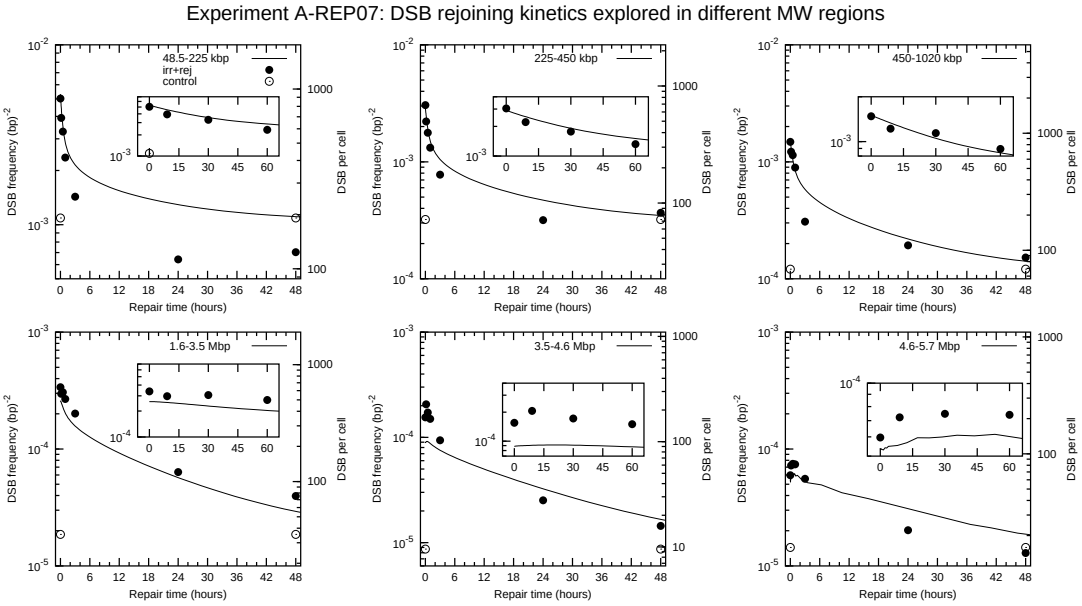

Figure 5.11: DSB rejoining kinetics observed in separate molecular weight regions in experiment A-REP07. (●): normalised frequency of DNA fragments per unit base pair or number of DNA fragments, irradiated samples; (○): same for unirradiated controls. Data are shown without errors since they refer to single determinations in one experiment. Lines are computer-simulations and the x-axis scale of the inset plots is in minutes, expanded in the first hour of post-irradiation incubation.

ried out on data averaged from six independent experiments for both radiation qualities and obtained with both methods of analysis illustrated in this paragraph and § 5.2. The

Summary of DSB rejoining kinetics analysis

	Direct Quantification			Monte Carlo simulations		
Radiation quality	F_{fast}	τ_{fast} (h^{-1})	τ_{slow} (h^{-1})	F_{fast}	τ_{fast} (h^{-1})	τ_{slow} (h^{-1})
X-rays	0.45±0.05	0.20±0.04	4±1	0.50±0.06	0.21±0.06	4±1
α-particles	0.61±0.05	1.2±0.2	19±5	0.6±0.1	0.8±0.3	20±10

Table 5.5: Results of the best fits of the first-order repair model (with two decaying exponentials, as in formula (5.1a) applied to data estimated using both the 'direct quantification' method and the Monte Carlo simulations, as illustrated above. Values are expressed as means±s.e. (n=6) and have been re-copied from tables 5.1–5.4.

values shown in table 5.5 indicate that the best-value parameters estimated from regression analysis of data obtained from either method of quantification are all consistent with each other. The direct quantification approach, considering its simplicity, provides the same kinetics results as the Monte Carlo simulations, although only the latter method allowed us to show that the kinetics are fragment size-independent. Moreover, the direct quantification method required a biased correction for the background damage, while the Monte Carlo simulation does not.

5.3.1 Fit of rejoining kinetics simulations to data that are corrected for the background damage

Previous DSB rejoining kinetics simulations were run during this project on experimental data-sets that had been corrected for the background damage by means of a 'region-to-region' subtraction of DNA mass-size distributions (see § 3.2.2.3 for a discussion on this corrective method). In these previous simulations, there was no need to distinguish between background and radiation-induced DSBs, since the correction for the background was performed on the experimental measurements to remove any trace of the background damage influence. The conclusion drawn from these simulations was that rejoining kinetics depend on fragment size, with smaller fragments rejoining more slowly than larger fragments. This finding agrees with recent results from Gauter *et al.* (2002) and in some respect with results by Johnston *et al.* (1998b). It was later understood that subtractions of DNA mass-size distributions cause distortions to the distributions themselves (see also figure 3.5) and that this could bias the experimental inference. Later on in the Thesis project, more sophisticated program codes were written to distinguish between background and radiation-induced breaks, so to be able to run simulations where radiation-induced breaks only were repaired, that could fit experimental data without any pre-correction. The central hypothesis made in the design of these new program codes was still that fragments of any size rejoin at the same rate, *i.e.* fragment size independent kinetics. Simulations using these newer programs have been shown in § 5.3. With the exception of the very long repair time samples (usually 48 hours, occasionally 24 hours), the agreement between model and experiment is satisfactory, indicating fragment size-independent rejoining kinetics, exactly the opposite as the result of the computer-simulations performed on subtracted data. Figure 5.12 puts in comparison the results of the application of both types of computer simulations (performed on subtracted data and on absolute data) on two data-sets: X-REP22 for X-rays (115 Gy) and A-REP08 for α-particles (100 Gy). These experiments were chosen from those that did not show *de novo* DNA fragmentation after incubation for 24 hours, to avoid bias.

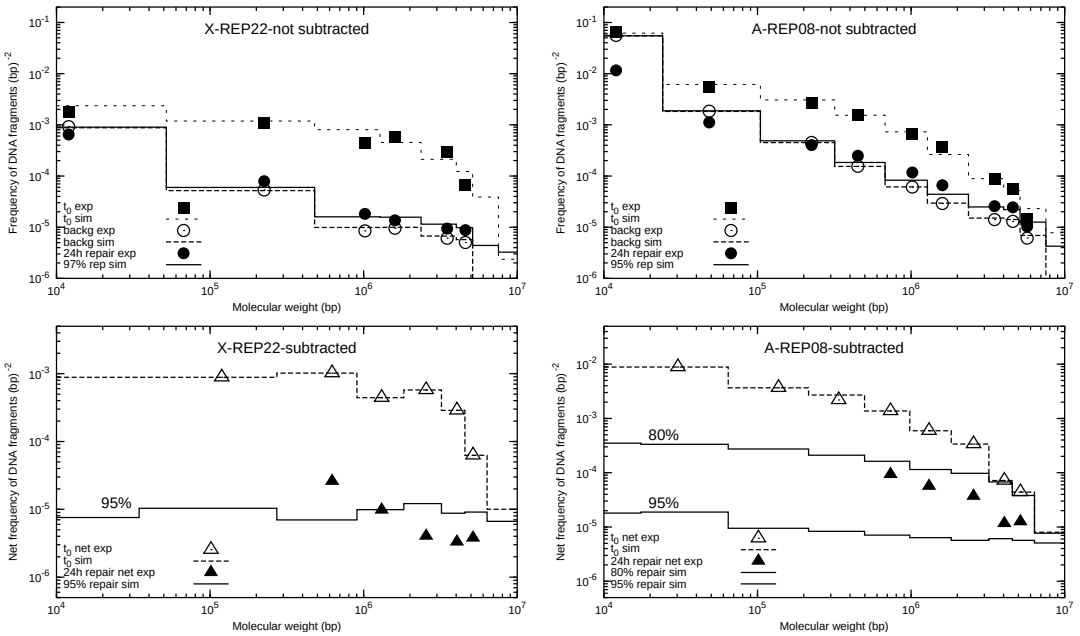

Figure 5.12: Results of DSB rejoining kinetics simulations on *un-corrected* (top two panels) and *corrected* (lower two panels) X-REP22 and A-REP08 experimental data-sets. Symbols (experimental determinations) in *top* panels: (■) initial DNA fragmentation, (○) background fragmentation and (●) DNA fragmentation after 24 hours repair-incubation. Lower panels: (△) 'net', *i.e.* corrected, initial DNA fragmentation, (▲) fragmentation after 24 hours repair-incubation. All step lines shown are best fits using computer-simulations of initial DNA fragmentation (dashed lines) and fragmentation plus DSB rejoining (solid lines) for various levels of $\mathcal{F}$ values as specified in each panel.

Simulations of un-corrected data are shown in the two upper panels, whereas corrected data are simulated in the lower two panels. The profiles obtained from the computer-simulations in the top and bottom panels relate to similar $\mathcal{F}$ values, for each experiment. Nevertheless, while the top panels indicate good agreement (supporting the hypothesis of fragment size-independent kinetics), the best fits in the lower panels are poor, suggesting deviations from the model, *i.e.* fragment size-dependent kinetics. The interpretation given here is that correction of experimental data for the background damage carried out as subtractions of DNA mass-size distributions are biased and should be avoided, if possible.

5.4 Computer-simulations of a low-dose DSB rejoining experiment with the PCC technique.

Low-dose simulations of a PCC rejoining kinetics experiment have been run using a similar approach to that described in § 4.5. Briefly, estimates of the DSB clustering properties of α-particles and X-rays made using PFGE at high doses, averaged over six independent experiments (see table 4.5) were used to simulate the initial fragmentation at doses below 10 Gy. DSB rejoining kinetics were simulated, and frequencies of double-stranded fragments smaller or larger than 20 Mbp, assumed to be the threshold size for a fragment to become visible under PCC conditions, were followed during the rejoining simulation. Assuming, for simplicity, first-order kinetics with a single exponential decay component (see § 3.2.4 and eq. 5.1b), the fraction of the initial DSBs that has been repaired in the computer simulation, $\mathcal{F}$, can be converted to elapsed repair time by solving eq. 5.1b for time.

$$1 - \mathcal{F} = \exp(-t/\tau) \Longrightarrow t = [-\ln(1 - \mathcal{F})] \cdot \tau \tag{5.2}$$

For simplicity it is assumed here that all breaks are repaired, *i.e.* a=0. This speeds-up the 'interpolation and solution' procedure that was employed in § 5.3, where a look-up table was employed. τ in eq. 5.2 has been set to 1 hour (Nasonova *et al.*, 2001) for simplicity. Using the DSB yields estimated from the computer-simulations of DSB induction applied to PFGE data (§ 4.4) at high doses, computer-simulations of a typical PCC rejoining kinetics experiment have been carried out after initial radiation doses below 10 Gy (down to 1 Gy) for both X-rays (figure 5.13) and α-particles (figure 5.14). The lines shown in these two figures refer to computer-simulations of number of excess fragments, that is counting all the fragments that are visible under a microscope, minus the number of chromosomes in a normal, non-aberrant cell, which in the case of human cells is 46.

Excess of PCC visible as well as total fragments, including those which PCC cannot detect, are shown. The kinetic curves could differ significantly if all fragments smaller than

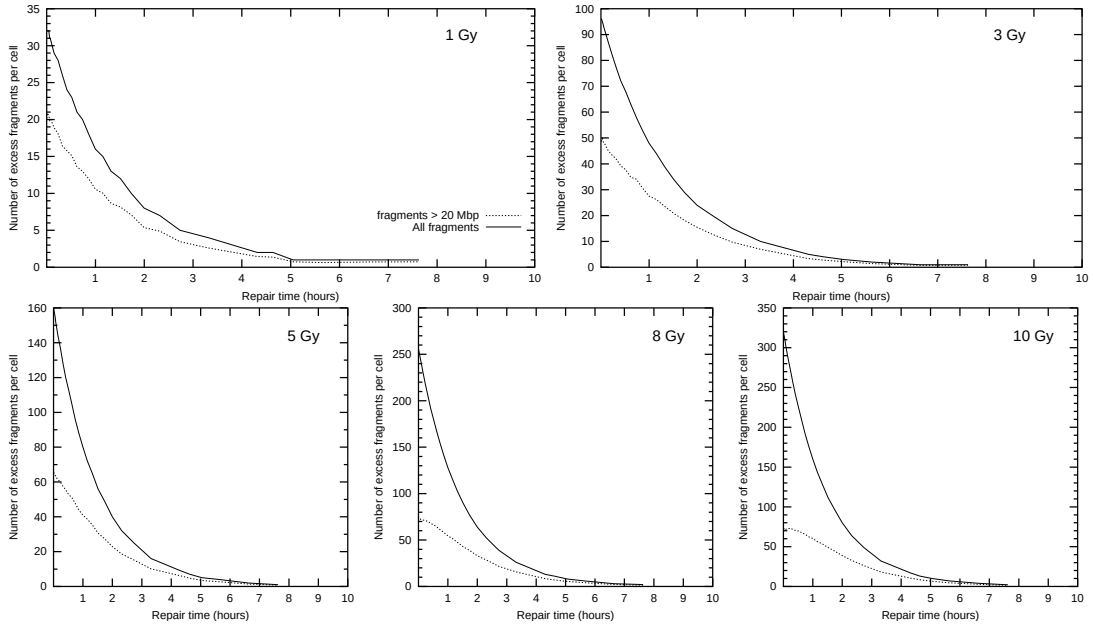

Figure 5.13: Simulations of rejoining kinetics of PCC fragments after an X-ray dose ranging from 1 to 10 Gy. Settings for the simulation of initial DNA fragmentation were taken from table 4.5.

20 Mbp were visible in PCC experiments, as also observed for PFGE experiments when including or excluding Mbp-sized fragments in the DSB rejoining experiments analysis (Stenerlow and Hoglund, 2002).

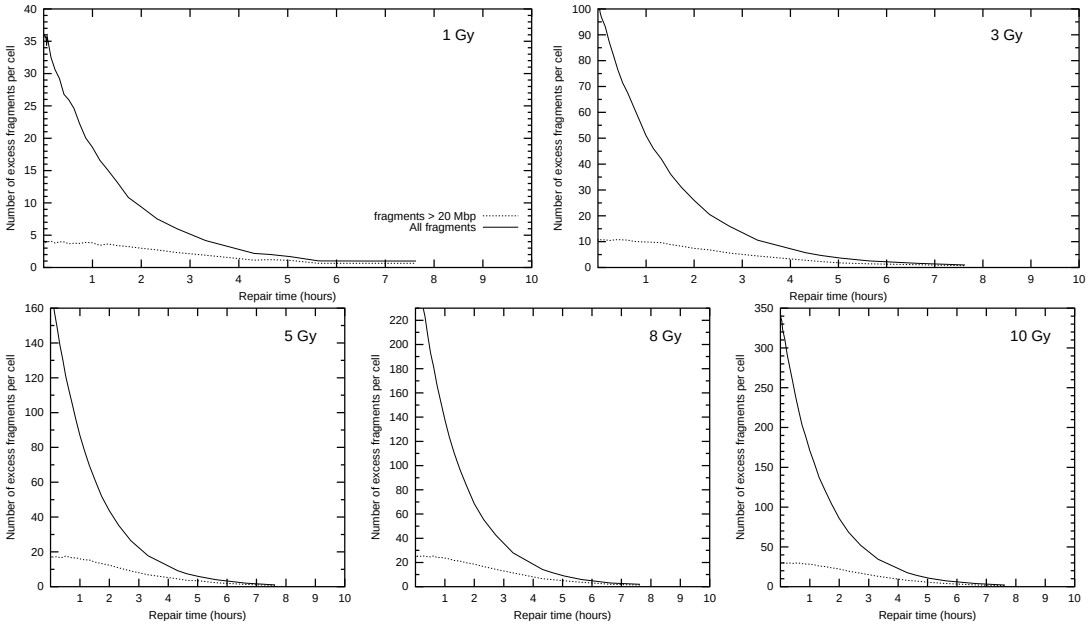

Figure 5.14: Simulations of rejoining kinetics of PCC fragments after an α-particle dose ranging from 1 to 10 Gy. Settings for the simulation of initial DNA fragmentation were taken from table 4.5.

Chapter 6

General Discussion

The three major results of this Ph.D. Thesis project are:

- The development of analytical and numerical methods for the quantification of double-strand break (DSB) yields and distributions, which do not require subtraction of the background damage that is measured in unirradiated control samples of pulsed field gel-electrophoresis (PFGE) experiments;
- the quantitative description of DSB clustering due to exposure to high-LET radiation, achieved by means of a Monte Carlo DSB clustering approach;
- the finding that DSB induced by both low and high-LET radiation appear to rejoin with kinetics that are independent of vicinity to other DSBs, within the DNA size-regions studied. This suggests that:

  > locally multiple damaged sites (LMDSs) are more important than regionally multiply damaged sites (RMDSs) in determining DSB rejoining kinetics.

These three results are now discussed in the context of previously reported data in the literature and predictions are made for future study.

6.1 Result I: treatment of background damage to DNA in PFGE

Quantification of DSB yields and distributions may lead to different results depending on whether DNA fragmentation data are analysed after correction for the background

damage or not. It was shown that DSB rejoining kinetics appear as fragment size-independent if uncorrected data are analysed. Conversely, when the background damage is subtracted, results indicate fragment size-dependent rejoining kinetics (see § 5.3 and 5.3.1). The interpretation given here is that a fragment size-dependent distortion is applied to the fragmentation profiles, when mass-size distribution values are subtracted. This problem can be described theoretically using the random breakage model, to show the effect of the subtractive procedure (see figures 3.4 and 3.5). A simple subtraction of the background DNA fragmentation pattern is erroneous, although alternative subtractive methods have been proposed in the past. A dose-dependent weighting factor that takes into account the extent of total DNA fragmentation observed in the unirradiated controls, as well as in the irradiated samples, may modulate the amount of background damage to be subtracted from each gel section, for an appropriate correction, thus limiting distortions in the fragment size distributions (Cedervall *et al.*, 1995, and personal communication). Nevertheless, a correction for the background damage carried out region by region cannot be accurate. The way the DNA mass signal 'moves' across the fragment size distribution while breaks are added or removed, *i.e.* while fragments are made smaller or larger, depends on the amount of DNA present in the next neighbour size regions (figures 3.5 and 3.4) and to a smaller extent even to more distant molecular weight regions. As breaks are added or removed, the amount of fragments of a certain size depends on the overall flux of fragments between the different molecular weight regions. A subtractive method to correct for the influence of the background damage should not be carried out region by region, as confirmed by our own studies of experimental data when these were analysed with methods of DNA DSB quantification that require such a correction.

The new approaches illustrated throughout this Thesis do not require pre-correction of experimental data. It was decided to adapt the functions employed for regression analysis, which are derived from the existing models, or to develop numerical methods that could account for both the non-linear and non-local mass-migration effects mentioned above, rather than manipulating the experimental data and potentially biasing the conclusions. The distortion caused by local subtraction procedures can lead to erroneous interpretations also in the analysis of initial radiation-induced DNA fragmentation. A departure of subtracted DNA fragmentation data from the random breakage model could be interpreted as due to clustered breakage, even for sparsely ionising radiation, which is thought to lead to the formation of randomly distributed damaged sites. This problem has been considered from the theoretical perspective using the BDRB approach (see also Pinto *et al.*, 2000) and from its application to experimental data that were obtained earlier, not as part of this project (Pinto, 1998).

For integral methods of analysis of DNA fragmentation, like the FAR or the *Q*-function methods, other ways of correction for the background damage exist, which do not require manipulations of experimental data (§ 3.2.1.1). When using these methods it is nevertheless assumed that the background damage measured in PFGE is randomly distributed, according to a mechanism that may not be distinguished from that of radiation. This does not appear to be the case, as shown for example in figures 4.5 for a few experiments carried out as part of this Thesis, or in studies by other workers (Belli *et al.*, 2001, 2002; Erixon and Cedervall, 1995; Höglund and Stenerlöw, 2001).

A central question is whether the background damage measured in PFGE experiments is representative of DNA damage to cells, or it is just an artifact of either the experimental procedures or data analysis. The large number of background DSBs measured may not necessarily reflect the damage present in the cells at the time of irradiation, but it may be produced only during the preparation of the samples for PFGE (Rydberg, 2000). Also, the large number of DSB that lead to the formation of 50 kbp or smaller fragments may be merely the result of an amplification of noise in the signal measured in this molecular weight region (Stenerlöw *et al.*, 2000). As suggested by Stenerlöw *et al.*, the uncertainties in the conversions from mass fraction measurements to number and frequency of DSBs using the set of equations 2.5 increase strongly as ΔM and $\bar{M}$ decrease, since for smaller DNA fragments the measured F_i values are affected by larger experimental uncertainties, and these uncertainties are amplified by the presence of smaller and smaller ΔM and $\bar{M}$ values of the denominator in eq. 2.5a. Following the arguments of Stenerlöw *et al.*, it may be argued that if F_i was set by the resolution limit of the PFGE assay at the approximate constant value of 0.001, and if both ΔM and $\bar{M}$ were to decrease approximately linearly with gel section number (gel sections further away from the wells contain smaller DNA fragments) one would expect from eq. 2.5a that the functional relationship between the frequency of DNA fragments n and the mass of the fragments M should follow a power-law with exponent $\simeq$-2, which on double logarithmic scales is a straight line of negative slope. The question is whether the power-law that describes the shape of the fragmentation patterns observed in the unirradiated controls indicates real correlated damage effects, or whether it is the result of a biased procedure, such as the conversion of very small mass fraction measured values to frequency of DNA fragments, with the aid of eq. 2.5. When the detection limits of PFGE are approached, the arguments made above suggest that the shape of the fragmentation profiles resembles a power-law purely due to the conversion made from mass fractions to frequency values. In this case, the observed power-law is due to a bias, and conversion to frequency of DNA fragments is not recommended. Nevertheless, for molecular weight regions where measurements of fractions of DNA mass are

significantly above the PFGE limits of sensitivity, one can safely exclude the effect of this systematic error. This project has employed a technique that allows measurements of DNA fragmentation in the range 30 kbp-5.7 Mbp, where the background damage pattern resembles that predicted by a power law. Comparison with results of other works suggests that a power-law may also describe well the shape of the fragmentation profiles measured in the unirradiated controls for much smaller fragments. Such works employed a more sensitive DNA labelling procedure than the present work, and the signal measured for kbp-size fragments was significantly above that of background, thus eliminating the problem of noise amplification discussed earlier (see Pinto *et al.*, 2000; Rydberg, 1996).

The origin of background damage in PFGE is not clear. In the attempt of finding potential mechanisms, the effect that lysis of cell membranes may have during preparation of the samples for PFGE is discussed here briefly. In one study employing the FAR method, Rydberg showed that radiation-induced heat-labile sites (HLSs)may be converted to DSBs during PFGE lysis, if this is carried out at 50°C with detergents and proteinase K, for an overnight exposure, as done in this PhD project (Rydberg, 2000). Rydberg showed that when exposure to lysis solution at 50°C is shorter, less DNA is extracted into the agarose gels. He suggested that a lysis treatment for 10 minutes may be sufficient to reveal the fragmentation effect of DSBs only, and that subsequent treatment may be responsible for converting radiation-induced only heat-labile sites (HLSs) into DSBs. Conversion of HLSs to DSBs is in fact a slow process with half times around 15–30 minutes, competing against repair of HLS, which takes place within 4 minutes from their initial induction, as observed in studies using an *in vitro* plasmid system (O'Neill, personal communication, and Jenner *et al.*, 2001). Using the FAR approach, Rydberg could not observe the same conversion effect in the unirradiated control samples, since the DNA fragmentation observed in unirradiated controls was independent of lysis time. Nevertheless, this putative time-dependent HLS to DSB conversion in unirradiated control cells was studied in Rydberg's work in cells that had already undergone prior lysis for 22 hours at 50°C . If conversion to DSB took place, it cannot be excluded that this happened in the first lysis. In summary, although Rydberg's study shows evidence of DSB conversion from radiation-induced HLSs, it remains unclear whether background DSBs in PFGE are caused by transformation of endogenous HLSs in the same way and to the same extent as shown for radiation-induced HLSs. PFGE lysis and electrophoresis runs may also convert some types of multiple damaged sites into double-strand breaks. For example, if an endogenous damaged base leads to a localised distortion of the sugar-phosphate backbone and lies near a SSB in an unirradiated cell, then shear forces during electrophoresis may cause strand breakage and produce a DSB which was not originally

present in the cell.

Background DNA damage in PFGE is described in this Thesis only in terms of size-distribution of the double stranded fragments that are a consequence of DNA breakage. In the analytical BDRB approach (§ 3.2.2.3), the background size distribution is assumed to follow a power-law (eq. 3.6), but no explanation is given regarding what mechanism might cause such a distribution. In the numerical version of the BDRB approach (§ 3.3.1.1), more flexibility is given to the description of the DNA fragmentation in unirradiated controls, but still no assumptions are made regarding the actual mechanism. Khvostunov and Andreev have attempted to predict what type of breakage mechanism would produce the fragmentation pattern that is observed in unirradiated controls of PFGE experiments. By computer-simulating several hypothetical mechanisms of breakage of three-dimensionally looped chromatin structures, they have been able to find a few mechanisms which lead to DNA fragmentation in reasonable agreement with the experimental patterns that are observed by several different investigators (Khvostunov and Andreev, 2001).

It could be argued that the unirradiated control fragmentation patterns of PFGE do not reflect damage to all the cells in the population, but the patterns may be averaged over a majority of normal, undamaged cells, and a sub-population of heavily damaged cells. In this case, PFGE procedures may be the origin of such heterogeneous fragmentation, but this may also be endogenous, at least in principle. Let us suppose that one has 10% FAR in the unirradiated control samples, where electrophoretic conditions are such that 10 Mbp is the exclusion size. Let us then consider the hypothesis that the FAR value measured is representative of DNA damage solely in the damaged sub-population. The entire genomic DNA content of these heavily damaged cells must be composed of fragments that are all smaller than 10 Mbp ($F_{<k=10\text{Mbp}}$=100%), so they can enter the gel and be detected, and account for 10% FAR averaged over the two populations. In this example, the remaining population is composed of cells that are not damaged, *i.e.* their chromosomes are intact. With a 6.4Gbp genome and all breaks equally spaced from each other, one would need at least 640 breaks per damaged cell. Nevertheless, in this case one would only predict the presence of one sharp DNA band at 10 Mbp, while fragmentation patterns observed in the unirradiated control samples appear smeared (see figure 4.1). Although there is evidence for background damage in PFGE to be induced by a clustered breakage mechanism (see for example figure 4.5), one can use the random breakage model just to predict, approximately, how many breaks should be induced to have $F_{<k=10\text{Mbp}}$=100% in a sub-population of heavily damaged cells. This can be done with the FAR implementation of random breakage (using eq. 3.2). It turns out that approximately 1000 DSBs correspond to virtually 0% chance for the survival of a fragment

larger than 10 Mbp. In practice, this is likely to be an underestimate, since the apparent DSB clustering in unirradiated controls implies that for the same FAR value, 10% in our example, there will be many more DSBs, as can be than estimated from integration of the power-law in eq. 3.6 (see also Pinto *et al.*, 2000). This calculation shows that for the background damage that is observed using PFGE to be the result of fragmentation of a sub-population of heavily damaged cells, these cells should contain several thousand breaks each. If this phenomenon was independent of PFGE, it should also be observed with other techniques. Experiments employing the 'comet' assay do not seem to reveal such a highly fragmented unirradiated control cell-population. Moreover, normal human fibroblasts are well known for their very low levels of spontaneous apoptosis, which could in principle be thought to be responsible for the putative extensive DNA fragmentation. A more complex scenario may be one where several cell populations exist, with varying levels of background damage, such that the average damage observed could be described with a power-law. Experiments that employ *in situ* labelling of γ-H2AX histone, which is extensively phosphorylated at the site of DSBs, show that unirradiated cells occasionally have very high numbers of foci (Kai Rothkamm *et al*, unpublished results). Currently however, there is no convincing evidence to prove that a sub-population of highly damaged cells is responsible for the background damage observed in PFGE.

Another possible interpretation is that PFGE *does* induce the background damage observed, only in a fraction of the cells. This damage may be induced, for example, when agarose plugs containing lysed cells, with DNA not protected by histone proteins, are handled after lysis for equilibration in electrophoresis buffer, and/or during sample loading in the wells of the agarose gels. Considering that the pores of the gellified agarose matrix are of size comparable to that of the cells diameter or below, *i.e.* a few μm, it is difficult to understand how shear forces during sample handling could produce such extensive DNA fragmentation that includes fragments of several kbp or hundreds of kbp.

That the DNA smeared mass distribution observed in the unirradiated controls is due to mitochondrial DNA can also be excluded. Although DNA of all mitochondria in mammalian cells accounts for about 1% of total cellular DNA mass, their genome is only about 16,500 base pairs, less than 10^{-5} times the size of the nuclear genome (Alberts *et al.*, 1994). Such a small genome cannot be responsible for the fragmentation pattern observed at the Mbp-scale and for several hundreds of kbp.

In summary, in this project, it has been hypothesised that background damage measured in PFGE is caused by electrophoresis procedures, hence independently of radiation, and that it is not present in normal cells. Moreover, it is considered to be equally distributed among all the cells encapsulated in an agarose plug. Given these hypotheses, it

may be worth stressing the difference between the picture observed of background damage in the BDRB method (§ 3.2.2.3) and that made in its numerical extension, designed to support radiation-induced clustered breakage (§ 3.3.1.1) in order to gain insights into how the damage may be distributed in each cell. In the analytical BDRB method, background damage in PFGE is described as if 46 virtual chromosomes exist, whose size is smaller than that of the original, intact chromosomes. Along with these virtual chromosomes, there is a widely dispersed fragmentation pattern, below 10 Mbp, whose origin lies in the fragmentation of the intact chromosomes, but fragments in this region can no longer be attributed to any chromosome. However, for the subsequent random breakage process which simulates radiation action, any shuffling of the above mentioned distribution would produce the same final fragmentation profile. A major uncertainty is probably the shape of the population of DNA fragments above 10 Mbp. With the numerical extension of this model, the hypothesis is that background fragments are equally distributed among all the 46 chromosomes present, as it is unknown whether individual chromosomes are more sensitive to this type of damage relative to each other. In the numerical model, background breaks occupy one contiguous region of each chromosome, covering a fraction of its length that is set by the experimental FAR value measured in the unirradiated controls (see figure 3.8). Alternatively, one may distribute the background fragments in several separated regions of each chromosome, still covering a fraction of the chromosome size equal to the FAR value, such that the distance between two contiguous regions occupied by background fragments defined a fragment that is larger than 10 Mbp. The total number of background breaks would be larger in this case, and the average background fragment size would be consequently smaller, but the shape of the fragmentation pattern below 10 Mbp could be identical. At high radiation doses, this alternative background arrangement would not produce different results from the one that was adopted in this study, which justifies the choice made. At low doses nevertheless, some differences may be evident. For the more dispersed, alternative geometry, Mbp-sized fragments would be produced as function of dose with a stronger linear component for sparsely ionising radiation. For the clustered geometry adopted here instead, one expects that two independent breaks are required to produce Mbp-sized fragments. The presence of a background break within a few Mbp from a randomly located radiation-induced DSB is unlikely for a linear production of fragments.

A very similar approach to the BDRB analytical method is the generalised broken stick (GBS) method developed independently by Belli *et al.* (2001). The rationale is identical to that of the BDRB method: the fragmentation pattern measured in irradiated samples must be the result of the super-imposition of background and radiation-induced breaks, and subtractions of profiles will inevitably lead to erroneous results.

6.2 Result II: quantification of initial yields of X-ray and α-particle induced double-strand breaks

Initial yields and distributions of DNA double-strand breaks (DSBs) have been measured in this study using pulsed field gel-electrophoresis and several mathematical and numerical methods of DSB quantification. Care has been taken to allow for the influence that background breaks have on the experimental outcome. It has been assumed here that all breaks that are not background breaks have been induced by radiation directly. There is an emerging concern about the type of DSBs that are detected by PFGE, in particular two hypotheses have been the subject of several studies by other investigators, conducted during this doctoral project, both stating that part of the DSBs measured are not directly due to radiation. Some of the measured breaks could be:

- Radiation-induced heat-labile site (HLS) that are converted to DSBs during the experimental procedures (Rydberg, 2000).
- Clustered lesions, which as consequence of attempted DNA repair are partly converted into DNA DSBs (Box *et al.*, 2001; Gulston *et al.*, 2002; Jenner *et al.*, 2001; Sutherland *et al.*, 2000). Such repair could in principle also take place in samples that are not deliberately subject to repair incubation, in the few minutes during the manipulations procedures when the samples are exposed to 37°C (see experimental methods, § 2.5). Also, these non DSB clustered lesions may be converted into breaks during electrophoresis procedures.

Production of HLSs appears to be mediated by OH radical species, as determined by varying the OH scavenging conditions in plasmid models (O'Neill, personal communication). It is also predicted that the extent of DSBs that could derive from conversion of HLS is LET dependent.

When using bacterial endonucleases such as Nth (endonuclease III) and Fpg (formamidopyrimidine DNA glycosylase) to convert non DSB clustered lesions into DSBs that could be detected with PFGE or conventional CFGE, it has been shown that a significant proportion of radiation-induced clustered lesions are not DSBs, for high-LET particles (Sutherland *et al.*, 2000), but even for γ radiation (Gulston *et al.*, 2002). The ratio of 'non-prompt' DSB to directly induced DSBs in human cells seem to be about 1, even for γ rays. That non-DSB clustered DNA lesions exist and are as abundant as prompt DSBs has a great importance for estimating risk of exposure to radiation, since some of these lesions appear difficult to repair. Some types of clustered DNA lesions seem in fact to stall the repair system (David-Cordonnier *et al.*, 2002; Weinfeld *et al.*, 2001). These

recent experimental findings may be challenging the role of radiation-induced direct DNA DSB as the important lethal lesion.

In summary, in this Thesis, it cannot be excluded that radiation-induced DSBs yields and distributions may be influenced by the presence of both heat-labile sites and non DSB clustered lesions, which would enhance the estimates of total DSB yields both in experiments where initial fragmentation is assayed and in those which included repair incubation. This factor, together with the necessity of using high radiation doses, at the time of increasing interest in the effect of radiation at low doses, raises the question as to whether conventional PFGE may still be the technique of choice for measuring DNA damage in the future. Nevertheless, results from this work are in good agreement with numerous published data, indicating that if such a problem exists, it may be encountered often. SCGE, commonly referred to as the 'comet' assay, may represent a valid alternative to PFGE. The neutral version of single cell gel-electrophoresis may be used at doses sensibly lower than that required by PFGE for fragmentation analysis, although conventional FAR analysis with PFGE can also be carried out at low doses. Lysis in single cell gel-electrophoresis (SCGE) is different from lysis in PFGE, and conversion of HLS to DSB could be less extensive. Perhaps the major limitation to the sensitivity of SCGE at low doses is due to the imaging techniques, rather than in the experimental technique itself (Johnston, personal communication). The advantage of SCGE over PFGE is nevertheless that the former allows the study of individual cells, so that in principle it may be used in conjunction to microbeam irradiation. On the other hand, spatial distribution of DNA damage cannot be studied as in PFGE, since molecular weight markers cannot be run in parallel.

Another low-dose, single cell technique that can be used to study DNA damage, particularly DSBs, has also emerged recently. This employs antibodies that are specific to a phosphorylated form of histone H2AX, (see § 1.2) when this becomes rapidly phosphorylated as a consequence of radiation induced injury (Paull *et al.*, 2000; Rogakou *et al.*, 1998). The dose required to detect γ-H2AX 'foci' is on the order of 1 Gy and this makes the technique perfectly adequate to study DNA damage in single cells subject to microbeam irradiation (Prise *et. al.*, unpublished results), especially when other biological end-points that necessitate low-doses are studied.

6.2.1 240 kVp X-rays induce randomly distributed breaks

Initial DNA fragmentation produced by 240 kVp X-rays has been measured experimentally and at first analysed with the FAR method (§ 4.3.1), direct DSB quantification (§ 4.3.3) and the background-dependent random breakage method (§ 4.3.4). Results of

the analysis with the first two methods indicate that estimates of DSB yields are a function of the experimental region analysed. This seems to suggest that a deviation from random breakage must occur (see table 4.4) and that application of methods based on random breakage to estimate yields of DSB induced after low LET radiation is perhaps inappropriate (see also Pinto *et al.*, 2002). The observed deviation from randomness is believed to be due in part to the subtractive procedure that is carried out to correct for the background damage to DNA. This subtraction in fact leads to an over-estimation of fragments in the hundreds of kbp region accompanied to under-estimation of larger fragments (see § 6.1). When the BDRB method has been employed, such deviation from randomness was significantly attenuated (table 4.4) strengthening the hypothesis that the putative non randomness of X-ray induced breaks distributions is mainly due to the conventional methods used to analyse experimental data. Other studies in the literature have generally found the distribution of low-LET induced DSBs caused by random breakage, with DSB yields either smaller of equal to those reported in the present study. Some exceptions exist, as for example in de Lara *et al.* (2001), where deviations from randomness were observed after ^{60}Co-γ irradiation, with a defect of fragments of about 100 kbp and an excess of Mbp-sized fragments. For comparison, see Prise *et al.* (1998), where results from different techniques are employed, and Prise *et al.* (2001) and table 6.1, where PFGE data only are shown together with those from this work, reported in table 4.4 in more detail. Results of analysis of fragmentation data with the numerical extension of the BDRB method (§ 4.4) also indicate that X-ray induced DSBs appear to be randomly distributed in the genome. DSB clustering simulations of X-ray induced fragmentation in fact produced a poorer fit to the data than the corresponding one for random breakage. Overall, yields of X-rays induced DSB are very similar to those published from other groups.

6.2.2 ^{238}Pu α-particles cause regionally clustered DNA breakage

Random breakage models do not fit experimental data of medium or high LET radiation induced DNA fragmentation. When applying random breakage models to fit α particles or light ions data, the DSB yields extrapolated to whole cells vary significantly with the experimental region investigated (see for example Höglund *et al.*, 2000; Newman *et al.*, 1997, as well as results from this work in § 4.3.1 obtained with a variable size threshold FAR method). For high LET radiation, indications of deviation from randomness are too significant to be solely due to erroneous corrections for the background damage. More recently, direct quantification has been employed to evaluate RBE values for DSB induction, although even in this case the estimates vary with the size of the

Inter-study comparison of DSB yields for low LET radiation. PFGE experiments

Cell type	radiation	method of analysis	DSB yield Gy^{-1} $bp^{-1} \times 10^{-9}$	reference
CHO	X-rays	FAR	$6 \cdot 0$	Ager and Dewey, 1990
CHO	X-rays	FAR	$4 \cdot 5 - 6 \cdot 7$	Iliakis *et al.*, 1991
Bladder Carcinoma	X-rays	distribution shape (§ 3.2.2.2)	$2 \cdot 7$	Whitaker and McMillan, 1992a
V79	γ	broken stick†	$4 \cdot 9 \pm 0 \cdot 4$	Friedl *et al.*, 1995
KE37/1	γ	distribution shape	$4 \cdot 0 \pm 0 \cdot 6$	Friedl *et al.*, 1995
GM38	225 kVp X-rays	FAR	$5 \cdot 8$	Löbrich *et al.*, 1996
GM38	225 kVp X-rays	direct quantification (§ 3.2.2.1)	$10 \cdot 7$	Löbrich *et al.*, 1996
V79	250 kVp X-rays	FAR	6.4	Newman *et al.*, 1997
V79	250 kVp X-rays	broken stick	8.9	Newman *et al.*, 1997
GM5758	^{60}Coγ	FAR	$5 \cdot 2$	Höglund *et al.*, 2000
GM5758	^{60}Coγ	direct quantification	$5 \cdot 8$	Höglund *et al.*, 2000
V79	^{60}Coγ	broken stick†	≈ 6	Kraxenberg *et al.*, 1998
K562-AP‡	^{60}Coγ	FAR-hybridisation	$7 \cdot 9$	Tabocchini *et al.*, 2000
K562-D	^{60}Coγ	FAR-hybridisation	$6 \cdot 3$	Tabocchini *et al.*, 2000
V79	^{60}Coγ	FAR	$4 \cdot 2$	Stenerlöw *et al.*, 1994
U-343MG	^{60}Coγ	FAR	$4 \cdot 2$	Stenerlöw *et al.*, 1994
LS-174T	^{60}Coγ	FAR	$4 \cdot 2$	Stenerlöw *et al.*, 1994
GM38	225 kVp x-rays	FAR	$5 \cdot 8$	Rydberg, 1996
V79	^{60}Coγ	direct quantification	$7 \cdot 0 \pm 0 \cdot 4$	Belli *et al.*, 2001
V79	^{60}Coγ	direct quantification	$6 \cdot 8 \pm 0 \cdot 3$	Belli *et al.*, 2002
V79	^{60}Coγ	FAR	$4 \cdot 0 \pm 0 \cdot 2$	Belli *et al.*, 2002
V79-4	^{60}Coγ	broken stick	7·6	de Lara *et al.*, 2001
RT112	^{60}Coγ	distribution shape	$6 \cdot 2$	Almodovar *et al.*, 1994
		this study		
AG01522B	240 kVp X-rays	FAR	$4 \cdot 5 - 10$	Pinto *et al.*, 2002
AG01522B	240 kVp X-rays	direct quantification	$4 \cdot 7 - 6$	Pinto *et al.*, 2002
AG01522B	240 kVp X-rays	BDRB	≈ 6	Pinto *et al.*, 2002

Table 6.1: Comparison of DSB yields for low LET radiation between the estimates from this and other studies employing PFGE.(†): the method used in these studies is based on random breakage, though not identical to any of the others that were employed in this study. (‡) 'AP' means actively proliferating, 'D' stands for butyric acid-induced differentiation.

fragments that are contributing to the DSB yield estimates, as also shown in this study in § 4.3.3. Mathematical models supporting clustered breakage, or computer-simulations of DNA breakage using reconstructions of both chromatin and charged particle track structure have provided a valid alternative to the random breakage model (Friedland *et al.*, 1999; Ponomarev *et al.*, 2001a; Sachs *et al.*, 1998). Experimental data on initial DNA fragmentation induced by ^{238}Pu α-particles have been analysed in this study using a simplified clustered breakage numerical approach, which has been fully developed throughout this project (§ 3.3.1.1). Results from quantitative comparison of the computer simulations to experimental data support the simple hypothesis that clusters of DSBs are located randomly in cells, and that each cluster contains, on average, six breaks all within ≈20 Mbp(summarised in table 4.5). This finding is compared following to results of other published results of Monte Carlo simulations of PFGE fragmentation data, considering current knowledge of high order chromatin structures (see figure 1.2). Table 6.2 also shows a comparison of DSB yields after high-LET radiation between several studies that employed PFGE and methods of DSB quantification either based on random breakage or on 'direct quantification'. The randomly located cluster (RLC) formalism by Sachs *et al.* also has two free parameters, and it has been employed to describe nitrogen ion-induced DNA fragmentation in human fibroblasts (Löbrich *et al.*, 1996) as well as 110 keV μm α-particles (Newman *et al.*, 1997, obtained using the same Pu source as in the present study). However, both data-sets used for analysis with RLC formalism were provided already corrected for the background damage by means of a subtraction of mass-length distributions (analysis in Sachs *et al.*, 1998). The best Monte Carlo fits with the RLC formalism to the α particle data set indicate an average cluster size of about 7 Mbp, and an average multiplicity of about 8. These results are not too different from those obtained from the simple approach developed in this work, since the cluster radius varies stochastically according to a uniform distribution in the present simulations, and to 10 Mbp maximum cluster radius there correspond a mean radius of 5 Mbp. The region covered by a cluster ultimately becomes approximately 10 Mbp, which can be compared to Sachs *et al.*'s result of 7 Mbp. The finding that clusters extend over several Mbp appears reproducible, although the mean breakage multiplicity per cluster is different. By quantification of the deviation from random breakage, without using computer models of DSB clustering, it was predicted that for 110 keV μm α-particles there is a 44% probability that a DSB is accompanied by another DSB, within 300 kbp (Newman *et al.*, 1997, V79 cells data). Although clustering at these kbp scales is evident in many studies, the cluster radius is under-estimated from the assumptions made by Newman *et al.* if compared to the one estimated in the present work. Mathematical considerations from others studies also predict that DSB clustering must extend up to several Mbp,

Inter-study comparison of DSB yields for high-LET radiation. PFGE experiments

Cell type	radiation	method of analysis	DSB yield Gy^{-1} $bp^{-1} \times 10^{-9}$	reference
VA13	32 keV/μm Ne	FAR	$0 \cdot 84$†	Rydberg *et al.*, 1994
VA13	190 keV/μm Fe	FAR	$0 \cdot 48$†	Rydberg *et al.*, 1994
GM38A	32 keV/μm Ne	FAR	$0 \cdot 86$†	Rydberg *et al.*, 1994
GM38A	190 keV/μm Fe	FAR	$0 \cdot 52$†	Rydberg *et al.*, 1994
U-343MG	125 keV/μm N	FAR	$3 \cdot 1$	Stenerlöw *et al.*, 1999
GM5758	40 keV/μm He	direct quantification	$8 \cdot 8 \pm 0 \cdot 2$	Höglund *et al.*, 2000
GM5758	80 keV/μm N	direct quantification	$8 \cdot 6 \pm 0 \cdot 9$	Höglund *et al.*, 2000
GM5758	125 keV/μm N	direct quantification	$8 \cdot 6 \pm 0 \cdot 3$	Höglund *et al.*, 2000
GM5758	175 keV/μm N	direct quantification	$7 \cdot 6 \pm 1 \cdot 0$	Höglund *et al.*, 2000
GM5758	225 keV/μm N	direct quantification	$6 \cdot 9 \pm 0 \cdot 7$	Höglund *et al.*, 2000
V79	110 keV/μm He	broken stick	$7 \cdot 76 \pm 0 \cdot 14$	Newman *et al.*, 1997
GM38	900 keV/μm Fe	FAR	$18 \cdot 9$	Löbrich *et al.*, 1996
GM38	24-29 keV/μm N	FAR	$12 \cdot 0$	Löbrich *et al.*, 1996
V79	31 keV/μm protons	direct quantification	$13 \cdot 1 \pm 0 \cdot 3$	Belli *et al.*, 2002
V79	123 keV/μm He	direct quantification	$8 \cdot 3 \pm 0 \cdot 3$	Belli *et al.*, 2002
		this study		
AG01522B	110 keV/μm He	FAR	$3 \cdot 4 - -13$	–
AG01522B	110 keV/μm He	direct quantification	$5 \cdot 6 - 10$	–
AG01522B	110 keV/μm He	BDRB	$7 - 9$	–
AG01522B	110 keV/μm He	clustered breakage simulations	$5 \cdot 5 \pm 0 \cdot 9$	–

Table 6.2: Comparison of DSB yields for high LET radiation between the estimates from this and other studies employing PFGE. †: RBE relative to X-rays in the same study.

when heavy ions with LET in the order of 10^3-10^4 keV μm are employed (Kraxenberg *et al.*, 1998).

If DSB clustering due to charged particle tracks extends to several Mbp, even as high as 10 Mbp, this may be due to the overlap of a charged particle track with one or more specific high orders of chromatin arrangement. Manuelidis described ordered chromatin structures with sizes in the order of 7–10 Mbp (Manuelidis, 1990). Intersecting such structures would cause DNA DSB clustering on the Mbp scale. High order organisation of $\approx$ 3 Mbp flexible chromatin giant loops, whose base points lie on a three dimensional random walk, are also suggested in the coordinated modelling and experimental work of Sachs *et al.* (1995) and Yokota *et al.* (1995), which provides evidence for such type of organisation to determine chromatin compaction from 0.15 to 190 Mbp. Interestingly, support for existence of 2·9 Mbp 'giant' looped domains comes from the work by Johnston *et al.* (1998a). It may be that several of these contiguous structures are hit after the passage of one energetic charged particle, with a resulting regional clustering of DNA damage extending up to several Mbp.

Sachs *et al.*, in the application of the RLC formalism to fit PFGE data on fragmentation induced by high LET particles, have assumed that to 1 Gy there correspond 10 radiation tracks, rather than leaving this as free parameter, which would have increased the degrees of freedom of the simulation. Such an assumption is not made in the numerical simulations of DSB clustering developed and applied in this work, since there was no explicit attempt to simulate singe-track effects. Nevertheless, it is interesting to attempt to find a connection between the results obtained here (table 4.5) and the effects of single particle traversals.

AG01522B fibroblasts are relatively thin cells (2–3 μm), and a single 110 keV μm^{-1} α particle traversing the cell nucleus is expected to deliver approximately 0.1 Gy. 1 Gy corresponds thus to an average of 10 α-particle traversals, although the number may fluctuate according to Poisson statistics. Due to the limited thickness of the cells, it can be hypothesised that each particle traversing the nucleus would intersect normally one and generally no more than two chromosome territories. Figure 6.1 gives a schematic representation of chromosome territories distributed in a human fibroblast. In practice, the cytoplasm stretches much further than represented in figure 6.1, and chromosome territories are believed to have overlapping regions, as described in the CT-IC model in § 1.2. For each particle track there will be up to two hits in distinct chromosome territories, hence 1 Gy may be related to a maximum of 20 chromosome territories hits. This may be regarded as an upper limit, since there is a chance that a particle will not intersect any chromatin at all, and some particles may hit only one chromosome territory. In fact, 20 independent α particle hits is probably overestimated, since from this study one

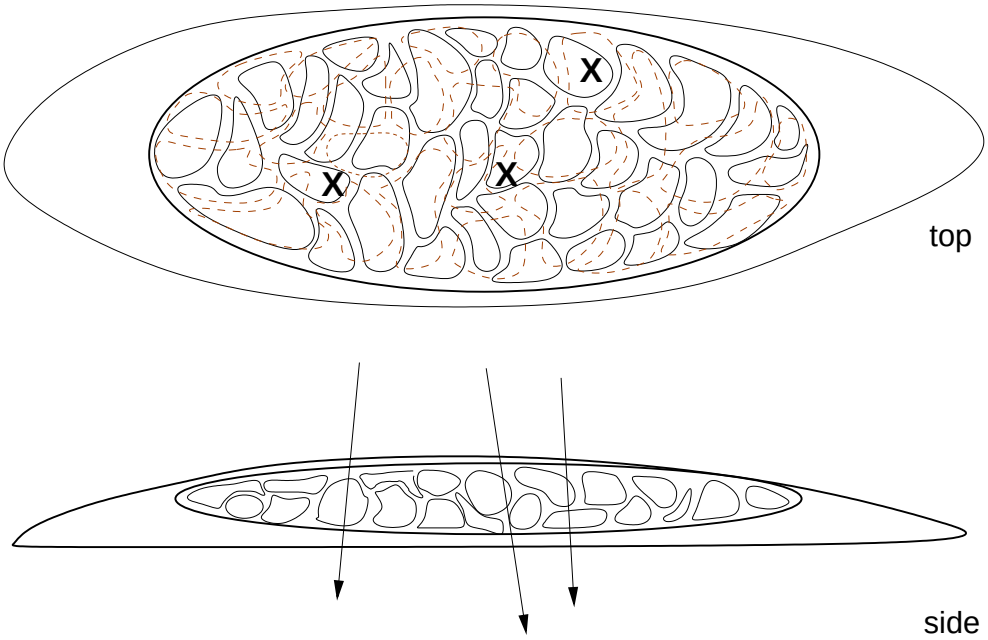

Figure 6.1: Single charged-particle tracks intersecting one or two distinct chromosome territories. Top panel: X symbols represent the point of traversal of one charged particle, viewed from the side in the lower panel. Dashed lines represent chromosome territories that lie in a background layer compared to those represented with a solid line. It is currently unknown whether the thickness of AG01522B cells is compatible with the existence of chromosome territories lying one above the other.

estimates a total of 35 DSBs, then the multiplicity of each cluster should be $\leq$2, that is, for one charged particle track intersecting a chromosome territory, only two breaks are induced. Based on results from Sachs *et al.* (1998) and simulations in this work, this is probably unlikely, for two breaks per cluster per chromosome would not lead to the fragmentation profile that is observed experimentally, which shows an excess of DNA fragments in the 100 kbp range compared to random breakage. Computer simulations for multiplicity set to two in fact provided poor fits to the data at all dose values available in this study. In figure 6.1, three particle tracks relates to an approximate dose of 0.3 Gy. According to the best fit of the DSB clustering simulations to the experimental data, $\approx$ 6 independent clusters are introduced in a cell per Gy, with an average multiplicity of 6, making about 36 DSBs on average, per Gy. The estimate for the number of chromosome territories involved is somewhat lower than the calculation made above (6 vs 20). If AG01522B were so thin that only one chromosome territory would be encountered per charged-particle track, not as shown in figure 6.1, then there would only be about 10 chromosome territories hits per Gy, as an upper estimate, that is 10 DSB clusters, and this may be better compared to the six independent clusters induced per Gy as predicted by the simulations in this work. Finally, it cannot be excluded that one α particle crossing the nucleus, or only one chromosome territory, may produce two track-correlated, although distinct, DSB clusters in the same chromosome. Although the simulation is not designed with one-track effects in mind, this event is unlikely but not impossible in the simulation (p=1/46).

The higher the dose, the less single track effects may be evident, as every chromosome would have received a similar number of track traversals, and roughly the same number of lesions. In this case, considering DSB clusters as independently and randomly located as in the present simulations may be a good approximation.

6.3 Result III: the relative role of LMDSs and RMDSs in determining DSB rejoining kinetics

Several experiments have been carried out as part of this project, in which cells have been incubated for up to 48 hours at 37°C , after an acute exposure to X-rays or α-particles, in order to evaluate DSB rejoining kinetics. Quantification of DSB rejoining kinetics has been accomplished either using the direct quantification method (§ 3.2.2.1) or via computer simulations of DSB repair (§ 3.3.3.1). Rejoining kinetics estimates obtained with either method were found to be consistent with each other, as summarised in table 5.5. The numerical method, applied to PFGE data, has also allowed us to test

whether DSBs are removed by the cellular repair machinery independently of their proximity to other DSBs. Data analysis in the 30 kbp–5·7Mbp region suggests that repair kinetics are consistent with the popular hypothesis that two types of DSB exist, with different reparabilities, and that α-particles induced breaks appear to rejoin more slowly. Moreover, results suggest that rejoining kinetics are not influenced by the distance between two contiguous breaks. This suggests that LMDSs may determine DSB rejoining kinetics, rather than damage that is regionally clustered between 30 kbp and 5·7 Mbp. This result has also been interpreted as evidence for fragment size-independent kinetics.Whether this may be extrapolated down to the kilo base pair or base pair region, that is for accompanied breaks taking place on one or few turns of the 30 nm chromatin fibre, or on lower order chromatin structures such as individual nucleosomes, is not clear. In fact, recent studies in oligonucleotides using extracts of repair enzymes show that locally clustered lesions impair repairability of DNA damage (David-Cordonnier *et al.*, 2002). Little is known about the repair kinetics of fragments whose size is $\leq$30 kbp. For fragments belonging to the size range studied in this project, there is evidence from other studies showing that the rejoining kinetics of some fragments are relatively slower, in contrast to the results presented here. Using a modified version of neutral filter elution (NFE) which employs a lysis procedure with Triton-X 100, which retain histone-depleted elements of high-order chromatin structures, namely nuclear matrix-DNA interactions, Johnston *et al.* demonstrated that breaks appearing as multiples within a 2·9 Mbp chromatin domain are processed by the V(D)J recombination-associated repair pathway, rejoining with slower kinetics than isolated breaks in such loops. These 2·9 Mbp looped domains were demonstrated to be independent of cell type (Johnston *et al.*, 1998a). It is difficult to compare the present data to those obtained from NFE-tx, since the latter ignores the contribution of fragments in the Mbp region that arise from single breaks in two adjacent 2·9 Mbp looped domains, whereas the technique employed here does not.

Results from this study show clearly that whether rejoining kinetics appear as fragment size-independent or as size-dependent depends on how experimental data are corrected for the unwanted DNA fragmentation caused by the background damage (§ 5.3.1). Since subtraction of background to irradiated and repaired fragmentation profiles results in an excess of small fragments, accompanied by a lack of Mbp-sized fragments one is tempted to conclude from the data that since small fragments are in excess, these must repair more slowly than large fragments, which in parallel appear depleted. Comparison to other experimental studies that handle the background damage in a similar fashion as shown here is necessary to test the conclusions from this work. It is proposed that fragment size-dependent kinetics were observed in this study due to a bias in the experimental procedures.

For low LET radiation only, and in CHO cells, an earlier study demonstrated that rejoining kinetics were fragment size-independent in the molecular weight range 1–10 Mbp (Dahm-Daphi and Dikomey, 1996). By contrast, evidence for small DNA fragments to repair with slow kinetics is provided in a recent study by Gauter *et al.* (2002). In that study, the popular method of analysing fragmentation patterns measured after irradiation and repair after incubation with the random breakage model is openly questioned. There is in fact no justification for interpreting such fragmentation profiles as due to some Gy-equivalent dose, since the removal of radiation-induced DSBs may in principle not reverse the initial induction process (see also, for comparison, the discussion in Pinto *et al.*, 2002). The study by Gauter *et al.* employs video-fluorometry of ethidium bromide stained gels, and an ingenious method to convert the mass-gel migration distance distribution to mass-fragment length distributions. Experimental determinations are obtained for several more fragment size values than in this study, which in contrast is based on physical gel sectioning. To study the fragmentation pattern in the complete distribution is potentially more accurate than physically sectioning the gels, since the latter method may smooth-out any fine structure in the mass-size distribution. There is nevertheless the risk that a weak signal may be below the sensitivity threshold of the imaging acquisition system. As the background damage is limited to a few % of the total DNA mass it should contribute to a faint signal if monitored on a continuous fragment size length scale. The problem is similar to that faced when, in the attempt to increase the size-resolution of ^{14}C or ^{3}H-based method of PFGE data quantification, one tries to cut thinner and thinner gel sections (§ 2.7). As a consequence, it may happen that the fragmentation pattern in the unirradiated controls is not correctly estimated with video fluorometry, and then not accounted for in the analysis of irradiated and repaired profiles. Another interesting point in the study by Gauter *et al.* (2002) is the choice of allowing cells to repair while embedded in agarose plugs, since with this method one has more control time allowed for repair. Repair was measured only up to 4 hours post-irradiation. During this doctoral project, several DSB rejoining kinetics studies were carried out initially with cells embedded in agarose plugs. The method was later abandoned since it was found that a competing *de novo* DNA fragmentation process was promptly triggered, perhaps due to the stress condition in which cells are exposed when embedded in a three dimensional agarose matrix (see § 2.4). As mentioned above, a comparison between rejoining kinetics results and whether proximity of DSBs plays a role in rejoining kinetics is greatly influenced by both experimental procedures and data analysis.

Excluding or including the signal contribution from small DNA fragments may affect estimates of DSB rejoining kinetics also in a different way. A recent study by Stenerlow and Hoglund (2002) shows how estimates of both slow and fast DSB rejoining kinetics

components, in the framework of a first-order repair kinetics model (§ 3.2.4), are affected by the presence of small DNA fragments in the experimental outcome. By varying the threshold size below which the number of fragments were counted at several repair times after both low and high LET radiation, Stenerlow and Hoglund show that estimates of F_{fast}, τ_{fast} and τ_{slow} vary, a result that they also obtained when DSB rejoining kinetics are studied in separate molecular weight intervals. One difficulty with the study by Stenerlow and Hoglund is that the authors have attempted to fit DSB rejoining data in restricted molecular weight regions with the equations provided by the first-order kinetics model. As also shown in the present study, Stenerlow and Hoglund stated that:

> "Analysis of rejoining in single size-intervals (but also in intervals that are cumulated, below a specified size, *personal note*) is complex and involves transfer of fragments from one size-interval to another; at the same time as fragments are rejoined and become larger, additional fragments, originating from rejoining of smaller pieces, will appear in that interval. . . ".

This very clear explanation by Stenerlow and Hoglund was essentially the main reason why rejoining kinetics in different size intervals were studied, in this work, with a computer-simulation that could account for all these non-local effects. The kinetics plots of figures 5.6, 5.7, 5.10 and 5.11 show that for some size intervals, specifically for larger fragments, one has a trend that is significantly different from an exponential decay with a double component. This is also evident in the work by Stenerlow and Hoglund themselves, in the 930-3500 kbp size region, where estimates of rejoining kinetics parameters were affected by large uncertainties due to the shallow slope of the slow rejoining phase. The shallow slope in this molecular weight region is due to the high rate of smaller fragments that, during rejoining, are entering this size region. This feature is even more evident in the 3500-5700 kbp region (figure 1, panel (e) in Stenerlow and Hoglund, 2002), where data cannot be fitted to a first order repair kinetics model at all, since the signal increases first, starting its decay only after the first hour of post-irradiation incubation.

Since the experimental data in this project do not allow us to discriminate between correct vs incorrect rejoining, the computer simulations have been designed to emulate correct DSB rejoining. This represents a major limitation both from the experimental and the theoretical point of view, for the results obtained in this project. In order to detect mis-rejoining at the Mbp scale and below, the technique developed by Löbrich *et al.* may be employed. According to recent data, mis-rejoining frequencies are in the order of 80%, if one allows also the slowly rejoining breaks to complete repair, even waiting for many days after radiation injury (M. Löbrich *et. al.*, unpublished results) This is in contrast to earlier data where it was believed that slowly rejoining breaks were ultimately reaching a

plateau phase, commonly referred to the level of breaks that could not be repaired. The recent observation by Löbrich *et. al.* provides evidence for all slowly rejoining fragments to be ultimately mis-rejoined. The numerical approach designed supports the existence of different type of breaks (see the object DSB in listing A.1), although in practice if mis-rejoining is to be modelled, it would be necessary to revise the chromosome geometry abstraction used in the codes, to allow for proximity of chromosome territories, as well as proximity of DSB ends that may originate from separate breaks.

That all the breaks are ultimately rejoined, although mis-rejoined, has been the basis of fitting DSB rejoining kinetics data in this study with a first-order kinetics model that does not contain a residual, unrepaired component (see eq. 3.11). An effect of such choice is that the slow repair half time τ_{slow} is much greater in this study compared to several published results of DSB rejoining kinetics, as can be seen in table 6.3, where results from PFGE experiments only are shown. The fast rejoining phase half-time also appears longer than for other published works, perhaps also influenced by the choice made for the fitting function.

6.4 Conclusion

The impact of background damage subtraction in PFGE data analysis has been described, and new methods have been developed and tested for the analysis of numerous DSB induction and rejoining experimental data obtained with the PFGE technique. When PFGE data are corrected for the effect of background damage by subtraction of the experimental determinations in the unirradiated controls, unwanted distortions are applied to the experimentally measured fragmentation patterns. Such distortions manifest themselves in an excess of double stranded fragments in the $\approx$ 100-500 kbp size region, always accompanied by depletion of larger, Mbp-sized fragments. When experimental data are treated as described, one may conclude that not only densely ionising radiation, but even low LET radiation such as 240 kVp X-rays can induce DNA double-strand breaks according to a clustered mechanism throughout the genome. Also, an excess of small DNA fragments is interpreted in DSB rejoining kinetics experiments as an indication of fragment size dependent kinetics: small DNA fragments would repair at a slower rate than Mbp-sized fragments.

Results obtained from the application of the method that have been developed in this project indicate that:

- when experimental data are corrected for the background damage using the procedures developed as part of the project, X-ray induced breaks appear to be dis-

Inter-study comparison of DSB rejoining kinetics for different types of radiation. PFGE studies

Cell type	radiation	method of analysis	f_{fast}	τ_{fast} (h^{-1})	τ_{slow} (h^{-1})	residual (%)	reference
GM578	$^{60}Co\gamma$	direct quantification†	0·59	0·13	1.5	–	Stenerlow and Hoglund, 2002
GM578	N 125 keV μm^{-1}	direct quantification‡	0·56	0·15	2·5	–	Stenerlow and Hoglund, 2002
V79/MeWo	6 MV X-rays	'dose-equivalent formalism'	0·5	0·25	1·67	7	Gauter *et al.* 2002
V79	$^{60}Co\gamma$	FAR	0·55	–	2·7±0·6	–	Stenerlöw *et al.* 1994
LS-174T	$^{60}Co\gamma$	FAR	0·76	–	4·5±0·3	–	Stenerlöw *et al.* 1994
U-343MG	$^{60}Co\gamma$	FAR	0·83	–	8·1±1·7	–	Stenerlöw *et al.* 1994
V79	He 55 keV μm^{-1}	FAR	0·52	–	2·2±0·6	–	Stenerlöw *et al.* 1994
LS-174t	He 55 keV μm^{-1}	FAR	0·68	–	3·1±0·6	–	Stenerlöw *et al.* 1994
U-343mg	He 55 keV μm^{-1}	FAR	0·78	–	3·9±1·7	–	Stenerlöw *et al.* 1994
GM5758	$^{60}Co\gamma$	direct quantification	0·93±0·03	0·32±0·13	1·3±1·0	4±3	Stenerlöw *et al.* 2000
GM5758	He 40 keV μm^{-1}	direct quantification	0·83±0·04	0·27±0·07	6·8±6·1	6±6	Stenerlöw *et al.* 2000
GM5758	N 80 keV μm^{-1}	direct quantification	0·84±0·04	0·28±0·03	2·7±0·5	5±2	Stenerlöw *et al.* 2000
GM5758	N 125 keV μm^{-1}	direct quantification	0·64±0·10	0·22±0·03	2·7±0·3	7±4	Stenerlöw *et al.* 2000
GM5758	N 175 keV μm^{-1}	direct quantification	0·71±0·02	0·25±0·12	2·1±1·5	12±4	Stenerlöw *et al.* 2000
GM5758	N 225 keV μm^{-1}	direct quantification	0·62±0·05	0·20±0·07	4·1±1·4	12±2	Stenerlöw *et al.* 2000
V79B	≈2·3 MeV neutrons	FAR	0·28±0·04	0·02±0·03	1·10±0·14	¶	Kysela *et al.* 1993a
XR-V15B	≈2·3 MeV neutrons	FAR	0·20±0·02	0·01±0·04	4·6±0·4	¶	Kysela *et al.* 1993a
V79B	250 kVp X-rays	FAR	0·62±0·05	0·04±0·02	0·83±0·17	¶	Kysela *et al.* 1993c
XR-V15B	250 kVp X-rays	FAR	0·53±0·01	0·06±0·01	6·6±1·1	¶	Kysela *et al.* 1993c
this study							
AG01522B	240 kVp X-rays	direct quantification	0·45±0·05	0·20±0·04	4±1	¶	
AG01522B	He 110 keV μm^{-1}	direct quantification	0·61±0·05	1·2±0·2	19±5	¶	

Table 6.3: DSB rejoining kinetics data from several published studies and this own, for direct quantification only. (†): fragments below 10 Mbp, (‡) fragments below 5·7 Mbp. (¶) assuming that all the breaks will ultimately be rejoined.

tributed randomly and uniformly throughout the genome of human cells,

- the mechanism of DSB induction by α-particles is consistent with a breakage process in which clusters of DNA DSBs are randomly and uniformly distributed, and within each cluster there can be on average six associated breaks within $\approx$18 Mbp,
- within the experimental size interval studied, spanning 30-5700 kbp, locally multiple damaged sites appear to be stronger determinants for DSB rejoining kinetics than regionally multiply damaged sites.

The two latter results combined together seem to suggest that the high radiation biological effectiveness of α-particles may be due to the local complexity of damage to DNA, that is to LMDS, hence to the nano-dosimetric property of this radiation, more than due to the ability of α-particles to cause regionally associated damage, that is to microdosimetric properties.

Appendix A

Examples of C++ computer program codes

In this Appendix, a few examples of C++ codes are illustated. The full program codes that were compiled to produce the executables for the DSB clustering simulations and DSB rejoining kinetics are omitted, since these would occupy too much space. However, excerpts from these codes are reported below to show the most relevant parts of the simulations of both DSB clustering and rejoining.

A.1 `DNAfragments` and `DSB` classes

Just like an integer, a float or a complex number type, a *class* is a user-defined type. The programmer designs it in order to be able to use it, and let other people use it, without remembering too many details of what's really inside it. If properly designed, a class can be used as any other object type. The user does not have access to all the elements of a class, so for example if you are given a remote control you just want to know what happens when you press its buttons, but you don't want to know about all the electronics that make the remote control work.

`DSB` and `DNAfragment` classes have been designed in a way that one could make operations with double-strand breaks and DNA double stranded fragments easily, such as building histograms, measuring sizes, repairing breaks, shuffling fragments, making χ^2 evaluations, without having to deal directly with numbers that would generate confusion. Listing A.1 introduces the `DSB` and `DNAfragment` classes, declaring data members and member functions, together with several functions that are 'friend' to the class, *i.e.* that have access to selected features of the class they are made friend to. A function declaration serves to give an idea of how is it used: which objects are passed to

it for its functioning and what type of object does it return when it has completed its job. The function definition instead is the detailed description of how the function is actually implemented. The functions declared in listing A.1 are defined in listing A.2. The other listings following show selected parts of the codes where DSB clustering and rejoining are implemented, and DSB and `DNAfragment` objects are employed.

Listing A.1: Declarations of `DNAfragments` and DSB classes plus facilitators

```
1  /* Fragments_and_Breaks.h
2  Declarations of the 'DSB' class and the 'DNAfragment' class
3  Designed and written beginning in May 2001 by Massimo Pinto
4  in Vitulazio (CE) - Italy and GCI, Northwood, Middx UK */
5  /**** Description ******/
6   // An Object of type 'DSB' is characterised by a coordinate on the
7   // chromosome (unigned long) where it is located and by a quality factor.
8   // An object of type 'DNAfragment' is characterised by its size and the
9   // quality of its two ends. The size is stored in an unsigned long
10  // integer, whereas the quality of the ends is stored as in an integer
11  // number, which can assume the following values:
12   // '0' if the break is an artifact of the technique that does not
13  // represent a real break in the cells
14   // '1' if the break is real and will be repaired correctly.
15   // '2' is a Telomere: a virtual rather than real break.
16   // '3' and following if the break has a chance of being
17  // mis-rejoined. The type of mis-rejoining will depend on the vicinity
18  // of other breaks that could be involved in mis-rejoining
19   // '4' is a radiation -induced break that cannot be repaired any
20  // further. For example, this is a ring that originated from two ends
21  // of the same fragment binding to each other.
22  // May 2001.
23  // The first implementation only goes up to quality of ends of type
24    // '0', '1' and '2' So, there is no support for mis-rejoining or for
25  // breaks that cannot be re-joined at all, yet.
26
27 /******** Declaration of the class DNAfragment ********/
28 #ifndef FRAGMENTS_AND_BREAKS
29 #define FRAGMENTS_AND_BREAKS
30 typedef unsigned long ulong;
31 typedef unsigned int uint;
32 #include<vector>
33 class DSB; /* You need to prototype this herem, since this is used in the
34                 DNAfragment class that is defined here below */
35 class DNAfragment {
36  protected:
37   friend class vector<DNAfragment>; /* The vector<> class is made
38   friend because there are rejoining () member functions that will need
39   to scan several elements of type DNAfragment within the same
40   vector<>. These functions are defined in this header file . There is
```

```
41    also a member function that creates a vector<DNAfragment> from a
42    vector<ulong>*/
43    friend class vector<DSB>; /* The classes vector<DSB> is also made
44                                 friend for the implementation of the
45                                 functions that transform vector<DSB> to
46                                 vector<DNAfragment> and vice-versa. */
47    // Data members
48    ulong size; /* Holds the size of the double-stranded fragment */
49    int first_end ; /* The quality of the first end */
50    int second_end; /* The quality of the second end */
51  public:
52    // Constructors
53    DNAfragment(); /* initialise to a fragment of 1 kbp length and simple
54                      ends */
55    DNAfragment(ulong a, int b = 1, int c = 1); // Initialise the
56    // fragment to size = a, both ends of quality "1".
57    DNAfragment(const DNAfragment&); // initialise to a fragment already given
58    // This is not a variable-sized object, as such, it should not need a destructor.
59    ~DNAfragment() {;} /* destructor */
60    // Query member functions, all in-lined due to their simplicity
61    ulong get_size () const{return size;}
62    int get_first_end () const{return first_end ;}
63    int get_second_end() const{return second_end;}
64    // Modifiers, in-lined as they are quite simple
65    void set_size(ulong a) {size = a;}
66    void set_first_end (int a) { first_end = a;}
67    void set_second_end(int a) {second_end = a;}
68    // Comparison functions and operators. Put here things like the
69    // operators ==, <, >, <=, >= and more comparison operators in case
70    // you need to use more sophisticated comparison criteria , for
71    // example checking whether the ends are similar , not just the size.
72    // Friend functions to implement rejoining and mis-rejoining
73    // The end_joining () function joins two contiguous ends if and only
74    // if these are perfectly reparable radiation-induced ends.
75    friend vector<DNAfragment> create_from_vec(vector<ulong> vec);
76    friend int end_tag(vector<DNAfragment> & vec, int index, int quality);
77    friend vector<DNAfragment> DSB_2_DNAfragment(const vector<DSB>);
78    friend vector<DSB> DNAfragment_2_DSB(const vector<DNAfragment>);
79    // For DSB repair
80    friend int end_joining(vector<DNAfragment> & vec, int index);
81    // For building fragment-type specific histograms
82    friend vector<ulong> DSB_2_fragment_sizes_with_quality(const
83                                                           vector<DSB>,
84                                                           const int ,
85                                                           const int );
86  };
87  /******** Declaration of the class DSB ********/
88  class DSB {
89    protected:
```

```
90  //      friend class vector<DNAfragment>; /* The vector<> class is made
91  //      friend because there are rejoining () member functions that will need
92  //      to scan several elements of type DNAfragment within the same
93  //      vector<>. These functions are defined in this header file . */
94    friend class vector<DSB>; /* Several features of DSB objects rely on
95                                 the vector<> functionality */
96    // Data members
97    ulong position ; /* Holds the coordinate */
98    int quality ; /* The quality of the dsb */
99   public:
100   // Constructors
101   DSB(); /* initialise a simple double strand break : ' zero ' coordinate
102             and type of break '1' */
103   DSB(ulong a, int b = 1); // Initialise the DSB to position = a , quality "1".
104   DSB(const DSB &);      // initialise to a DSB already existing
105   ~DSB() {;}     /* destructor */
106   // Query member functions , all in-lined due to their simplicity
107   ulong get_position () const{return position;}
108   int get_quality () const{return quality;}
109   // Modifiers , in-lined as they are quite simple
110   void set_position (ulong a) {position = a;}
111   void set_quality ( int a) { quality = a;}
112   friend void reset_quality (vector <DSB> & vec, int); /* Resets all
113   the DSBs as simple radiation -induced, i .e . type 1. */
114
115   // Comparison functions and operators .
116   // Friend functions to implement rejoining and mis-rejoining
117   // The end_joining () function joins two contiguous ends if and only
118   // if these are perfectly repairable radiation -induced ends.
119   friend vector<DSB> create_from_vector(const vector<ulong> vec, const
120                                         int q);
121   friend void make_DSB_vec(vector <DSB> & vec1, const vector <ulong>
122                            vec2, const int q);
123   friend int tag_a_break(vector<DSB> & vec, int index, int quality );
124   friend vector<DNAfragment> DSB_2_DNAfragment(const vector<DSB>);
125   friend vector<DSB> DNAfragment_2_DSB(const vector<DNAfragment>);
126   friend vector<ulong> DSB_2_ulong_sizes(const vector<DSB>);
127
128   /* Facilitators to count the number of DSB of a given quality in a
129      vector and in a vector of vectors */
130   friend int count_DSB_type(const vector<DSB> vec, const int quality);
131   friend int count_DSB_type_many_chromosomes(const vector < vector<DSB> > vec_of_vecs,
132                                              const int quality );
133
134   // For DSB repair
135   friend int remove_DSB(vector <DSB> & vec, const int index, const int quality);
136 };
137
138 // Functors
```

```
139
140 /* A class of objects that are designed to compare DNA fragments
141 according to size and DSBs according to their position */
142
143 class less_than
144 {
145   public:
146     bool operator () ( const DNAfragment& Arg1, const DNAfragment& Arg2
147                        )
148                     { return Arg1.get_size() < Arg2.get_size () ; }
149   bool operator () ( const DSB& Arg1, const DSB& Arg2
150                        )
151                     { return Arg1.get_position() < Arg2.get_position () ; }
152 };
153 #endif
```

Listing A.2 contains the explicit definitions of all the functions that have been declared in listing A.1.

Listing A.2: Definitions of `DNAfragments` and DSB classes plus their facilitators

```
1
2 #include "Fragments_and_Breaks.h"
3
4 /*********************************************************/
5 /******** Class DNAfragments function definitions ********/
6 /*********************************************************/
7
8  // Constructors
9
10 DNAfragment::DNAfragment() /* Default constructor: initialises a
11                                fragment of 1 kbp lenght as default . The
12                                ends are assumed to be 'good', i.e. they
13                                are reparable radiation -induced breaks.*/
14 {
15   size = 1000L;
16    first_end  = 1;
17   second_end = 1;
18 }
19
20 DNAfragment::DNAfragment(ulong a, int b = 1, int c = 1)
21 {
22   size = a;
23    first_end  = b;
24   second_end = c;
25 }
26
27 DNAfragment::DNAfragment(const DNAfragment &f) // Copy constructor
28 {
29   size = f.size;
```

```
30     first_end  =  f . first_end ;
31    second_end = f.second_end;
32  }
33
34  //  Friends
35
36  int  end_joining(vector<DNAfragment> & vec, int index) // Joins two
37     //  contiguous  ends as  long  as  they  are  reparable
38  {
39    if   ( ( index  + 1) < ( int )  vec.size () )
40      { /* Proceed with  these  two  fragments  only   if   they  both   exist   in
41             the  vector ,  otherwise  you have to   return  */
42        if   ( ( vec[index ]. get_second_end() == 1) &&
43             (vec[index+1]. get_first_end   () == 1) )   /*  If   the  ends to  be
44                                                              processed are  of  type
45                                                               '1' */
46          { /*  First   copy the  fragment  " sum" in  the   position   ' index ' */
47            vec[index ]. set_size (vec[index ]. get_size () +
48                                   vec[index+1].get_size  () );
49            vec[index ]. set_second_end(vec[index+1].get_second_end());
50            vec.erase(&vec[index+1]); /* Deletes  the  element  at  index  +
51                                         1 */
52            return  0;  /* The two fragments  have been  repaired  */
53          }
54        else
55          return  1;  /* One of  the  ends was not  reparable  */
56      }
57    else
58      return  2;  /* You have caught the   last   fragment  in   the   vector :
59                    index+1   falls    now out  of   the   vector    itself   . */
60  }
61
62  vector<DNAfragment> create_from_vec(vector<ulong> vec)
63  {
64    vector <DNAfragment> temp;
65    for  ( uint  i  = 0;  i  < vec.size (); ++ i )
66      {
67        DNAfragment buff(vec[i],1,1);
68        temp.push_back(buff);
69      }
70    return  temp;
71  }
72
73  //  end_tag ()  changes the  second end of  vec[ index ]  and the    first    end of
74  //  vec[ index +1],  thus  changes the    attributes    of  the  break  between
75  //  them . The  limit    of    its    action   may be vec. size ()  or  any  other
76  //    limit  . When tagging the  ends of   the  fragments  in  a   certain    bin ,
77  //  then  your  " limit  " has got  to  be  that   of  the  upper   limit    of  the  bin ,
78  //  or  you  risk    to    fall    in  the  next  bin . " Quality  " is  the    quality    of
```

```
79  // the break that you want to set.
80
81  int end_tag(vector<DNAfragment> & vec, int index, int limit, int quality)
82  {
83    if ((index + 1) < limit ) /* We are inside the region to process */
84      {
85        vec[index].set_second_end(quality);
86        vec[index+1].set_first_end (quality );
87        return 0;
88      }
89    else return 2; /* You have gone out of the limits */
90  }
91
92  // operators
93
94  bool operator< (const DNAfragment & a, const DNAfragment & b)
95  {
96    ulong size_a=a.get_size ();
97    ulong size_b=b.get_size ();
98    return (size_a < size_b);
99  }
100
101 DNAfragment operator+ (const DNAfragment &a, const DNAfragment &b)
102 {
103   DNAfragment temp(a.get_size()+b.get_size(),a.get_first_end (), b.get_second_end());
104   return temp;
105 }
106
107 /*********************************************/
108 /******* Class DSB function definitions *******/
109 /*********************************************/
110
111  // Constructors
112
113 DSB::DSB() /* Default constructor : initialises a DSB at position
114                 '0L'. The quality factor is by default set to '1',
115                 i.e. it's a genuine radiation -induced DSB. */
116 {
117   position = 0L;
118   quality  = 1;
119 }
120
121 DSB::DSB(ulong a, int b = 1) /* Explicit constructor : specifies the
122                                 DSB coordinate and the DSB quality . */
123 {
124   position = a;
125   quality = b;
126 }
127
```

```
128 DSB::DSB(const DSB &f) /* Copy constructor: creates an identical
129                           DSB. */
130 {
131   position = f.get_position();
132   quality = f.get_quality();
133 }
134
135 void reset_quality(vector<DSB> & vec, int q)
136 {
137   for (uint i = 0; i < vec.size(); ++i)
138     vec[i].set_quality(q);
139 }
140
141 // Friends
142
143 void make_DSB_vec(vector<DSB> & vec1, const vector<ulong>
144                   vec2, const int q)
145 {
146   for (uint i = 0; i < vec2.size(); ++i)
147     {
148       DSB buff(vec2[i],q);
149       vec1.push_back(buff);
150     }
151   return;
152 }
153
154 vector<DSB> create_from_vector(const vector<ulong> vec, const int q) /* This
155 is useful if you have a vector of ulongs, representing coordinates,
156 and want to create a vector of DSBs from it. All you need to do is to
157 add the information regarding the quality of the break, which by
158 default is set to '1'.*/
159 {
160   vector<DSB> temp;
161   for (uint i = 0; i < vec.size(); ++i)
162     {
163       DSB buff(vec[i],q);
164       temp.push_back(buff);
165     }
166   return temp;
167 }
168
169 // operators
170
171 bool operator< (const DSB & a, const DSB & b)
172 { /* The ordering criterium is on the sole position, regardless of the
173      quality of the ends. */
174   ulong pos_a=a.get_position();
175   ulong pos_b=b.get_position();
176   return (pos_a < pos_b);
```

```
177 }
178
179 /*********************************************/
180 /****** Inter-class function definitions ********/
181 /*********************************************/
182
183 // DSB_2_DNAfragment() transforms a vector of <DSB>s into a vector of
184 // <DNAfragment>
185
186 vector<DNAfragment> DSB_2_DNAfragment(const vector<DSB> the_DSB_vec)
187 { /* position_second - position_first requires the_DSB_vec to be
188       sorted */
189   vector<DNAfragment> buff; /* Elements will be 'push_back'ed here */
190   for (uint j = 0; j < (the_DSB_vec.size() -1); )
191     {
192       int quality_first = the_DSB_vec[j].get_quality ();
193       int quality_second = the_DSB_vec[++j].get_quality ();
194       ulong position_first = the_DSB_vec[--j].get_position();
195       ulong position_second = the_DSB_vec[++j].get_position();
196       DNAfragment temp;
197       temp.set_size(position_second - position_first );
198       temp.set_first_end ( quality_first );
199       temp.set_second_end(quality_second);
200       buff.push_back(temp);
201     }
202   return buff;
203 }
204
205 // DNAfragment_2_DSB() transforms a vector of <DNAfragment> into a
206 // vector of <DSB>s.
207
208 vector<DSB> DNAfragment_2_DSB(const vector<DNAfragment>
209                                 the_DNAfrag_vec)
210 {
211   vector<DSB> buff; /* Elements will be 'push_back'ed here */
212     ulong abscissa = 0L;
213     DSB temp;
214     for (uint j = 0; j < the_DNAfrag_vec.size(); )
215       {
216         //       int quality_first = the_DNAfrag_vec[j]. get_first_end ();
217         int quality_second = the_DNAfrag_vec[j].get_second_end();
218         ulong this_frag_size = the_DNAfrag_vec[j].get_size ();
219         abscissa += this_frag_size ;
220         temp.set_position(abscissa);
221         temp.set_quality(quality_second);
222         buff.push_back(temp);
223         ++j;
224       }
225       temp.set_position(0L);
```

```
226         temp.set_quality (0);  /* a telomere is a DSB of type 2 */
227         buff.insert(buff.begin(),temp);
228 //          buff[buff.size()-1]. set_quality (2);
229       return buff;
230 }
231
232 // Friends of the DSB class
233
234 //  DSB_2_fragment_sizes_with_quality () extracts the size of the
235 // fragment that is delimited by two ends of the same given
236 //  quality . Breaks of any other quality are considered absent, they do
237 // not chop down the sizes. This is very nice for extracting the fragment
238 // size distribution of the background or radiation -induced breaks
239 // only. You always need to specify the telomeres so two ' quality '
240 // values are necessary.
241
242 vector<ulong> DSB_2_fragment_sizes_with_quality(const vector<DSB>
243                                                 the_DSB_vec, const int
244                                                 quality1, const int
245                                                 quality2)
246 { vector <DSB> copy_with_q1_q2_only;
247  for (uint i = 0; i < the_DSB_vec.size(); ++i)
248    {
249      DSB temp = the_DSB_vec[i];
250       if ((temp.get_quality() == quality1 ) || (temp.get_quality() == quality2))
251         copy_with_q1_q2_only.push_back(temp);
252    }
253  vector <ulong> distances = DSB_2_ulong_sizes(copy_with_q1_q2_only);
254  return distances;
255 }
256
257 // DSB_2_ulong_sizes () transforms a vector of <DSB> into a vector of
258 // ulongs, where the distances between all the DSBs, without
259 //  distinction , are written down. Simplified from DSB_2_DNAfragment()
260
261 vector<ulong> DSB_2_ulong_sizes(const vector<DSB> the_DSB_vec)
262 { /* position_second - position_first requires the_DSB_vec to be
263       sorted */
264   vector<ulong> buff; /* Elements will be 'push_back'ed here */
265   for (uint j = 0; j < (the_DSB_vec.size() -1); )
266     {
267       ulong position_first = the_DSB_vec[j].get_position ();
268       ulong position_second = the_DSB_vec[++j].get_position();
269       ulong temp = position_second - position_first ;
270       buff.push_back(temp);
271     }
272   return buff;
273 }
274
```

```
275 int remove_DSB(vector <DSB> & vec, const int index, const int quality)
276 {
277   if (vec[index]. get_quality () == quality )
278     {     vec.erase(vec.begin()+index);
279     return 1; /* the break was successfully removed */
280     }
281   else return 0; /* the break was not to be repaired */
282 }
283
284 int count_DSB_type(const vector<DSB> vec, const int quality)
285 {
286   int sum=0;
287   for (uint j = 0; j < vec.size(); ++ j)
288     {
289       if (vec[j ]. get_quality () == quality )
290         sum++;
291     }
292   return sum;
293 }
294
295 int count_DSB_type_many_chromosomes(const vector < vector<DSB> > vec_of_vecs,
296                                     const int quality )
297 {
298   int total_sum = 0;
299   for (uint i = 0; i < vec_of_vecs.size(); ++ i)
300     {
301       total_sum += count_DSB_type(vec_of_vecs[i], quality );
302     }
303   return total_sum;
304 }
```

A.2 double-strand break clustering

Listing A.3 shows a part of the program code that was written to produce the executable program for the DSB clustering simulations. Objects of type DSB are employed here, whereas `DNAfragments` are used more extensively when looking at the size of fragments created for accumulating fragment size frequencies (not shown).

Listing A.3: the DSB clustering routine

```
666 /* ***************** */
667 /* Clustering begins */
668 /* ***************** */
669
670 int clustered = 0; /* The number of additional breaks
671                       added in this cluster . It 's a
672                       counter . */
```

```
673 double multiplicity = 0.0; /* The stochastic value for
674                                 each cluster
675                                   multiplicity . */
676
677 /* The number of EXTRA breaks to be located in THIS cluster is drawn
678    from a Poisson distribution with parameter ExpectCorrBreaks that
679    was read from the initialisation file */
680
681  multiplicity = PoissonDeviate(ExpectCorrBreaks,mtrand1);
682
683 if ( multiplicity >= 1.0) {
684   /* If at least one more break is to be added */
685   clustered = 0; /* counter for the number of additionally clustered
686                     breaks that we shall add now */
687
688   /* I moved the lines of code that set the cluster radius before the
689      while () loop because the cluster radius should be set BEFORE the
690      extra breaks are added in the cluster . Otherwise there is no real
691      clustering going on, since for every extra break there is a new
692      dice throw to set the cluster radius . Rather, I have in mind that
693      the cluster radius is a property of the cluster as a whole,
694      rather than its individual DSBs */
695
696   ulong temp_Cluster_Radius =
697     mtrand1.randInt(MaxClusterRadius);
698
699                 while (clustered < ( ( int ) multiplicity ) )
700                   {
701                   ulong clustered_break = 0L; /* The object where the
702                   temporary position of the clustered break is stored */
703
704                   /* We now examine a few different cases for the
705                      process of adding the breaks within the same
706                      cluster . These cases depend on the vicinity of
707                      the cluster centre to the telomeres and the value
708                      of the current cluster radius that has been drawn
709                      above . */
710
711                   if ( ( temp_Cluster_Origin > temp_Cluster_Radius)
712                     && ( ( temp_Cluster_Origin +
713                           temp_Cluster_Radius) < Chromosome_size) )
714                     { /* ' if ' case one: the cluster sits well
715                     somewhere inside the chromosome: generate a break
716                     nearby according to a uniform probability where
717                      temp_Cluster_Origin is the centre . */
718                         ulong LeftLimit = temp_Cluster_Origin -
719                           temp_Cluster_Radius;
720                         clustered_break = mtrand1.randInt(2*temp_Cluster_Radius);
721                         clustered_break += LeftLimit ;
```

```
722                 }
723             else if (temp_Cluster_Origin <
724                     temp_Cluster_Radius)
725                 { /* ' if ' case 2: the cluster radius spans
726                 down to the left telomere of the current
727                 chromosome. The uniform probability
728                  distribution for the localisation of the extra
729                 breaks in this cluster is not centred on
730                  temp_Cluster_Origin : it starts right on the
731                  left telomere and spans up to
732                  temp_Cluster_Origin + temp_Cluster_Radius
733                 which for convenience I call RightLimit . */
734                   ulong RightLimit = temp_Cluster_Origin +
735                     temp_Cluster_Radius;
736                   clustered_break = mtrand1.randInt(RightLimit);
737                   /* It is implicitly shifted to the right of
738                      the left telomere since this is in the
739                      null abscissa . */
740                 }
741         else if ((temp_Cluster_Origin +
742                   temp_Cluster_Radius ) >
743                  Chromosome_size)
744           { /* ' if ' case 3: the cluster contains the
745                 right telomere . Again , liker for the
746                 previuos case , the interval is smaller
747                 than the one in case 1 */
748             ulong LeftLimit = temp_Cluster_Origin -
749               temp_Cluster_Radius;
750             clustered_break = mtrand1.randInt(Chromosome_size - LeftLimit);
751             clustered_break += LeftLimit ;
752           }
753
754         /* Transform the clustered break into a DSB and
755            add it to the current chromosome, since you
756            have not left the chromosome since the
757            coordinate of the origin of the cluster was
758            set before . */
759
760         DSB clustered_DSB(clustered_break,1);
761         Diploid_Genome[this_chr].push_back(clustered_DSB);
762
763         /* Notice that in this way you come out with a
764            Diploid_Genome[ this_chr ] vector that is not
765            sorted . You will need to sort it later . */
766
767         TotalBreaks++; /* Record that one more break has
768                           been generated */
769         clustered++; /* Record also that you have added
770                         another break to ' this ' cluster
```

```
771                                    since you have a fixed
772                                     multiplicity as your upper
773                                    limit . */
774
775                        } /* Ends the while () loop that was locating as many
776                             breaks as the temporarily extracted multiplicity
777                             value */
778  } /* Ends clustering if multiplicity was > 1 */
779
780  /** ---Clustered part ends --**/
781   .....
```

A.3 double-strand break rejoining routines

Listing A.4 shows the relevant part of the DSB rejoining routine. The function 're-move_DSB()' and a few others appearing in this listing were defined in listing A.2. Only the part of the program code that is most relevant to the DSB rejoining aspect is shown.

Listing A.4: the DSB rejoining routine

```
895   /**********************************/
896   /**********************************/
897   /*            Rejoining part            */
898   /**********************************/
899   /**********************************/
900
901   /* How many breaks are to be repaired . The count has to be
902   made on the breaks that you consider to be reparable ,
903   i .e . those of type '1' and may be a fraction of those of
904   type '0', in a future potential implementation . */
905
906   int to_be_repaired =
907   ( int )(count_DSB_type_many_chromosomes(Diploid_Genome,1)*repair);
908
909   for ( int count = 0; count < to_be_repaired ; ) {
910     /* Randomly selects the chromosome where the DSB to be
911     repaired shall be found */
912     int this_chr = mtrand1.randInt(45);
913     if (reparable_DSB_per_chromosome[this_chr] > 0) {
914       /* Go ahead with rejoining if there are breaks to be
915       repaired in this chromosome */
916       int this_DSB =
917       mtrand1.randInt(Diploid_Genome[this_chr].size() -
918       1); /* A DSB is chosen randomly in
919       the selected chromosome */
920       if (remove_DSB(Diploid_Genome[this_chr],this_DSB,1)
921       == 1) { /* If the break selected for removal is a
```

```
922             suitable break, remove it ... */
923             reparable_DSB_per_chromosome[this_chr]--;
924             count++; /* ... and take two notes of it. The
925              first is decrementing the number of DSB
926             that are still available for removal in
927             this chromosome. The second is the
928             counter for the number of breaks
929             repaired */
930           }
931         }
932       }
933       .....
```

Acknowledgements

First of all I wish to thank my supervisors: Dr. Kevin Prise, Prof. John Hartley and my group leader, Prof. Barry Michael, for the support, the trust, and the ability to guide me trough a project that ended up in something much bigger and more fascinating that I could have possibly thought at the beginning. I have very much appreciated the attention that of you have paid to make sure that students in your group were always given the best opportunities. You have made sure I could participate to international congresses, workshops and those EEC consortia meetings, where questions raised made me think about what was I doing in depth.

If it had not been for Barry's attempts to persuade me to try to design computer models that had to be as simple as possible, right now I would be probably still be struggling with something far too sophisticated for the purposes of this project.

Virtually everything I know about PFGE, cell culture and laboratory work in general was thought to me by Dr. Heidi Newman. I owe you really much, Heidi.

Thanks to people in my group, in particular Melvyn for technical support, Stuart and Peppe, with whom I shared a lot of time discussing statistics and computer programming strategies.

People in the Gray Cancer Insitute from other research groups: Mick Woodcock, Peter Wardman and Marjorie Hance, Chris Martindale, Boris Vojnovic for the time generously spent trying to improve the sensitivity of PFGE, Ros Locke, Ross Maxwell, Nicola Ward, and all the mechanical workshop staff (also for fixing my bike a few times).

People from the CoMPLEX interest group at the University College London, for helping with programming and design of computer codes. A special thanks goes to James Heald, for advice on how to solve the many problems encountered with the 'recognise and tag' approach. A sincere thanks also goes to all those people that decided to reply (for free!) to tens and tens of my requests of help launched on the Usenet newsgroups which were dedicated to programming in C++, algorithms, the Linux programming environment and alike.

Thanks a lot to my flatmate Alex for cheering me up during the last year of the project, and pushing me up the Chiltern hills on my bike. Even more, for introducing me to Oscar Peterson's jazz piano.

Grazie alla mia famiglia, tutta, per l'appoggio e l'incoraggiamento. Più di chiunque altri: Renata, ancora una volta hai dimostrato di essere di enorme apoggio e di avere una fiducia praticamente illimitata nei miei confronti, sono molto fortunato e mi lamento troppo. Lorenzo, sembrerebbe che hai forse fatto poco, ma hai fatto in realtà davvero tantissimo.

Anche Akbar, tra un lancio di palla ed una finta rissa hai fatto in modo che si potesse fare delle felici pause.

This project would not have been possible without the support of the Sir Samuel Scott of Yews Trust, the Nuclear Fission Safety Programme of the European Union, and from Gray Laboratory Cancer Research Trust.

Northwood, 24th October 2002

Bibliography

AGER, D. D. and DEWEY, W. C., 1990, Calibration of pulsed field gel electrophoresis for measurement of DNA double-strand breaks. *International Journal of Radiation Biology*, **58**, 249–259. 52, 162

ALBERTS, B., BRAY, D., LEWIS, J., RAFF, M., ROBERTS, K. and WATSON, J. D., *Molecular Biology of the Cell* (Garland Publishing Inc., 1994), third edition. 157

ALMODOVAR, J. R. D., STEEL, G., WHITAKER, S. and MCMILLAN, T., 1994, A comparison of methods for calculating DNA double strand break induction frequency in mammalian cells by pulsed field gel electrophoresis. *International Journal of Radiation Biology*, **65**, 641–649. 162

ALPER, E. L., *Radiation Biophysics* (Academic Press, 1990), second edition. 65

BADIE, C., ILIAKIS, G., FORAY, N., ALSBEIH, G., CEDERVALL, B., CHAVAUDRA, N., PANTELIAS, G., ARLETT, C. and MALAISE, E. P., 1995, Induction and rejoining of DNA double-strand breaks and interphase chromosome breaks after exposure to X rays in one normal and two hypersensitive human fibroblast cell lines. *Radiation Research*, **144**, 26–35. 30, 124

BALLARINI, F., BIAGGI, M., MERZAGORA, M., OTTOLENGHI, A., DINGFELDER, M., FRIEDLAND, W., JACOB, P. and PARETZKE, H. G., 2000, Stochastic aspects and uncertainties in the prechemical and chemical stages of electron tracks in liquid water: a quantitative analysis based on Monte Carlo simulations. *Radiation and Environmental Biophysics*, **39**, 179–188. 76

BARENSDEN, G. W., Responses of cultured cells, tumours and normal tissues to radiations of different linear energy transfer. In: EBERT, M. and HOWARD, A., editors, *Current Topics of Radiation Research*, volume IV (North-Holland Publishing Company, Amsterdam, 1968), pages 293–356. 18

BARKAS, W. H., Nuclear Research Emulsion. Techniques and Theory. volume 1 (Academic Press, New York, 1963), pages 366–381. 16

BECKER, D. and SEVILLA, M. D., 1993, The chemical consequences of radiation damage to DNA. *Advances in Radiation Biology*, 121–180. 14

BEDFORD, J. S. and GOODHEAD, D. T., 1989, Breakage of human interphase chromosomes by alpha particles and X-rays. *International Journal of Radiation Biology*, **55**, 211–216. 121

BELLI, M., CERA, F., CHERUBINI, R., HAQUE, A. M., IANZINI, F., MOSCHINI, G., SAPORA, O., SIMONE, G., TABOCCHINI, M. A. and TIVERON, P., 1993, Inactivation and mutation induction in V79 cells by low energy protons: re-evaluation of the results at the LNL facility. *International Journal of Radiation Biology*, **63**, 331–337. 16

BELLI, M., CERA, F., CHERUBINI, R., IANZINI, F., MOSCHINI, G., SAPORA, O., SIMONE, G., TABOCCHINI, M. A. and TIVERON, P., 1991, Mutation induction and RBE-LET relationship of low-energy protons in V79 cells. *International Journal of Radiation Biology*, **59**, 459–465. 16

BELLI, M., CERA, F., CHERUBINI, R., IANZINI, F., MOSCHINI, G., SAPORA, O., SIMONE, G., TABOCCHINI, M. A. and TIVERON, P., 1994, DNA double-strand breaks induced by low energy protons in V79 cells. *International Journal of Radiation Biology*, **65**, 529–536. 26, 31

BELLI, M., CHERUBINI, R., FINOTTO, S., MOSCHINI, G., SAPORA, O., SIMONE, G. and TABOCCHINI, M. A., 1989, RBE-LET relationship for the survival of V79 cells irradiated with low energy protons. *International Journal of Radiation Biology*, **55**, 93–104. 16

BELLI, M., CHERUBINI, R., GALEAZZI, G., MAZZUCATO, S., MOSCHINI, G., SAPORA, O., SIMONE, G. and TABOCCHINI, M. A., A new facility for radiobiological studies with proton beams: survival and DNA damage in mammalian cells. In: ONORI, S. and TABET, E., editors, *Physics in Environmental and Biomedical Research* (World Scientific Publishing, Singapore, 1986), pages 109–113. 16

BELLI, M., CHERUBINI, R., GALEAZZI, G., MAZZUCATO, S., MOSCHINI, G., SAPORA, O., SIMONE, G. and TABOCCHINI, M. A., 1987, Proton irradiation facility for radiobiological studies at 7 MeV Van De Graaf accelerator. *Nuclear Instruments and Methods in Physics Research, A*, **256**, 576–580. 16

BELLI, M., CHERUBINI, R., VECCHIA, M. D., DINI, V., ESPOSITO, G., MOSCHINI, G., SAPORA, O., SIGNORETTI, C., SIMONE, G., SORRENTINO, E. and TABOCCHINI, M. A., 2001, DNA fragmentation in mammalian cells exposed to various light ions. *Advances in Space Research*, **27**. 31, 56, 65, 69, 70, 76, 98, 154, 158, 162

BELLI, M., CHERUBINI, R., VECCHIA, M. D., DINI, V., ESPOSITO, G., MOSCHINI, G., SAPORA, O., SIMONE, G. and TABOCCHINI, M. A., 2002, DNA fragmentation in V79 cells irradiated with light ions as measured by pulsed-field gel electrophoresis. I. Experimental results. *International Journal of Radiation Biology*, **78**, 475–482. 31, 56, 57, 65, 69, 154, 162, 164

BELLI, M., GOODHEAD, D. T., IANZINI, F., SIMONE, G. and TABOCCHINI, M. A., 1992, Direct comparison of biological effectiveness of protons and alpha-particles of the same LET. II. Mutation induction at the HPRT locus in V79 cells. *International Journal of Radiation Biology*, **61**, 625–629. 16

BEREZNEY, R., 1991, The nuclear matrix: a heuristic model for investigating genomic organization and function in the cell nucleus. *Journal of Cellular Biochemistry*, **47**, 109–123. 19, 21

BLOCHER, D., 1988, DNA double-strand break repair determines the RBE of alpha-particles. *International Journal of Radiation Biology*, **54**, 761–771. 30

BLÖCHER, D., 1990, In CHEF electrophoresis a linear induction of dsb corresponds to a nonlinear fraction of extracted DNA with dose. *International Journal of Radiation Biology*, **57**, 7–12. 52, 54, 56, 63

BOX, H. C., BUDZINSKI, E. E., DAWIDZIK, J., PATRZYC, H. B. and FREUND, H. G., 2001, A novel double lesion in X-irradiated DNA consists of a strand break and a base modification. *Radiation Research*, **156**, 215–219. 159

BOYLE, S., GILCHRIST, S., BRIDGER, J. M., MAHY, N. L., ELLIS, J. A. and BICKMORE, W. A., 2001, The spatial organization of human chromosomes within the nuclei of normal and emerin-mutant cells. *Human Molecular Genetics*, **10**, 211–219. 28

BURKART, W., JUNG, T. and FRASCH, G., 1999, Damage pattern as a function of radiation quality and other factors. *Comptes rendus de l'Académie des sciences–Série III*, **322**, 89–101. 24, 25

CEDERVALL, B., 1995, *Analysis of X-ray induced DNA double strand breaks using pulsed field gel electrophoresis. Application to the study of radiosensitivity of human cells.*. Ph.D. Thesis, Department of Medical Radiation Physics and Medical Radiobiology, Karolinska Institutet, Stockholm. 55

CEDERVALL, B. and KALLMAN, P., 1994, Randomly distributed DNA double-strand breaks as measured by pulsed field gel electrophoresis: a series of explanatory calculations. *Radiation and Environmental Biophysics*, **33**, 9–21. 50, 54

CEDERVALL, B. and LANGE, C. S., 1998, Analysis of DNA mass distributions in pulsed-field gels to determine DNA dsb induction and rejoining kinetics. In: *Abstracts of the 46th Annual Meeting of the Radiation Research Society*, Nashville: Radiation Research Society, Abstract P20-379. 54, 55

CEDERVALL, B. and RADIVOYEVITCH, T., 1996, Methods for analysis of DNA fragment distributions on pulsed field gel electrophoretic gels. *Electrophoresis*, **17**, 1080–1086. 54

CEDERVALL, B., WONG, R., ALBRIGHT, N., DYNLACHT, J., LAMBIN, P. and DEWEY, W. C., 1995, Methods for the quantification of DNA double-strand breaks determined from the distribution of DNA fragment sizes measured by pulsed-field gel electrophoresis. *Radiation Research*, **143**, 8–16. 54, 61, 62, 153

CEDERVALL, B. E. and MCMILLAN, T. J., 2002, The fraction of DNA released on pulsed-field gel electrophoresis gels may differ significantly between genomes at low levels of double strand breaks. *Radiation Research*, 247–249. 40

CHARLESBY, A., 1953, Molecular-Weight changes in the degradation of long chain polymers. *Journal of the Royal Statistical Society*, 120–128. 25, 32, 54, 68, 122

CHATTERJEE, A., MACCABEE, H. D. and TOBIAS, C. A., 1973, Radial cutoff LET and radial cutoff dose calculations for heavy charged particles in water. *Radiation Research*, **54**, 479–494. 17

CHRISTENSEN, R. C., TOBIAS, C. A. and TAYLOR, W. D., 1972, Heavy-ion-induced single- and double-strand breaks in ϕX-174 replicative form DNA. *International Journal of Radiation Biology and Related Studies in Physics and Chemistry*, **22**, 457–477. 26

CHU, G., VOLLRATH, D. and DAVIS, R., 1986, Separation of large DNA molecules by contour clamped homogenous electric fields. *Science*, **234**, 1582–1585. 45

COHOON, J. and DAVIDSON, J., *C++ Program Design: An Introduction to Programming and Object Oriented Design* (McGraw-Hill, 1997). 74

COLE, A., MEYN, R. E., CHEN, R., CORRY, P. M. and HITTELMAN, W., Mechanisms of cell injury. In: MEYN, R. E. and WITHERS, H. R., editors, *Radiation Biology in Cancer Research* (Raven Press, New York, 1980), pages 33–58. 23, 24

CONTOPOULOU, C. R., COOK, V. E. and MORTIMER, R. K., 1987, Analysis of DNA double strand breakage and repair using orthogonal field alternation gel electrophoresis. *Yeast*, **3**, 71–76. 32, 54, 59

COOK, V. E. and MORTIMER, R. K., 1991, A quantitative model of DNA fragments generated by ionizing radiation, and possible experimental applications. *Radiation Research*, **125**, 102–106. 32, 59

COQUERELLE, T. M., WEIBEZAHN, K. F. and LUCKE-HUHLE, C., 1987, Rejoining of double strand breaks in normal human and ataxia-telangiectasia fibroblasts after exposure to 60Co gamma-rays, 241Am alpha-particles or bleomycin. *International Journal of Radiation Biology and Related Studies in Physics and Chemistry*, **51**, 209–218. 30

CORNFORTH, M. N. and BEDFORD, J. S., 1987, A quantitative comparison of potentially lethal damage repair and the rejoining of interphase chromosome breaks in low passage normal human fibroblasts. *Radiation Research*, **111**, 385–405. 26

CREMER, T. and CREMER, C., 2001, Chromosome territories, nuclear architecture and gene regulation in mammalian cells. *Nature Reviews Genetics*, **2**, 292–301. 22

CUCINOTTA, F. A., NIKJOO, H., O'NEILL, P. and GOODHEAD, D. T., 2000, Kinetics of DSB rejoining and formation of simple chromosome exchange aberrations. *International Journal of Radiation Biology*, **76**, 1463–1474. 72

DAHM-DAPHI, J. and DIKOMEY, E., 1996, Rejoining of DNA double-strand breaks in X-irradiated CHO cells studied by constant- and graded-field gel electrophoresis. *International Journal of Radiation Biology*, **69**, 615–621. 169

DARROUDI, F. and NATARAJAN, A. T., 1991, Studies on the origin of chromosomal alterations induced by ionising radiations: utilization of repair-deficient mammalian mutant cells. In: CHAPMAN, J. D., DEWEY, W. C. and WHITMORE, G. F., editors, *Radiation Research, a Twentieth-century perspective*, volume 1 (Academic Press, San Diego, 1991). 26

DAVID-CORDONNIER, M. H., CUNNIFFE, S. M., HICKSON, I. D. and O'NEILL, P., 2002, Efficiency of incision of an AP site within clustered DNA damage by the major human AP endonuclease. *Biochemistry*, **41**, 634–642. 159, 168

DE LARA, C. M., HILL, M. A., JENNER, T. J., PAPWORTH, D. and O'NEILL, P., 2001, Dependence of the yield of DNA double-strand breaks in Chinese hamster V79-4 cells on the photon energy of ultrasoft X rays. *Radiation Research*, **155**, 440–448. 161, 162

DEUTSCH, J. M., 1988, Theoretical Studies of DNA During Gel Electrophoresis. *Science*, **240**, 922–4. 45

DURANTE, M., FURUSAWA, Y., GEORGE, K., GIALANELLA, G., GRECO, O., GROSSI, G., MATSUFUJI, N., PUGLIESE, M. and YANG, T. C., 1998a, Rejoining and misrejoining of radiation-induced chromatin breaks. IV. Charged particles. *Radiation Research*, **149**, 446–54. 121

DURANTE, M., GEORGE, K., WU, H.-L. and YANG, T. C., 1998b, Rejoining and misrejoining of radiation-induced chromatin breaks. III. Hypertonic treatment. *Radiation Research*, 68–74. 121

DURANTE, M., GROSSI, G. F., PUGLIESE, M., NAPPO, M. and GIALANELLA, G., Correlation between chromosome damage and cell killing in mammalian cells exposed to photons or hadrons. In: AMALDI, U. and LARSSON, B., editors, *Adrontherapy in Oncology* (Excerpta Medica, Elevier Science, 1994), pages 712–716. 26

EASTMAN, A. and BARRY, M. A., 1992, The origins of DNA breaks: a consequence of DNA damage, DNA repair, or apoptosis? *Cancer Investigation*, **10**, 229–240. 24, 27

ELIA, M. C. and NICHOLS, W. W., 1993. Application of programmable, autonomously controlled electrode (PACE) technology to the development of an improved pulsed field gel electrophoresis assay for DNA double strand breaks in mammalian cells. Technical Report 1. 47

ELKIND, M. M., 1985, DNA Damage and Cell Killing: Cause and Effect? *Cancer*, **56**, 2351–2363. 23

ELKIND, M. M. and SUTTON, H., 1959, X-ray damage and recovery in mammalian cells in culture. *Nature*. 27

ERIXON, K. and CEDERVALL, B., 1995, Linear induction of DNA double-strand breakage with X-ray dose, as determined from DNA fragment size distribution. *Radiation Research*, **142**, 153–162. 65, 154

FILIPSKI, J., LEBLANC, J., YOUDALE, T., SIKORSKA, M. and WALKER, P. R., 1990, Periodicity of DNA folding in higher order chromatin structures. *The EMBO Journal*, **9**, 1319–1327. 19, 20, 22

FINCH, J. T. and KLUG, A., 1976, Solenoidal model for superstructure in chromatin. *Proceedings Of The National Academy Of Sciences (U.S.A.)*, **73**, 1897–1901. 21

FLOWERS, B., *An Introduction to Numerical Methods in C++* (Oxford University Press, 2000), second revised edition. 74

FOLKARD, M., PRISE, K. M., VOJNOVIC, B., DAVIES, S., ROPER, M. J. and MICHAEL, B. D., 1989, The irradiation of V79 mammalian cells by protons with energies below 2 MeV. Part I: Experimental arrangement and measurements of cell survival. *International Journal of Radiation Biology*, **56**, 221–237. 16, 38

FOLKARD, M., PRISE, K. M., VOJNOVIC, B., NEWMAN, H. C., ROPER, M. J. and MICHAEL, B. D., 1996, Inactivation of V79 cells by low-energy protons, deuterons and ^{3}He ions. *International Journal of Radiation Biology*, 729–738. 16

FORAY, N., ARLETT, C. and MALAISE, E., 1997a, Radiation-Induced DNA Double-Strand Breaks and the Radiosensitivity of Human Cells: A Closer Look. *Biochimie*, **79**, 567–75. 26, 30, 34

FORAY, N., BADIE, C., ALSBEIH, G., FERTIL, B. and MALAISE, E. P., 1996, A new model describing the curves for repair of both DNA double-strand breaks and chromosome damage. *Radiation Research*, **146**, 53–60. 72

FORAY, N., PRIESTLEY, A., ALSBEIH, G., BADIE, C., CAPULAS, E. P., ARLETT, C. F. and MALAISE, E. P., 1997b, Hypersensitivity of ataxia telangiectasia fibroblasts to ionizing radiation is associated with a repair deficiency of DNA double-strand breaks. *International Journal of Radiation Biology*, **72**, 271–283. 30

FOWLER, J. F., 1999, Is repair of DNA strand break damage from ionizing radiation second-order rather than first-order? A simpler explanation of apparently multiexponential repair. *Radiation Research*, **152**, 124–136. 71, 72

FOX, J. C., 1990, Evidence to support the existence of efficient DNA double-strand break rejoining in a radiosensitive mutant of V79-4 following irradiation with 250 kVp X-rays or neutrons. *Mutation Research*, **235**, 41–7. 30

FOX, J. C. and MCNALLY, N. J., 1988, Cell survival and DNA double-strand break repair following X-ray or neutron irradiation of V79 cells. *International Journal of Radiation Biology*, **54**, 1021–1030. 30

FOX, J. C. and PRISE, K. M., 1993, DNA lesions: linear energy transfer and radiosensitive mutants. *British Journal of Radiology*, **suppl.**, 48–52. 26, 27

FRIEDL, A., KRAXENBERGER, A. and ECKARDT-SCHUPP, F., 1995, An Electrophoretic Approach to the Assessment of the Spatial Distribution of DNA Double Strand Breaks in Mammalian Cells. *Electrophoresis*, **16**, 1865–1874. 162

FRIEDLAND, W., JACOB, P., PARETZKE, H. G., MERZAGORA, M. and OTTOLENGHI, A., 1999, Simulation of DNA fragment distributions after irradiation with photons. *Radiation and Environmental Biophysics*, **38**, 39–47. 32, 76, 84, 163

FRIEDLAND, W., JACOB, P., PARETZKE, H. G. and STORK, T., 1998, Monte Carlo simulation of the production of short DNA fragments by low-linear energy transfer radiation using higher-order DNA models. *Radiation Research*, **150**, 170–182. 32, 76

FRIEDLAND, W., JAKOB, P., PARETZKE, H. G. and STORK, T., Simulation of strand breaks and short DNA fragments in the biophysical model PARTRAC. In: GOODHEAD, D. T., O'NEILL, P. and MENZEL, H. G., editors, *Microdosimetry: an interdisciplinary approach* (The Royal Society of Chemistry, Cambridge, 1997), pages 43–46. 76

GAUTER, B., ZLOBINSKAYA, O. and WEBER, K. J., 2002, Rejoining of radiation-induced DNA double-strand breaks: pulsed-field electrophoresis analysis of fragment size distributions after incubation for repair. *Radiation Research*, **157**, 721–733. 127, 147, 169, 172

GOODHEAD, D. T., Relationship of microdosimetric techniques to application in biological systems. In: KASE, K. R., BJAERNGARD, B. E. and ATTIX, F. H., editors, *Dosimetry of ionizing radiations*, volume 2 (Academic Press, Orlando, 1987), pages 1–89. 17

GOODHEAD, D. T., 1994, Initial events in the cellular effects of ionizing radiations: clustered damage in DNA. *International Journal of Radiation Biology*, **65**, 7–17. 24, 25

GULSTON, M., FULFORD, J., JENNER, T., DE LARA, C. and O'NEILL, P., 2002, Clustered DNA damage induced by γ radiation in human fibroblasts (HF19), hamster (V79-4) cells and plasmid DNA is revealed as Fpg and Nth sensitive sites. *Nucleic Acids Research*, in press. 159

HABER, J., 2000, Partners and pathways repairing a double-strand break. *Trends in Genetics*, **16**, 259–264. 28

HARDER, D., Pairwise lesion interaction. Extension and confirmation of of Lea's model. In: FIELDEN, E. M., FOWLER, J. F., HENDRY, J. H. and SCOTT, D., editors, *Radiation Research*, volume 2 (Taylor and Francis, London, 1987), pages 318–324. 17

HEILMANN, J., TAUCHER-SCHOLZ, G. and KRAFT, G., 1995, Induction of DNA double-strand breaks in CHO-K1 cells by carbon ions. *International Journal of Radiation Biology*, **68**, 153–62. 57

HÖGLUND, E., BLOMQUIST, E., CARLSSON, J. and STENERLÖW, B., 2000, DNA damage induced by radiation of different linear energy transfer: initial fragmentation. *International Journal of Radiation Biology*, **76**, 539–547. 31, 50, 57, 59, 65, 69, 161, 162, 164

HÖGLUND, E. and STENERLÖW, B., 2001, Induction and rejoining of DNA double-strand breaks in normal human skin fibroblasts after exposure to radiation of different linear energy transfer: possible roles of track structure and chromatin organization. *Radiation Research*, **155**, 818–825. 31, 32, 50, 57, 71, 99, 154

HOLLEY, W. R. and CHATTERJEE, A., 1996, Clusters of DNA induced by ionizing radiation: formation of short DNA fragments. I. Theoretical modeling. *Radiation Research*, **145**, 188–199. 25, 32, 76

ICRP, 1980. Recommendations, Report 30. Technical report, International Commission on Radiological Protection. 16

ILIAKIS, G., 1991, The role of DNA double strand breaks in ionizing radiation-induced killing of eukaryotic cells. *Bioessays*, **13**, 641–648. 25, 52

ILIAKIS, G., OKAYASU, R. and SEANER, R., 1988, Radiosensitive xrs-5 and parental CHO cells show identical DNA neutral filter elution dose-response: implications for a relationship between cell radiosensitivity and induction of DNA double-strand breaks. *Int J Radiat Biol*, **54**, 55–62. 26

ILIAKIS, G. E., CICILIONI, O. and METZGER, L., 1991, Measurement of DNA double-strand breaks in CHO cells at various stages of the cell cycle using pulsed field gel electrophoresis: calibration by means of ^{125}I decay. *International Journal of Radiation Biology*, **59**, 343–357. 162

INTERNATIONAL HUMAN GENOME SEQUENCING CONSORTIUM, 2001, Initial sequencing and analysis of the human genome. *Nature*, **409**, 860–921. 49, 59, 68

JEGGO, P. A., 1998a, DNA breakage and repair. *Advances in Genetics*, **38**, 185–218. 28

JEGGO, P. A., 1998b, Identification of genes involved in repair of DNA double-strand breaks in mammalian cells. *Radiation Research*, **150**, S80–S91. 26, 28, 30

JEGGO, P. A. and KEMP, L. M., 1983, X-ray-sensitive mutants of Chinese hamster ovary cell line. Isolation and cross-sensitivity to other DNA-damaging agents. *Mutation Research*, **112**, 313–327. 26

JENNER, T. J., BELLI, M., GOODHEAD, D. T., IANZINI, F., SIMONE, G. and TABOCCHINI, M. A., 1992, Direct comparison of biological effectiveness of protons and alpha-particles of the same LET. III. Initial yield of DNA double-strand breaks in V79 cells. *International Journal of Radiation Biology*, **61**, 631–637. 16

JENNER, T. J., FULFORD, J. and O'NEILL, P., 2001, Contribution of base lesions to radiation-induced clustered DNA damage: implication for models of radiation response. *Radiation Research*, **156**, 590–593. 155, 159

JOHANSEN, L., The contribution of water-free radicals to the X-ray inactivation of bacteria. In: *Cellular Radiation Biology* (Williams and Wilkins, Baltimore, 1965), pages 103–106. 19

JOHNSTON, P., MACPHAIL, S., BANÀTH, J. and OLIVE, P., 1998a, Higher Order Chromatin Structure-Dependent Repair of DNA Double Strand Breaks:Factors Affecting Elution of DNA from Nucleoids. *Radiation Research*, **149**, 533–542. 22, 29, 31, 165, 168

JOHNSTON, P., MACPHAIL, S., STAMATO, T., KIRCHGESSNER, C. and OLIVE, P., 1998b, Higher Order Chromatin Structure Dependent Repair of DNA Double Strand Breaks: Involvement of the V(D)J Recombination Double Strand Break Repair Pathway. *Radiation Research*, **149**, 455–462. 22, 29, 31, 147, 168

KEMP, L. M., SEDGWICK, S. G. and JEGGO, P. A., 1984, X-ray sensitive mutants of Chinese hamster ovary cells defective in double-strand break rejoining. *Mutation Research*, **132**, 189–196. 26

KHVOSTUNOV, I. K. and ANDREEV, S. G., 2001, Biophysical analysis of radiation induced initial DNA fragmentation. In: *Abstracts of the 13th symposium on Microdosimetry, Stresa (Lake Maggiore), Italy*, Poster D4. 76, 156

KILTIE, A. E., ORTON, C. J., RYAN, A. J., ROBERTS, S. A., MARPLES, B., DAVIDSON, S. E., HUNTER, R. D., MARGISON, G. P., WEST, C. M. and HENDRY, J. H., 1997, A correlation between residual DNA double-strand breaks and clonogenic measurements of radiosensitivity in fibroblasts from preradiotherapy cervix cancer patients. *International Journal of Radiation Oncology, Biology and Physics*, **39**, 1137–144. 56

KILTIE, A. E., RYAN, A. J., SWINDELL, R., BARBER, J. B., WEST, C. M., MAGEE, B. and HENDRY, J. H., 1999, A correlation between residual radiation-induced DNA double-strand breaks in cultured fibroblasts and late radiotherapy reactions in breast cancer patients. *Radiotherapy Oncology*, **51**, 55–65. 56

KODAMA, Y., NAKANO, M., OHTAKI, K., DELONGCHAMP, R., AWA, A. A. and NAKAMURA, N., 1997, Estimation of minimal size of translocated chromosome segments detectable by fluorescence *in situ* hybridization. *International Journal of Radiation Biology*, 35–39. 123

KRAXENBERG, F., WEBER, K. J., FRIEDL, A. A., ECKARDT-SCHUPP, F., FLENTJE, M., QUICKEN, P. and KELLERER, A. M., 1998, DNA double-strand breaks in mammalian cells exposed to γ rays and very heavy ions. *Radiation and Environmental Biophysics*, 107–115. 69, 86, 162, 165

KÜHNE, M., ROTHKAMM, K. and LÖBRICH, M., 2000, No dose-dependence of DNA double-strand break misrejoining following alpha-particle irradiation. *International Journal of Radiation Biology*, **76**, 891–900. 71

KUZMINOV, A., *Recombinationl repair of DNA damage, Molecular Biology Intelligence Unit* (Springer–Verlag, 1996). 28, 29

KYSELA, B., 1994, *Ionizing radiation-induced DNA damage and repair in relation to biological function*. Ph.D. Thesis, Dept. of Biology and Biochemistry, Brunel University. 40, 44, 56, 57

KYSELA, B. P., ARRAND, J. E. and MICHAEL, B. D., 1993a, Relative contributions of levels of initial damage and repair of double-strand breaks to the ionizing radiation-sensitive phenotype of the Chinese hamster cell mutant, XR-V15B. Part II. Neutrons. *International Journal of Radiation Biology*, **64**, 531–538. 71, 172

KYSELA, B. P., MICHAEL, B. D. and ARRAND, J. E., 1993b, Field-inversion gel electrophoresis analysis of the induction and rejoining of DNA double-strand breaks in cells embedded in agarose. *Radiation Research*, **134**, 107–111. 56

KYSELA, B. P., MICHAEL, B. D. and ARRAND, J. E., 1993c, Relative contributions of levels of initial DNA damage and repair of double strand breaks to the ionizing radiation-sensitive phenotype of the Chinese hamster cell mutant, XR-V15B. Part I. X-rays. *International Journal of Radiation Biology*, **63**, 609–616. 71, 172

LEA, D., *Action of radiation on living cells* (University Press, Cambridge, 1946). 3, 19

LEHMANN, A. R. and ORMEROD, M. G., 1970, The replication of DNA in murine lymphoma cells (L5178Y). I. Rate of duplication. *Biochimica et Biophysics Acta*, **204**, 128–143. 61

LITWIN, S., 1969, The Distribution of Radioactive Recovery in Randomly Cut and Segmented DNA. *Journal of Applied Probability*, **6**, 275–284. 32, 54

LÖBRICH, M., COOPER, P. K. and RYDBERG, B., 1996, Non-random distribution of DNA double-strand breaks induced by particle irradiation. *International Journal of Radiation Biology*, **70**, 493–503. 31, 48, 57, 69, 162, 163, 164

LÖBRICH, M., IKPEME, S., HAUB, P., WEBER, K. J. and KIEFER, J., 1993, DNA double-strand break induction in yeast by X-rays and alpha-particles measured by pulsed-field gel electrophoresis. *International Journal of Radiation Biology*, **64**, 539–546. 31

LÖBRICH, M., KÜHNE, M., WETZEL, J. and ROTHKAMM, K., 2000, Joining of correct and incorrect DNA double-strand break ends in normal human and ataxia telangiectasia fibroblasts. *Genes Chromosomes & Cancer*, **27**, 59–68. 71

LÖBRICH, M., RYDBERG, B. and COOPER, P. K., 1995, Repair of x-ray-induced DNA double-strand breaks in specific Not I restriction fragments in human fibroblasts: joining of correct and incorrect ends. *Proceedings Of The National Academy Of Sciences (U.S.A.)*, **92**, 12,050–12,054. 28, 71, 170

MANUELIDIS, L., 1990, A view of interphase chromosomes. *Science*, **250**, 1533–1540. 22, 165

MATSUMOTO, M. and NISHIMURA, T., 1998, Mersenne Twister: A 623-Dimensionally Equidistributed Uniform Pseudo-Random Number Generator. *ACM Transactions on Modeling and Computer Simulation*, **8**, 3–30. 78

MIRKOVITCH, J., GASSER, S. M. and LAEMMLI, U. K., 1987, Relation of chromosome structure and gene expression. *Philosophical transactions of the Royal Society of London. Series B: Biological sciences*, **317**, 563–574. 19

MONTROLL, E. and SIMHA, R., 1940, Theory of depolymerization of long chain molecules. *Journal of Chemical Physics*, **8**, 721–727. 25, 32, 54

MUNRO, T. R., 1970, The relative radiosensitivity of the nucleus and cytoplasm of Chinese hamster fibroblasts. *Radiation Research*, **42**, 451–470. 3

NASONOVA, E., GUDOWSKA-NOWAK, E., RITTER, S. and KRAFT, G., 2001, Analysis of Ar-ion and X-ray-induced chromatin breakage and repair in V79 plateau-phase cells by the premature chromosome condensation technique. *International Journal of Radiation Biology*, **77**, 59–70. 124, 149

NCRP, 1979. Tritium and other radionuclide labelled organic compounds incorporated in genetic material. Technical report, National Council on Radiation Protection, Washington, DC. 3

NEWMAN, H. C., PRISE, K. M., FOLKARD, M. and MICHAEL, B. D., 1997, DNA double-strand break distributions in X-ray and α-particle irradiated V79 cells: evidence for non-random breakage. *International Journal of Radiation Biology*, **71**, 347–363. 31, 32, 41, 48, 57, 61, 62, 69, 161, 162, 163, 164

NEWMAN, H. C., PRISE, K. M. and MICHAEL, B. D., 2000, The role of higher-order chromatin structure in the yield and distribution of DNA double-strand breaks in cells irradiated with X-rays or alpha-particles. *International Journal of Radiation Biology*, **76**, 1085–1093. 57, 69

OLIVE, P., BANÁTH, J. and MACPHAIL, S., 1994, Lack of Correlation Between Radiosensitivity and DNA Double Strand Break Induction and Rejoining in Six Human Tumor Cell Lines. *Cancer Research*, 3939–3946. 30

OLIVE, P. L., 1998, The role of DNA single- and double-strand breaks in cell killing by ionizing radiation. *Radiation Research*, **150**, S42–S51. 25, 26, 30

PAINTER, R. B., *Radiation Biology in Cancer Research* (Raven Press, New York, 1979), pages 59–68. Eng. 3

PANTELIAS, G. E. and MAILLIE, H. D., 1983, A simple method for premature chromosome condensation induction in primary human and rodent cells using polyethylene glycol. *Somatic Cell Genetics*, **9**, 533–547. 121

PASTINK, A., EEKEN, J. C. and LOHMAN, P. H., 2001, Genomic integrity and the repair of double-strand DNA breaks. *Mutation Research*, **480-481**, 37–50. 28

PAULL, T. T., ROGAKOU, E. P., YAMAZAKI, V., KIRCHGESSNER, C. U., GELLERT, M. and BONNER, W. M., 2000, A critical role for histone H2AX in recruitment of repair factors to nuclear foci after DNA damage. *Current Biology*, **10**, 886–895. 21, 67, 160

PINTO, M., 1998. *Alterazioni molecolari indotte da radiazioni sparsamente ionizzanti: studi sperimentali e teorici*. *Laurea* dissertation, Università degli studi di Napoli 'Federico II', Facoltà di Scienze Matematiche, Fisiche e Naturali. Corso di Laurea in Fisica. 153

PINTO, M., NEWMAN, H. C., PRISE, K. M. and MICHAEL, B. D., 2000, Quantification of DNA damage by PFGE: development of an analytical approach to correct for the background distribution. *International Journal of Radiation Biology*, **76**, 741–748. 57, 61, 62, 63, 65, 67, 68, 153, 155, 157

PINTO, M., PRISE, K. M. and MICHAEL, B. D., 2002, Quantification of radiation induced DNA double-strand breaks in human fibroblasts by PFGE: testing the applicability of random breakage models. *International Journal of Radiation Biology*, **78**, 375–388. 32, 50, 57, 59, 61, 65, 67, 68, 69, 161, 162, 169

PINTO, M., PRISE, K. M. and MICHAEL, B. D., in prep., Rejoining of DSB induced by 240 kVp X-Rays or ^{238}Pu α-particles in human fibroblasts: experimental PFGE studies and computer-simulations. *in prep*. 32

PONOMAREV, A. L., BRENNER, D., HLATKY, L. R. and SACHS, R. K., 2000, A polymer, random walk model for the size-distribution of large DNA fragments after high linear energy transfer radiation. *Radiation and Environmental Biophysics*, **39**, 111–120. 32, 70, 76

PONOMAREV, A. L., CUCINOTTA, F. A., SACHS, R. K. and BRENNER, D. J., 2001a, Monte Carlo predictions of DNA fragment-sized distributions for large sizes after HZE particle irradiation. *Physica Medica*, **17 Suppl 1**, 153–156. 76, 163

PONOMAREV, A. L., CUCINOTTA, F. A., SACHS, R. K., BRENNER, D. J. and PETERSON, L. E., 2001b, Extrapolation of the DNA fragment-size distribution after high-dose irradiation to predict effects at low doses. *Radiation Research*, **156**, 594–597. 76

PRISE, K. M., 1994, Use of radiation quality as a probe for DNA lesion complexity. *International Journal of Radiation Biology*, **65**, 43–48. 24, 27

PRISE, K. M., AHNSTRÖM, G., BELLI, M., CARLSSON, J., FRANKENBERG, D., KIEFER, J., LÖBRICH, M., MICHAEL, B. D., NYGREN, J., SIMONE, G. and STENERLÖW, B., 1998, A review of dsb induction data for varying quality radiations. *International Journal of Radiation Biology*, **74**, 173–184. 26, 31, 57, 161

PRISE, K. M., DAVIES, S. and MICHAEL, B. D., 1987, The Relationship Between Radiation Induced DNA Double Strand Breaks and Cell Killing in Hamster V79 Fibroblasts Irradiated with 250 kVp X-Rays, 2.3 MeV Neutrons or ^{238}Pu α Particles. *International Journal of Radiation Biology*, **52**, 893–902. 26

PRISE, K. M., FOLKARD, M., DAVIES, S. and MICHAEL, B. D., 1990, The irradiation of V79 mammalian cells by protons with energies below 2 MeV. Part II. Measurement of oxygen enhancement ratios and DNA damage. *International Journal of Radiation Biology*, **58**, 261–277. 16, 26

PRISE, K. M., FOLKARD, M., NEWMAN, H. C. and MICHAEL, B. D., 1994, Effect of radiation quality on lesion complexity in cellular DNA. *International Journal of Radiation Biology*, **66**, 537–542. 27

PRISE, K. M., PINTO, M., NEWMAN, H. C. and MICHAEL, B. D., 2001, A review of studies of ionizing radiation-induced double-strand break clustering. *Radiation Research*, **156**, 572–576. 24, 26, 31, 44, 55, 57, 161

PŘIDAL, I. and LOKAJIČEK, M. V., 1984, A model of DSB-repair kinetics. *Journal of Theoretical Biology*, 81–90. 73, 93

RADIVOYEVITCH, T., HOEL, D. G., CHEN, A. M. and SACHS, R. K., 1998a, Misrejoining of double-strand breaks after X irradiation: relating moderate to very high doses by a Markov model. *Radiation Research*, **149**, 59–67. 73

RADIVOYEVITCH, T., HOEL, D. G., HAHNFELDT, P. and SACHS, R. K., 1998b, Size distributions of misrejoining DNA fragments in irradiated cells. *Mathematical Biosciences*, **149**, 107–136. 73, 91

RADIVOYEVITCH, T., HOEL, D. G., HAHNFELDT, P. J., RYDBERG, B. and SACHS, R. K., 1998c, Recent data obtained by pulsed-field gel electrophoresis suggest two types of double-strand breaks. *Radiation Research*, **149**, 52–58. 73

RAGNI, G. and SZYBALSKI, W., 1962, Molecular radiobiology of human cell lines. II. Effects of thymidine replacement by halogenated analogues on cell inactivation by decay of incorporated radiophosphorous. *Journal of Molecular Biology*, 338. 3

RIEF, N. and LÖBRICH, M., 2002, Efficient rejoining of radiation-induced DNA double-strand breaks in centromeric DNA of human cells. *The Journal of Biological Chemistry*, **277**, 20,572–20,582. 34

ROGAKOU, E. P., PILCH, D. R., ORR, A. H., IVANOVA, V. S. and BONNER, W. M., 1998, DNA double-stranded breaks induce histone H2AX phosphorylation on serine 139. *Journal of Cellular Biochemistry*, **273**, 5858–5868. 21, 160

ROOTS, R. and OKADA, S., 1972, Protection of DNA molecules of cultured mammalian cells from radiation-induced single-strand scissions by various alcohols and SH compounds. *International Journal of Radiation Biology and Related Studies in Physics and Chemistry*, **21**, 329–342. 19

ROTHKAMM, K., KÜHNE, M., JEGGO, P. A. and LÖBRICH, M., 2001, Radiation-induced genomic rearrangements formed by nonhomologous end-joining of DNA double-strand breaks. *Cancer Research*, **61**, 3886–3893. 31, 71

RYDBERG, B., 1996, Clusters of DNA damage induced by ionizing radiation: formation of short DNA fragments. II. Experimental detection. *Radiation Research*, **145**, 200–209. 25, 76, 155, 162

RYDBERG, B., 2000, Radiation-induced heat-labile sites that convert into DNA double-strand breaks. *Radiation Research*, **153**, 805–812. 154, 155, 159

RYDBERG, B., HOLLEY, W. R., SAIRA MIAN, I. and CHATTERJEE, A., 1998, Chromatin conformation in living cells: support for a zig-zag model of the 30 nm chromatin fiber. *Journal of Molecular Biology*, **284**, 71–84. 21, 32, 76, 86

RYDBERG, B., LÖBRICH, M. and COOPER, P. K., 1994, DNA double-strand breaks induced by high-energy neon and iron ions in human fibroblasts. I. Pulsed-field gel electrophoresis method. *Radiation Research*, **139**, 133–141. 164

SACHS, R. K., BRENNER, D. J., HAHNFELDT, P. J. and HLATKYS, L. R., 1998, A formalism for analysing large-scale clustering of radiation-induced breaks along chromosomes. *International Journal of Radiation Biology*, **74**, 185–206. 32, 69, 163, 165, 167

SACHS, R. K., CHEN, A. M. and BRENNER, D. J., 1997a, Review: Proximity effects in the production of chromosome aberrations by ionizing radiaiton. *International Journal of Radiation Biology*, **71**, 1–19. 83

SACHS, R. K., CHEN, A. M., SIMPSON, P. J., HLATKY, L. R., HAHNFELDT, P. and SAVAGE, J. R., 1999a, Clustering of radiation-produced breaks along chromosomes: modelling the effects on chromosome aberrations. *International Journal of Radiation Biology*, **75**, 657–672. 32, 91

SACHS, R. K., HAHNFELD, P. J. and BRENNER, D. J., 1997b, The link between low-dose response relations and the underlying kinetics of damage production/repair/mis-repair. *International Journal of Radiation Biology*, 351–374. 71

SACHS, R. K., PONOMAREV, A. L., HAHNFELDT, P. and HLATKY, L. R., 1999b, Locations of radiation-produced DNA double strand breaks along chromosomes: a stochastic cluster process formalism. *Mathematical Biosciences*, **159**, 165–87. 70, 163

SACHS, R. K., VAN DEN ENGH, G., TRASK, B., YOKOTA, H. and HEARST, J. E., 1995, A random-walk/giant-loop model for interphase chromosomes. *Proceedings Of The National Academy Of Sciences (U.S.A.)*, **92**, 2710–2714. 22, 165

SCHRÖDINGER, E., *What is life?* (Cambridge University Press, 1944). 3, 23

SCHWARTZ, D. and CANTOR, C., 1984, Separation of yeast chromosome-sized DNA molecules by pulsed field gradient gel electrophoresis. *Cell*, **37**, 67–75. 41, 44, 46

SCHWARTZ, D. C. and KOVAL, M., 1989, Conformational dynamics of individual molecules during gel electrophoresis. *Nature*, **338**, 520–522. 45

SPARROW, A. H., *Cellular Radiation Biology* (Williams & Wilkins, Baltimore, 1965), pages 199–222. 3

STAMATO, T. D. and DENKO, N., 1990, Asymmetric field inversion gel electrophoresis: a new method for detecting DNA double-strand breaks in mammalian cells. *Radiation Research*, **121**, 196–205. 52, 57

STENERLÖW, B., BLOMQUIST, E., GRUSSELL, E., HARTMAN, T. and CARLSSON, J., 1996, Rejoining of DNA Double Strand Breaks Induced by Accelerated Nitrogen Ions. *International Journal of Radiation Biology*, **70**, 413–420. 32

STENERLÖW, B., CARLSSON, J., BLOMQUIST, E. and ERIXON, K., 1994, Clonogenic Cell Survival and Rejoining of DNA Double Strand Braks: Comparisons Between Three Cell Lines After Photon or He Ion Irradiation. *International Journal of Radiation Biology*, **65**, 631–639. 162, 172

STENERLOW, B. and HOGLUND, E., 2002, Rejoining of double-stranded DNA-fragments studied in different size-intervals. *International Journal of Radiation Biology*, **78**, 1–7. 32, 44, 50, 57, 71, 150, 169, 170, 172

STENERLÖW, B., HÖGLUND, E. and CARLSSON, J., 1999, Induction and rejoining of large DNA fragments after ion irradiation. *Radiation Research*, **151**, 642–648. 32, 57, 71, 164

STENERLÖW, B., HÖGLUND, E., CARLSSON, J. and BLOMQUIST, E., 2000, Rejoining of DNA fragments produced by radiations of different linear energy transfer. *International Journal of Radiation Biology*, **76**, 549–557. 32, 44, 59, 67, 71, 104, 106, 154, 172

STEWART, R. D., 2001, Two-lesion kinetic model of double-strand break rejoining and cell killing. *Radiation Research*, 365–378. 73

SUTHERLAND, B. M., BENNET, P. V., SIDORKINA, O. and LAVAL, J., 2000, Clustered DNA damages induced in isolated DNA and in human cells by low doses of ionizing radiation. *Proceedings Of The National Academy Of Sciences (U.S.A.)*, **97**, 103–108. 159

SUTHERLAND, B. M., BENNET, P. V. and SUTHERLAND, J. C., 1996, Double strand breaks induced by low doses of γ rays or heavy ions: quantitiation in nonradioactive DNA. *Analytical Biochemistry*, 53–60. 43, 58

TABOCCHINI, M. A., ROTHKAMM, K., SIGNORETTI, C., RISSE, J., SAPORA, O. and LÖBRICH, M., 2000, Formation and repair of DNA double-strand breaks in gamma-irradiated K562 cells undergoing erythroid differentiation. *Mutation Research*, **461**, 71–82. 162

TAINER, J. A., 2000, DNA structural biochemistry of DNA damage recognition and repair pathway progression. In: *Abtracts of the 47th Annnual Meeting of the Radiation Research Sociey*, volume S01–4. 14

TAYLOR, B., GREENSTEIN, J. P. and HOLLAENDER, A. E., 1948. *Archives of Biochemistry and Biophysics*, 19–31. 25

THACKER, J., STRETCH, A. and GOODHEAD, D. T., 1982, The mutagenicity of α-particles from ^{238}-Pu. *Radiation Research*, **92**, 343–352. 38

TIMOFÈEFF-RESSOVSKY, N. V., ZIMMER, K. G. and DELBRÜCK, M., 1935, Uber die Natur der Genmutation und der Genstruktur. *Nachr. a.d. Biologie d. Ges. d. Wiss. Göttingen*, **1**, 189–245. 23

TOBI, S. E. and MCMILLAN, T. J., 1997, Techniques for the measurement of DNA strand breaks in mammalian cells. Extended Abstract from 'Radiation Damage to DNA: Techniques, Quantitation and Mechanisms', Bowness-on-Windermere, Lake District, UK, April 19–24, 1997. *Radiation Research*, 481–452. 43

TOBIAS, C., 1985, The Repair-Misrepair Model in Radiobiology: Comparison to Other Models. *Radiation Research*, **104**, S77–S95. 72

VON SONNTAG, C., HAGEN, U., SCHÖN-BOPP, A. and SCHULTE-FROHLINDE, D., *Radiation Induced Strand Breaks in DNA: Chemical and Enzymatic Analysis of End Groups and Mechanistic Effects.*, volume 9 (Academic Press, 1981), pages 109–142. 24

WALLRATH, L. L., LU, Q., GRANOK, H. and ELGIN, S. C., 1994, Architectural variations of inducible eukaryotic promoters: preset and remodeling chromatin structures. *Bioessays*, **16**, 165–170. 21

WARD, J. F., 1981, Some biochemical consequences of the spatial distribution of ionizing radiation-produced free radicals. *Radiation Research*, **86**, 185–195. 24

WARD, J. F., 1994, The complexity of DNA damage: relevance to biological consequences. *International Journal of Radiation Biology*, **66**, 427–432. 14, 25, 27

WARD, J. F., 1995, Radiation mutagenesis: the initial DNA lesions responsible. *Radiation Research*, **142**, 362–368. 25

WARD, J. F., Nature of Lesions Formed by Ionising Radiation. In: NICKOLOFF, J. and HOEKSTRA, M., editors, *DNA Repair in Higher Eukaryotes*, volume 2, chapter 5 (Humana Press Inc., Totowa NJ, 1998), pages 65–84. 23

WEINFELD, M., RASOULI-NIA, A., CHAUDRY, M. A. and BRITTEN, R. A., 2001, Response of base excision repair enzymes to complex DNA lesions. *Radiation Research*, **156**, 584–589. 159

WHITAKER, S. J. and MCMILLAN, T. J., 1992a, Oxygen effect for DNA double-strand break induction determined by pulsed-field gel electrophoresis. *International Journal of Radiation Biology*, **61**, 29–41. 162

WHITAKER, S. J. and MCMILLAN, T. J., 1992b, Pulsed-Field Gel Electrophoresis in the measurement of DNA double strand break repair in xrs-6 and CHO Cell Lines: DNA degradation under some conditions interferes with ther assesment of double strand break rejoining. *Radiation Research*, **130**, 389–392. 40

WHITAKER, S. J., UNG, Y. C. and MCMILLAN, T. J., 1995, DNA Double Strand Break Induction and Rejoining as Determinants of Human Tumour Cell Radiosensitivity. A Pulsed Field Gel Electrophoresis Study. *International Journal of Radiation Biology*, **67**, 7–18. 25

WIDOM, J., 1992, A relationship between the helical twist of DNA and the ordered positioning of nucleosomes in all eukaryotic cells. *Proceedings Of The National Academy Of Sciences (U.S.A.)*, **89**, 1095–1099. 21

WIDOM, J., Structure, dynamics, and function of chromatin in vitro. In: *Annual review of biophysics and biomolecular structure*, volume 27 (Annual Reviews, 1998), pages 285–327. 21

WINTERS, T. A., PASTWA, E., MEZHEVAYA, K. and NEUMANN, R. D., 2001, Repair of radiation-induced DNA double-strand breaks is dependent upon end-group complexity and radiation quality as determined by *in vitro* end joining using a human HeLa cell extract. In: *VIIth International Workshop on Radiation Damage to DNA, Nouan le Fuzelier, France*. 74

YOKOTA, H., VAN DEN ENGH, G., HEARST, J. E., SACHS, R. K. and TRASK, B. J., 1995, Evidence for the organization of chromatin in megabase pair-sized loops arranged along a random walk path in the human G0/G1 interphase nucleus. *Journal of Cell Biology*, **130**, 1239–1249. 22, 165

Index

Attached Publications

PAPER I PINTO, M., NEWMAN, H. C., PRISE, K. M. and MICHAEL, B. D., 2000, Quantification of DNA damage by PFGE: development of an analytical approach to correct for the background distribution. *International Journal of Radiation Biology*, **76**, 741–748.

PAPER II PRISE, K. M., PINTO, M., NEWMAN, H. C. and MICHAEL, B. D., 2001, A review of studies of ionizing radiation-induced double-strand break clustering. *Radiation Research*, **156**, 572–576.

PAPER III PINTO, M., PRISE, K. M. and MICHAEL, B. D., 2002, in the proceedings of the 13th Symposium on Microdosimetry, Stresa, Lake Maggiore, Italy, May 27-June 1, 2001, DSB rejoining after irradiation of human fibroblasts with X-rays or alpha-particles: PFGE studies and numerical models. *Radiation Protection Dosimetry*, **99**, 133–136.

PAPER IV PINTO, M., PRISE, K. M. and MICHAEL, B. D., 2002, Quantification of radiation induced DNA DSBs in human fibroblasts by PFGE: testing the applicability of random breakage models. *International Journal of Radiation Biology*. **78**, 375-388.